Cholestasis-Induced Cognitive Decline: Neurological Mechanisms and Therapeutic Implications

Lucy May Gee

Institute of Biosciences,

Faculty of Medical Sciences

This thesis is submitted for partial fulfilment of the degree Doctor of Philosophy

October 2020

Abstract:

Cognitive dysfunction occurs during the cholestatic liver disease Primary biliary Cholangitis (PBC). Patients experience with short-term memory and concentration deficit, termed 'brain fog'. This can be debilitating and severely affect quality of life, with no beneficial treatments (Newton, Hollingsworth et al. 2008)

In this thesis, using the murine Bile Duct Ligation (BDL) model and *in vitro* modelling with human neuronal cells, I investigated the effects of cholestasis on the blood-brain barrier (BBB) and resultant changes within the brain. This study focussed on the hippocampus due to its crucial role in learning and memory. Changes to BBB could be observed from day 6, including astrocyte detachment, and permeability using MRI. By day 10 mice had visual spatial memory deficits, neuroinflammation was seen within the hippocampus, and changes were observed in gamma frequency oscillations. Interestingly, neurons in the hippocampus possessed features of senescence in cholestatic mice (telomere associated DNA damage, and P21+ RNA), highlighting parallels in pathology between the liver (where senescence is known to occur during cholestasis) and the brain. This effect was mirrored during *in vitro* studies, where neurons treated with PBC patient serum (to simulate pathological exposure to bile acids) also displayed increased sen-B-gal, a feature of senescence.

In another strand, I examined the ability of both approved (ursodeoxycholic acid, Obeticholic Acid) and experimental (Bezafibrate) therapies to modify cognitive processes. Only Obeticholic Acid provides a potential therapeutic due to its *in vivo* and *in vitro* effects. Strikingly, OCA improve cognition and reduces neuronal senescence in BDL mice and *in vitro* when neurons are pre-treated before serum treatments.

Therefore, the data presented in this thesis implicates senescence as a key pathological feature of cholestatic disease not just in the liver but also in brain where it has been previously linked to poor cognition (Baker, Wijshake et al. 2011, Fielder, Tweedy et al. 2020). Further investigation of early intervention with OCA may prove beneficial to patients experiencing cognitive deficit.

Acknowledgements;

I would like to thank my supervisors Fiona, Dave, Fiona and Peter for their continued support throughout the time of my PhD. Thank you to Fibrosis Lab for being my main base, and to FLB lab for adopting me partway through.

Thank you to Jack Leslie for help with running the flow cytometry experiments, Ben Millar and Claire Richardson for the set up for the behavioural testing protocols, and Rainie for always being there to give technical assistance for any animal work. Thanks to UG student RuoXie who completed some of the counts for immunofluorescent brain stains. Thank you to valued collaborators Diana Jurk and Tom Bird and his student Christos, for staining help and advice on anything senescence related in the brain and liver respectively. Thanks to Beth Stoll, for showing me that science could be interesting.

Dedications;

To my parents, without your endless love and support none of this would have been possible.

Abbreviations List:

Bile duct ligation (BDL)

Bile Duct Resection (BDR)

Bile acid (BA)

Obeticholic Acid (OCA)

Ursodeoxycholic Acid (UDCA)

non-alcoholic steatohepatitis (NASH)

Bezafibrates (BF)

Open Field (OF)

Blood-brain barrier (BBB)

Neurovascular Unit (NVU)

Brain Microvascular Endothelial Cells (BMECs)

Hepatic Encephalopathy (HE)

Sucrose rich artificial cerebral-spinal fluid (SaCSF)

Artificial cerebral-spinal fluid (aCSF)

Carbachol (Cb)

Micromolar (µM)

Room temperature (RT)

phosphocreatine responses (PCr)

cardio pulmonary exercise testing (CPET),

quality of life (QOL)

resting-state functional magnetic resonance imaging (rsfMRI)

Diffusion Tensor Imaging Magnetic Resonance Imaging (DTI-MRI)

interferon gamma (IFN- γ)

lipopolysaccharide (LPS)

Arginase1 (arg1)

Nitric oxide synthase (iNOS)

Rotations per minute (RPM)

Glial acidic fibrillary protein (GFAP)

Electron microscopy (EM)

Fluorescence Activated Cell Sorting (FACs)

Biliary Epithelial Cells (BECs)

Ductular Reaction (DR)

Phosphate Buffered Saline (PBS)

Distilled water (dH20)

Parvalbumin (PV)

Peroxisome Proliferator-Activated Receptor (PARR)

Aspartate Transaminase (AST)

Alanine Transaminase (ALT)

Alkaline Phosphatase (ALP)

Cytochrome P450 cholesterol 7A1-hydroxylase (CYP7A1)

Cytochrome sterol 27-hydroxylase (CYP27A1)

Carbontetrachloride (CCL4)

α-naphthylisothiocyanate (ANIT)

apical sodium-dependent bile acid transporter (ASBT)

Pregnane X receptor (PXR)

Farnesoid X Receptor (FXR)

tumour necrosis factor-α (TNF-α)

interleukins 4 and 10 (IL4, IL10)

transforming growth factor beta (TGF-β)

Takeda G protein Coupled receptor (TGR5)

Lithocholic Acid (LCA)

Taurocholic acid (TCA)

Glycoursodeoxycholic acid (GUDCA)

chenodeoxycholic acid (CDCA)

monozygotic (MZ)

Hepatic stellate cells (HSC)

Table list:

Figure List

1. Chapter One - General Introduction

1.1. The Normal Functional Anatomy of the Human Liver and Biliary Tree

1.1.1. Liver

The organ of the liver is primarily responsible for several processes including detoxification, energy homeostasis, cholesterol and fat processing in conjunction with the biliary system. It also represents the largest visceral organ by volume, spanning the upper abdomen (Rogers and Dintzis 2012).

The liver is comprised of four lobes, in order of size; the right, the left, the caudate and the quadrate lobe. The lobes have complex interlinking functionality. The major blood supply (70%) of the liver comes from the portal vein. The portal vein is mirrored by the bile ducts which run in parallel throughout, giving rise to the classic 'portal triad' formation seen in liver histology first reported by Ludwig (Ludwig 1987).

The portal triad is the centre of the functional units of the liver; named lobules or hepatic acinus. These comprise of aforementioned portal triad (a bile duct, portal vein and hepatic artery) with bridging formation of hepatocytes. This construction causes a graded oxygen content across different areas of the lobule, partitioning areas of the liver into metabolic zones (figure 1). These zones are crucial for the normal functioning of the liver. The zones represent flexible metabolic attributes of hepatocytes, and can be modified and shifted into either a more oxygen dependent or glycolytic state along with other metabolic modifications.

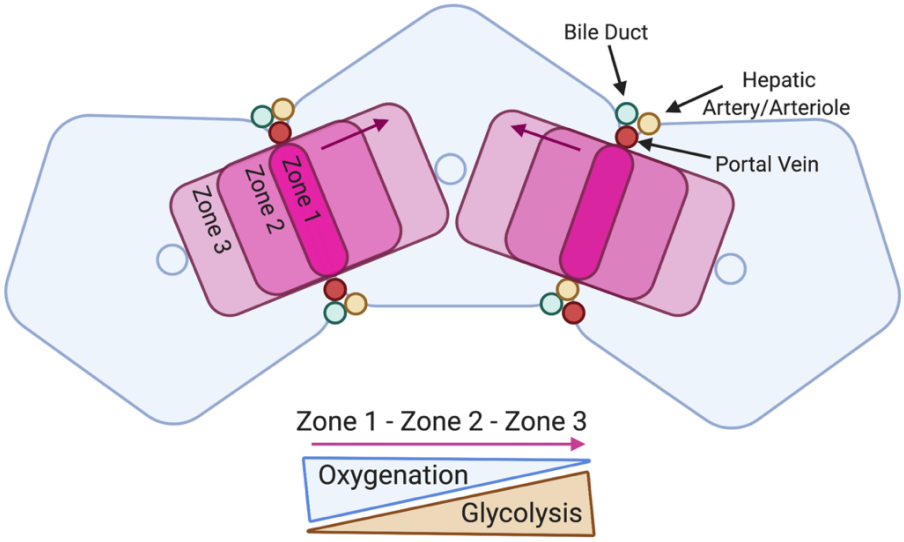

Figure 1. The metabolic and functional organisation of the liver.

1.1.2. The Biliary Tree

The biliary tree in humans is a complex system of interlobular, septal and major ducts intersected at one end with the Canals of Hering and the other the extrahepatic bile ducts, delivering bile to the gallbladder. Bile has many roles in the body, most famously it is the major pathway for cholesterol degradation.

In this pathway bile acids are formed as end-products of degraded cholesterol and must be excreted via the intestines through to the faeces. The normal composition of the bile is 97% water, 0.7% bile acids, 0.2% bilirubin, 0.51% fats (cholesterol, fatty acids, and lecithin) (Barrett and Ganong 2012). Bile is made in the liver by the hepatocytes and secreted into the bile canaliculi via the apical membrane. Adjacent hepatocytes have adjoining apical membranes separated via tight junctions(Anderson and Van Itallie 1995). This both sticks hepatocytes together and ensures the bile acids don't diffuse from the bile flow. During cholestatic injury, distressed hepatocytes can change their bile secretion patterns, disrupting the tight junction and leading to perturbed flow, resulting in bidirectional bile flow back into the intercellular space and out into the liver (Boyer 1983).

Bile secretion differs depending on the area of the lobule in which the hepatocyte resides. Hepatocytes from the periportal regions are exposed to and produce higher concentrations of bile salts, resulting in a larger size of canaliculi in these regions (Layden and Boyer 1978). Once within the biliary tree, tracts are lined with cholangiocytes (also termed biliary epithelial cells) -the major cell type lining the biliary epithelium.

Smaller ducts are lined by between 4-5 cholangiocytes, while larger ducts can be lined by up to 40 (Glaser, Francis et al. 2006). Classically, cholangiocytes are mitotically dormant however they have been shown to proliferate in response to noxious stimuli such as carbontetrachloride (CCL4) (LeSage, Benedetti et al. 1999), α-naphthylisothiocyanate (ANIT), or cholestasis (Glaser, Lam et al. 2010). It is thought that smaller cholangiocytes (lining small ducts) have a larger proliferative capacity than larger cholangiocytes (lining large ducts). Cholangiocyte proliferation, termed ductular reaction (DR) also occurs during cholestatic biliary disease in humans (Sell 1998).

1.1.3. Differences in the Liver and Biliary Tree between humans and rodents

Rodents provide a good model species for study of the liver and biliary tree. However, there are some key differences in the structural organisation. In mice, livers spans the entire subdiaphragmatic space and accounts for 6% of total body weight, 3x as much as humans (Rogers and Dintzis 2012). Rodents also have fewer intermediary ducts, possessing mainly large and small ducts (Alpini, Roberts et al. 1996).

Another key difference in rats is the absence of the gall bladder, first reported in 1922 (McMaster 1922). While the cause of this is not known it is thought that due to the nature of a rat's diet (low fats) and the way in which they continuously forage for food a gallbladder is not evolutionarily necessary, and the liver is able to produce sufficient bile without a need for storage.

1.2. Bile Salts Function, Composition and Regulation

As aforementioned, the bile is partly made up of bile acids. These have long been described as digestive detergents, acting as detergents to emulsify circulating fat globules. While these bile acids do have a primary role in the breakdown of cholesterol (over half of cholesterol is broken down this way (Insull 2006)), they are also bioactive steroids hormones with key roles in processes such as energy homeostasis.

Bile acids are produced solely in the liver, by hepatocyte undergoing a series of catabolic reactions producing bile from cholesterol under the power of the enzyme cholesterol 7α-hydroxylase (CYP7A1). Due to their control of cholesterol homeostasis the levels of bile acids in the enterohepatic circulation is tightly regulated, through the transcription of CYP7A1 (Russell & Setchell, 1992) (Pullinger, Eng et al. 2002). CYP7A1 is the rate limiting enzyme in the classical pathway of bile acid synthesis, leading to the repression of bile acid synthesis via negative feedback loops.

The primary bile acids in humans cholic acid (CA) and chenodeoxycholic acid (CDCA) are ordinarily synthesised by hepatocytes under CYP7A1 in the classical pathway. More rarely their synthesis can be initiated by mitochondrial CYP7A1, which is found in other cell types in the liver including macrophages (Hylemon, Zhou et al. 2009).

After synthesis in the liver, bile acids are secreted and absorbed into the intestine (figure 2). The main transporter responsible for bile acid transport from the apical (canicular) membrane is BSEP (Childs, Yeh et al. 1995). The importance of BSEP was discovered in progressive familial intrahepatic cholestasis subtype 2 (PFIC-2) patients. A lack of functional BSEP in these patients leads to severe decrease in normal bile acid concentration (1% of normal), highlighting BSEP as the major canalicular bile acid transport mechanism (Strautnieks, Kagalwalla et al. 1997).

Upon reaching the large intestine primary bile acids undergo further processing via deconjugation and dehydroxylation by gut bacteria. This processing forms secondary bile acids such as chenodeoxycholic acid (CDCA) conversion to lithocholic acid (LA)

(Ridlon, Kang et al. 2006). Unconjugated bile acids can be absorbed passively in the ileum, and conjugated bile acids are actively transported by bile acid transporters (Wilson, Lindsey et al. 1968) back to the liver. In humans, bile acids are stored primarily in the gallbladder, and are released after each meal.

In the gallbladder bile acids and cholesterols along with phospholipids and micelles, which solubilise cholesterols and also reduce bile acid toxicity. This allows bile acids to facilitate absorption of dietary vitamins and lipids in the small intestine. Upon release into the intestines, bile acids are then reabsorbed into the ileum and taken back to the liver (via portal tract) for re-excretion into the bile by the hepatocytes. In the ileum terminal bile acids are absorbed into the enterocyte actively by the apical sodium-dependent bile acid transporter (ASBT) and secreted back to portal circulation via basolateral Ostα/Ostβ transporters, which have a key role in preventing accumulating bile acid toxicity (Ferrebee, Li et al. 2018) and are a major basolateral bile acid transport system in the intestine and many other epithelial cells (Dawson, Hubbert et al. 2005). Hepatocytes take up bile acids by Na+-taurocholate co-transporting polypeptide (NTCP) and organic anion transporters (OATPs) for re-secretion back into the gallbladder (Figure 2).

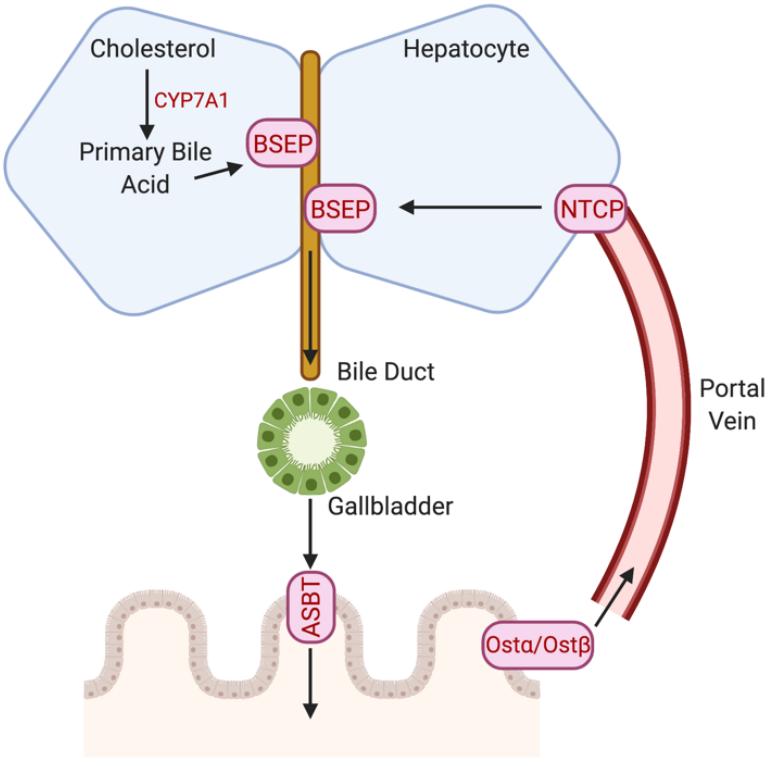

Figure 2. Active mechanisms of bile acid transport through the liver and biliary system.

The bile acids found in mammalian species are so called 'modern' C24 bile acids. These bile acids form the majority of the human bile pool and consist of chains 24 carbon atoms long (Hofmann, Sjövall et al. 1992). The bile acid pools of other more 'primitive' vertebrates such as sharks or amphibians are commonly 25, 26 or 27 carbon atoms in length. Mammalian bile acids are conjugated with glycine or taurine, in humans at a ratio of about 4:1 (Warren, Chalmers et al. 2006).

1.3. Key Bile Acid Receptors and their Specific Roles

1.3.1. Farnesoid X Receptor (FXR)

Farnesoid X Receptor (FXR) is a nuclear bile acid receptor with functions in metabolism, and a pivotal role in regulating liver inflammation and regeneration (Meng, Wang et al. 2010, Zhang, Wang et al. 2012). It is expressed in a variety of tissues such as liver, adipose tissue, pancreas, kidney and the vascular wall (Huber, Murphy et al. 2002).

Several papers indicate that FXR has a key role in gene regulation of hepatic bile acid synthesis, bile acid secretion from the gall bladder, absorption into the intestine and hepatic bile acid uptake, thus highlighting its role in mechanisms of bile acid homeostasis throughout its cycle (Kuipers, Claudel et al. 2004).

FXR can be activated by both free and conjugated bile acids. Hydrophobic bile acids are more potent agonists. Chenodeoxycholic acid (CDCA) is the natural compound of highest affinity (EC50 ~ 10 µM) (Wang, Chen et al. 1999) and deoxycholic acid and lithocholic acid bind with weaker affinity. Hydrophilic bile acids such as muricholic acid and ursodeoxycholic acid cannot activate FXR (Li, Jadhav et al. 2013). Intercept's artificial compound Obeticholic Acid can activate FXR with a potency 100x stronger than CDCA (De Magalhaes Filho, Downes et al. 2016).

1.3.1.1. Regulation of Bile Acid Synthesis by Farnesoid X Receptor

Bile acid synthesis is largely controlled by the transcriptional regulation of CYP7A1, the main rate limiting step in bile synthesis in the liver (Chiang 2009). It is also well known that bile acids are responsible for repressing CYP7A1 gene expression, generating an effective negative feedback loop. This feedback mechanism allows the liver to effectively increase or decrease bile acid synthesis and the resulting pool, maintaining constant levels.

Inhibition feedback of CYP7A1 is controlled by FXR. This nuclear receptor is expressed in both hepatocyte and enterocytes, and induces small heterodimer partner (SHP), to repress transcriptional regulator liver-related homologue-1 (LRH-1). This in turn binds to the CYP7A1 promotor, inhibiting CYP7A1 synthesis and reducing bile acid production (Heuman, Hylemon et al. 1989, Goodwin, Jones et al. 2000). Inhibition is induced via a cascade mediated by small heterodimer partner (SHP) and various transcription factors which bind the bile acid response elements in the promoter region of CYP7A1 (Stroup,

Crestani et al. 1997). Other cytochrome 450 enzymes involved in BA synthesis can also be regulated in this way, for example CYP8B1 (Yang, Zhang et al. 2002).

However, SHP deficient mice are still able to repress CYP7A1 expression, through bile acid stimulation and through FXR agonism. This therefore suggests other FXR mediated feedback regulation of CYP7A1 must exist in place of SHP knockout (Kerr, Saeki et al. 2002). Concurrently, FXR has also been shown to induce fibroblast growth factor-15 (FGF-15) (FGF-19 in murine), which can also affect CYP7A1 transcription, highlighting a role for FXR as a master regulator of bile acid synthesis. FGF-15 infusion in mouse studies, either directly into circulation or specifically in liver tissue caused repression of CYP7A1 mRNA (Inagaki, Choi et al. 2005).

Conversely, when mice lack functional FXR, bile acid synthesis is upregulated, CYP7A1 expression increased, and pool size increased (Sinal, Tohkin et al. 2000) illustrating the importance of FXR in inhibition of bile acid synthesis.

1.3.1.2. Role of Farnesoid X Receptor in Lipid Metabolism

It has long been known that bile acid sequestrants reduce total and low-density lipoprotein in the plasma. Patients on bile acid supplements decrease their high-density lipoprotein whereas cholestyramine treatment (bile acid sequestrant) can increase HDL cholesterol levels (Shepherd, Packard et al. 1979).

1.3.2. Takeda G Protein 5 Receptor

TGR5 is a G-protein coupled receptor, also named G-protein bile acid-activated receptor (GP-BAR1). TGR5 is widely expressed in many tissues, including the intestine, gallbladder, liver, and brain (Maruyama et al., 2002). In the liver TGR5 is expressed mainly in Kupffer cells and sinusoidal cells, with no TGR5 expression in hepatocytes (Keitel, Donner, Winandy, Kubitz, & Haussinger, 2008; Keitel et al., 2007). When

activated, TGR5 stimulates cAMP synthesis, leading via intracellular signalling cascades to increases in nitrous oxide and the complex phosphorylation of CD95 (Reinehr & Haussinger, 2004). This reduces bile acid- induced apoptosis in the sinusoidal cells, which are regularly exposed to high levels of bile acids from the portal circulation post-meals.

1.4. Primary Biliary Cholangitis (PBC)

Primary Biliary Cholangitis (PBC) is an autoimmune liver disease of the bile duct. Immune system attack causes destruction of the intrahepatic bile ducts, selectively targeting intrahepatic cholangiocytes. The disease also causes progressive cholestasis of the liver, defined as 'decrease in bile flow due to impaired secretion by hepatocytes or obstruction of intra/extra-hepatic bile ducts. Ultimately the build-up of bile acids in the hepatic circulation leads to inflammation and fibrosis of the liver, which can advance to cirrhosis at the later stages of the disease. In 26% of cases this leads to liver failure within 10 years of diagnosis (Washington 2007).

Clinically, PBC is a heterogeneous disease, causing difficulties in diagnosis and treatment. Patient presentation can range from asymptomatic and slow progressing cholestasis diagnosed only from abnormal liver biochemistry to advanced cirrhosis (Long, Scheuer et al. 1977, Crowe, Christensen et al. 1985). It is clear that PBC represents a variety of patients, with as spectrum of disease states reflecting ongoing dynamic processes of bodily wide and local organ injury.

1.4.1. Anti-Mitochondrial and Anti-Nuclear Antibodies

The pathophysiology of PBC was identified in the 1980s as a loss of tolerance to ubiquitous mitochondrial autoantigens the E2 subunit at the mitochondrial pyruvate dehydrogenase complex (PDC-E2), causing targeted injury at the small ducts. This leads to an autoimmune response driven by mitochondrial autoantigen intolerance, primarily

within the liver causing inflammatory response (cholangitis), progressing to cholestasis (prohibition/ disruption of bile flow) and on to cirrhosis of the liver. The presence of anti-mitochondrial antigens (AMA) is largely used for clinical diagnosis, however these are present only in 90-95% of cases (Hirschfield 2011). It is thought that AMAs are the most specific immune marker of any autoimmune disease.

AMAs specifically recognise the lipoylated domains on immunodominant epitopes where lipoic acid is attached at the lysine group (K) 173. T cells and B cells both possess the lipoylated K173 group, leading to CD4 T cell being enriched 100-150-fold in the liver and lymph nodes. CD8 T cells (PDC-E2 specific) in the liver also possess this domain and so are upregulated by 10 fold (Kita , Lian et al. 2002, Kita, Matsumura et al. 2002).

AMA negative patients show no obvious differences from AMA positive patients, and present similarly based on criteria of age, sex and liver (Lindgren, Glaumann et al. 2009). This goes against the paradigm of AMA positivity as central to PBC diagnosis and progression, and has sparked debate on the true pathogenesis of PBC.

More recently, other autoantibodies have been linked with the disease. Antinuclear antibodies (ANAs) are autoantibodies attacking the nuclear fraction of the cell, and occur in around 50% of patients. They are clinically significant, and can be prognostic indicators (their presence informs of more severe disease) (Nakamura, Takii et al. 2006, Nakamura, Kondo et al. 2007). However, the pathogenic significance of these is unclear.

Clinical laboratories typically use fluorescence microscopy to detect changes in the nucleus, such as dotted nuclei or rimmed patterns. Specific components linked with nuclear pore complex gp120 and sp100 have been implicated in prognostic testing. Recent studies have shown that higher titres of AMA specific antibodies anti-gp210 and anti-sp100 can be associated with more advanced disease (Gatselis, Zachou et al. 2013), whereas only mildly elevated anti-sp100 titres were associated with a better long term

prognosis. More recently these biomarkers of progression have been investigated in trials (Huang, Han et al. 2019).

1.4.2. Histology and Immune Response

PBC is an organ specific autoimmune disease, with the small hepatic ducts the main target of autoimmune attack. The disease has a complex interplay of genetics or environmental factors with the adaptive immune system contributing to disease onset and progression.

PBC has a very distinct histology, categorised into four stages. First comes periportal inflammation with ductular lesions, moving on to secondary increased periportal lesions and hepatitis. The third stage is defined by loss of normal hepatic architecture and bridging fibrosis, followed by cirrhosis of the liver at stage four. These stages are often accompanied by 'florid lesions' - areas of intense inflammatory response and resulting necrosis (Ludwig, Dickson et al. 1978). The inflammatory infiltrate resulting in the lesions is heterogeneous, consisting of large numbers of lymphocytes that are closely associated with distressed and necrotic BECs, as well as both resident and infiltrating macrophage populations (Kobayashi, Kakuda et al. 2014). This large-scale inflammation leads to occlusion at the ducts and portal veins accompanied by ductular reaction. Figure 3 below from (Smyk, Rigopoulou et al. 2012) gives examples of histological staging.

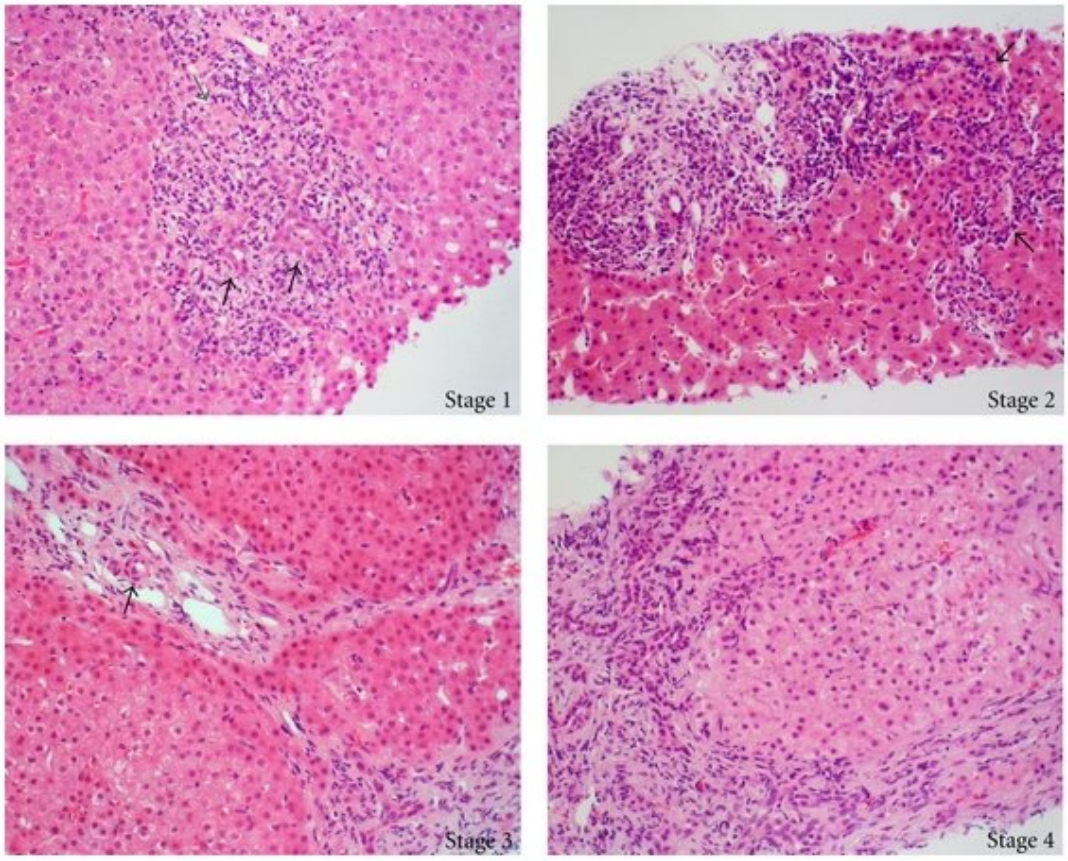

Figure 3. Figure is taken from (Smyk, Rigopoulou et al. 2012). The four histological stages of PBC begin with inflammatory infiltrate leading to extensive periportal inflammation and ductular reaction. Stage 3 is bridging fibrosis through the tissue finally followed in stage 4 by cirrhosis.

1.4.3. Ductular Reaction

Ductular reaction is a key pathological feature of PBC. It is defined as an expansion and proliferation at the duct, via expansion of ductules or by differentiation of hepatic progenitor cells (HPC) into biliary structures. Ductular reaction requires two key interlinked processes; the proliferation of the epithelium at the duct and the aggravation by bile acids leading to fibrosis. Both mesenchymal and inflammatory cell accompany the expansion of BECs that surround the biliary tract. HPC expansion exists as a compensatory mechanism in the event of liver damage, when hepatocytes become distressed (Roskams 2003). In association with this ductular reaction, hepatic stellate cells become activated and proliferate, depositing extra cellular matrix in a fibrotic

response(Milani, Herbst et al. 1990). It remains unclear which of these events occur first, however the combination results in an expanded and distorted duct.

BECs play a key role in ductular rearrangement. During PBC BECs begin to express a reactive phenotype of a combination of chemokines and cytokines along with angiogenic factors similar to during liver development which encourage proliferation (Strazzabosco and Fabris 2012). Phenotypic changes to these cells create paracrine connections with stromal cells such as hepatic stellate cells and Kupffer cells (Fabris and Strazzabosco 2011).

1.4.4. Adaptive Immune Response in PBC

Adaptive immune response in PBC is thought to be activated as a consequence of autoimmune response. The triggers resulting in the autoimmune response remain unclear, however molecular mimicry has been suggested. PDC-E2 reactive T cell lines (the primary PBC autoantigen) have been shown to be cross reactive with E.Coli peptides, which may provide some insight into the pathogenesis of PBC (Shimoda, Nakamura et al. 2000).

1.4.4.1. CD8 T Cells

Overall, CD8+ T cells are key in the pathogenesis of PBC. They infiltrate the portal regions throughout disease progression in ample numbers (Kita , Lian et al. 2002) and infact a PBC phenotype can be induced by transfer of CD8 T cells from dnTGF-βRII mouse model of PBC in to wild type C57/Bl6 mouse strain (Yang, Lian et al. 2008). Other PBC emulating mouse models show the development of lesions is paired with huge CD8 T cell infiltration (Wakabayashi, Yoshida et al. 2009).

1.4.4.2. CD4 T Cells

CD4 T cells also infiltrate the peri-portal hepatic regions both in PBC and in animal models. Increased CD4 T cells can be seen accumulating specifically within the portal tracts (Lan, Salunga et al. 2009) compared to other regions of the liver. Other studies show that Th1 cells mediate initial immune response, which is then perpetuated by Th17 cells in established disease (Yang, Ma et al. 2014).

Other T cells populations have also been investigated in PBC. The presence of IL-6 in the bile duct suggests that Th2 cell cytokines lead to cell damage by antibody dependent cytotoxicity (Yasoshima, Kono et al. 1998).

1.4.5. Aetiology and Risk Factors

As with many autoimmune diseases, PBC has a complex and heterogeneous inheritance. There is a high level of predominance in women (approx. 10:1 in the UK), and is particularly common in postmenopausal women. Though it is less common in men, male patients tend to present at an younger age and have a more severe disease phenotype (Carbone, Mells et al. 2013), and were less likely to show response once they began treatment with UDCA.

Reasons for the high female predominance in PBC are scarce. Women who develop PBC at a younger age also show a clear reduction in response to first line treatment UDCA (Carbone, Mells et al. 2013) like men. As cholestasis is seen in pregnancy, it seems likely that this effect could be influenced by the effects of female sex hormones such as oestrogen, the receptors for which are expressed on liver populations such as cholangiocytes (Alvaro, Invernizzi et al. 2004).

Another hypothesis is that PBC may be influenced by changes in sex chromosomes. X linked disease such as Turner's syndrome can have autoimmune symptoms causing

chronic cholestasis, and additionally several key immune tolerance genes such as FOXP3 are coded for by the X chromosome (Powell, Buist et al. 1982). Women with PBC also have frequent X chromosome monosomy, suggestive of X chromosome instability (Invernizzi, Miozzo et al. 2004).

1.4.5.1. Genetic Risk and Risk alleles

There is some monozygotic (MZ) twin concordance in PBC, suggesting an element of genetic inheritance (Selmi, Mayo et al. 2004). However, studies in discordant MZ twin pairs show there are marked differences in epigenetic modifications such as DNA methylation and additional copy number variants resulting from duplications or rearrangement (Selmi, Cavaciocchi et al. 2014).

The prevalence of PBC risk in first degree relatives of those with the condition is approximately 0.72% and 1.2% (Hirschfield and Invernizzi 2011). However, this becomes much higher if female to female relatives (such as mother-daughter) are investigated (Lazaridis, Juran et al. 2007).

In the past decade, Genome Wide Association Studies (GWAS) have led to some progress in mapping the genetic susceptibility to the disease. Susceptibility loci have been identified are mainly within the Human Leukocyte Antigen complex (HLA). This is encoded on the major histocompatibility complex and is responsible for regulation of the human immune response. Both Canadian (Hirschfield, Liu et al. 2009) and Italian (Liu, Invernizzi et al. 2010) GWAS have confirmed susceptibility loci for PBC falling within the HLA, and two main genes outside of the HLA IL12A and IL12RB2 both of which encode interleukin 12.

1.4.5.2. Environmental Factors

There have been several environmental factors reported as influencing the pathogenesis of PBC. The prevalence of PBC is markedly different in different countries and regions. Within the UK incidence of PBC is highest in the North East (Prince, Chetwynd et al. 2001) and South Wales (Metcalf and James 1997). There could be a number of reasons for this; firstly, PBC is more prevalent in areas of socioeconomic deprivation. The North East is a typically deprived region, which can cause large scale differences in demographic and produces many confounding variables, making it tricky to discern specific risk factors for PBC development. Historically, it is a coal mining region, as is South Wales, likely leading to the large-scale environmental release of chemical compounds. Areas of Coal mining activity have been found to be associated with PBC diagnosis hotspots in the North East of England (Dyson, Blain et al. 2019). However other risk factors such as smoking (Gershwin, Selmi et al. 2005), have long been reported higher in lower socioeconomic groups (Hiscock, Bauld et al. 2012).

Xenobiotics have been at the forefront of environmental candidates for the triggering of PBC, largely because of their associations with several other autoimmune diseases such as systemic sclerosis. There are several candidates for xenobiotic compounds in PBC from compounds present in cigarettes as mentioned above, to compounds found in pesticides, food additives, and hair dyes (Amano, Leung et al. 2005). There is also evidence to suggest that the auto-immune reaction may be due to the activation of the immune system following pathogenic response. Several pathogens have been investigated from Escherichia coli (Burroughs, Rosenstein et al. 1984) (a bacteria commonly implicated in UTIs). A summary of genetic and environmental risk factors can be found below (Figure 4).

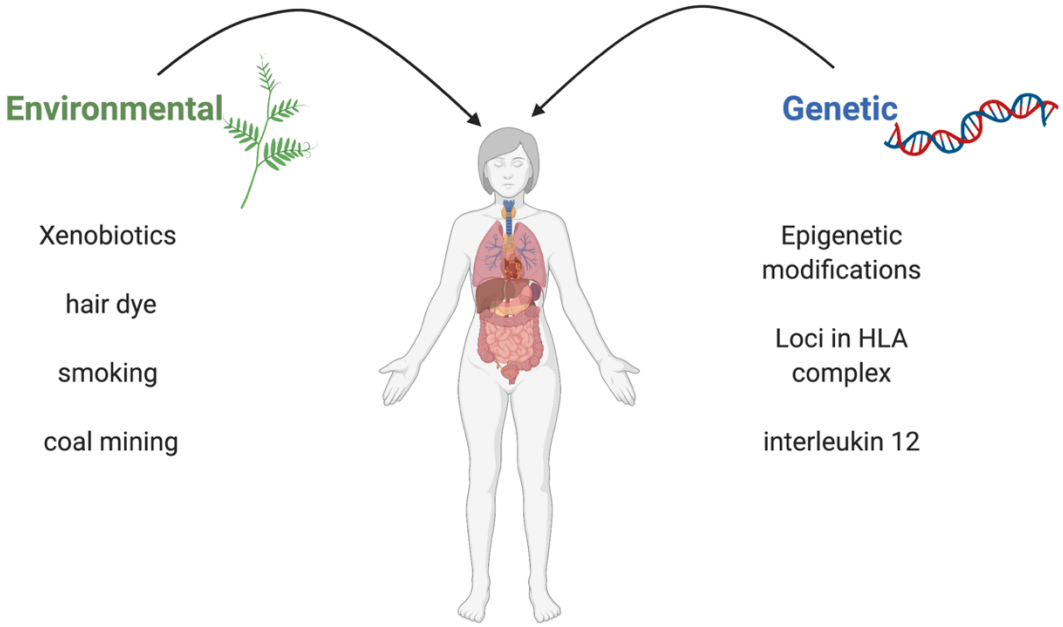

Figure 4.Environmental and genetic risk factors in the development of PBC.

1.4.5.3. Diagnosis and Symptoms

At the time of diagnosis, a large portion of patients are asymptomatic (20-61%) (Prince, Chetwynd et al. 2004). Patients with PBC can remain symptomless for up to 10 years, however once symptoms appear time until transplant is around 10 years (Washington 2007). Better testing procedures and AMA testing have improved the likelihood of early diagnosis.

The introduction of large-scale qualitative methodology such as the PBC-40 questionnaire has highlighted the associations of certain symptom presentation and low quality of life scores. The most common symptoms at presentation are pruritus and fatigue. However, these are often the most debilitating, causing patients to stay in their homes and affecting daily function

1.4.5.4. Pruritis

Pruritus causes uncomfortable itching in patients. It can range from mild and tolerable to immobilising, leading to sleep disturbance, depression and reduced quality of life. The itch generally occurs in a diurnal pattern, with an intense late evening itching period. Possible causes of the itching sensation include accumulation of bile acids in the tissues and/or stimulation of brain centres involved in sensation, which may have evolved as a protective reflex against noxious stimulation in the body. Despite how common and how severe this itching can be, the exact pathophysiology of pruritis remains unclear.

Evidence shows that when bile acids are injected subcutaneously, a pruritis itch occurs, supporting the hypothesis of tissue bile acid accumulation (Varadi 1974). Additionally, bile acid monologue drug treatments such as ursodeoxycholic acid (UDCA) do little to cessate these pruritic symptoms (Ricci, Hofmann et al. 1998).

There is evidence to suggest that itch has an interlinked neurological pathology. Opioid antagonists and serotonin reuptake inhibitors such as nalextrone and sertraline both have mild anti pruritic activity. However, the most potent anti-pruritic effect and therefore the most common prescribed treatment is rifampicin the Pregnane X receptor (PXR) agonist (EASL 2009), suggesting that much of the itch originates in the liver and that bile acids have a large contribution to the overall symptomatology.

1.4.5.5. Fatigue

Fatigue is one of the most common and debilitating symptoms of PBC. A complex symptom set, it is reported to occur in anywhere between 40-80% pf patients (Witt-Sullivan, Heathcote et al. 1990, Goldblatt, Taylor et al. 2002, Poupon, Chrétien et al. 2004). Of those experiencing fatigue 68% have spells lasting over 6 months(Cauch-Dudek, Abbey et al. 1998), and 20% experience debilitating fatigue leaving them unable to work (Dyson, Wilkinson et al. 2016). As well as working fatigue can also severely impact other factors such as mental health, family and social life. Studies using the UK-PBC cohort have shown that fatigue is the symptom which causes the greatest impact

on perceived quality of life for patients (Mells, Pells et al. 2013), making it an important target for therapy.

However, no therapy as currently used impacts fatigue, including first- and second-line therapies UDCA (Heathcote, Cauch-Dudek et al. 1994) and OCA (Nevens, Andreone et al. 2016). Even liver transplantation in end stage disease does nothing to improve fatigue (Carbone, Bufton et al. 2013).

The pathophysiology of fatigue, as with many of the other symptoms remains poorly understood. Fatigue can be broadly characterised in two components; peripheral and central fatigue. Peripheral fatigue is often described as loss of energy and is related to muscle weakness. It has been shown that fatigued PBC patients are quicker to tire upon repeated hand grip testing. Interestingly, fatigue is correlative with rate of grip strength decline on repeat testing (Goldblatt, James et al. 2001).

Muscle acidosis may be a contributing factor, and has been found to be caused by mitochondrial dysregulation in the muscle of patients. Studies have shown fatigued patients have a higher ratio of phosphocreatine responses (PCr) to ATP in both working arm muscle (Hollingsworth, Newton et al. 2008) and cardiac muscle (Jones, Hollingsworth et al. 2010). Using cardio pulmonary exercise testing (CPET), PBC patients were found to have significantly lower anaerobic threshold than controls. Changes in aerobic anaerobic metabolism in fatigued patients contribute to muscle acidosis. Intramuscular acidosis leads to increased muscle fatigue during sustained activity, resulting in reduced contractile force and longer recovery times (Allen, Lannergren et al. 1995).

The central component is often self-described by patients as ‘brain fog’ and has several neurophysiological changes resulting in depression sleep disturbance and cognitive abnormalities. It is likely that central fatigue is intricately interlinked with cognitive symptoms in PBC. Fatigued patients have been found to have delayed sleep timing

leading to disturbed sleep and excessive daytime somnolence (Montagnese, Nsemi et al. 2013).

1.4.5.6. Cognitive Symptoms

Cognitive impairments are most often reported as problems relating to concentration and memory. These occur in many patients, with 80% reporting mild cognitive impairment and 50% showing moderate to severe issues with concentration and memory (Newton, Hollingsworth et al. 2008). They have a large negative impact on patient quality of life, leaving patients unable to function normally (Hale, Newton et al. 2012). Despite this, cognitive deficits are often under diagnosed, and written off as fatigue based. One of the main issues face by patients with cognitive symptoms is that they do not correlate with disease progression (Newton, Bhala et al. 2006), or to histological markers of liver disease severity (Newton, Hollingsworth et al. 2008) and is not reversed by transplantation.

1.4.5.6.1. Inclusion of Cognitive Symptoms Within the PBC-40

Because of this ambiguity, most quality of life (QOL) research in PBC until 2005 had been focussed on fatigue despite the fact that there is evidence of a separate mechanisms of cognitive deficit with abnormalities seen in attentional, concentration and psychomotor testing (Tarter, Hegedus et al. 1987, Floreani, Marchiori et al. 1995). The invention and subsequent inclusion in clinical assessment of scoring systems such as the PBC-40 (Jacoby, Rannard et al. 2005) have allowed the definitive separation of fatigue and cognitive deficit as symptoms by providing specific cognition based questions in the assessment.

Cognitive symptoms have been separately categorised and is addressed by six questions in the PBC-40 questionnaire 'In the last 4 weeks:

- I had to make a lot of effort to remember things
- I had difficulty remembering things from one day to the next
- My concentration span was short because of PBC
- I had difficulty keeping up with conversations
- I found it difficult to concentrate on anything
- I found it difficult to remember what I wanted to do' (Jacoby, Rannard et al. 2005)

1.4.5.6.2. Human Brain Imaging Studies in PBC

This kind of recognition has led to more in depth analysis of the effects of PBC both physiologically on the brain itself and on the day-to-day functional capacity of patients. White matter lesions (WML) have been identified in patients, from early stages of the disease, suggesting there is damage foci in the brain of patients, perhaps in areas of high neuroinflammatory susceptibility (Newton, Hollingsworth et al. 2008). The density of lesions was found to be correlated with severity of cognitive deficit in these studies, and deficits were also associated with autonomic dysfunction (measured in systolic blood pressure) where lower blood pressure was associated with cognitive dysfunction. Lesion density was found to be greater in the frontal lobe, an area important in higher level executive function.

In addition to physical changes to the brain, functional magnetic resonance studies of deep grey matter structures in the brains of PBC patients (Mosher, Swain et al. 2017) have revealed changes in the functional connectivity of patients. Using 20 patients and 21 matched controls Mosher et al studied resting state functional connectivity in several deep brain structures (the hippocampus, amygdala, thalamus and putamen) via resting-state functional magnetic resonance imaging (rsfMRI). The signals created by rsfMRI are synchronous in functional brain networks, either within or between brain regions.

The study shows PBC patients exhibit several rsFC changes in key brain regions. They report an increased rsFC within the putamen, amygdala, hippocampus and thalamus. As suggested by the authors, this could be as a result of chronic immune cell infiltration resulting in connectivity changes within the brain (D'Mello, Le et al. 2009). Changes such as these in key functional areas modulating memory and adaptive function (hippocampus, amygdala) could feasibly be responsible for the changes in cognition experienced by patients.

Mosher et al also found altered rsFC in the connections between the putamen and the motor cortex. In light of previous studies linking changes in motor cortex excitability with fatigue symptoms, it is likely that the shift in rsFC is related to fatigue symptoms. However, similar shift in rsFC between the putamen and regions important in attentional control (IFG) and working memory (superior frontal gyrus, inferior parietal gyrus) are more likely to be functionally related to cognitive deficits, highlighting the functional separation of the two symptoms. The researchers were also able to correlate these rsFC changes in the deep brain to performance in working memory tasks, fatigue and itch.

Subsequent follow up studies have investigated more closely the hippocampal structure and found reduced hippocampal volume in PBC patients (Mosher, Swain et al. 2018). As concluded by the study, this is likely correlative with neuroinflammation and resultant oxidative stress within and surrounding the hippocampus, due to iron deposition. In depth analysis of key hippocampal sub-structures revealed significant changes to the subiculum, CA4 and dentate gyrus. As the patients in this particular study are only on average 6 years after diagnosis, brain structural changes begin early in the disease process.

Sophisticated functional imaging techniques such as Diffusion Tensor Imaging Magnetic Resonance Imaging (DTI-MRI) have unveiled changes to fractional anisotropy in patients

to significant levels in the thalamus (Grover, Southern et al. 2016). The thalamus is an important relay centre in the brain, and therefore may be implicated in the executive function and attentional deficit reported by patients. In conjunction the study reported change in T1 weighted MRI showing abnormalities in all brain regions studied including the thalamus, caudate putamen, and global pallidus.

Other groups who have used DTI have also found few differences. A German study from 2018 reported no significant changes to DTI in any brain regions in PBC patients (Zenouzi, von der Gablentz et al. 2018). However, this study also found few changes in cognition score, and only selected functional deficit based not in working memory or executive function domains, but in verbal fluency measurements.

1.4.5.7. Overlap between Fatigue and Cognitive Symptoms

Studies such as these and more highlight the complex interlinking mechanisms of fatigue and cognitive dysfunctions in PBC. Peripheral fatigue can often occur separately, whereas the symptoms of central fatigue are more complex, as they are closely associated with cognitive dysfunction, and likely have overlapping pathologies. This is highlighted by studies such as Mosher et al 2017 showing connectivity changes in key functional areas such as the hippocampus can be correlated with both working memory tasks and fatigue.

Differences in sampling and patient selection can cause a high variability in cognitive studies. Due to the huge variety in symptoms experienced by patients and the overlap between fatigue and cognitive domains, it becomes difficult to tease apart functional differences associated with different brain regions and contributing to different symptoms. The aforementioned German study targeted a highly fatigued patient set, with little cognitive symptoms, whereas the study by Grover et al stratified patients based on cognitive domains in the PBC-40 questionnaire. Another complicating issue is the interplay between pre cirrhotic cognitive changes in PBC, and the development of

post cirrhotic hepatic encephalopathy. Though pre cirrhotic symptoms and their pathology is less studied, publications such as these corroborate evidence of cognitive symptoms outside of classic late stage hepatic encephalopathy. This highlights the need for further study of the mechanistic basis of cognitive dysfunction in cholestatic liver diseases such as PBC.

1.5. Hepatic Encephalopathy (HE)

Hepatic encephalopathy (HE) is a severe and debilitating brain condition rising from end-stage cirrhotic liver disease, occurring in around 40% of cirrhotic patients (Poordad 2007). He begins at minimal stage (stage 1) with mild confusion and changes to verbal fluency and impaired sleep-wake cycle and progresses through to severe HE (stage3-4), resulting in confusion, and ultimately the patient becomes comatose (Amodio, Montagnese et al. 2004). HE is a well-established prognostic indicator for PBC, and one patients rarely recover from – stage 4 HE is associated with high mortality rates (Wong, Gish et al. 2014, Bajaj, O'Leary et al. 2017).

1.5.1. Pathogenesis of HE

1.5.2. Hyper-ammonia

The hepatology community has outlined hyper ammonia as the classical cause of HE. Ordinarily the healthy liver is responsible for much of the processing of ammonia during the urea cycle. The liver transforms ammonia into urea which is split between the kidney and intestines for disposal through urine, and further transformation and faecal expulsion respectively. The intestine also creates most of the ammonia found in the bodily circulation through the deamination of amino acids, releasing it back into the portal circulation for transport to the liver. The liver uptakes around 85% of produced ammonia (fig 4). In cirrhotic conditions, the stressed hepatocytes in the liver are unable to process ammonia. This causes a build-up of ammonia that is unable to be transformed

and excreted. This causes an overload of ammonia in portal circulation. However due to overloading of the liver, portal hypertension occurs, leading to a much larger concentration of ammonia in the systemic circulation (figure 5).

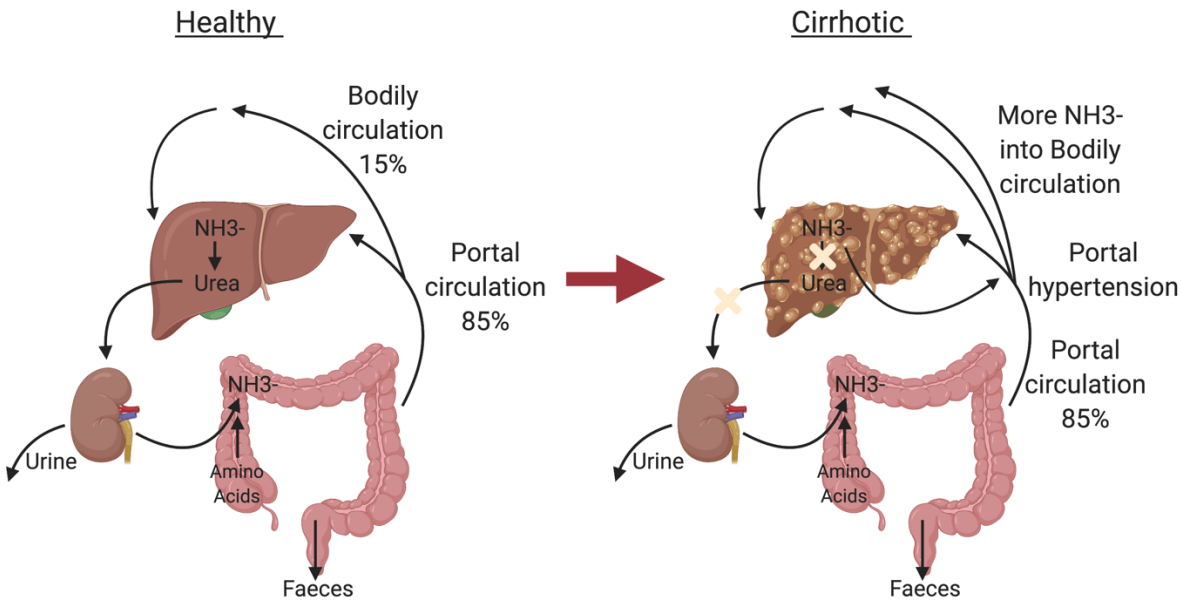

Figure 5. Ammonia circulation in healthy and cirrhotic liver.

A high concentration of circulating ammonia can lead to permeability at the blood brain barrier through induced changes at tight junctions (Ott and Larsen 2004). Usually cerebral ammonia is detoxified via glutamine synthetase expressed by astrocytes, and converted into glutamine. Accumulation of glutamine within astrocytes leads to swelling which is causative of oedema (Wright, Davies et al. 2007).

1.6. Treatments for PBC

Treatments are thoroughly reviewed as introduction in Chapter 4 (page 96).

1.7. The Blood-Brain Barrier in Health and Disease

The blood brain barrier forms a protective environment between the brain and the rest of the body. It allows the free movement of water and permeable molecules and also allows some molecules by active transport. Lipid solubility plays a large role in the passage of molecules through the blood brain barrier and is affected by many factors such as charge and tertiary structure (Banks 2009).

The BBB is organised into neurovascular units (NVU), as first described by Harder et al in 2002 (Harder, Zhang et al. 2002). NVUs consist of the brain capillary endothelium, pericytes (Lai and Kuo 2005) along with associated astrocytic end-feet and neurons (Cohen, Ehret et al. 1995) as seen in figure 6. Each component is intricately linked with the other, establishing one whole functional unit. NVUs provide a highly efficient system, regulated by gap junctions and ion channels to enable the transport of ions and neuro-modulatory molecules between the blood and the brain (Gordon, Choi et al. 2008).

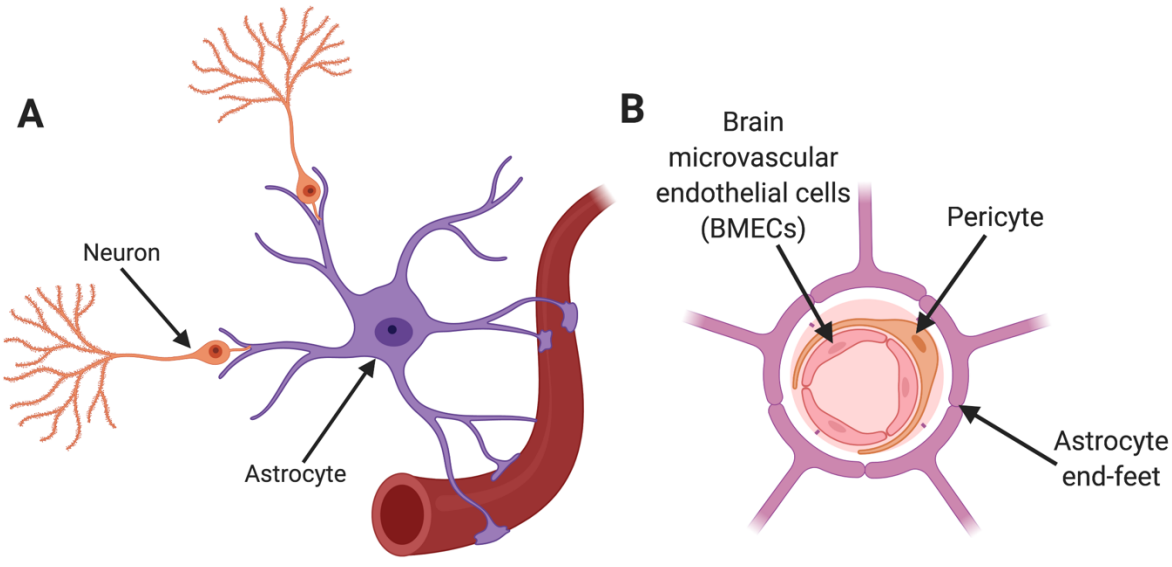

Figure 6. A) Anatomical layout of the Blood-brain barrier, with astrocytes forming attachment both to the vessel and neurons. B) Cross sectional diagram of a blood vessel indicating astrocyte end-feet, pericyte and microvascular endothelial cells.

1.7.1. Astrocytes

The role of the astrocyte at the blood brain barrier was first questioned in Camilo Golgi's famous work (reprint can be found here (Golgi, Bentivoglio et al. 2001) originally published in 1886), where he noted the close proximity of astrocyte end-feet with the cerebrovasculature. After this it was not re-examined until much later by Davson and Oldendorf (Davson and Oldendorf 1967). It is now known that astrocytes play an important role in maintaining separation of the central nervous system and the rest of the bodily circulation, including regulation of ionic flow, nutrients and macromolecules into the CNS.

Initial descriptions of astrocytes vastly underestimated their role, pinning them as neuronal and structural support cells both within the NVU and wider brain functions. This was questioned by Cornell-Bell, who went on to show the astrocytes express glutamate sensitive ion channels, and are able to propagate calcium waves within their own cytoplasm but also to each other, promoting long-range communication (Cornell-Bell, Finkbeiner et al. 1990).

Astrocytes are incredibly versatile and are able to communicate with both blood vessels and neurons simultaneously. They are involved in bidirectional communication at the synapse, expressing G-protein coupled receptors that can sense neurotransmitters and stimulate the appropriate gliotransmitter response (reviewed here (Santello, Calì et al. 2012). By release of these gliotransmitters, astrocytes are able to modulate synaptic communication.

Gliotransmission means astrocytes are able to communicate efficiently not just with neurons but with cells such as pericytes and endothelial cells at the barrier. This allows modification of processes such as vasodilation in accordance with neuronal activity in order to maintain intricate balance of energy consumption by neurons and the delivery of energy producing molecules such as ATP in the blood.

1.7.2. Pericytes

Pericytes sit closely associated with endothelial cells and provide them with structural support. Pericytes are essential to NVU function as they sit between the brain parenchyma and the blood vessels facilitating communication between the two. More recently interest in pericytes has grown, and in the last ten years key discoveries have been made about their function, such as their ability to regulate the BBB through signalling factors, influencing both the tight junctions of endothelial cells and the attachment of astrocyte end-feet (Armulik, Genové et al. 2010). It has since been reported that reduced pericyte number can cause increased BBB permeability through tight junction loss (Sengillo, Winkler et al. 2013), and pericytes control the flow of molecules between the blood stream and the brain, solidifying them as key modulators of BBB function.

Additionally, pericytes also have roles in the neuroinflammatory response – they can express inflammatory cytokines and present their antigens to immune cells, recruit them to allow their passage into the brain (Rustenhoven, Jansson et al. 2017). In response to inflammatory cytokines such as IL-1B or TNF- α inflammatory signals are released along with matrix metalloproteinase 9 (MMP-9) which can directly lead to BBB breakdown (Herland, van der Meer et al. 2016).

1.7.3. Evidence of BBB dysfunction in cholestatic liver disease

Over the past 10 years, support has been building for the hypothesis that the circulation of toxic bile acid and related molecules could facilitate BBB breakdown and allow neurological changes. Proof of bile acid related BBB breakdown is scarce and much is

limited to in vitro modelling of human cells. These studies largely focus on the tight junction aspects of BBB integrity.

In these experiments treatment with unconjugated bilirubin (UCB) led to a bi-phasic response, of which the second phase caused the reduction in zonula occludens (ZO)-1 and β-catenin levels, thus leading to reduction of tight junctions and cell-to-cell contacts (Palmela, Sasaki et al. 2012). Similar effects were also seen by the group using LPS, or a combination of both LPS and UCB (Cardoso, Kittel et al. 2012). These changes could potentially increase para-cellular permeability and allow bile acid entry into the brain in pathogenic conditions.

Bile acids themselves seem to exert pleiotropic effects at the barrier. In vitro follow up to the above studies shows pre-treatment with hydrophilic bile acids UDCA or glycoursodeoxycholic acid (GUDCA) confer protection against UCB induced barrier permeability (Palmela, Correia et al. 2015). Later studies indicate that both hydrophobic bile acids such as chenodeoxycholic acid (CDCA) and hydrophilic bile acids such as deoxycholic acid (DCA), but not UDCA can permeabilize the BBB. This study not only provides early evidence that cholestasis can be detrimental to BBB function, but that individual bile acids such as CDCA and DCA can mediate this effect and are able to permeabilize the BBB both *in vitro* and *in vivo* (Quinn, McMillin et al. 2014). Seemingly, the effects of bile acids at the barrier are more complex than being able to state a positive or negative effect, rather they are likely to have complex interactions, based on characteristics such as hydrophobicity, charge and conjugation.

1.8. Neuroinflammation

Neuroinflammation is an inflammatory response within the brain, mediated by cytokines chemokines or other neuro-reactive molecules produced largely by either infiltrating immune cells or resident neuroglia (microglia and astrocytes).

1.8.1. Microglia

The microglia are the resident macrophage type cell of the brain. They are responsible many of the innate immune functions within the brain, including immune regulation by cytokine production and in immunosurveillance and phagocytic engulfment. Generally, they comprise around 10% of the cell population (Lawson, Perry et al. 1992)and mirror many of the characteristics of their cousins the macrophage, namely myeloid lineage (Ginhoux, Greter et al. 2010) and their slow turnover (Lawson, Perry et al. 1992).

Even when in their resting state, microglia are constantly surveilling the surrounding area for any miniscule changes in homeostasis. They respond to disruptions in ions such as potassium and ATP molecules released from damaged cells (Davalos, Grutzendler et al. 2005), as well as directly to immune threats (virus, bacteria, or foreign stimuli). They become activated and change their shape, with a swollen soma and retracted processes. This change is associated with increased expression of calcium binding protein Iba1 (Ito, Imai et al. 1998), which is often used for immunohistological measurement.

Reactive microglia can be broadly classified into distinctive states of reactivity; an inflammatory and neurotoxic state known as M1 and a resolutory and neuroprotective state known as M2 (Boche, Perry et al. 2013). However, even cells within these phenotypes can display diverse characteristics and undergo phenotype switching. M1 microglia can be activated via both interferon gamma (IFN- γ) and lipopolysaccharide (LPS) signalling, and release pro inflammatory cytokines such as tumour necrosis factor-α (TNF-α), IL-6 etc (full list in Figure 7). M2 phenotype microglia can be induced by interleukins 4 and 10 (IL4, IL10) and release anti-inflammatory molecules IL-10 and transforming growth factor beta (TGF-β) (Colton, Mott et al. 2006, Boche, Perry et al. 2013). These two phenotype of microglia can be stratified by the presence of a series of cell surface markers, most commonly Arginase1 for M2 microglia, and iNOS for M1 microglia.

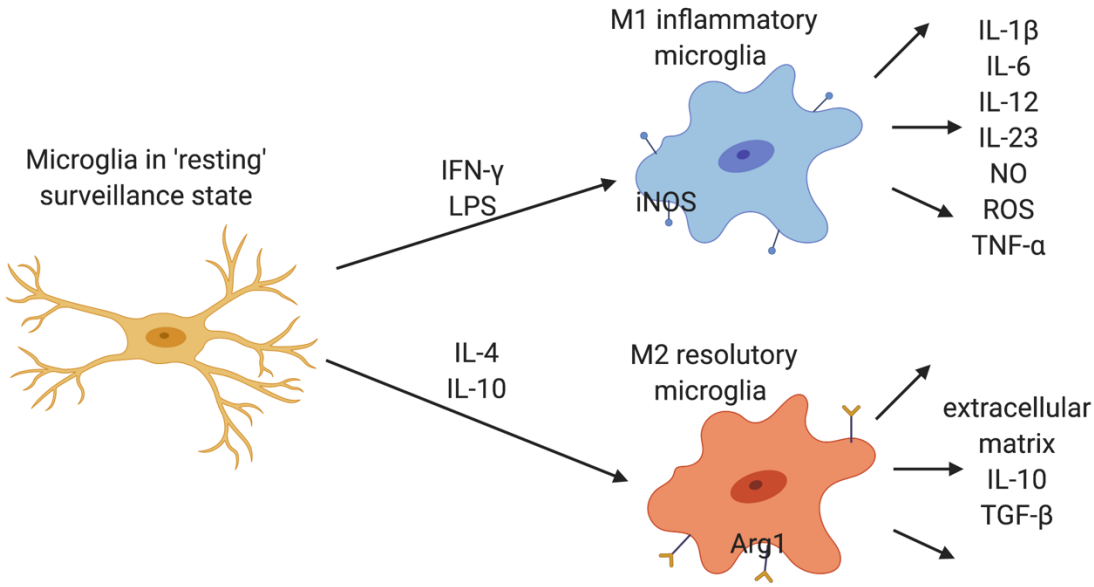

Figure 7. Differential activation states of microglia and their associated cytokine outputs.

Besides inflammation, microglia also have emerging roles in memory and learning through a process called synaptic pruning. During development, weaker synapses are regularly phagocytosed by microglia as the brain matures (Paolicelli, Bolasco et al. 2011). More recently, this process has also been implicated in synapse loss in neurodegenerative disorders such as Alzheimer's disease (Hong, Beja-Glasser et al. 2016).

1.8.2. Astrocytes

As well as their active role at the blood-brain barrier, astrocytes also have diverse functions in neuroinflammation and modulation of neuronal signalling. They make up around 35% of all cells in the central nervous system, and are key regulators of pathogenic immune response and response to neuronal injury.

Astrocytes are able to detect and respond to a number of inflammatory stimuli. As a part of their response to CNS injury they become activated, and form a scar known as gliosis or astrogliosis. This is protective, and ensures any inflammatory stimuli or neurotoxic compounds remain trapped at the injury site. Before the point of scar

formation, many morphological and phenotypic changes occur, including activation, a process which leads to increased expression of astrocyte distinctive markers such as glial fibrillary acid protein (GFAP) and vimentin. Increases in GFAP have been robustly linked to support of neuronal activity in a number of pathological states including epilepsy (Steward, Torre et al. 1992).

Similarly to microglia, differential activation phenotypes have been discovered in astrocytes. These have been as A1 neurotoxic astrocytes and A2 resolutory astrocytes, in keeping with the common nomenclature generated for microglia. A1 astrocytes can be induced by classically activated microglia (M1) through the secretion of inflammatory factors (IL-1α, TNF α) and complement factors such as C1q. Once in the A1 activation state, astrocytes lose the ability to support healthy neuronal activities such as synaptogenesis and instead induce the neuronal cell death (Liddelow, Guttenplan et al. 2017). As with M1 microglia, the number of A1 astrocytes is increased in age, particularly in hippocampal and striatal regions with these regions seeing both a larger number of A1 associated genes, and a higher fold of upregulation (Clarke, Liddelow et al. 2018). The particular neurotoxin inducing neuronal death is yet to be identified (as in Figure 8).

A2 phenotype astrocytes are protective, and are induced in models such as middle cerebral artery occlusion (MCAO), where astrocytes play a key role in the regeneration of tissue following ischaemia. This was initially proposed by Sofroniew (Sofroniew 2009) who observed in conditions of ischaemia, astrocytes play a key role in BBB repair, reducing immune cell infiltration and limiting neuron damage. Astrocytes were extensively profiled from the MCAO model by Ben Barres and colleagues. They found release of key neurotrophic factors from astrocytes in the MCAO model, including leukaemia inhibitory factor (LIF), Cardiotrophin-like cytokine factor 1 (CLCF1) and thrombospondins (Zamanian, Xu et al. 2012), which are capable of helping to repair lost synapses (Eroglu, Allen et al. 2009).

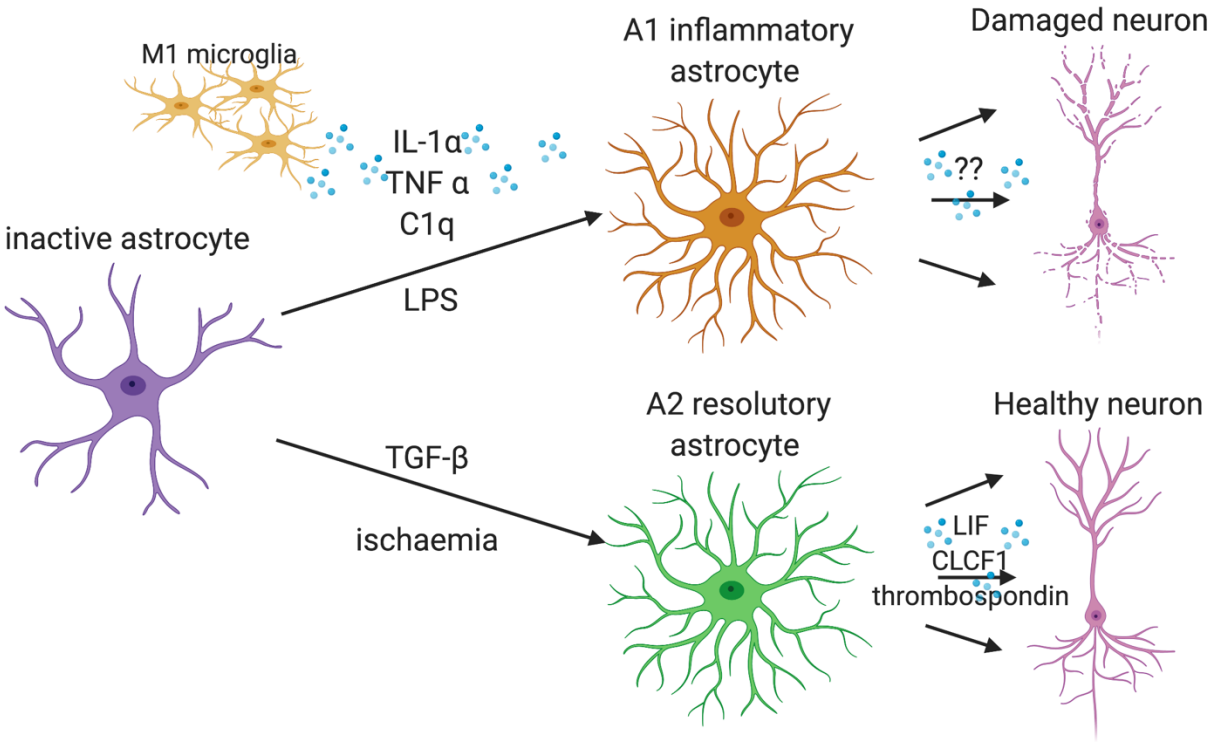

Figure 8. Stimulation of differential activation states of astrocytes and their associated cytokine outputs.

1.9. Cellular Senescence

Cellular senescence is a complex process leading to a loss of replicative capacity in somatic cells. It was first described in 1961 by Hayflick and Moorhead (Hayflick and Moorhead 1961). When exposed to stress (endogenous or exogenous), a cell may activate a cascade which produces a senescence phenotype, meaning a cell can no longer divide and loses its function. This state is phenotypically distinct from other states such as quiescence, or terminal differentiation (Munoz-Espin and Serrano 2014, R. Pacheco-Rivera 2017).

Senescent cells become unresponsive to stimulation and demonstrate a distinctive metabolic and epigenetic phenotype. Senescence is implicated in a variety of standard age related and pathological processes including in liver cancers and cholestatic disease such as PBC (Sasaki, Ikeda et al. 2005). There are several differing biological processes associated with cellular senescence, the replicative senescence described by Hayflick being just one of them(Munoz-Espin and Serrano 2014). This means that there is no definitive marker of senescence, as this can differ between organ and pathology.

1.9.1. Telomere Dysfunction and Replicative Senescence

Most mitotic cells have a limited replicative capacity before they enter a state of senescence. This is also known to occur in vitro, indeed this is how it was first observed by Hayflick and Moorhead, leading to the coining of the term 'Hayflick's limit', which states that a normal human fetal cell population will divide successfully between 40 – 60 times before entering a senescent state (Hayflick and Moorhead 1961).

Telomeres are found at the end of the chromosomes and cap the encoding regions of the genome (Campisi and d'Adda di Fagagna 2007, R. Pacheco-Rivera 2017). This forms a barrier which protects the integrity and genomic stability of chromosomes. Telomeres are formed of the protein complex named Shelterin (de Lange 2005, R. Pacheco-Rivera 2017). Telomerase activity adds telomere repeat sequences onto the end of telomeres,

therefore ensuring that they maintain their length (Munoz-Lorente, Cano-Martin et al. 2019). Without the action of telomerase, telomeres shorten with each cell division until a point at which DNA damage response (DDR) becomes triggered, ultimately leading to senescence. Telomere shortening has been found to be directly correlative with the induction of cellular senescence (Harley, Futcher et al. 1990). This has been demonstrated in mice, where longer telomeres are associated with increased lifespan and healthier ageing (Munoz-Lorente, Cano-Martin et al. 2019).

Somatic cells do not express telomerases, therefore limiting their replication and causing naturally occurring age related replicative senescence (R. Pacheco-Rivera 2017). Telomeres are shortened by around 50-200 base pairs per replication (Harley, Futcher et al. 1990, Herbig, Jobling et al. 2004, Campisi and d'Adda di Fagagna 2007). This loss inevitably destabilises the Shelterin complex, dislodging it and resulting in the exposed telomeric ends being recognised as a DNA break and activating the DDR (de Lange 2005, Victorelli and Passos 2017). These induced senescent cell accumulate throughout lifespan and can contribute to age related disease onset. Additionally, there are several genetic disorders resulting from telomerase mutations, including within the liver (Calado, Regal et al. 2009).

1.9.2. DNA damage and Oncogene Induced Senescence

The DDR can also occur as a result of other insults which lead to premature cellular senescence in response to noxious stimuli. Breaks in DNA, either single or double strand break drive chromosome instability, resulting in the phosphorylation of gamma H2AX histone via activation and binding of ATM and ATR protein kinases (d'Adda di Fagagna, Reaper et al. 2003, Herbig, Jobling et al. 2004).

ATM also works to phosphorylate essential checkpoint kinases checkpoint-1 (CHK1) and checkpoint-2 (CHK2), which trigger a cascade leading to cell-cycle arrest (d'Adda di Fagagna, Reaper et al. 2003, Hernandez-Segura, Nehme et al. 2018). This and other

pathways drive cellular senescence. Key drivers of cell cycle arrest include cyclin dependent kinase (CDK) inhibitors p16, p15 and p21 (Hernandez-Segura, Nehme et al. 2018). Ordinarily, CDK's phosphorylate proteins at different stages of the cell cycle, tightly regulating arrest and growth. The key parallel pathways involved in the induction of cell cycle arrest are p53-p21 and p16-Rb (d'Adda di Fagagna, Reaper et al. 2003).

P53 as a key tumour suppressor and 'guardian of the genome', conserving genomic stability. When DDR is activated multi-site phosphorylation of P53 and MDM2 degradation suppress P53 (Zhang, Xiong et al. 1998), leading to activation of P21. As a CDK inhibitor P21 functions to promote cell cycle arrest at G1/S phase. Pro-senescent P21 can also be activated in a P53 independent manner, through TGF-β signalling (Datto, Li et al. 1995). The p53/P21 pathway is paramount to the senescence response. Inhibition of P21 is able to prevent the occurrence of senescence entirely (Brown, Wei et al. 1997, Dirac and Bernards 2003). Several interlinking processes, such as telomere shortening, cellular or oxidative stress, all lead to the process of P53 activation through the DDR, ultimately evoking senescence.

Another key CDK inhibitor P16, also plays a key role in senescence induction. Ordinarily P16 regulates the cell cycle through inhibiting Rb phosphorylation (Herbig, Jobling et al. 2004) and accelerating the cycle through to S phase. Several different methods of senescence induction such as telomere shortening have been shown to effect P16, either epigenetically or via interference with Rb protein (Smogorzewska and de Lange 2002). There is also evidence implicating the 16/Rb pathway in oxidative stress-induced senescence through MAPK which is induced by reactive oxygen species (ROS).

1.9.3. Reactive Oxygen Species (ROS)

Reactive oxygen species (ROS) are a product of cellular oxygen metabolism, occurring naturally in the body. Certain types of ROS such as superoxides are highly reactive molecules that can exert varying biological effects. Ordinarily ROS species are highly regulated in the body and sequestered by naturally occurring antioxidants (R. Pacheco-Rivera 2017). Therefore, cells with higher anti-oxidant capacity also tend to show a higher threshold for replicative senescence and slower telomere shortening (Kornienko, Smirnova et al. 2019). Telomeres are highly susceptible to oxidative damage, likely due to displacement of shelterin complexes by ROS, leaving telomeres vulnerable (von Zglinicki, Saretzki et al. 1995, Coluzzi, Leone et al. 2019).

1.9.4. Senescence Associated Secretory Phenotype (SASP)

A major hallmark of senescence is the senescence associated secretory phenotype, or SASP. The name SASP refers to the collection of chemo and cytokines secreted from senescent cells (Maciel-Baron, Morales-Rosales et al. 2016). The secretion of SASP from a senescent cell can also influence the behaviour of surrounding cells, inducing senescence through paracrine signalling. SASP is difficult to define as a specific secretory signature, given that it can vary greatly between organ and the cell type in question, as well as the induction stimuli (Maciel-Baron, Morales-Rosales et al. 2016). Despite this, some core components remain conserved, such as IL-6, IL-8 and TGF- β, which can be observed in a fairly consistent manner across cell types. It seems likely therefore that the SASP allows communication between distressed and senescent cells and co-ordinates the immune response (Krizhanovsky, Yon et al. 2008, Ogrodnik, Miwa et al. 2017, R. Pacheco-Rivera 2017).

1.9.5. Senescence in Liver Disease

Senescence is a pathological hallmark of cholestatic liver disease. In 2005, the Japanese Yakanuma group discovered a common senescence phenotype was found to occur in

the liver during DR, with surrounding biliary epithelial cells (BECs) becoming senescent In PBC patients (Sasaki, Ikeda et al. 2005). In the context of cholestasis BECs also incur DNA damage and telomere shortening (Sasaki, Ikeda et al. 2008), both known causes of cellular senescence (Collado, Blasco et al. 2007). This led to several key discoveries including the realisation that senescence occurs in many liver diseases rising from persistent injury and DR (Sasaki, Ikeda et al. 2010), and in many cases can drive the pathology of these conditions(Ogrodnik, Miwa et al. 2017).

Hepatocytes also frequently become senescent following liver injury, and can contribute to the DR phenotype and resulting fibrosis (Lu, Bird et al. 2015). This process can lead to sustained inflammation and exacerbation of disease phenotype.

In turn the induction of senescence in hepatic cell types leads to the release of inflammatory cytokines, known as the senescence associated secretory phenotype or SASP. SASP can have a large effect on the microenvironment, triggering the induction of senescence in nearby cells (Nelson, Wordsworth et al. 2012). This effect is induced through both paracrine and autocrine signalling. Within the liver, key SASP chemokines include several TGFβ family ligands such as VEGF, CCL2 and CCL20, as well as IL-6 and IL-8 which are sustained across cell types (Acosta, Banito et al. 2013). CCL2 is known to have a key role in macrophage recruitment through receptor CCR2 (Gregory, Morand et al. 2006), and also acts to sustain senescence through its CXCR2 receptor (Acosta, O'Loghlen et al. 2008).

1.9.6. Senescence in Neurons

The cellular process of senescence occurs throughout every organ in the body. Within the brain it has been found that senescence like phenotypes do occur in neurons during normal ageing processes (Jurk, Wang et al. 2012), despite them being post mitotic. In ageing mice, several markers of senescence (B-galactosidase, P21) and senescence associated signalling (IL-6, ROS) were found in various neuronal populations. At 32

months these features occurred in 40–80% of Purkinje neurons and 20–40% of cortical and hippocampal neurons.

So far, little is known about the impact of senescence features and low grade 'inflammaging' (often attributed to SASP chemokines IL-6 and IL-8) on neuropathology such as degenerative diseases. Astrocytes are a key brain cell population, and have been long associated with the pathology of several neurodegenerative diseases (Maragakis and Rothstein 2006). In stressed conditions astrocytes have been found to undergo changes in their function such as cell cycle arrest, reduced telomere length, P16, P21 and P53 expression and other key senescence processes both *in vitro* (Bitto, Sell et al. 2010), and *in vivo* in patients with Alzheimer's disease (Bhat, Crowe et al. 2012). Astrocytes have been found to be more susceptible to oxidative stress induced senescence than other cell types such as fibroblasts, suggesting that senescence may be more common in the brain than other organs. As these stressed astrocytes cease to function, they can pass on this phenotypic switch to the neurons they are co-cultured with. This induces glutamatergic distress, signalling changes and cell death (Limbad, Oron et al. 2020).

1.10. Aims of the PhD

The aims of this PhD are as follows:

- Utilize the BDL model to assess the effects of cholestatic disease on several parameters – liver damage, cognition and fatigue, the function and morphology of the blood brain barrier, changes within the hippocampus including neuron cell loss, neuroinflammation, senescence.

- Using the BDL model, assess functional changes in the hippocampus through local field potential electrophysiology to look at changes in network gamma frequency oscillation.

- Utilize the BDL model to assess the effects of 1st line (UDCA), 2nd line (OCA), and experimental (bezafibrate) therapy on liver, cognitive and CNS changes observed in mice following BDL.

- Use in vitro neuronal cell models to investigate changes in neurons exposed to BDL or PBC patient serum and elucidate mechanisms of neuronal dysfunction.

2. Chapter Two - Methods and Materials

2.1. Animals

All mice used in these studies were of C57/Bl6 genotype, male and purchased from Envigo. All procedures were in accordance with the UK Animals (Scientific Procedures) Act 1986 and European Union directive 2010/63EU and in accordance with the arrive guidelines.

2.2. Bile Duct Ligation (BDL) Surgery

BDL surgery was performed when animals were 8-12 weeks and at least 25g in weight. BDL surgery involves the gall bladder being tied and cut, preventing flow of the bile and causing cholestasis. All mice were humanely euthanised at 10 days post-surgery and organs harvested as outlined in figure 8 below. Bile Duct Ligation (BDL) is a common model for progressive cholestatic liver disease in mice, which transitions through three phases. Phase 1. In the early phase, bile leaking into the liver causes biliary and hepatic injury and inflammation, which typically peaks around days 3-5. Phase 2. Cholestatic liver damage persists initiating a progressive ductular reaction and fibrogenic response, days 5 - ~14. Phase 3, which is not studied here, causes advanced fibrosis and then cirrhosis with possible onset of ascites, typically from days 14-21 (Abshagen, König et al. 2015).

When drug treatments were used, these were integrated into the surgery schedule either prophylactically from 3 days prior to surgery or therapeutically from 3 days post-surgery. Mice received buprenorphine post-operative pain relief, were monitored and clinically scored daily and were kept at 25°C in a heated cabinet. Drug treatments were

given at the following concentrations: Obeticholic Acid (OCA) 0.03%, Ursodeoxycholic Acid (UDCA) 0.5%, Bezafibrates (BF) 0.5% w/v.

For all studies with behavioural testing, treatments were integrated into powdered chow diet under the assumption that each mouse would eat 3g of chow per day. For the flow cytometry experiments, mice were oral gavaged with either control or drug dispensed in a volume of 100µl per mouse per day. Behavioural studies followed plan outlined below (Figure 9), where mice underwent Open Field testing on day 9 and Y maze testing on day 10 post-surgery. Surgery was performed by Prof Fiona Oakley.

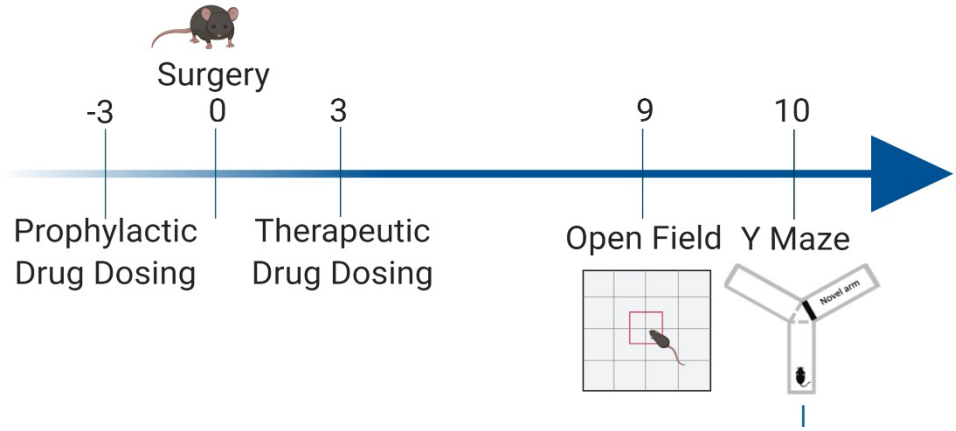

Figure 9. Experimental Drug Dosing schedule BDL mice.

2.3. Behavioural Testing

2.3.1. Open Field

Open field testing was used to assess locomotor activity in mice (Seibenhener and Wooten 2015). Poor locomotor activity in mice can be related to fatigue. Fatigue is in some cases associated with poor cognition in PBC patients and therefore is of interest in this thesis. Open field testing involves allowing the mouse to move freely around on a samsung tablet contained securely in a specially constructed box. A software is used to record the animals free movement for 5 minutes, with a reduction in movement indicative of fatigue in the animal.

Mice were moved into behavioural testing room at least 1 hour prior to testing, and all BDL animals placed onto heated pads. Animals were then individually placed into a testing area measuring 25.66 x 17.53cm onto a Samsung Galaxy Tab 2 10.1 for 5 minutes. Steps and distance travelled were recorded using MouseTrapp© software.

2.3.2. Y Maze

In order to compare the BDL model to the human cognitive deficit, the Y-maze was selected. This is a hippocampal dependent task measuring visual spatial memory (Kraeuter, Guest et al. 2019). This task was selected with discussion between Dave Jones, who described the clinical phenotype seen in patients and mouse behavioural expert Claire Richardson in order to select the most appropriate test to assess spatial and hippocampal dependent memory, which form part of the patient phenotype.

Mice were moved into behavioural testing room at least 1 hour prior to testing, and all BDL animals placed onto heated pads. Y maze arena had three arms of 40cm identified as A1 A2 A3, each with a differentiating marker at the end of the arm. Mice were assigned different start arms in a rotating allocation. In the T1 phase mice were placed into the maze with only two arms open for 5 minutes to explore the arena. The mice were then removed to a clean cage for 1 minute (fresh cage used per cage of mice). Then

in T2 mice were returned to the maze in the starting position with the novel arm opened for 2 minutes, and allowed to explore. A camera was set up above the maze to record movements and the video files analysed via Ethovision software. Animals who showed no movement were excluded from analysis. (UDCA study; BDL n=1, pro-UDCA BDL n=1, Ther-UDCA BDL n=1. OCA study; BDL n=2, pro-OCA-BDL n=2 BDL, Ther-OCA n=1, Beza study Beza n=2).

2.4. Liver Histology

2.4.1. Terminal Tissue Collection

At the point of harvest livers histology is taken from 3 transverse sections. These are taken from the large lobe, the bi-lobulated lobe and the triangular lobe. The spleen is used as a positive control in IHC. For histological analysis, each lobe was sampled and tissues were fixed with 10% formalin for 24 hours. After this time, they were switched to 70% ethanol, embedded in paraffin and sliced to 5µm.

2.4.2. Picrosirius Red

Protocol for Picrosirius red is first described in (Wright, Issa et al. 2001). Tissue dewaxed in 2x 5 minutes in clearene, 5 minutes in 100% ethanol and 5 minutes in 70% ethanol. Slides were then transferred to distilled water for 3x 3 minutes. Tissues were moved to 0.2% phosphomolybdic acid in distilled water (DI) for 5 minutes and then washed for 3x 3 minutes with DI water before being placed into 0.1% Sirius red F3B in picric acid solution for 90 minutes. They were washed again 3x 3 minutes in DI water and changed to a 0.01M hydrochloric acid (HCL) solution for 2 minutes, washed 3x again and dehydrated through ascending alcohol concentrations into clearene for 5 minutes before being mounted in pertex mounting media.

2.4.3. General Liver IHC Procedure on FFPE tissue

This protocol was adapted from (Oakley, Meso et al. 2005). Adaptions to the protocol for individual stains are listed below in table 1, and section 2.4.4). Tissues underwent

dewaxing protocol as described above. Endogenous peroxidases were blocked using 2% hydrogen peroxide solution in methanol for 15 minutes and slides washed in PBS. Antigen retrieval was performed using the method outlined in table 1 diluted in water and heated in the microwave for 20 minutes, removed and allowed to cool. After being washed with PBS slides were mounted into a sequenza and blocked sequentially with avidin and biotin for 20 minutes each. Blocking was performed with 1:5 dilution relevant serum (outlined in table 1 below) in PBS for 20 minutes before primary antibody was applied for an hour at room temperature.

The slides were washed 3x in PBS and incubated with secondary antibody for 2 hours before being washed in PBS 3x and Vector ABC tertiary applied for 1 hour. Slides were washed again 3x in PBS before 100µl DAB reaction mixture was applied to each slide for 1-5 minutes each. After a brief PBS wash tissue was counterstained in Meyers Haemotoxylin and washed in running tap and Scot's water before being dehydrated as stated above and mounted using pertex mounting medium.

Table 1. Antibodies and block procedure used for each antibody for liver histology

Stain	Primary Antibody	Secondary Antibody	Block + Antigen Retrieval
α-SMA – for activated myofibroblasts	α-SMA FITC conjugated 1:1000 sigma Aldrich F3777	Sw Biotinylated anti-fluorescein 1:300 Dako E0353	20% Pig Serum Citrate microwave
Cytokeratin 19 – ductular expansion	Rb polyclonal to Cytokeratin19 1:250 Abcam - ab84632	Sw anti-rabbit biotinylated 1:300 DAKO E0353	20% Pig Serum Citrate microwave
P21 – for senescent cells	Rat polyclonal to P21 (HUGO) abcam ab107099	Gt anti rat biotinylated 1:200 Vectorlabs BA-9400	20% Pig Serum 1mM EDTA soln

2.4.4. Stain Specific Modifications in Liver Histology

For P21 staining in liver tissue was pre-boiled in dH20 for 10 minutes before the EDTA antigen retrieval step.

2.4.5. Imaging and Analysis for Liver

Image analysis was performed using a Nikon Eclipse Upright Brightfield microscope and NIS-Elements BR analysis software. For all liver IHC analysis images are taken at 100x magnification and 4 images taken per lobe, totalling 12 images per animal. Large vessels were excluded from analysis. Optical density was calculated using a threshold that was established on several images before being applied to the whole cohort. A percentage of stained area was calculated from this for PSR, α-SMA and CK19 stains. For p21 an object count threshold was established and applied to all tissues.

2.5. Mesoscale Discovery (MSD)

Levels of IFN-γ, IL-1β, IL-2, IL-4, IL-5, IL-6, IL-10, IL-12p70, KC/GRO, TNF-α in the serum of sham and BDL mice were detected using the V-PLEX Proinflammatory Panel 1 Mouse Kit (K15048D).

2.6. Liver Enzymes

Alanine aspartate transferase (AST) and alkaline phosphatase (ALP) were measured using standard protocols in the clinical pathology department at the Royal Victoria Infirmary.

2.7. Brain Histology

Brain histology was performed on fixed paraffin embedded sections at 5µm thickness. Protocol was adapted from (Lin, Patel et al. 2017) Tissues were dewaxed as per liver protocol above (section 2.4.3). Slides were washed with PBS and microwaved for 20 minutes with Vector labs citrate-based antigen unmasking solution (H-3300-250) diluted in water. After cooling, tissue permeabilization was performed with 0.25% triton X-100

in PBS for 15 minutes before slides were blocked for 2 hours with 5% donkey serum block. Slides were incubated with primary antibody overnight at 4°C, at the concentrations shown below (table 2).

On the second day slides were washed 3x over an hour with 0.1% Triton-X100 in PBS and the secondary antibody applied in block solution at the dilutions indicated below. Tissue was washed a final time with 3x 0.1% PBST before DAPI was applied in blocking solution for 10 minutes at 1:1000 concentration. Slides were mounted using Vectorshield prolong gold anti fade mounting media (P36930).

Table 2. Antibodies and blocking procedure for each antibody for brain histology.

Antibody	**Stains**	**Primary Antibody**	**Secondary Antibody**	**Block + Antigen Retrieval**
NeuN	Mature neurons	Ms monoclonal 1:150 Abcam ab104224	Dk anti-mouse fluorescent 594 1:250 Life technologies A21203	5% donkey serum Citrate microwave
SOX2	Neuro-progenitors	Gt polyclonal 1:300 Santa Cruz SC17320	Dk anti-goat fluorescent 647 1:250 life technologies A21447	5% donkey serum Citrate microwave
GFAP	Mature astrocytes	Rb polyclonal 1:300 Dako ZO334	Dk anti-rabbit fluorescent 488 1:250 life technologies A21206	5% donkey serum Citrate microwave

Iba1	Mature microglia	Gt polyclonal 1:200 Abcam ab5076	Dk anti-goat fluorescent 647 1:250 life technologies A21447	5% donkey serum Citrate microwave
Parvalbumin	GABAergic interneurons	Ms monoclonal 1:10000 Sigma-Aldrich P3088	Dk anti-mouse fluorescent 594 1:300 life technologies A21203	5% donkey serum Citrate microwave
Calretinin	Excitatory interneurons and projection neurons	Ms monoclonal 1:150 Milipore MAB1568	Dk anti-mouse fluorescent 594 1:250 life technologies A21203	5% donkey serum Citrate microwave
γ-H2A.X	DNA damage	Rb monoclonal 1:250 Abcam ab11174	Gt anti-rabbit 1:200 Life technologies A11008	1:60 goat serum Citrate microwave
FXR	Farnesoid X Receptor	Rb polyclonal 1:150 Invitrogen PA5-40755	Dk anti-rabbit fluorescent 488 1:250 life technologies A21206	5% donkey serum Citrate microwave
RecA	Endothelial marker	Ms monoclonal 1:200 Abcam ab9774	Dk anti-mouse fluorescent 594 1:200 life technologies A21203	5% donkey serum Citrate microwave

2.7.1. Brain Histology Analysis

In order to obtain images of the whole dentate gyrus, 3 images were taken per animal (figure 10A). Counts were taken only from within the granule cell layers of the dentate gyrus as highlighted in figure 10D, in order to minimise the differences in sampling and dentate gyrus size between animals. Cell type counts are represented as a percentage of total cells. Total cells were calculated by counting DAPI positive cells in cell counter extension in Matlab version 2012b. Each cell type was then calculated as a percentage of DAPI + cells.

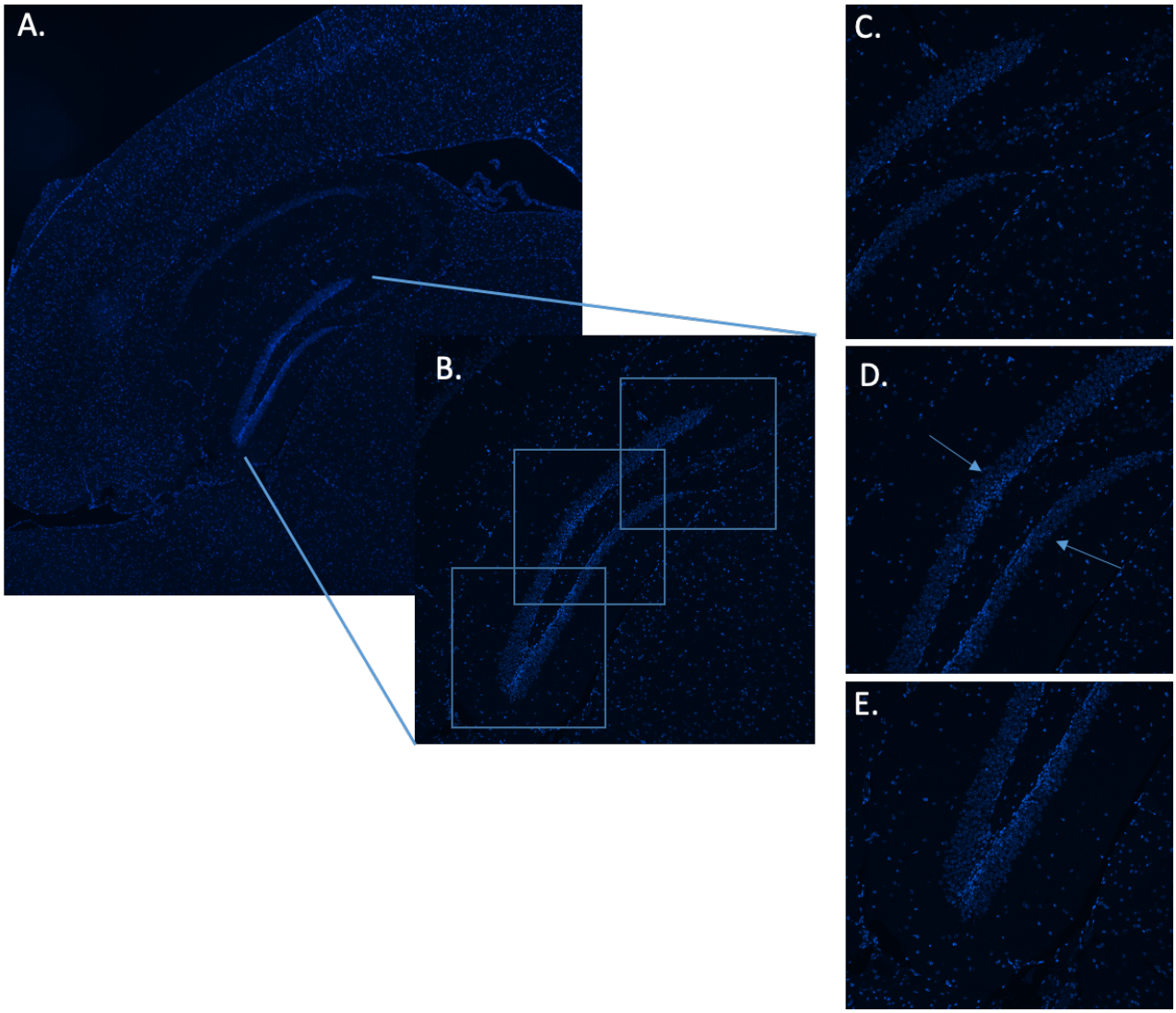

Figure 10. Counting strategy for histology in the dentate gyrus. A) Zoomed out image showing the whole structure of the DG at 10x. B) in order to capture images of a high quality, 3x 20x images were taken per animal, capturing the whole DG structure C-E) show example images. Counts were taken within the densely populated granule cell layer region highlighted in D.

2.7.2. Brain P21 RNA-ish

RNA-ISH was performed after RNAscope protocol from Advanced Cell Diagnostics Inc. (ACD). Tissues underwent dewaxing protocol as described above. Endogenous peroxidases were blocked using 2% hydrogen peroxide solution in methanol for 15 minutes and slides washed in PBS. Slides were washed with PBS and slides heated for 30 minutes. Following this slides were washed in dH_20 and 100% ethanol and air dried. Sections were treated with protease plus for 30 minutes at 40°C, washed with H_2O and incubated with p21 probe for 2 hours at 40°C.

Slides were washed in H20 and incubated with AMP1 for 30 minutes at 40°C, washed with wash buffer and incubated with AMP2 for 15 minutes at 40°C. This was repeated with wash buffer and AMP3 for 30 minutes, then washed and AMP4 for 15 minutes, both at 40°C. With washes in between AMP5 and AMP6 were applied, for 30 and 15 minutes respectively at room temperature. Finally, RNAscope 2.5 HD Reagent kit-RED was used for chromogenic labelling. After counterstaining with haematoxylin, sections were dehydrated, mounted with Pertex and coverslipped.

2.7.3. Immuno-triple Fish for Telomere staining

This protocol is first described in (Hewitt, Jurk et al. 2012). Slides were heated and rehydrated through alcohol as previously outlined and underwent a sodium citrate antigen retrieval. Non-specific binding was blocked with 30 minutes incubation in 1:60 Goat serum. Slides were blocked with Avidin and Biotin before being wash and incubated with γ-H2A.X antibody (table 2) overnight at 4°C at a 1:250 dilution. Slides were washed 3x with PBS and incubated with biotinylated secondary antibody for 30 minutes diluted in block with Goat serum at a 1:200 concentration. Sections were washed in PBS and incubated with Avidin DCS (vectorlab) at 1:500 concentration for 30 minutes.

After γ-H2A.X IF, slides were washed three times in PBS, crosslinked with 4% paraformaldehyde for 20 minutes and dehydrated in graded ethanol. Sections were

denatured for 10 min at 80°C in hybridization buffer (70% formamide (Sigma UK), 25 mM MgCl2, 0.1 M Tris (pH 7.2), 5% blocking reagent (Roche, Germany)) containing 2.5 µg ml−1 Cy-3-labelled telomere-specific (CCCTAA) probe (Panagene), followed by hybridization for 2 hour at RT in the dark.

Slides were washed with 70% formamide in 2 × SSC for 15 minutes, followed by washes in 2 × SSC and PBS for 10 minutes. Sections were incubated with DAPI, mounted and imaged. In-depth Z-stacking was used (a minimum of 40 optical slices with × 63 objective) followed by Huygens (SVI) deconvolution. Number of TAF per cell was assessed by quantification of partially or fully overlapping (in the same optical slice) signals from telomere probe and γ-H2A.X in slice-by-slice analysis, 100 cells per animal or as many neurons as present.

2.7.4. Super Resolution Imaging

Immunofluorescent staining was undertaken as described above. In order to stain the astrocytic attachment to blood vessels sections were co-stained with anti-GFAP rabbit polyclonal antibody and endothelial wall antibody (RecA) (table 2). Sections were imaged using a Leica SP8 confocal (inverted) gSTED 3D Super resolution microscope.

2.7.5. Electron Microscopy

At point of harvest hippocampi were sub-dissected and finely chopped. Tissue was fixed in 2% glutaraldehyde 0.1M cacodylate buffer overnight, and then post fixed in 1% osmium tetroxide before being dehydrated in acetone and embedded in epoxy resin. The blocks sectioned ultrathin and sliced both longitudinally and transversely and stained with uranyl acetate and lead citrate and imaged on a Philips CM100 TEM with tungsten filament.

For analysis, 10 blood vessel images were taken per animal. Astrocyte coverage was calculated using imageJ. Images were set using the ingrained scale on the image, the relative diameter of the whole vessel, and the astrocyte coverage was calculated as a

percentage by dividing whole diameter by astrocyte coverage and multiplying by 100. Endothelial thickness was measured on the same ten images per animal. For each vessel endothelial thickness was sampled at 10 places, evenly spaced around the vessel, and averaged to account for variability in thickness of the vessel. For both measurements the final number for the animal (n=4 per group) total was calculated as an average of the 10 images captured for that animal.

2.8. Flow Cytometry

A panel of fluorescently labelled antibodies was designed in order to determine the specific expression of Farnesoid X Receptor on brain microvascular endothelial cells (BMEC) in the hippocampus. Flow cytometry in the brain, and the selection of Sca1 as a marker of microvascular endothelial cells was adapted from (Wylot, Konarzewska et al. 2015, Au - Martin, Au - El-Behi et al. 2017).

Additionally, we characterised the ARG1 (M2) and iNOS (M1) phenotype of resident and infiltrating immune cells. Antibody mixtures were prepared in a total volume of 30µl of FACs buffer (with or without a permeabilisation agent depending on the presence of the proteins internally or externally). The antibody concentrations are described in Table 3.

Mice were euthanised humanely, perfused through the left ventricle and the brain removed. The left and right hippocampus was sub-dissected out and placed in Hanks Buffered Saline Solution (without calcium and magnesium, HBSS (-)). The brain sample was finely chopped and a digestion cocktail containing 1ml PBS, 123µl Liberase (low thermolysin grade from Roche) and 200µl DNase and placed in an incubator at 37°C for 45 minutes. The digested brain was then put through a 70µm cell strainer and rinsed through with HBSS (-) to ensure collection of all tissue. Cells were centrifuged for 6 minutes at 400g and supernatant discarded and cells re-suspended in 5ml HBSS. Cells had 30% Percoll (diluted in PBS) slowly underlaid. They were centrifuged for 30 minutes at 900g with 0 brake so the interphase is not disrupted. The fat and myelin layer should settle at the top of the liquid interphase and be pipetted gently off. Other cell fractions

remain in a pellet at the bottom of the tube. Pellet is re-suspended in 200ul PBS and transferred to a 96 well round bottom plate.

Cells are span at 1500rpm for 2 minutes and supernatant discarded before 50ul Live/Dead stain mix is added (if being used). Cells incubated with L/D at 4°C for 15 minutes before spun at 1500rpm and 200ul FACs buffer (PBS and 1% Fetal calf serum) added to each well. To stain intracellular proteins, the cells undergo a 2-step staining procedure.

First the cells were incubated with the cell surface antibodies for 30 minutes at 4°C (CD45, Sca1, CD31, CD11b, F4/80). They are then washed in FACs buffer and fixed and permeabilised for 15 minutes each at 4°C. Fixation was achieved by incubating the cells in 4% paraformaldehyde and permabilisation step done using 1x Perm wash (BD Biosciences).

Intracellular antibodies were diluted to the required concentration (outlined in table 3) in 1X Perm Wash diluted in FACs buffer and were incubated with the antibody mix for 30 minutes at 4°C. If a secondary antibody conjugation was required (marked with * in table), cells were then incubated with the secondary antibody after intracellular staining, following which they were washed twice in FACs buffer and re-suspended in 100µl of FACs buffer ready to run on the flow cytometer. Cells were read on either a FACSCanto II or BD FACSDiva v8 and analysis was performed using FlowJo software.

*Table 3. Antibodies used for flow cytometry experiments. *denotes a secondary antibody conjugation*

Antigen	Fluorophore	Vendor	Dilution
Live/Dead	BV241	Life Technologies	1/100
FXR	AF594*	Thermofisher Scientific	1/50
CD45	BV510	Biolegend	1/50
CD11b	PerCP-Cy5.5	Biolegend	1/500
Sca1	APC	Biolegend	1/50
ARG1	PE	R&D	1/50
INOS	PE-Cy7	eBioscience	1/50
Ly6G	BV780	eBioscience	1/50
F4/80	FITC	eBioscience	1/50

2.9. Electrophysiology

2.9.1. Electrophysiology Preparation

Animals were killed humanely by anaesthetic overdose with inhaled isoflurane and intramuscular injection ketamine (≥100 mg kg−1) and xylazine (≥10 mg kg−1) as previously described by the group (Driver, Racca et al. 2007). When all reflex (flinch reflex, pedal withdrawal reflex) disappeared animals were transcardially perfused with at least 25mls of sucrose rich artificial cerebral-spinal fluid (SaCSF) - composed of (mM) 252 sucrose, 3.0 KCl, 1.25 NaH_2PO_4, 24 $NaHCO_3$, 2.0 $MgSO_4$, 2.0 $CaCl_2$ and 10 glucose. The brain was removed and sliced to 450um horizontal slices with a Leica VT1000S vibratome in ice cold SaCSF.

Slices were trimmed to the hippocampal region and moved into a holding chamber at RT for 1 hour before being transferred to the recording chamber and maintained at 32-34°C at an air liquid interface between normal aCSF (sucrose replaced with 126 mM NaCl) and humidified 95% O2/5% CO2. Oscillations were evoked with 10µM cholinergic agonist Carbachol, to activate transmission through acetylcholine receptors. The chemical composition of SaCSF and aCSF are outlined in table 4.

Table 4. Chemicals required to make 1 Litre of artificial cerebral spinal fluid.

Chemical Name	Formula	Vendor	Amount in aCSF Solution (mM)
Sucrose	C12H22O11	Sigma-Aldrich (16104)	252
Potassium chloride	KCl	VWR International (101985M)	3
Sodium dihydrogen orthophosphate	NaH2PO4	VWR International (307164T)	1.25
Sodium bicarbonate	NaHCO3	Tocris (3152)	24
Magnesium sulphate	MgSO4	Sigma-Aldrich (M7506-M)	2
Calcium chloride	CaCl2	VWR International (275844L)	2
Glucose	C6H12O6	VWR International (101176K)	10
Sodium chloride	NaCl	Sigma-Aldrich (S7653)	126

2.9.2. Recording and data acquisition

Extracellular recording electrodes were filled with normal aCSF (resistance 2–5 MΩ), and field recordings taken from the border between stratum radiatum and stratum lacunosum moleculare in CA3. Recordings were taken with Axoclamp-2B amplifier (Axon Instruments Inc., Union City, CA, USA) and extracellular data filtered at 0.001–0.4 kHz low-using Bessel filters. Mains noise was deducted with a Humbug (Digitimer, Welwyn Garden City, Herts, UK), and data redigitized at 10 kHz using an ITC-16 interface

(Digitimer, Welwyn Garden City, UK). Axograph 4.6 software (Axon Instruments Inc., Union City, CA, USA) was used for data acquisition and analysis.

2.9.3. Data analysis

To generate power spectra Axograph used Fourier analysis using 60 seconds per 10-minute recording. This was used to calculate peak frequency and area power (area under the peak). Mouse gamma frequency oscillation was measured at frequencies between 15 and 49 Hz. Oscillations were categorized as stable when area power measured within ±10% for three consecutive 10 min recording intervals. Rhythmicity was measured using the first side peak amplitude of the auto-correlations performed over 1 s traces, and was shown on the rhythmicity index on a scale between 0-1. Multiple slices were gained from each animal, and as such data reported in this publication is shown as N to represent the animal number and n for slice number.

2.10. Neurotoxic Effects of Cholestatic Serum In Vitro

2.10.1. Growth and Differentiation of 97 Cell Line

Cells were derived from foetal forebrain by Peter Hanson and Chris Morris. The differentiation protocol is adapted from (Kurzawa-Akanbi, Hanson et al. 2012), which uses the same cells. The cells were passaged using trypsin-EDTA solution and were seeded into a geltrex coated 48 well cell culture plate at a density 5,000 cells per well with 250µl of proliferation media. They were allowed to proliferate for 2 days before the proliferation media was withdrawn and replaced with differentiation media. Growth medium was replaced with differentiating medium containing Dulbecco's modified Eagle's medium /F12 supplemented with 10% heat-inactivated Foetal Bovine Serum (Sigma), N-1, B27 and N-2 for 2 weeks before beginning experimental procedure. For chamber slides cells were plated at a density of 10,000 cells/chamber.

2.10.2. Neurotoxic Effect of Serum from Cholestatic Mice

Blood was extracted via right ventricular cardiac puncture at harvest from mice that underwent either sham or BDL surgery (10 days). These were left at RT for at least 30

minutes to allow clotting and spun at 8,000rpm for 10 minutes before collecting the clear serum layer and discarding the red blood cell pellet. Serum samples were stored at -80^{o}C.

On the day of the experiment serum samples were thawed on ice, vortexed and heat inactivated for 30 minutes at 60^{o}C. They were diluted in media to the desired concentration and added to the plate for 72 hours.

2.10.3. Neurotoxic effects of PBC patient serum

Human serum was obtained from the UK-PBC bioresource of samples from well characterised PBC patients experiencing cognitive symptoms as defined by the UK-PBC cohort questionnaire. Serum samples were stored long term at -80^{o}C. Serum samples were thawed on ice, vortexed and heat inactivated for 30 minutes at 60^{o}C. Samples were diluted in media to desired concentration added to the plate for 72 hours.

2.10.4. Alamar Blue Cell Viability Assay

To determine the effect of treatment with cholestatic serum on cell viability, the Alamar blue reduction assay was used. Sterile filtered alamar blue (1mg/ml) was added to fresh media to a final concentration of 5% alamar blue. The media was removed from all wells and replaced with 250µl alamar blue solution per well and plate returned to incubator for around 1 hour until a colour change can be observed in the control wells.

Alamar blue solution (100µl) was removed from each well and added to a 96 well plate, allowing for two technical replicates. The cell viability was determined using a TECAN Nano M+ fluorescent plate reader at 530nm excitation and 590nm emission. Done for day 0 (background reading) and media was then replaced with serum dosed media, after 72hours cell viability measurement was repeated. This assay was performed before and after each cell dosing experiment.

In order to assess cell viability, alamar blue readings at day 0 and 3 were averaged from 2x technical replicate and 3x measured wells (biological replicate) and calculated as a percentage change over time.

2.10.5. B-galactosidase Senescence Assay

This assay was performed using kit ab228562 purchased from abcam. The kit was reconstituted according to the manufacturer's instructions. Cells were washed briefly with PBS and fixed for 10 minutes in formaldehyde prior to assay. ß-galactosidase solution was added to wells (250µl for 48 well plate, 400µl for chamber slides) and incubated in a sealed bag at 37 ^{o}C for 3 hours. Cells were washed 3x with sterile PBS before being stored at 4 ^{o}C in 70% glycerol. Cells were imaged on a Zeiss axioimager microscope. To get an average senescence score per condition, 4 areas were analysed per well, and three well repeats per condition were averaged.

2.10.6. Immunocytochemistry (ICC)

Cells were fixed for 10 minutes with 4% PFA before being washed 3x with ice cold PBS to remove residue. Permeabilisation step was performed using 0.2% Triton-X100 in PBS for 10 minutes and cells were then washed in PBS and blocked in 5% of the corresponding serum block with 0.1% Triton-X100 in PBS for 1 hour. Primary antibodies were applied overnight at 4^{o}C at a concentration of 1:1000 in the block buffer of 1%BSA, 0.1% Triton-X100 in PBS. Cell were placed in a humidified chamber on a rocker.

The next day cells were washed 3x in PBS and secondary antibody was applied at 1:1000 for 1 hour at room temperature. Secondary antibody was diluted in the same buffer as the primary antibody. Cells were washed 3x again with PBS and incubated for 10 minutes with DAPI in the buffer solution at 4^{o}C. Slides were mounted immediately using Vectorshield prolong gold antifade mounting media and glass coverslips. Images were taken on Zeiss Axioimager 2 at Bioimaging unit Newcastle university. ROI feature on ImageJ was used in order to measure expression per cell and per nucleus. 10 Cells per image were analysed to get an average and 4 images taken per treatment.

2.10.7. LiCor Fluorescent Western Blot

Wet nitrocellulose membrane for 2 minutes in 1X PBS. Then wet for 1 minute in methanol 100% and rinse with ultrapure water. Membrane blocked in Intercept blocking buffer (li-Cor 927-60000) for 1 hour at RT on a rocker, ensuring enough block to cover the membrane. Primary antibody diluted 1/2000 in 0.2% Tween 20 + PBS (TBST). FXR antibody used is Thermofisher Scientific (PA5-40755), TGR5 antibody is R&D systems MAB4286. Primary antibody is incubated with the blot overnight at 4 °C on rocker.

Pour off antibody solution and rinse membrane 3 times in 1X TBST (0.1% tween 20). Secondary antibody was then added (IRDye 680RD used) at a concentration of 1:15,000 in 0.2% Tween20 in Intercept Blocking buffer for 1 hour at RT on rocker. Membrane was rinsed with 1X TBST (01% Tween20) 3 times. Membrane was scanned on the Odyssey Imaging System.

2.11. Statistical Analysis

Data are always presented as mean ± standard error of the mean (SEM), where *, **, *** and **** equals P values of <0.05, <0.01, <0.001 and <0.0001 respectively. P values were calculated using GraphPad prism using an ANOVA with Tukey Post-hoc test, or unpaired T-Test. For non-parametric analysis, Kruskal Wallis test was used for groups +2, Mann whitney U was used for groups of 2.

3. Chapter Three - Cognitive deficits and underlying brain pathology occur during BDL-induced Cholestasis

3.1. Introduction

As previously discussed, the pathology behind cognitive deficit is of yet largely unknown. In order to begin characterising these deficits molecularly, cellularly and functionally first an animal model must be chosen that recapitulates these deficits as widely as possible.

3.1.1. Bile Duct Ligation as a Model for Cholestatic Liver Disease

The bile duct ligation (BDL) model provides a robust and largely replicable murine surgical model of cholestatic liver disease. The model recapitulates many of the major hepatic complications of cholestatic autoimmune liver disease. Including biliary obstruction, portal and peri-portal fibrosis (A), collagen deposition (Fiorucci, Antonelli et al. 2004, Abshagen, König et al. 2015), jaundice, ductular reaction (DR) (B), immune cell infiltration and peri-ductular senescence (C). Example rodent BDL histology can be seen in figure 10.

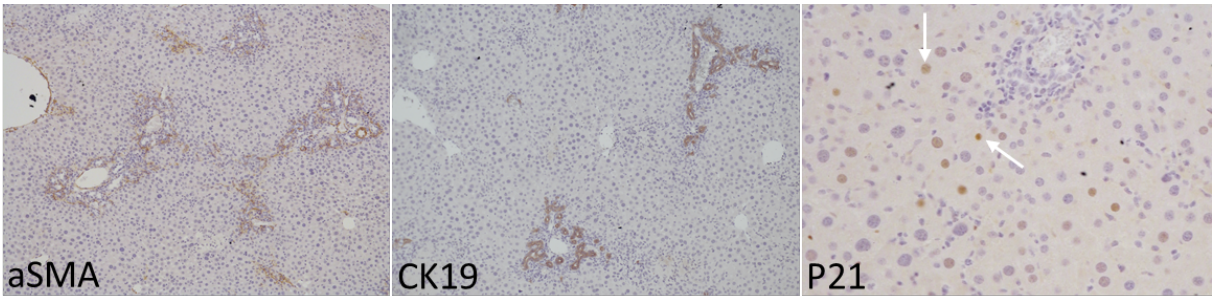

Figure 11. Example histology showing (A) periportal fibrosis, (B) ductular reaction, (C), senescence.

3.1.2. Evidence for Memory Impairments in BDL

Crucially, limited evidence in rodents shows BDL also recapitulates central spatial memory deficits seen in PBC patients. Several studies have reported by 21 days post-surgery (but not 7 or 14) rats were found to possess significant learning and motor impairment when assessed using the Morris Water Maze (Montes, Alcaraz-Zubeldia et al. 2001, Huang, Hsieh et al. 2004, Hosseini, Alaei et al. 2014). Spatial memory deficits are also seen in mice at 21 days post BDL when subjected to T maze testing (Magen, Avraham et al. 2009) (comparable to Y maze). This study also reports locomotor activity deficits in Open Field tests.

3.1.3. Changes in Circulating Inflammatory Cytokines

Previous studies using BDL or BDR animals have shown that by day 5, peripheral monocytes are recruited to the brain via CCR2 (Kerfoot, D'Mello et al. 2006), and can activate resident microglia(D'Mello, Le et al. 2009). These monocytes attach to the endothelial wall through P- selectin (D'Mello, Riazi et al. 2013) and cause monocyte mediated microglial activation through TNF-α. Brain infiltrating monocytes were found at higher concentration in key brain areas such as the motor cortex, hippocampus and basal ganglia.

The hippocampus is an important brain region, controlling highly intricate and diverse functionality. The hippocampus is susceptible to BBB breakdown and indeed recent

studies in humans have shown that BBB breakdown at the hippocampus leaves the brain vulnerable to cognitive impairment (Nation, Sweeney et al. 2019). Therefore, it seems significant that monocytes were found at high concentrations in this key region.

These circulating inflammatory factors are likely to affect both the BBB and the normal homeostatic function of the brain. As 'changes in neurotransmission that give rise to behavioural alterations in such diseases occur before the development of overt pathological CNS tissue damage, but after cerebral immune cell infiltration has occurred' (Pollak, Ovadia et al. 2003). Thus, by day 10 when moderate disease has developed, changes will likely occur to the BBB and susceptible brain areas experience neuroinflammation.

3.1.4. Evidence for Blood-Brain Barrier Dysfunction in BDL

The blood brain barrier ordinarily provides a physical and metabolic barrier from between the bodily circulation and the brain. The semi permeable barrier comprises of brain microvascular endothelial cells (BMECs) with specialised tight junction properties, alongside pericytes and astrocytes exerting synergistic functions. In our studies we have focussed mainly on astrocyte attachment at the vessel as these provide the key cell to cell signalling between the BBB and functional changes in neurons. Endothelial cells, astrocyte and neuron grouping is known as the neurovascular unit, along with pericytes or secondary cells such as interneurons, myocytes and components of the extracellular matrix (ECM) (shown below). The neurovascular unit (NVU) provides a primary mechanism of brain communication and homeostasis, enabling dynamic vasoconstriction and vasodilation first described by Harder in 2002 (Harder, Zhang et al. 2002).

To date, there is little concrete *in vivo* evidence of changes in the blood brain barrier occurring in rodent models of cholestasis. Studies so far have been mainly focussed around hepatic encephalopathy (HE); a state characterised by cirrhosis. Though not

directly relevant to my PhD studies, these rodent papers provide an insight into the BBB alterations that can occur as a result of bile acid and other secondary molecules such as ammonia. Several papers have found alterations in BBB as a result of HE, such as cerebral oedema, which indicates changes to BBB function (Mouri, Mourabit et al. 2017)

Early studies by Jaqueline Wahler and Mark Swain in rats showed ANIT and BDL induced cholestasis led to a decrease in blood to brain transfer constant (Ki) compared to Sham controls, both in the drug induced ANIT model by day 7 and BDR by day 5. This data is indicative of changes to BBB function and macrostructure (Wahler, Swain et al. 1993), in early cholestatic disease.

We hypothesised that by 10 days post BDL significant changes to the liver including significant myofibroblast activation, and collagen deposition as has been well described in the literature (Abshagen, König et al. 2015). We also hypothesised that the changes structure of the BBB, as well as neuroinflammatory cell types such as microglia and astrocytes will occur, and these cell types will be activated into an M1 phenotype.

3.2. Study Rationale

Our initial studies were run up to 10 days and liver fibrosis, DR, circulating inflammation, cognition, microvascular changes at the blood brain barrier, changes to brain resident cell populations, senescence in the liver and brain and electrophysiological gamma wave oscillations were assessed. A smaller study of animals was harvested at day 6 to investigate early changes to circulating inflammatory markers, the blood brain barrier, fatigue score, and neuronal/glial cell populations.

Previous studies in the field have reported changes to the BBB by day 5 post BDL (Wahler, Swain et al. 1993). However behavioural changes have not been identified until day 21 (in rats and mice) (Magen, Avraham et al. 2009). Therefore, we expect to see an immune response by day 6 - including changes in circulating inflammatory markers and

neuroinflammation. Behavioural deficits may not occur until day 10 (if at all in this timeframe). It is likely that we will begin to see changes in neuronal network excitability and oscillation capacity by day 10, alongside resulting in memory deficit.

As BDL provides a severe cholestatic model (indeed in many labs is unable to be run as long as 21 days), we aim to look at earlier time points in the disease course to assess subtle changes to the brain architecture and resulting cognitive decline. By day 10, these animals experience significant fibrosis and inflammation, however they are pre-cirrhotic. This allows us to look at changes that occur early in the cholestatic process, before reaching a point of cirrhosis where such hepatic and neurological changes may be irreversible. Studying a cholestatic animal model at these time points allows us to pick apart a mechanism not of late stage Hepatic Encephalopathy (HE) (where treatment is likely to have little effect), or minimal HE which is also defined as occurring during cirrhosis, but earlier still in the disease spectrum.

Circulating and brain infiltrating macrophages in the brain (and their activation phenotype) were assessed via fluorescence activated cell sorting (FACs). This method was also used to assess endothelial cells of the BBB. Electron microscopy was used to assess nanoscopic changes to BBB integrity and to assess astrocytic end-feet attachment at the vessel. Astrocytes themselves were assessed for proliferation using immunofluorescent marker GFAP.

Other cell types were also assessed for changes using immunofluorescence; neurons (NeuN), microglia (Iba1), fast spiking interneurons (Parvalbumin), and progenitors (SOX2). All data showing brain tissue is rodent brain isolated or imaged from the hippocampus, mainly CA3 and Dentate gyrus, as these are the areas most significantly associated with spatial memory deficits.

Telomere associated foci (TAF) and P21 RNA-ish were used to calculate the number of neurons that were senescent. Together these form a confirmatory battery of tests. TAFs

assess DNA damage co-localised at the shortened ends of telomeres, and p21 forms part of the senescence associated pathways.

The standardised behavioural tests used were open field for activity and Y maze for spatial memory and were initially designed and performed by Dr. Claire Richardson (behavioural expert) and repeated by Dr Ben Millar and myself. Behavioural tests were selected by agreed discussion between clinicians at Newcastle upon Tyne hospital trust and academic researchers specialising in animal behaviour (Dr. Claire Richardson) at Newcastle University. In line with 3Rs animal welfare guidelines behavioural tests were never done on the same day as this is known to affect naturalistic behaviours and causes undue stress (Võikar, Vasar et al. 2004). Workflow for testing can be found in figure 12.

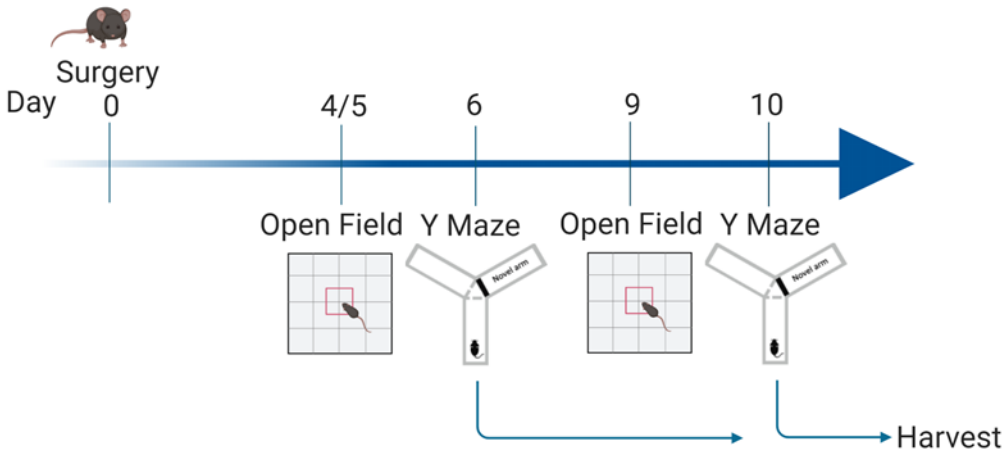

Figure 12. Workflow for behavioural testing experiments

3.3. Aims

The main aims of the research comprising Chapter three are as follows:

- Assess fatigue and visual spatial memory deficits present in BDL mice at 5- and 9-days post-surgery when compared to sham operated animals.

- Assess liver function enzymatically (AST and ALP) and assess histologically (PSR, α-SMA, CK19, p21) damage to the liver by day 10 of BDL.

- Employ techniques to assess BBB of sham and BDL animals at day 6 and 10 post-surgery, in order to investigate early loss of BBB function during cholestasis (EM, MRI, FACs, Super Resolution imaging).

- Assess changes to neuronal (neurons, neural progenitor) and inflammatory (astrocytes, microglia) cell types within the hippocampus which may contribute to overall disease phenotype.

- Assess immune cell activation phenotype in the liver, circulation and brain.

- Assess senescence as a common multi-organ mechanism for dysfunction in cholestatic disease.

3.4. Results

3.4.1. Some Pathological Changes Occur by Day 6

3.4.1.1. Bile duct ligated mice show no fatigue by day 6 post-surgery

At 5 days post-surgery in our murine model, there were no statistical differences in results from open field testing between sham (n=5) and day 5 BDL mice (n=7). Distance travelled (FIG 13A), number of steps taken (FIG 13B) and speed of movement (FIG 13C) all show a similar trend of a small reduction between the sham and BDL groups. This is likely to indicate the beginnings of subtle fatigue like symptoms, with a minor reduction in activity in the BDL group, though this doesn't reach significance.

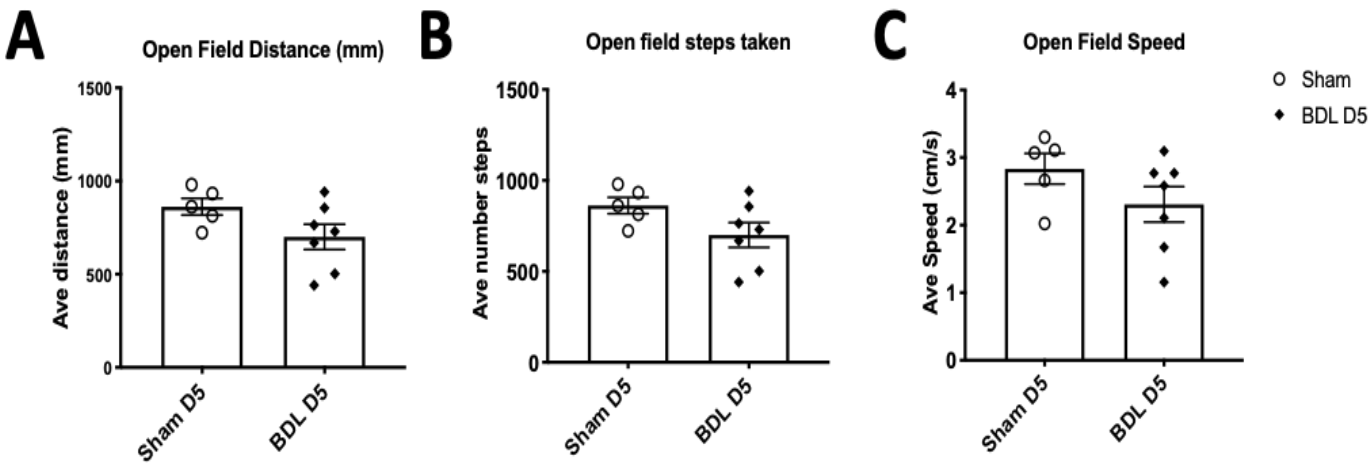

Figure 13. Open field outputs for the duration of the 5 minute trial (A) distance covered in mm (B) steps taken (C) average speed travelled. N= 5 sham and N = 7 BDL animals.

3.4.1.2. BDL mice show subtle changes at the BBB by Day 6

Astrocytes are key to the function of the BBB, and without them brain microvascular endothelial cells are unable to form a working barrier (Rubin, Hall et al. 1991). As the astrocyte end-feet are in close contact with the vessels themselves, these are known to act as 'injury sensors' to noxious molecules such as circulating inflammatory cytokines (in addition perhaps In this case to bile acids themselves) (Robel, Berninger et al. 2011). In response to injury become activated, move away from the vessel and proliferate in order to 'plug the gaps' in the BBB.

At day 6, electron microscopy nanoscopic analysis revealed reduced astrocyte coverage at the vessel (FIG 14E). This is indicative of early changes to the normal ultrastructure of the BBB within the hippocampus, and likely resultant changes to ionic permeability. This is likely to be in the early process as astrocyte number isn't changed between the sham and day 6 BDL animals. The number of pericytes (FIG 14D), and their observed phenotype looks to still be conserved at this stage in the disease process. The structure of the vessels themselves also looks to be conserved; there are no significant changes in the endothelial wall thickness (FIG 14A) or average vessel circumference (FIG 14B).

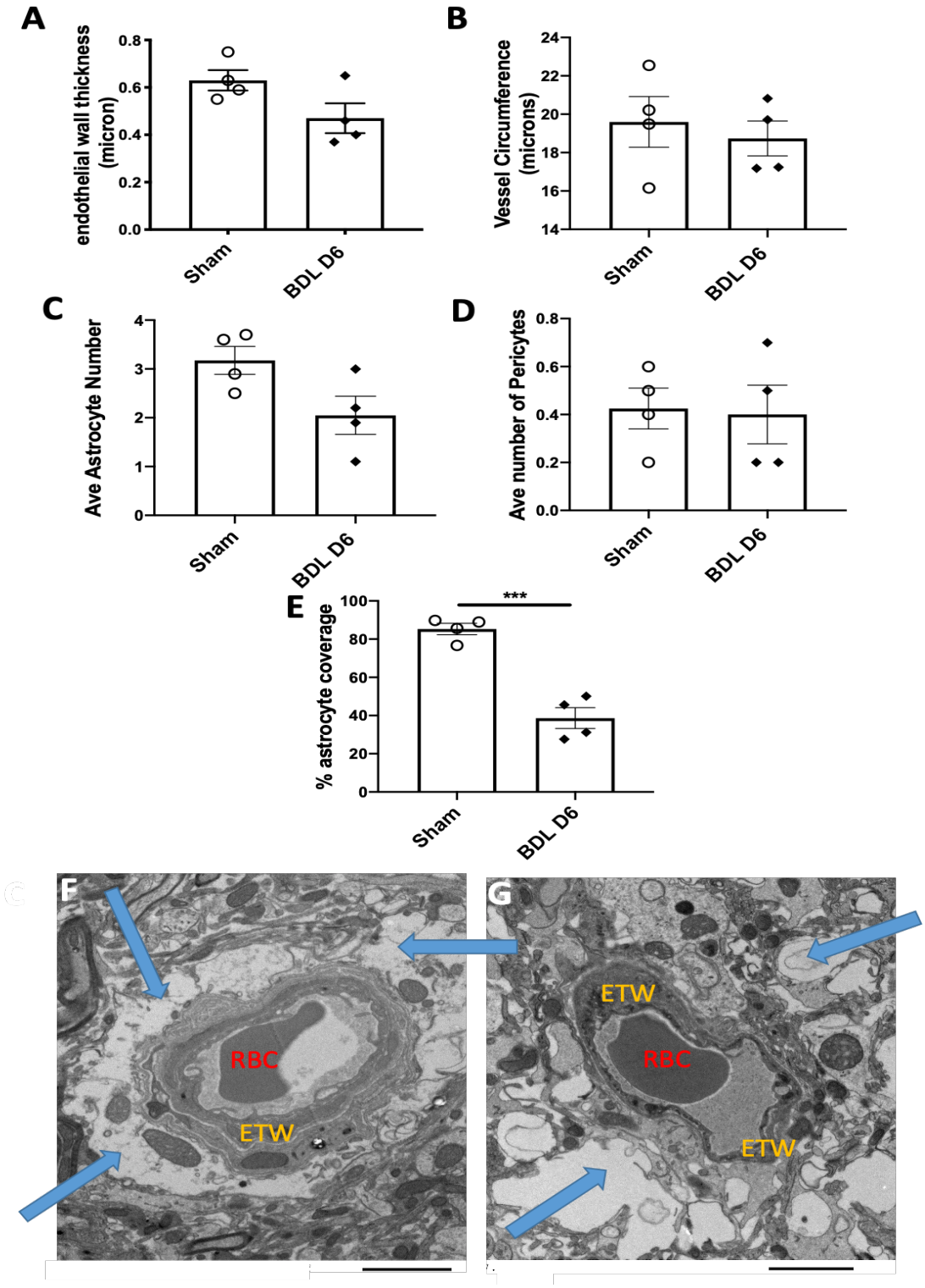

Figure 14. transmission electron microscopy study day 6 bile duct ligation. (A) Endothelial wall thickness (B) vessel circumference in microns (C) astrocyte count (D) pericyte count are similar between sham and BDL animals. (E) percentage astrocyte coverage was significantly reduced in BDL animals. (F) sham image showing full coverage of astrocyte end-feet (G) BDL day 6 image showing reduced astrocyte end-feet coverage. Endfeet are denoted by blue arrows, RBC denotes red blood cell and ETW denotes endothelial wall. Scale = 2microns. N=4 sham N= 4 BDL day 6 animals. 10 vessels imaged per animal and averaged to get final number. Data represented as mean +/- SEM, statistics T.TEST.

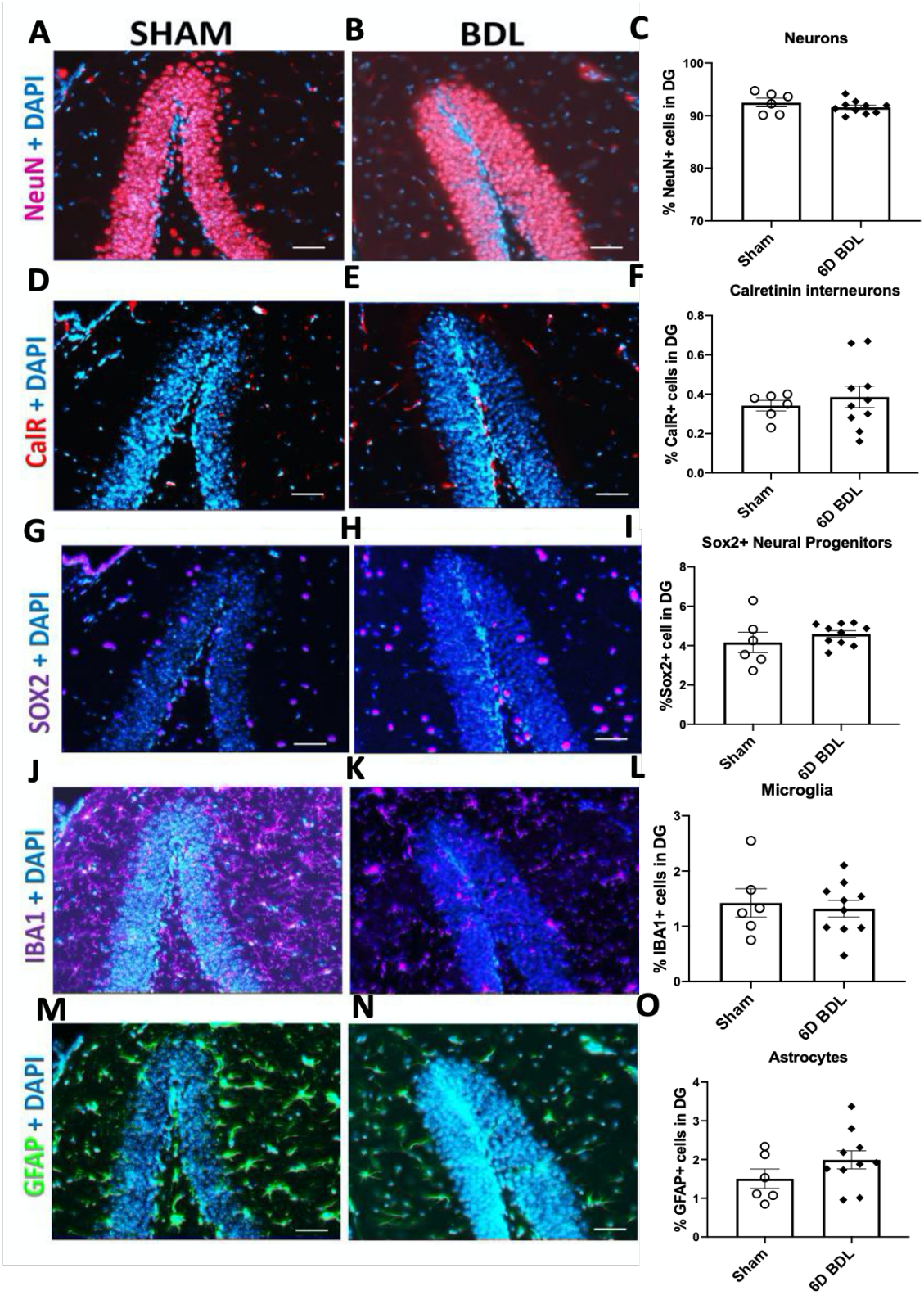

Figure 15. Immunofluorescent stainingof cell populations in the dentate gyrus (A,B,C) Neurons (D, E, F) calretinin interneurons (G, H, I) SOX2+ progenitor cells (J, K , L) iba1+ microglia (M,N, O) GFAP+ astrocytes. all similar between sham and day 6 BDL mice. N=6 sham N= 10 day 6 BDL. Scale = 50 µm. Data represented as mean +/- SEM, statistics T.TEST. Images are shown with DAPI overlay, counts taken within granule cell boundary of the dentate gyrus and represented as a % of DAPI.

3.4.1.1. BDL mice show no changes in brain resident cell types by day 6

By day 6 BDL mice show little change in the numbers of key brain resident cell types within the hippocampus such as neurons (FIG 15A, B, C), calretinin+ interneuron (FIG 15D, E, F) progenitors (FIG 15G, H, I), microglia (FIG 15J, K, L), and GFAP= astrocytes (FIG15 M, N, O). This data indicates that by this early stage in disease there is little progression of the neuronal disease process. Astrocytes usually provide the first response to injury, and are possibly beginning to show a proliferative phenotype in the dentate gyrus increasing from mean value of 1.5% astrocytes to 2% astrocyte population of total cells.

3.4.2. Pathological Changes by Day 10 BDL

3.4.2.1. Changes to the Liver Biochemistry by Day 10 BDL

By day 10 after bile duct ligation mice show significant changes to liver enzymes. Aspartate transaminase (AST) (FIG 16A) was more than doubled in the serum of BDL mice when compared with sham operated animals. This is indicative of large amounts of liver damage. An even more significant increase in alkaline phosphatase (ALP) (FIG 16B) indicates damage to the ductular cells and gall bladder of the level that is expected from BDL surgery.

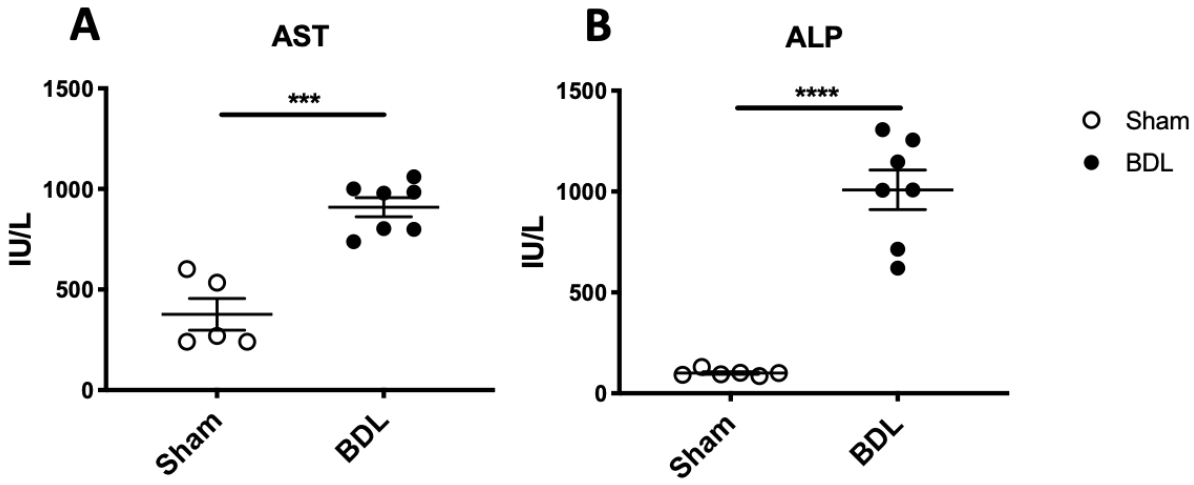

Figure 16. Liver Biochemistry measurements. BDL day 10 animals had significantly raised Aspartate transaminase (AST) (A) and alkaline phosphatase (ALP) (B). N= 6 Sham N= 7 BDL day 10. Data represented as mean +/- SEM, statistics T.TEST. These tests were performed by staff scientists at Royal Victoria Infirmary Hospital labs, Newcastel upon Tyne.

3.4.2.2. Histological Changes to the Liver by Day 10 BDL

Mice show significant pro fibrotic features by day 10 post BDL surgery. There was a significant increase in activated myofibroblasts, (α-SMA), (FIG 17A, B, C), collagen deposition as seen in Picrosirius red (PSR) stain (FIG 17D, E, F), a common and well characterised phenotype of fibrosis that is likely to contribute to raised liver enzymes seen in Figure 15 and altogether indicates a pro-inflammatory environment.

DR occurred by day 10 as seen in the cytokeratin 19 (CK19) histology (FIG 17G, H, I). DR, known pathologically as biliary hyperplasia is a common and robust feature of cholestatic disease, where the bile ducts undergo proliferation of the biliary epithelial cells and subsequent remodelling in response to injury (Roskams, Theise et al. 2004). In the case of BDL a large portion of this occurs at the large ducts (Alpini, Glaser et al. 1998).

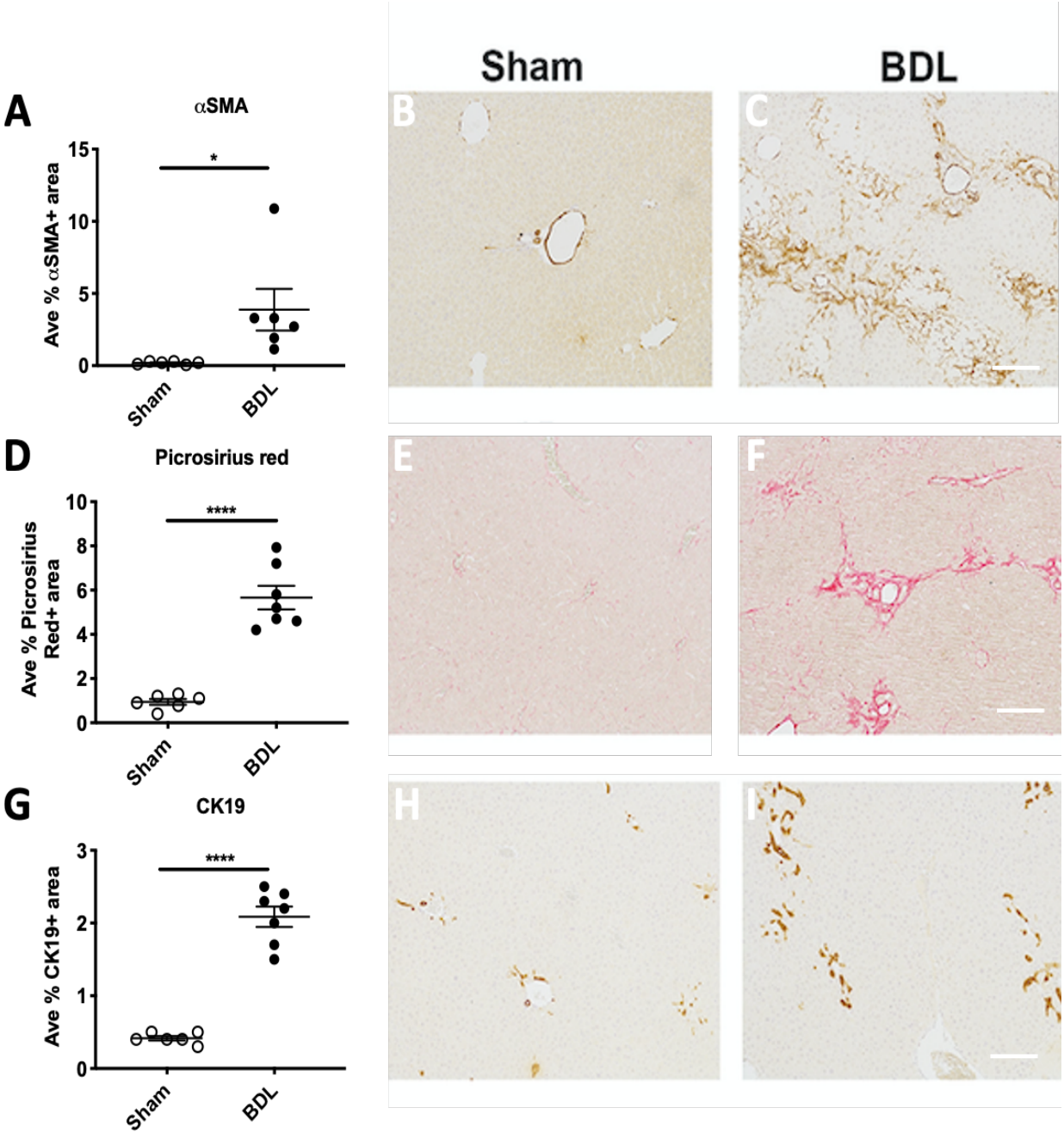

Figure 17. Liver histology day 10 BDL animals. BDL animals had significantly increased activated myofibroblasts (A) example images of sham (B) and BDL (C), significantly increased collagen deposition (D), example images of sham (E) and BDL (F). Ductular proliferation was significantly increased in day 10 BDL livers (G), example histology for sham (H) and BDL (I). Scale = 50 µm. N= 6 Sham N= 7 BDL day 10 animals. Data represented as mean +/- SEM, statistics T.TEST.

3.4.2.3. Bile duct Ligated mice show Hepatic Senescence and DNA damage by day 10

As previously discussed, liver senescence is a well characterised symptom in patients with PBC. Ductular senescence was assessed here and cells sorted into parenchymal (mainly hepatocytes as labelled here) and non-parenchymal cell types (comprising of cell types such as BECs/cholangiocytes, sinusoidal endothelial cells, stellate cells, Kupffer cells, and intrahepatic lymphocytes) based on cell size criteria. These cells make up 60% and 40% of liver mass respectively. Hepatocytes are usually thought of as the 'functional' cells of the liver, however non parenchymal cells have important roles in hepatotoxicity and regeneration. Both parenchymal and non-parenchymal cells are sensitive to P21 mediated senescence. In the BDL model by day 10 an average of 16% of hepatocytes are senescent whereas less than 1% of hepatocytes exhibit senescence in Sham animals (FIG 18B, E, F). Senescence was also induced in non-parenchymal cells (FIG 18A), to a lesser extent than in hepatocytes, likely because hepatocytes are sensitive to oxidative damage.

Hepatocytes also showed DNA damage as measured by γ-H2AX (FIG 18D), in similar levels to non-parenchymal cells, indicative of a global hepatic DDR. DNA damage is significantly increased in non-parenchymal cells (FIG 18C).

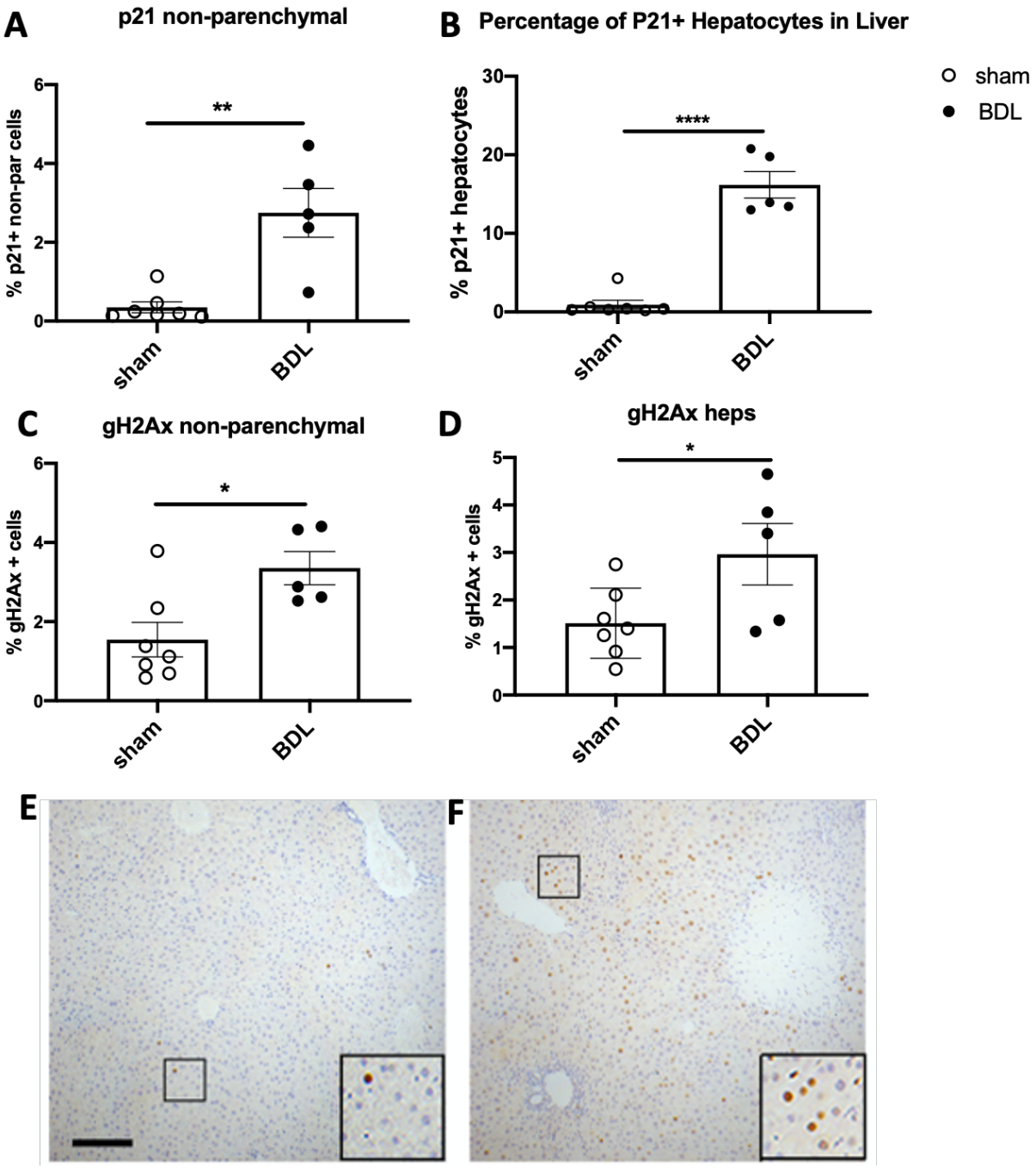

Figure 18. Senescence (p21+) and DNA damage were assessed in the Liver of sham and day 10 BDL animals. (A) non parenchymal cells and (B) hepatocytes showed more senescence in BDL animals. DNA damage was also higher in the non parenchymal (C) and hepatocytes (D) in BDL animals. Histology images showing (E) sham and (F) BDL day 10 liver. Scale = 100micron. Data generated by collaborators Thomas Bird and Christos Kiourtis at Beatson Institute Glasgow, using HALO software. N=7 Sham animals N= 5 BDL day 10 animals. Data represented as mean +/- SEM, statistics T.TEST.

3.4.2.4. Circulating inflammatory Factors are raised in BDL mice

Mesoscale discovery (MSD) inflammatory panel was run on serum from the day 10 BDL cohort (FIG 19). MSD readout revealed significant increase in inflammatory cytokines interferon gamma, IL10, IL-1B, IL-2, IL-4, IL-5, and TNFα. The only inflammatory output that was not significantly increased was KC gro (CXCL1) which is implicated in neutrophil recruitment. IL-6, a member of the senescence associated secretory phenotype (SASP) in hepatocytes was hugely inflated in the BDL animals.

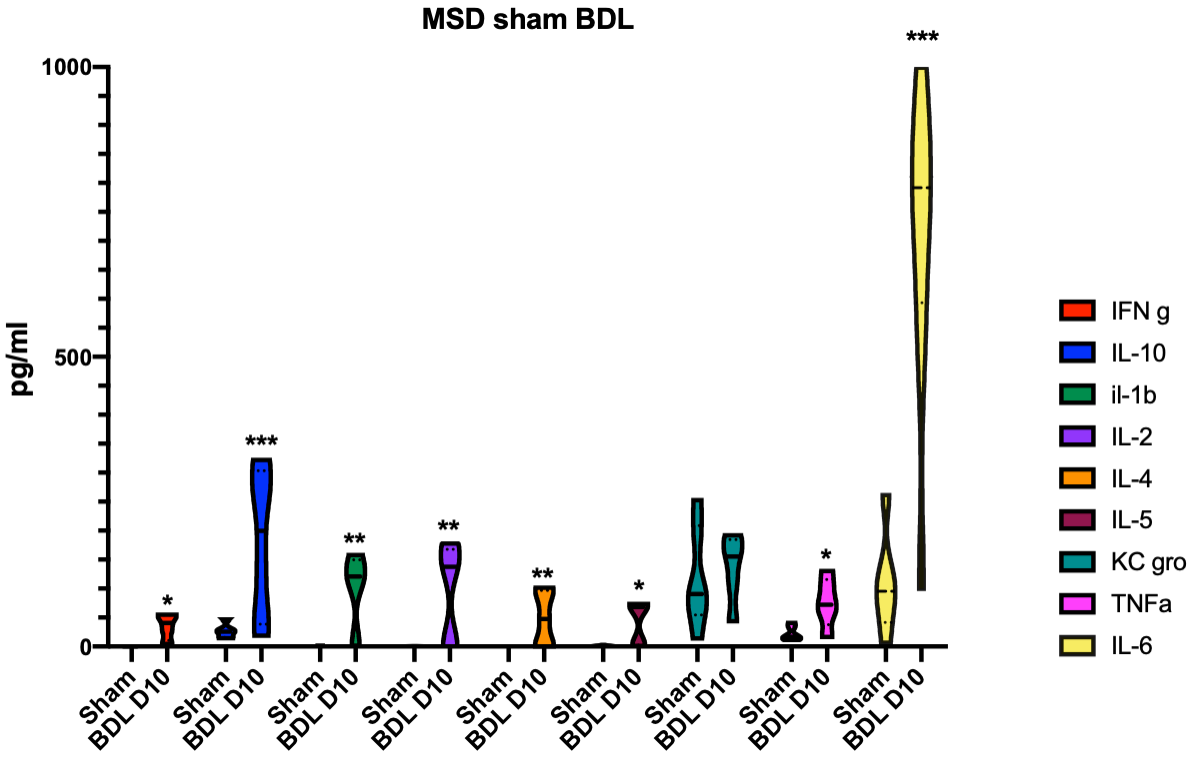

Figure 19. Mesoscale discovery data showing the serum concentrations of key cytokines between sham and BDL day 10 mice. Represented as picogram per mililiter. N= 6 sham and N= 5 BDL animals. Statistics multiple T.Test.

3.4.2.5. BDL Mice show Fatigue by Day 10 Post-Surgery

Bile duct ligated mice (n= 6) showed significant reduction in both the distance moved (FIG 20A) and number of steps taken (FIG 20B) in open field testing by day 9 post-surgery when compared to sham (n= 6). In addition, the BDL group also showed a reduction in speed of movement by day 9 (FIG 20C), indicative of central fatigue. This data is indicative of fatigue symptoms in rodents appearing much earlier than previously reported, as Hosseini et al found no motor impairment at day 7 or 14 in rats. Our study shows significant locomotor activity deficit occurs as early at 9 days post-surgery.

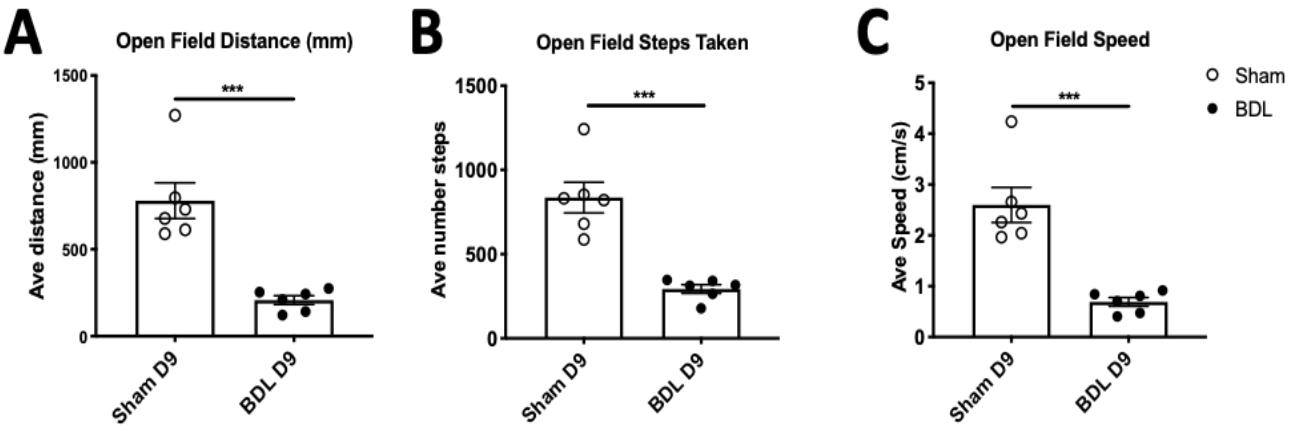

Figure 20. Open field data indicates significant reductions in distance travelled (A), step taken (B), and speed of travel in BDL mice by day 9. . N=6 Sham animals N=6 BDL day 9 animals. Data represented as mean +/- SEM, statistics T.TEST.

3.4.2.6. Bile duct ligated mice show spatial memory deficit by day 10 post-surgery

BDL animals shows a significant reduction in spatial memory by day 10 (n=9) compared to sham (n=8) animals when using hippocampal dependent task, the Y maze, and proportional time spent in novel arm as the primary output. Sham animals exhibit naturalistic exploratory behaviour when in the Y maze, and spent the majority of their time exploring the novel space as seen in the heatmaps as has been long recorded

natural test behaviour (Dember and Fowler 1959). In the example heatmaps shown where A1 is the novel arm (FIG 21A) sham animals spent average of 80% of trial time in the novel arm, On the other hand, BDL animals spend an average of 39% of the trial time in the novel arm (FIG 21B, C) a number only marginally above statistical probability. The heatmaps (FIG 21A and B) indicate example movement pattern of each group when A2 is the start arm, and A1 is the novel arm.

Though latency to entering novel arm (FIG 21E) showed greater variation in the BDL groups, there is a trend towards these animals taking longer to enter the novel space. This is likely to be due to animals with impaired memory not recognising the space as novel, despite spatial memory cues at the end of each arm (FIG 21D). This may also be indicative of decreased motivation in the BDL animals (Wright and Conrad 2005) perhaps due to fatigue symptoms.

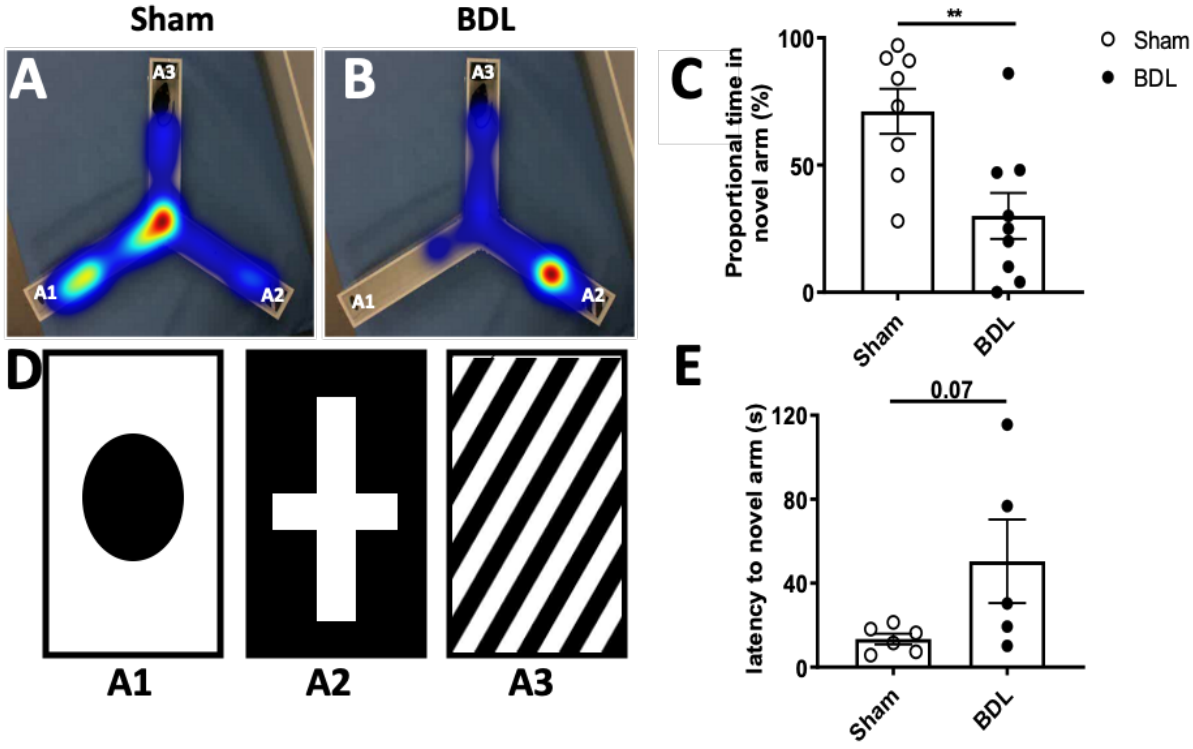

Figure 21. Y maze data indicates a visual-spatial memory impairment in BDL animals by day 10. Heatmaps showing (A) sham and (B) BDL movement in the Y-maze. (C) BDL mice show reduced time spent in the novel arm (D) diagram showing schematics present at the end of each arm of the maze. (E) BDL animals showed longer latency to entering the novel arm (P=0.07). N= 8 sham N=8 BDL. Data represented as mean +/- SEM, statistics T.TEST.

3.4.2.7. Bile duct ligated mice show aberrant astrocyte interactions at the blood brain barrier

In order to look at specific changes at the vessel, a step wise protocol of techniques was employed (FIG 22C) from a microscopic (confocal microscopy) through to looking at specific cell-cell interactions at a nanoscopic scale (electron microscopy).

Hippocampal astrocytes, the primary modulatory glial cell of the BBB significantly proliferated in BDL mice by day 10 when investigated by histology (FIG 22A). This suggests a loss of integrity at the barrier, leading to astrocyte activation and proliferation (astrogliosis). Super resolution imaging of astrocyte specific behaviour at the vessels (FIG 22A), stained again by GFAP (green) and vessels by RecA (red) indicates a change in morphology to an activated state, and a reduction in coverage at the vessel itself. Activation of astrocytes is most easily characterised by swelling of the soma and processes and increased expression of intermediate filament proteins such as Glial acidic Fibrillary protein labelled here (Pekny and Nilsson 2005). It represents the universal response of an astrocyte to noxious stimuli, such as infiltrating inflammatory cytokines or damage at the vessel.

Flow cytometry enabled a cell specific assessment of microvascular endothelial cells that make up the BBB. When labelled using Sca1, microvascular endothelial cell numbers were significantly reduced in BDL animals at day 10 (FIG 22D), indicative of BBB damage and adding to the mounting evidence of BBB dysfunction in this model.

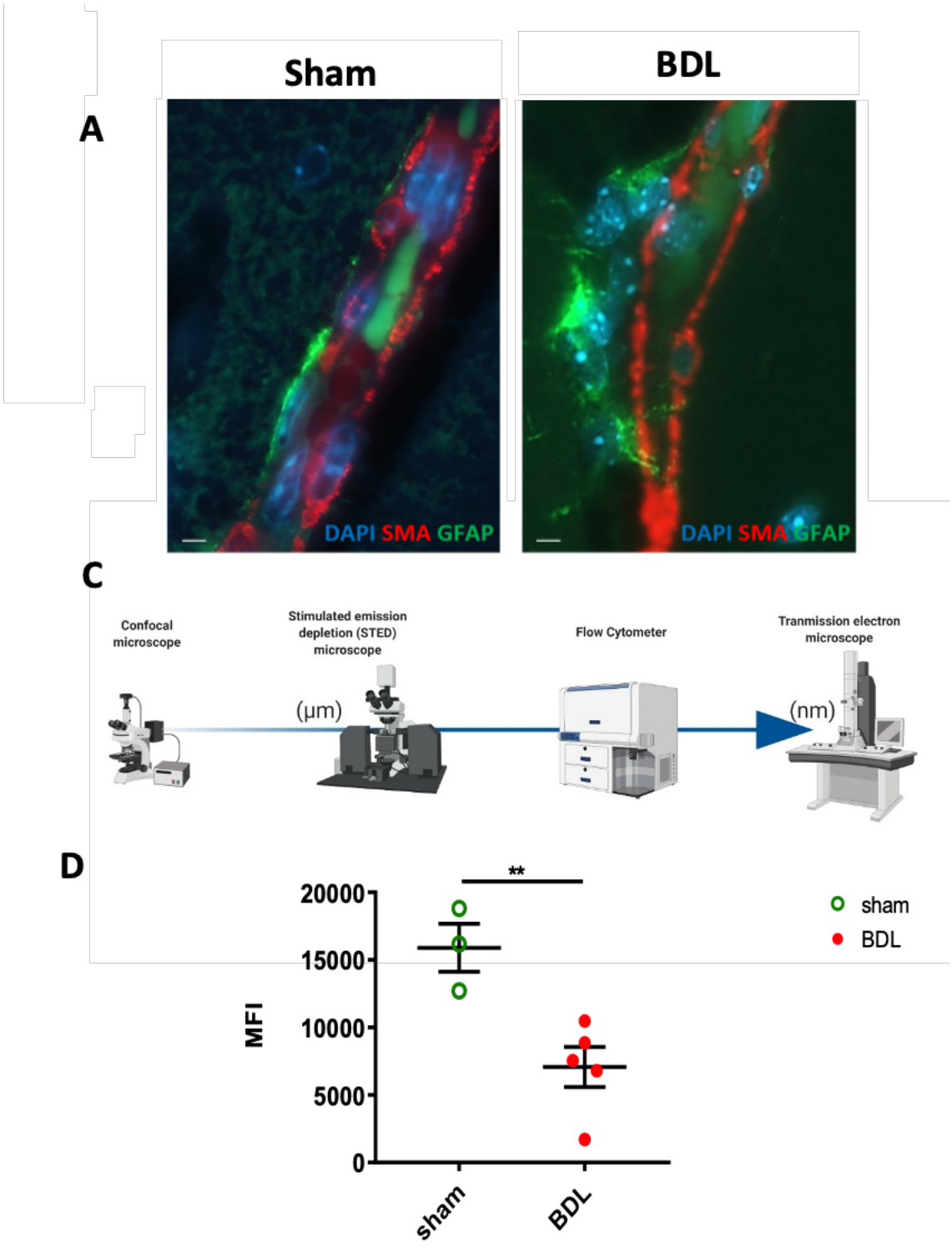

Figure 22. Immunohistologcial and flow cytometry assessment of BBB. (A) Super Resolution image of blood vessels in the DG of Sham and BDL animals. BDL animals show proliferative and poorly attached GFAP+ astrocytes in green. ReCA stained vessel in red. (C) a workflow diagram of the BBB work (D) Flow cytometry data showing a reduction in Sca1+ endothelial cells in BDL amimals. N=3 Sham animals N=4 BDL. Scale 20µm. Data represented as mean +/- SEM and statistics are T.TEST. The image in (A) was taken during my masters.

3.4.2.8. Bile duct ligated mice have reduced astrocyte coverage at the blood brain barrier

Electron microscopy (EM) revealed reduced astrocyte coverage at the blood vessels (FIG 23E), and showed gaps between astrocytes and the vessel, likely caused by astrogliosis and scars forming between the vessel surface and astrocyte. Astrocyte coverage at the vessel was reduced from 83% to 55%, a large reduction.

This is supported by histological analysis indicating astrocyte proliferation (FIG 25A), and evidence from EM data shown here. Morphological changes can be seen in the EM cross sectional images, where sham (A) shows astrocytes (white arrows) tightly associated with the vessel with thin end feet enveloping the diameter of the vessel. Conversely, in the BDL image (B) astrocytes are more in number, swollen, and detached from the vessel in a manner seen in other EM studies (Haley and Lawrence 2016). This data indicates that there is a loss of astrocyte coverage; ergo increased permeability at the BBB in the BDL model.

Endothelial wall thickness was also assessed using EM in the BDL model. There were no significant differences in either circumference (FIG 23D), or pericyte number (FIG 23F). However, the decrease in endothelial wall thickness (FIG 23C), may be related to the loss of MFI in hippocampal endothelial cells observed in flow cytometry data. A lack of differences in the circumference at vessels confirms that the vessels sampled were of comparable size, and so the effects seen in the astrocyte population (for example the astrocyte count), are likely to be due to the pathological state and not biases in sampling.

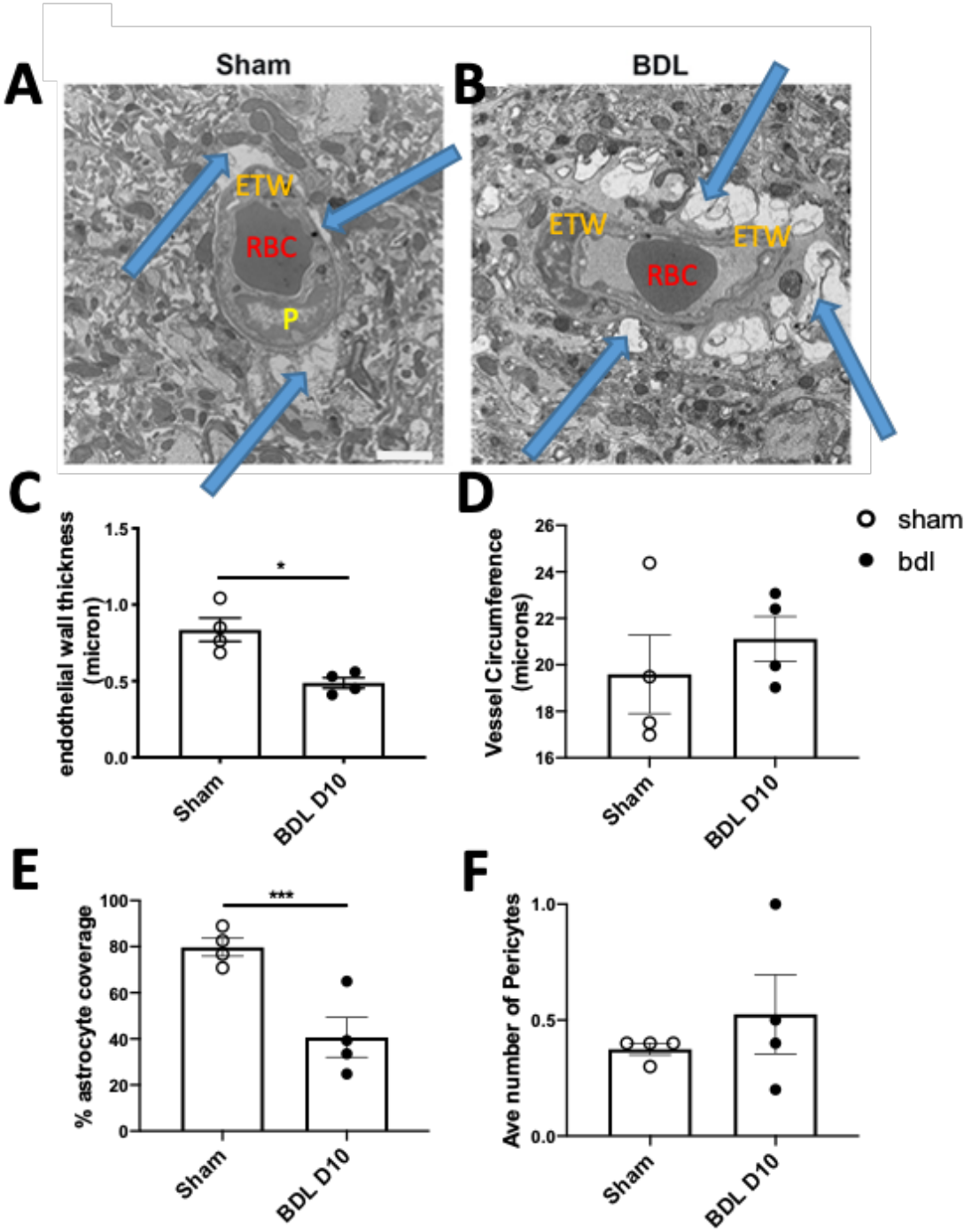

Figure 23. Transmission electron microscopy data for sham and BDL day 10 mice. Histology shows astrocyte endfeet surrounding (A) sham and (B) BDL day 10 animals. (C) endothelial wall thickness was significantly reduced in BDL day 10 animals. (D) vessel circumference and (F) average number of pericytes was comparable between sham and BDL day 19 animals. (E) percentage astrocyte coverage was significantly reduced in day 10 BDL mice. . Endfeet are denoted by blue arrows, RBC denotes red blood cell, ETW denotes endothelial wall, P denotes pericyte. N=4 sham and N=4 day 10 BDL animals. Scale = 2 microns. Data represented as mean +/- SEM, statistics T.TEST. This data was presented as a part of my masters thesis.

3.4.2.9. Magnetic Resonance imaging assessment of Blood-Brain Barrier breakdown in BDL

BDL animals showed an increased contrast in the hippocampal region after gadolinium injection (FIG 24A, C). This indicates a higher amount of gadolinium contrast agent is able to enter the brain in the BDL animals, and thus that the BBB is leaky in the hippocampus of the BDL group. Despite only having 3 animals per group, there seems to be an increase in contrast in the BDL animal group, though this does not reach significance. This data was generated with help from Andrew Blaimire and Saimir Luli.

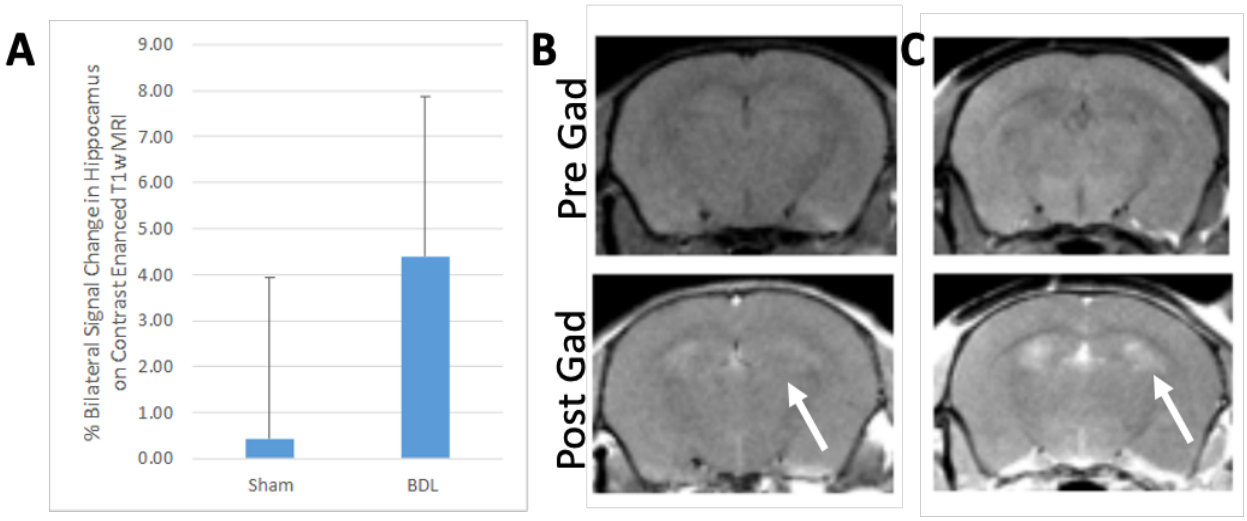

Figure 24. (A) Gadolinium enhanced T1 weighted MRI indicate a leaky blood-brain barrier in BDL animals. (B) Pre and post gadolinium injection shows little contrast change in sham animals. (C) Contrast change can be seen in BDL day 10 animals. N= 3 sham and N=3 BDL day 10 animals. This data was generated with help from Andrew Blaimire and Saimir Luli.

3.4.2.10. BDL mice show some neuroinflammation by day 10

Hippocampal cell type changes were assessed in the BDL cohort harvested at day 10. In the dentate gyrus, an area where we have found BBB breakdown (FIG 23, 24) histological analysis indicates a significant proliferation of astrocytes, indicative of

neuroinflammatory response in this area (FIG 25A). As well as proliferating, astrocyte adopt a 'reactive' phenotype (FIG 25C) characterised by enlarged cell body and increased thickness of processes with fewer sweeping processes (Wilhelmsson, Bushong et al. 2006) instead of the inactivated astrocytes seen in sham animals (FIG 25B).

Astrocytes do not have a proliferative nature, and in response to insult ordinarily increase in number around 2-3-fold. Here astrocytes are seen to proliferate 1.5x as an average, corroborating the literature, and also indicative of early (pre peak) neuroinflammatory response.

Astrocytes activate in response to noxious stimuli or cytokines such as TNF-α. Often astrocytes and microglia activate in tandem, and can influence the activation status and phenotype of one another in a cytokine dependent manner (Liddelow, Guttenplan et al. 2017). Microglia are also proliferating and activating in BDL by day 10, and show a trend towards significance ($p=0.09$) (FIG 25D). In the BDL animals' microglia look by eye to show an ameboid phenotype and ramification (densifying and contracting of processes) (FIG 23F) when compared to the sham surgery group (FIG 25E), however this needs quantification.

In order to investigate the specific activation phenotype of the microglia, FACs was employed. FACs analysis showed the total number of macrophages in the hippocampus was hugely increased (FIG 25G). Cells were sorted according to F4/80 positivity (macrophage marker) and phenotyped according to iNOS (M1) and Arg1 (M2) expression. M1 phenotype microglia were significantly increased in BDL animals, as expected (FIG 25I). However, these was also a significant increase in Arg1+ microglia, indicative of a restorative M2 macrophage phenotype (FIG 25J). When calculated as a percentage of all macrophages, the BDL animals had a total of 54% M1 activated macrophages and 46% M2 activated macrophages, in comparison to sham animals who had 58% M1 macrophages. This data indicates a diverse activation phenotype in the microglia, both inflammatory and resolutory.

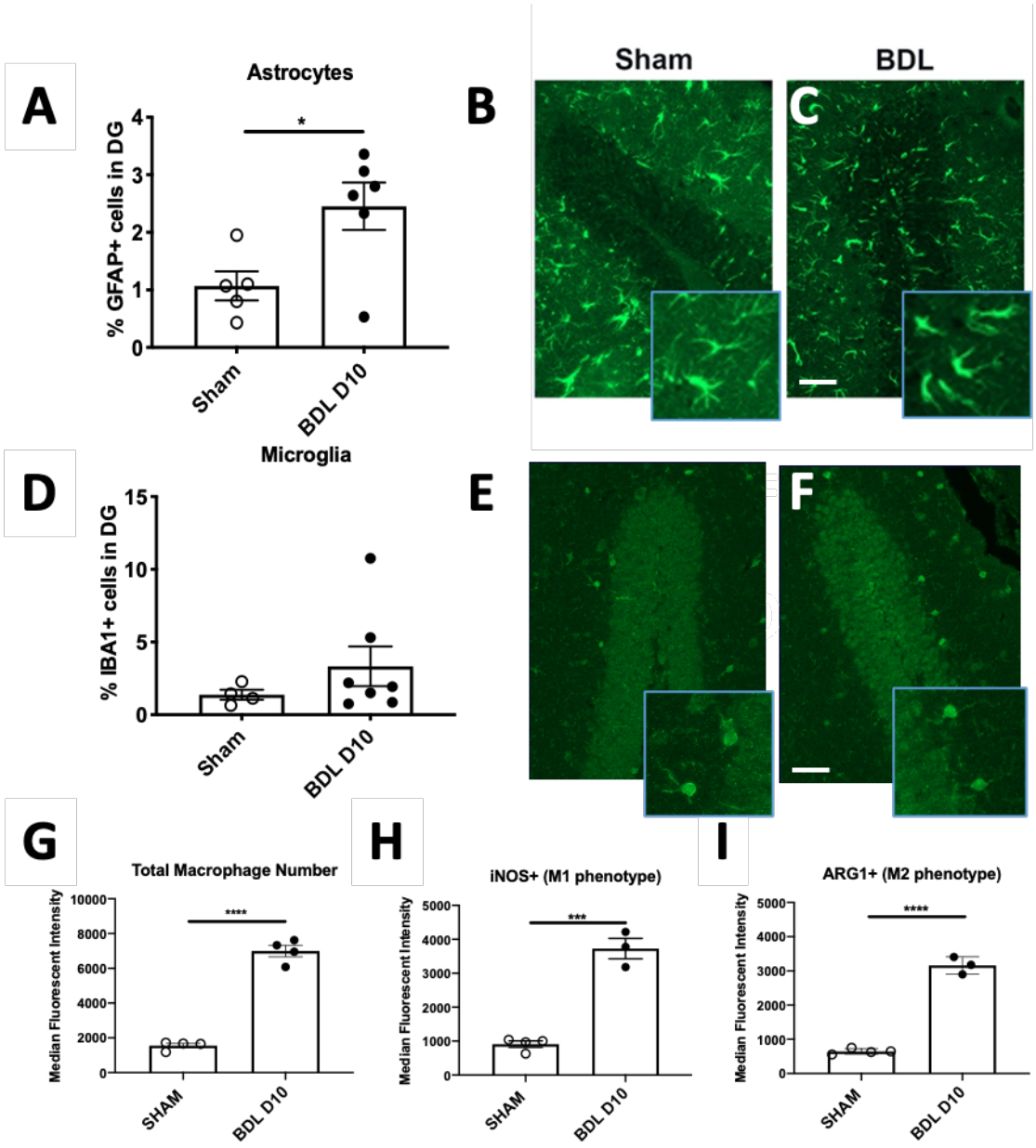

Figure 25. Immunofluorescent and fluorescence associated cell sorting for inflammatory cell types. (A) astrocyte number were significantly increased between (B) sham and (C) BDL day 10 mice. (D) there was no increase in microglia between (E) sham and (F) BDL day 10 mice. (G) inflitrating macrphage number was significantly increased in BDL mice. Both (H) M1 and (I) M2 macrophage phenotype number were increased. Histology N=5 sham N=6 BDL. FACs N=4 sham and N=4 BDL. Scale = 50 microns. Data represented as mean +/- SEM, statistics T.TEST.

3.4.2.11. BDL mice show damage to neuronal populations by day 10

Different neuronal and interneuron populations were assessed histologically for loss of positivity. Neurons within the granule cell layer (FIG 26A, B) were found to be significantly less NeuN+ in the BDL animals than in sham animals. NeuN expression can be modulated by a number of processes, usually NeuN is described as a pan neuronal marker, meaning all healthy neurons express it. A loss of neurons specifically within the granule cell layer has been shown to result in spatial memory deficit (Colicos and Dash 1996), indicating a mechanism for behavioural deficit in this model.

NeuN loss in the BDL animals often showed a similar pattern of staining loss in the inner granule cell layer and dentate gyrus crest (FIG 26C, G). The inner granule cell layer is where adult neurogenesis occurs, however we didn't see a reduction in SOX2 (immature neuron) expression here (FIG 26D, E, F). This may have been skewed by the SOX2 stain also picking up immature astrocytes in the early stages of their differentiation.

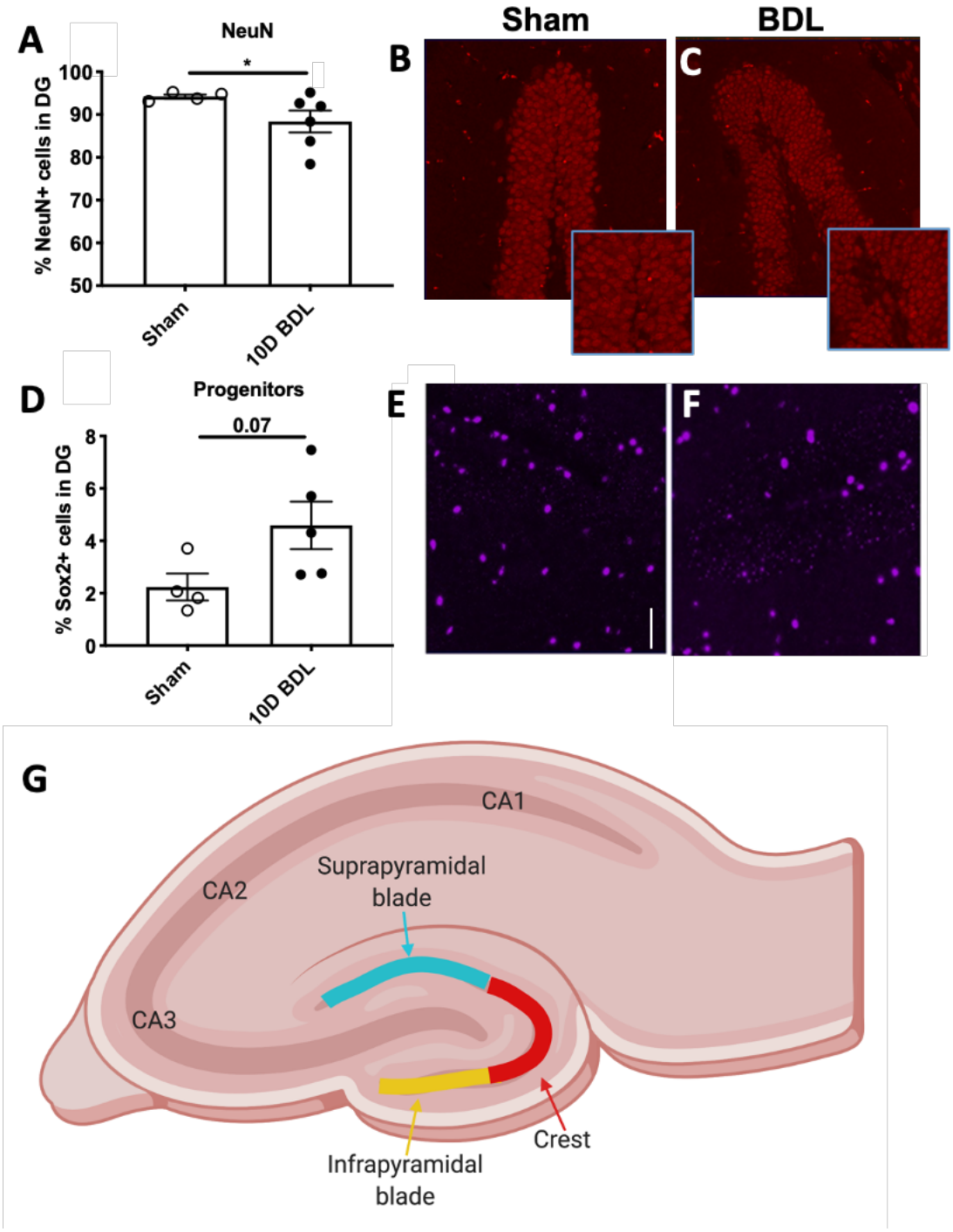

Figure 26. Immunofluoescent staining of Neuronal populations within the dentate gyrus. (A) Neun+ neurons were significantly reduced in Day 10 BDL animals. (B) sham animals showed intact staining, whereas (C) BDL showed areas of missing NeuN neurons. (D) Neural progenitors were increased in BDL group, this did not reach significance. (E) sham and (F) BDL staining SOX2+ progenitors looked similar. (G) diagram outlining subregions of the dentate gyrus. N=4 sham N= 6 BDL day 10 animals (one exlcuded in the Sox2 stain group). Scale = 50µm. Data represented as mean +/- SEM, statistics T.TEST.

3.4.2.12. BDL animals show neuronal senescence by day 10

Senescence is a process of cell cycle arrest, preventing the normal cellular function. When neurons become dysfunctional in response to cellular stressors such as oxidative stress DNA damage or SASP they enter a senescent state, losing ordinary function. Neuronal senescence was investigated in several ways in order to unpick phenotypic changes. Expression of checkpoint protein P21 RNA (how many neurons were producing P21 RNA and how much of it) was measured alongside Telomere Associated Foci (TAF) staining. An integrative approach taking into account both DNA damage via γ-H2AX and uncapping of telomeres, two intricately linked processes that occur in tandem (Hewitt, Jurk et al. 2012).

In BDL animals both the number of P21+ neurons, and the number of foci per neuron in the DG (FIG 27B and C) and CA3 (FIG 27E and F) were significantly increased, indicating a strong senescence phenotype in both regions. While the percentage increases of P21 expression in both regions were similar between sham and BDL, there were area differences between the DG and CA3 in the baseline level of senescence in the sham group. The average percentage of P21 RNA + neurons in the DG is 14% whereas in the CA3, this is 34%.

Neuronal populations in the CA3 have a high proportion of pyramidal cells. There are publications suggesting pyramidal cells in the CA3 are susceptible to oxidative stress (Cruz-Sánchez, Gironès et al. 2010), as well as further recent studies indicating that fast spiking basket cells in the CA3 are very sensitive to oxidative stress (Morishita, Cabungcal et al. 2015). Stress responses and resultant DDR in the CA3 may account for the higher levels of P21 RNA. TAFs show higher levels of DNA damage in BDL animals, and a higher percentage of TAF+ neurons (FIG 27G), and more than double the number of co-localising TAFs per neuron (FIG 27I).

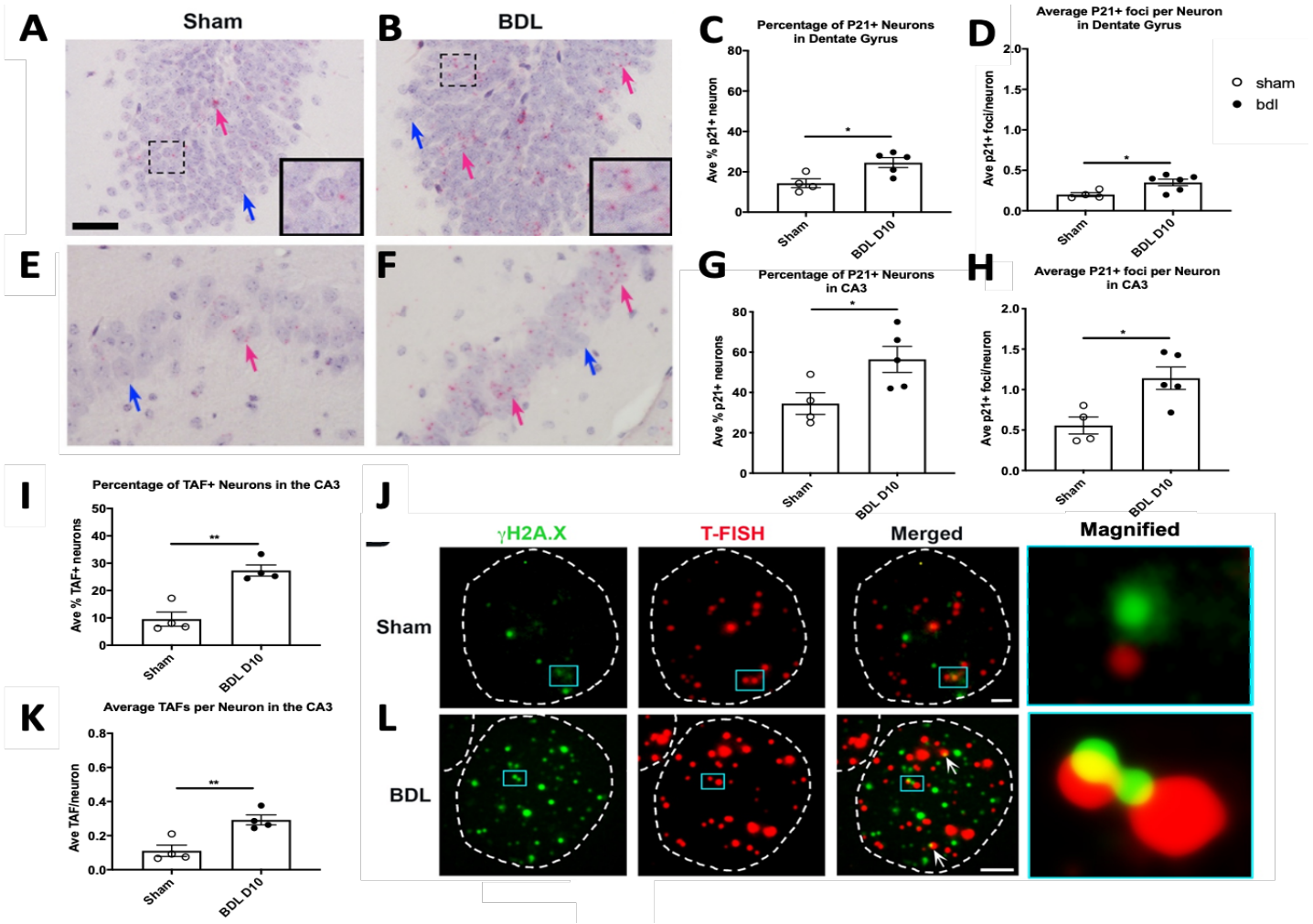

Figure 27. Neuronal senescence staining. (A) sham dentate gyrus showed less P21 RNA than (B) BDL. (C)Percentage of P21+ neurons and (D) AVG P21 foci were incereased in BDL animal dentate gyrus. (E) sham CA3 showed less P21 RNA than (F) BDL. (G) Percentage of P21+ neurons and (H) AVG P21 foci per neuron were increased in BDL. (I) Percentage of Telomere associated foci (TAF) was also increased in CA3 of (L)BDL animal compared to (J) sham. (K) AVG TAFs per CA3 neuron was also increased in BDL day 10 animals. Scale P21 = 50 microns. Scale TAF =1.5µm (Sham), 1.2µm (BDL). Data represented as mean +/- SEM, statistics T.TEST. Staining oerformed by Diana Jurk, analysis performed by me

3.5. A Summary of Key Findings from Chapter 3

- BDL causes deficits in visual – spatial memory (Y maze) and fatigue (Open Field) by day 10 when compared to Sham operated animals.

- There are key changes to BBB morphology (EM, STED imaging) and permeability (MRI) by day 10 BDL, which together are highly indicative of loss of BBB function in the BDL mice leaving the brain permeable to toxins produced during cholestasis.

- There are key changes to cell types within the brain by day 10. NeuN positivity is lost, and a significant portion of neurons within the CA3 and DG have a senescent phenotype, an outcome which may contribute to the cognitive deficit.

- Inflammatory cell types microglia and astrocytes are upregulated in the hippocampus in BDL animals by day 10, indicative of neuroinflammation.

3.6. Conclusions

Results from this chapter clearly show cholestasis causes cognitive impairment as well as hepatic damage in the BDL model. The liver phenotype seen in the mice has been well characterised by other groups (Abshagen, König et al. 2015) and is recapitulated in this experimental data set. Myofibroblast activation and proliferation (FIG 17A), collagen deposition (FIG 17D), DR (FIG 17G), and senescence of hepatocytes and non-parenchymal cells (FIG 18A, B) all occur by day 10. This model is severe, with quickly progressing cholestasis. This is also indicated by fibrosis and DNA damage (FIG 18C, D) by day 10, and also the increased presence of liver enyzmes such as AST (FIG 16A), which is released from stressed hepatocytes. There is also a significant increase in ALP (FIG 16B), another enzyme released upon damage to the ducts and increases step wise in relation to ductular damage, allowing tracking of the disease progression in these BDL animals. Though BDL

represents a severe cholestatic model, by day 10 mice haven't yet developed cirrhosis (Tag, Sauer-Lehnen et al. 2015). Utilizing this earlier end-point in our study allowed us to assess pre-cirrhotic changes to cognitive function.

The presence of a phenotype of senescence is corroborative with human data showing that cholestatic liver diseases such as PBC induce a phenotype of senescence in the ductular cells (which we see in our studies as non-parenchymal cell fraction), and in peri-ductular hepatocytes (hepatocyte fraction) (Sasaki, Ikeda et al. 2005). These senescent cells in patients are found to undergo both telomere shortening and DNA damage (Sasaki, Ikeda et al. 2008). In our model we have found evidence of DNA damage around the ducts (FIG 18C), again in keeping with reported changes in the cholestatic liver in humans.

Behavioural deficits are yet to occur by day 6 (FIG 13), but are prominent by day 10 (FIG 20, FIG 21), with both activity and spatial memory domains affected. This correlates with fatigue seen commonly in PBC patients (Newton, Bhala et al. 2006) and also with visual spatial deficit seen in patients (Newton, Hollingsworth et al. 2008). Therefore, the BDL model goes some way to recapitulating cholestasis induced cognitive decline, and its associated phenotype of fatigue. Cognitive phenotype has been associated with physical changes in the hippocampus in patients (Mosher, Swain et al. 2018). Changes in cognitive function in cholestatic mice using hippocampal dependent tasks allows a measurement more comparable to the human phenotype.

Results from this chapter indicate a powerful circulating inflammatory phenotype, both from inflammatory cytokines (FIG 19) and macrophage activation (FIG 25). There is an increase in activated macrophages within the brain itself (FIG 25). Previous publications show monocyte recruitment to the brain leads to signaling to and activation of resident microglia (Kerfoot, D'Mello et al. 2006) or that circulating monocytes themselves can infiltrate the brain through a compromised barrier (D'Mello, Le et al. 2009). Evidence from our data of BBB dysfunction lends itself to the idea of circulating immune infiltration.

By day 10 astrocytes possess an abhorrent phenotype at the barrier (EM fig, STEM at BBB), and are activated leading to proliferation (FIG 25A) when counted both at the barrier and

generally within the dentate gyrus of the hippocampus. Microglia become activated and change phenotype, attracting more astrocytes via the inflammatory feedforward loop, modulated chiefly by TNF-α (D'Mello, Le et al. 2009). In our models we saw a significant increase of the pro-inflammatory cytokine's TNF-α alongside other inflammatory cytokines such as IL-6 (FIG 19). In turn the neuroinflammatory processes induce dysfunction and leakiness at the barrier. The hippocampus has been found to be more susceptible to BBB damage, both in normal age and pathological conditions such as traumatic brain injury (Montagne, Barnes et al. 2015). This may explain why breakdown in the hippocampus is affected in diseases such as cholestatic disease caused by a circulating inflammatory phenotype.

By day 10, NeuN expression appeared to be lost in some granule cells in the crest of the dentate gyrus (FIG 26A). Despite NeuN expression being lost, the cells remained DAPI positive, pointing towards a loss of function rather than cell death. This has been reported in disease states due to apoptosis, and can lead directly to a cognitive deficit (Colicos and Dash 1996). When we investigated the senescence phenotypes of the granule cells, we found large increase in both the expression of p21 RNA (FIG 27 C, D, G, H), and the presence of DNA damage foci at uncapped telomere ends, named Telomere associated foci (TAFs) (FIG 27I, K). In BDL mice P21 RNA was present in more neurons in the DG (35% neurons) and CA3 (50% neurons) areas key in spatial memory (FIG 27C, G). In addition, there were more RNA copies in these regions in BDL mice than in Sham operated animals (FIG 27D, H). This senescence phenotype is a candidate to be the underlying cause of the behavioural deficits experienced by BDL mice.

Currently there are no studies published linking senescence of peripheral organs with induced senescence within post mitotic neurons in the brain. In ageing, multiple organ senescence occurs, primarily due to pro inflammatory cytokine secretion, termed 'inflammaging' (Franceschi, Bonafè et al. 2000). In our data we have shown that BDL animals show increased senescence in the hippocampus of the brain as well as within the liver. We also see huge increases in circulating inflammatory cytokines, detected by MSD using serum samples. Particularly cytokines such as IL-6, which are known to be secreted from senescent hepatocytes (Irvine, Skoien et al. 2014) and forms a part of the SASP.

We have also demonstrated the presence of breakdown of the normal function of the blood brain barrier. A non-functional or leaky barrier allows inflammatory cytokines infiltration and to exertion of effects in the brain, infiltrating key regions such as the hippocampus, and leading to the induction of senescence within the neurons there. In tandem, the induced activation of brain resident immune cells such as microglia and astrocytes, causes neuroinflammatory cascade, a damaging process mediated by M1 microglia. Due to intricate coupling at the neurovascular unit, astrocytes that are activated into an A1 phenotype induced by microglia have damaging effects at the neuron, reducing synaptogenesis, neuronal health and can even induce neuronal death (Liddelow, Guttenplan et al. 2017). Here, by unknown mechanisms- neuroinflammatory, activated astrocytes have induced a senescent phenotype in hippocampal neurons, possibly via SASP signaling within the hippocampus (figure 28).

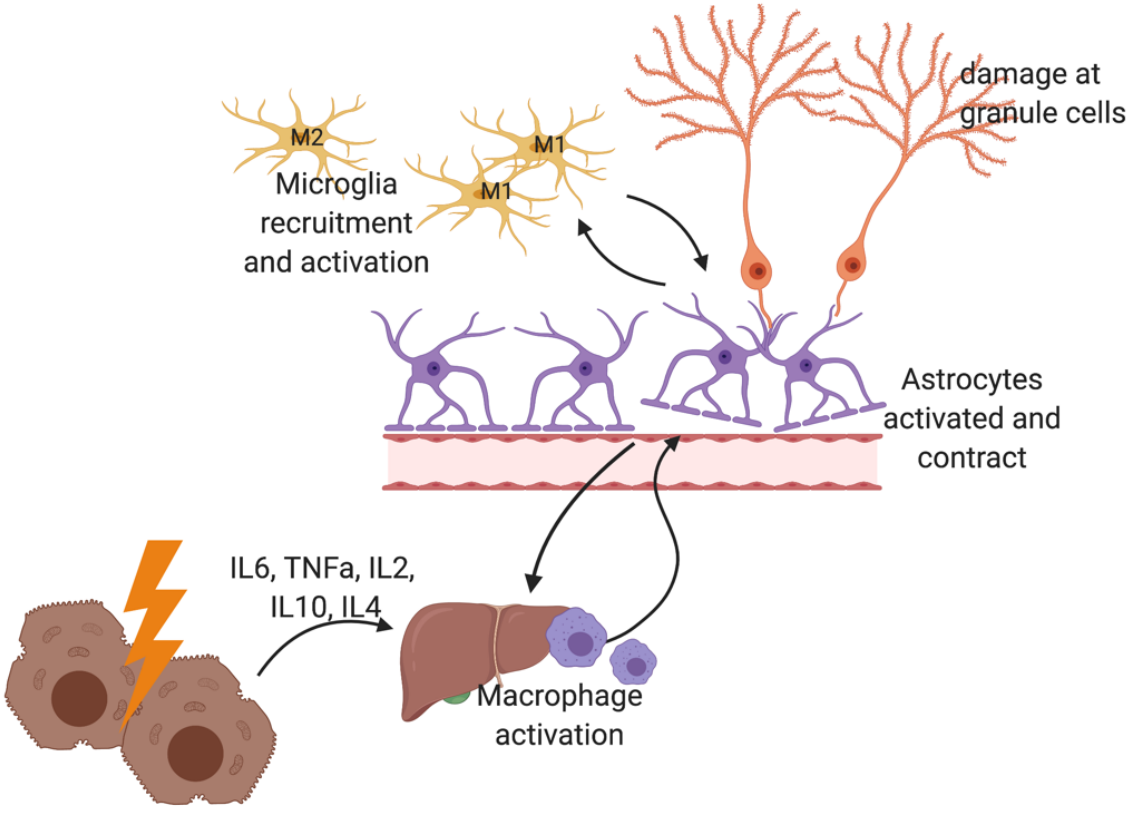

Figure 28.Schematic outlining possible mechanism of action of neuron damage within the hippocampus.

4. Chapter Four – The effects of Primary Biliary Cholangitis drug treatments on cognitive symptoms during BDL-induced Cholestasis

4.1. Introduction

Thus far, the search for effective therapeutics for cognitive symptoms in PBC has been fruitless. In fact, as currently used no treatment – both drug or liver transplantation - improves the cognitive symptom set at all (Pells, Mells et al. 2013). As transplantation improves other features (liver biochemistry, fibrosis) and effectively 'resets' the disease course (recurrence rates are 1 in 3), it seems likely then that cognitive symptoms possess an intrinsically linked but distinct pathological mechanism. Symptoms are likely triggered by the liver pathology but once kick started can self-aggravate and continue despite resolution of hepatic insult. Therefore, the failure of current therapy may be related to a lack of direct action on the pathological processes within the brain.

There are only two drug therapies currently approved for the treatment of PBC. The first is the first line therapy Ursodeoxycholic acid (UDCA) which has a high proportion of none responders and second-line therapy Obeticholic Acid (OCA) a more recently FDA approved (2016).

4.1.1. Ursodeoxycholic Acid (UDCA)

UDCA is a naturally occurring bile acid, first approved for use in 1997. It works by increasing bile flow, thereby diluting the bile acids present in the body and reducing natural production of bile acids from the bile ducts via negative feedback, as well as weak anti-oxidant properties. The use of UDCA is associated with improved liver biochemistry, increased survival and reduction in liver transplants.

Although it does not provide a cure, UDCA improves transplant free survival at time points of both 10 and 35 years (Poupon, Bonnand et al. 1999, Floreani, Caroli et al. 2011). UDCA is the currently recommended first treatment option for PBC treatment by the European Association for the Study of Liver (EASL) guidelines (13-15 mg/kg/d) (EASL 2009). Despite improved liver biochemistry (serum AST ALT and ALP), 40-50% are classified as unresponsive to UDCA therapy and therefore have little resulting therapeutic benefit. To date, there is little understanding of the pathological differences between UDCA responders and non-responders. Prognostic outcomes vary hugely between the groups, with UDCA non -responders representing an at-risk patient population, with a greater likelihood of faster disease progression (Corpechot, Abenavoli et al. 2008, Kuiper, Hansen et al. 2009).

4.1.1.1. UDCA Mechanism of Action

UDCA works by three main mechanisms. The presence of UDCA has been found to stimulate biliary secretion and therefore reduce bile acid toxicity in both animal models (Kitani, Ohta et al. 1985) and patients (Jazrawi, de Caestecker et al. 1994). Therefore, many of the beneficial effects seen in those treated with UDCA in part come from enhanced elimination of toxic compounds from the liver, in particular hepatocytes.

Though the exact anti-cholestatic mechanisms of UDCA remain unclear, hepatoxic effects during cholestasis are counteracted by stimulating mechanisms of biliary excretion. UDCA can stimulate the expression of the transporter proteins required for biliary secretion through the canicular membrane (Jazrawi, de Caestecker et al. 1994) in humans, it is known to encourage insertion of transporters in the canicular membrane such as Mrp2

and Bsep in rodents, thereby stimulating excretion and removal of toxic compounds from the liver (Beuers, Bilzer et al. 2001, Dombrowski, Stieger et al. 2006).

Other postulated effects include reducing the toxic effects of bile acids on the phospholipid bilayer by increasing the hydrophobic bile acid load in the system (UDCA is the most hydrophilic bile acid) and thereby reducing cell death and expelling hydrophobic damaging bile acids such as lithocholic acid *in vivo* (Takano, Ito et al. 1994).

Several *in vitro* experiments have also indicated a likely anti-apoptotic role for UDCA, through preventing mitochondrial depolarization and reducing the production of the resulting ROS in hepatocytes (Rodrigues, Fan et al. 1998). UDCA has also been found to stimulate pro-survival signals in injured hepatocytes through cyclic adenosine monophosphate (CAMP) (Webster and Anwer 1998) or nuclear factor kappa-light-chain-enhancer of activated B cells (NF-κB) mediated mechanisms.

4.1.2. Obeticholic Acid (OCA)

The Farnesoid X Receptor (FXR) agonist OCA was FDA approved in 2016 following the reported ALT improvements in the large scale POISE study (Nevens, Andreone et al. 2016), becoming the first drug approved for use in the treatment of PBC in nearly 20 years. The largest reported adverse outcome of the trial was pruritis, which continues to be the most commonly reported side effect and reason for drug discontinuation. Currently the prescription guidelines of OCA state usage only in conjunction with UDCA in cases of non-response (after 1 year follow up on UDCA) or alone in rare cases of UDCA intolerance (Hirschfield, Dyson et al. 2018).

4.1.2.1. OCA Mechanism of Action

A series of conducive mechanisms have been reported for OCA pharmacology. It has reported anti cholestatic, anti-inflammatory and anti-fibrotic effects in a variety of diseases (Mudaliar, Henry et al. 2013, Hirschfield, Mason et al. 2015), and is currently

undergoing the FDA approval process to be the first drug treatment available for the fibrosis induced during non-alcoholic steatohepatitis (NASH), following positive results from the REGENERATE study (Younossi, Ratziu et al. 2019).

OCA is a semi-synthetic 6-ethyl derivative of natural chenodeoxycholic acid (Pellicciari, Fiorucci et al. 2002) and potent FXR-receptor agonist, binding with an affinity 100x stronger than the natural ligand CDCA (De Magalhaes Filho, Downes et al. 2016). The FXR receptor provides a powerful therapeutic target against PBC due to its regulation of bile flow (discussed in chapter One). Therefore, FXR can act within the liver stimulating biliary excretion of toxic bile acid compositions through mechanisms similar to UDCA. It can also work directly through stimulation of FGF-19 (human) or FGF-15 (mouse) release in the gut.

FXR activation of SHP (its downstream target) has been shown to have anti-fibrotic effects *in vivo* and *in vitro* (Fiorucci, Antonelli et al. 2004), with FXR agonists such as OCA preventing the onset of fibrosis directly through inhibiting collagen gene expression in HSCs. It also influences inflammatory processes within the liver. FXR KO mice have been shown to aberrant cellular processes, triggering inflammation and the development of tumours (Yang, Huang et al. 2007). Follow-up research implicates a direct modulatory effect via NF-κB agonism, implicating FXR as a master hepatic regulator of inflammation (Wang, Chen et al. 2008). The identification of a role for FXR key immunomodulatory implicates FXR and its agonists as key therapeutic targets in a number of diseases.

4.1.3. Bezafibrates (BZ)

Bezafibrate is one of the fibrate family of peroxisome proliferator-activated receptor-α (PPARα) agonists (though studies indicate secondary effects on both PPARγ and PPARδ) that are currently being investigated for use in PBC. The fibrate drug class have been approved for medical use since 1978 but are not currently approved for use in PBC.

Patients trials combining UDCA and Bezafibrate treatment have shown promising improvements in key prognostic indicators such as liver biochemistry (AST/ALT/ALP) (Corpechot, Chazouillères et al. 2018, Agrawal, Majeed et al. 2019), and need for transplantation (Corpechot, Chazouillères et al. 2019) when compared to UDCA monotherapy. This makes Bezafibrate the most likely drug candidate to be next approved for use in PBC.

4.1.3.1. Bezafibrate Mechanism of Action

Bezafibrate works on PPARs, a nuclear receptor family that are abundant in the liver. It exerts many of its pharmacological effects on PPAR-α, which is highly expressed in hepatocytes. However, as previously mentioned, effects are also propagated secondarily through PPAR-δ and PPAR-γ. PPAR-δ is equally distributed through various liver resident cell types, such as hepatocytes, cholangiocytes, Kupffer cells, and stellate cells whilst PPAR-γ exists largely in Kupffer cells.

PPARs are classically known as lipid lowering drugs and are used for treatment in conditions such as atherosclerosis. Fibrates are able to increase fatty acid oxidation, leading to a reduction in low-density lipoprotein (LDL) in plasma and triggering a reduction in LDL-cholesterol levels (Staels, Dallongeville et al. 1998).

In the context of cholestatic disease, fibrate action through PPAR-α downregulates processes of BA synthesis by inhibiting key BA synthesising enzymes cytochrome P450 cholesterol 7A1-hydroxylase (CYP7A1) and cytochrome sterol 27-hydroxylase (CYP27A1) (Post, Duez et al. 2001). Agonism at this receptor can repress CYP7A1 activity by 60%, reducing hepatocyte BA production.

Fibrates also have anti-inflammatory effects. Historically, this was thought to be through PPAR-α, which has long been shown to inhibit IL-6 production through repression of NF-κB (Delerive, De Bosscher et al. 1999). It now seems likely that this is only part of the story. More recent studies show promising anti-inflammatory effects and resulting reduction in cholangitis using drugs that effect PPARγ (Nozaki, Harada et al. 2013) and PPARδ

(Haczeyni, Wang et al. 2017). The latter of these induced a multi-centre clinical trial for the agent Seladelpar (Jones, Boudes et al. 2017).

4.2. Study Rationale

As currently used, no PBC treatment has any effect on cognitive symptoms, including transplantation. The following studies were designed to evaluate the benefit of early therapeutic intervention with drug candidates that are either approved for use in PBC (UDCA, OCA), or are being currently investigated in trial (Bezafibrate). There were assessed individually for efficacy and potential for cognitive benefit in a controlled and replicable animal model of cholestasis, that recapitulates the cognitive symptoms seen in humans.

Primary studies (highlighted as such) investigating UDCA and OCA efficacy used a prophylactic and therapeutic dosing schedule in order to assess time dependent effects on behavioural and histological changes. Clearly, in a patient prophylactic dosing is impossible. However, this allows us begin to pick apart the mechanism of cholestasis-induced cognitive decline, especially in the brain where it is not known clearly whether damage is cause via primary cascades within the brain (independent pro inflammatory signalling cascades triggered within the brain) or by secondary mechanisms (pro inflammatory signalling from the liver).

In later studies (bezafibrate studies and later OCA studies), drug dosing treatments were started on the day of surgery after prophylactic and therapeutic dosing schedules showed little discrepancy. The testing parameters of the studies were the same as the animal studies in chapter one liver histology, behavioural testing using Open Field and Y maze, hippocampal cell type histology, FACs, senescence staining, were all assessed.

UDCA and OCA were used in this study as they represent the current 1st and 2nd line therapies approved for use in patients. No drug treatments as currently used improves cognitive symptoms in patients, however models such as BDL provide a unique opportunity to explore mechanisms of cognitive decline and the ability (or inability) of

conventional, approved, drug treatments to impact disease course if used early in the disease process.

PPAR agonists are currently being explored for approval in patients and are an attractive therapeutic option for patients, in part due to itch experienced with other anti-cholestatic agents such as OCA. The experiments outlined in this chapter allowed a direct comparison between novel treatments such as Bezafibrate and current treatment options (FIG 29). This allowed in depth investigation into the effect of Bezafibrate with focus on cognitive symptoms, an avenue which has been little explored in previous animal models.

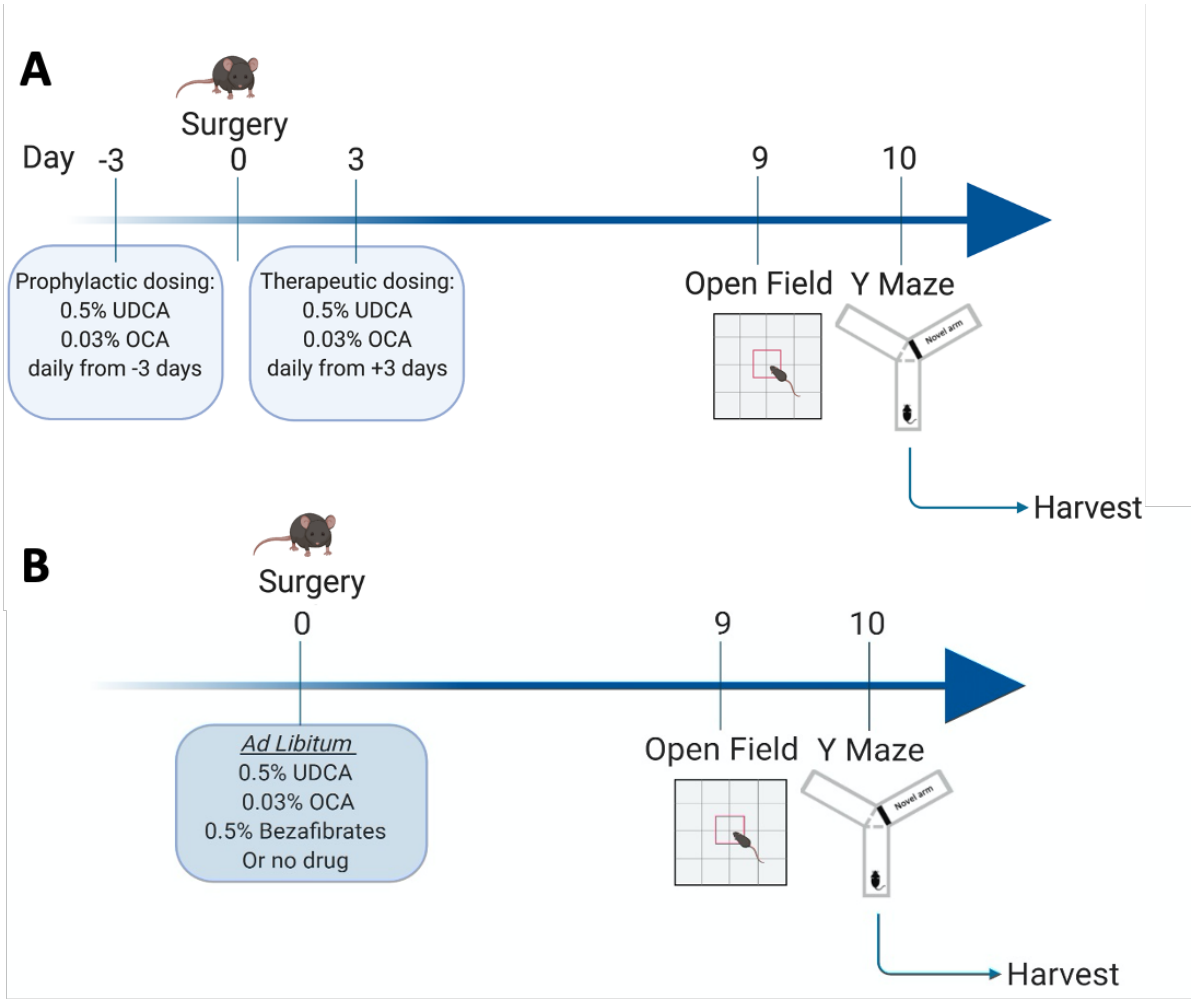

Figure 29 Experimental timelines for drug intervention studies (A) Prophylactic and therapeutic dosing schedule (B) ad libitum dosing schedule from day of surgery.

4.3. Aims of the Chapter

- To compare the therapeutic effects of administering either the first or second line PBC drug therapies UDCA and OCA in the BDL animal model of cholestatic liver disease.

- In addition, compare the therapeutic benefit of Bezafibrate, an experimental PPAR agonist to currently used therapies.

The therapeutic effects to be assessed are:

- Liver damage and histology (fibrosis, activated myofibroblasts, ductular proliferation)

- Cognitive function and memory (Y maze), fatigue (Open Field).

- Histology of neuronal and inflammatory (astrocytes, microglia) cell types.

- Neuronal Senescence within the hippocampus.

Additional experiments for treatments with positive therapeutic benefit:

- Functional and morphological assessment at the blood brain barrier

4.4. Ursodeoxycholic acid Study

4.4.1. UDCA shows little therapeutic benefit in liver histology outputs

This study replicates histological increase in collagens, activated myofibroblasts and DR previously reported in result chapter one. Treatment with 0.5% (500mg/kg) UDCA both prophylactically and therapeutically had little impact on liver histology in the BDL model. Activated myofibroblasts (α-SMA, FIG 30A) were still upregulated during BDL compared to sham, accompanied by an increase in collagen deposition (Picrosirius red) (FIG 30E). Both the parameters remained upregulated despite the UDCA treatment. Ductular reaction (CK19) was also still upregulated (FIG 30I), mirroring results from the previous study (Chapter Three FIG 17). UDCA prophylactic intervention did not improve the DR phenotype and may have marginally exacerbated the phenotype, possibly due to increase bile flow in the days prior to surgery. Therapeutic dosing of UDCA made no change to DR.

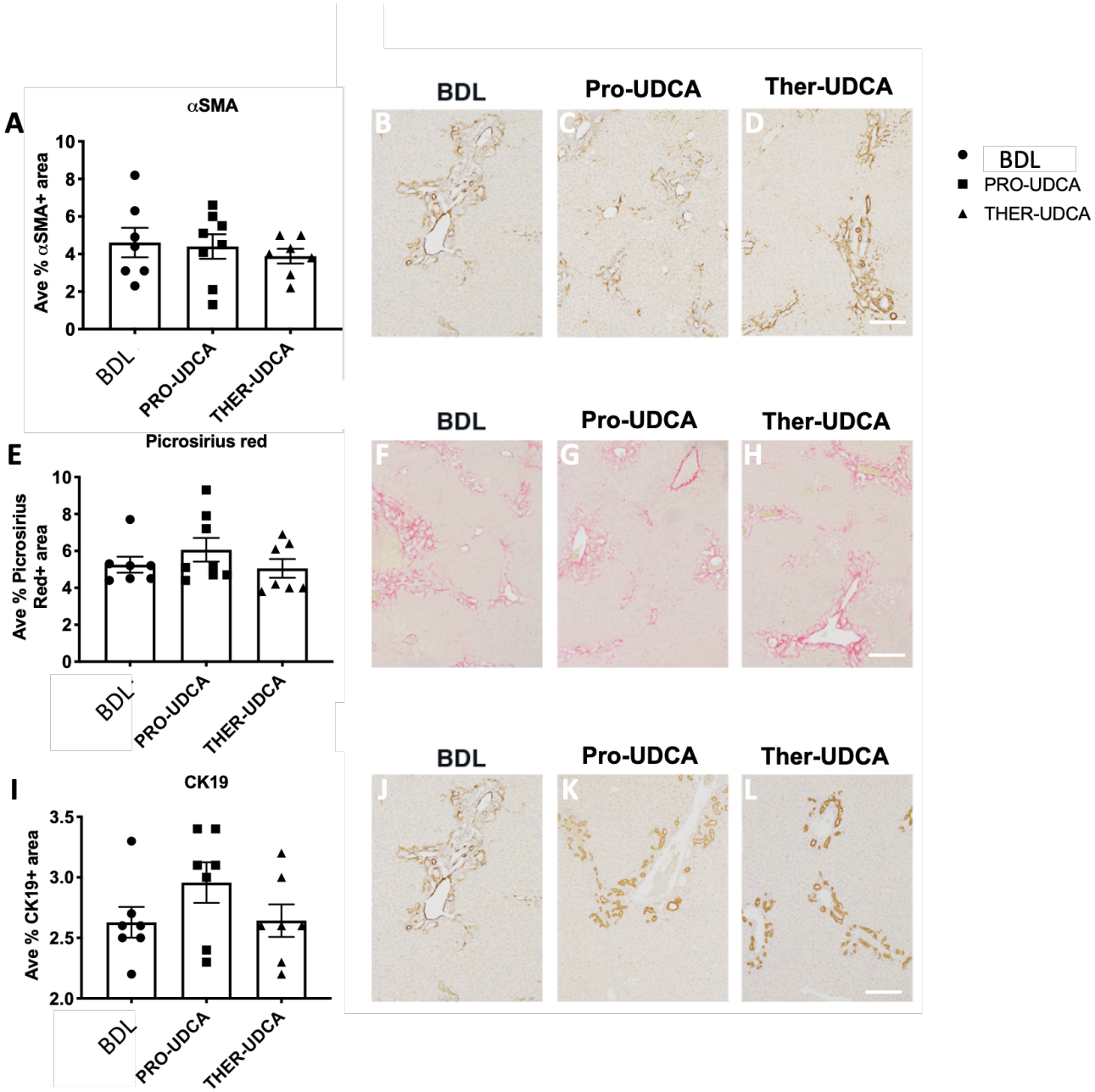

Figure 30.Liver histology from the UDCA dosing study. (A) percentage cover of activated myofibroblasts were similar between (B) BDL day 10, (C) prophylactic UDCA and (D) Therapeutic UDCA dosing. (E) fibrosis was similar been (F) BDL, (G) prophylactic UDCA and (H) therapeutic UDCA. (I) ductular proliferation was similar between (J) BDL (K) prophylactic UDCA and (L) therapeutic UDCA. Scale = 100µm. N=7 BDL, N= 8 pro UDCA N= 7 Ther UDCA. Data represented as mean +/- SEM. Statistics ANOVA.

4.4.2. UDCA Treatment did Not Affect Senescence in the Liver

Senescence staining in the liver showed no differences in p21 positivity in either non parenchymal cells (FIG 31A) or hepatocytes (FIG 31B) in the liver between BDL and either UDCA treated group. The non-parenchymal group showed a small trend towards decease with prophylactic UDCA treatment.

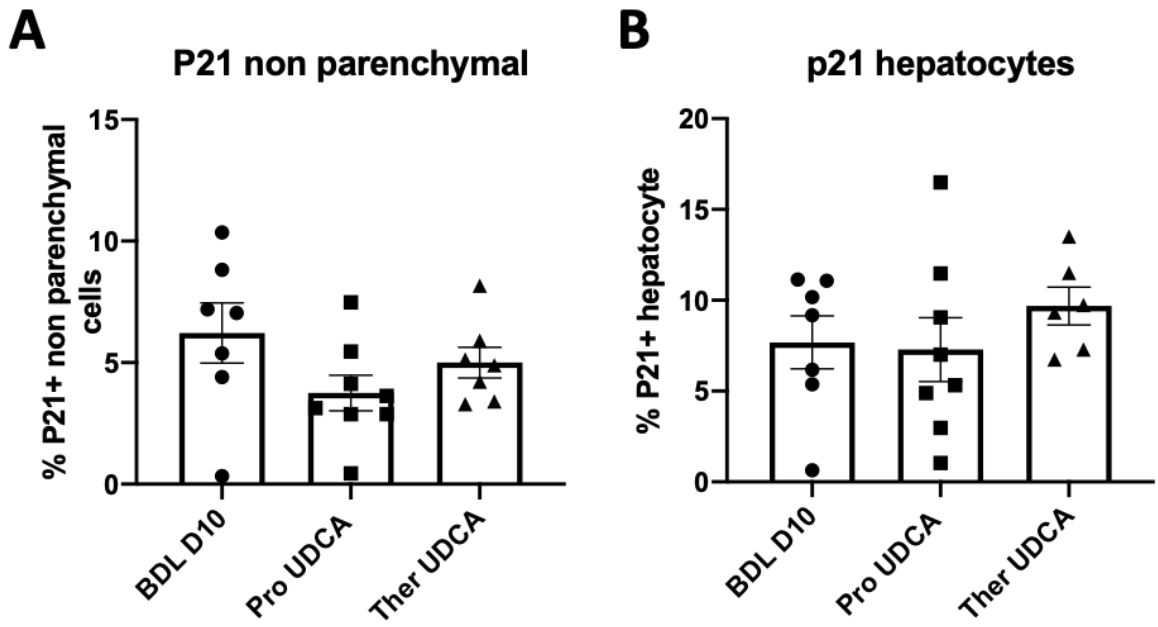

Figure 31. P21 stain from the liver of BDL untreated mice, or treated prophylactically or therapeutically with UDCA. (A) There were no differences in percentage of p21+ parenchymal cells in the liver (B) There were no differences in the percentage of p21+ hepatocytes between any group. N=7 BDL N= 8 prophylactic UDCA N=6 Therapeutic UDCA. Data represented as mean +/- SEM statistics ANOVA. Data analysed using HALO system with thanks to collaborators Thomas Bird and Christos Kiourtis.

4.4.3. UDCA Treatment had No Effects on Behaviour

Neither prophylactic nor therapeutic dosing with UDCA showed improvement in behavioural testing. Open Field steps taken were similar between all three groups (FIG 32A), though the data set is variable. This data illustrates the animal may still be experiencing fatigue, and therefore have no prevention or alleviation of cognitive symptoms with treatment.

Y maze output time spent in the novel arm was also similar between the three groups (FIG 32C), indicating there is no improvement in the visual-spatial memory impairment in the treated group. Figure 32B, D and E depicts heatmaps from all three treatment arms where the start arm is A2 and the novel arm A3. The animals in all three groups exhibited no preference for the novel arm.

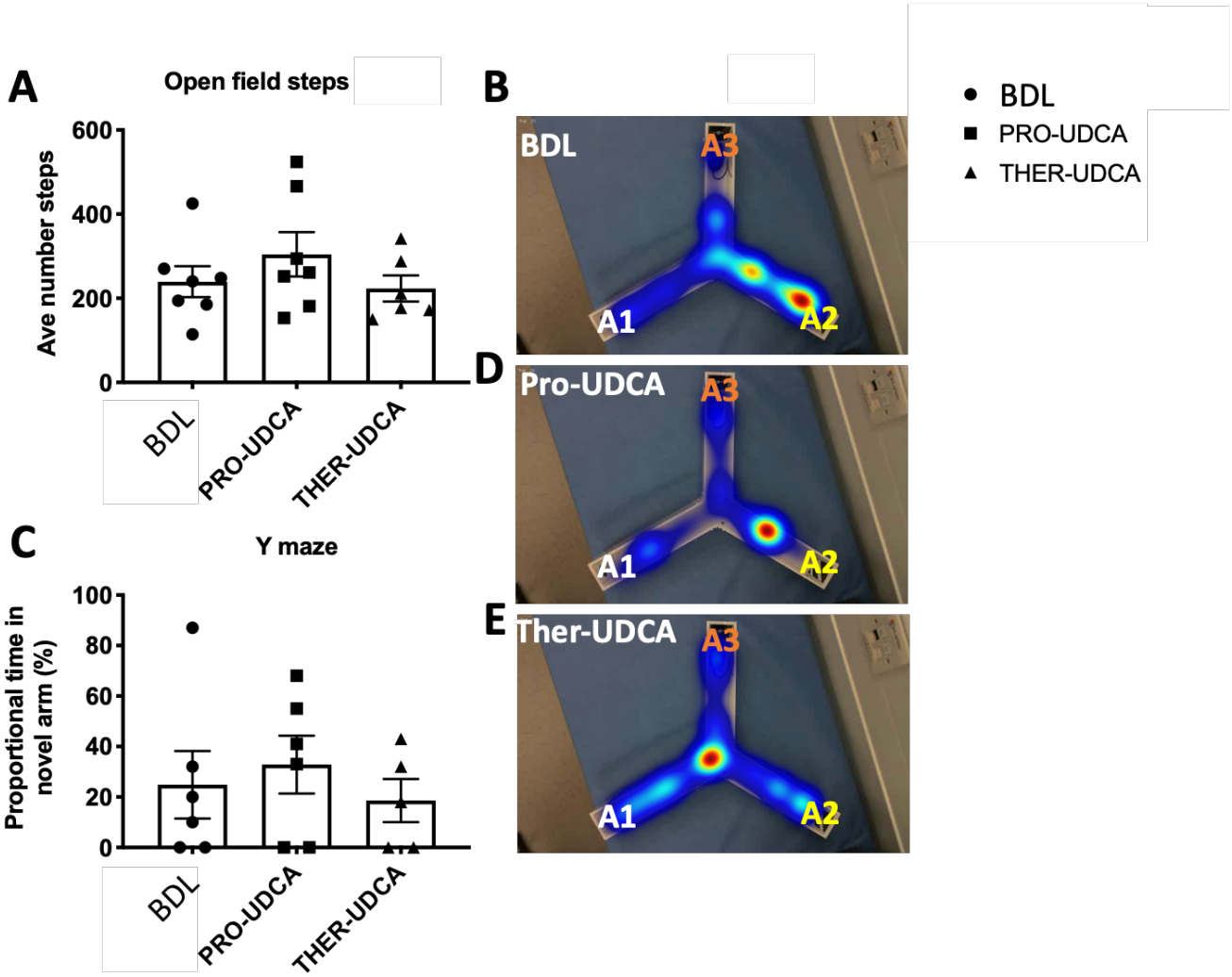

Figure 32. Behavioural testing for UDCA study. (A) UDCA treated and BDL untreated mice took similar number of steps in the Open Field. (C) animals spent similar time in the novel arm in the Y maze, (B) example heatmap of BDL mice, (D) prophylactically treated UDCA mice, and (E) therapeutically UDCA treated mice. N=7 BDL N= 7 pro UDCA mice N=6 Ther UDCA mice. 1 BDL and 1 pro UDCA mice excluded from the Y-maze analysis on the basis that they didn't move from the start arm. Data represented as mean +/- SEM statistics ANOVA.

4.4.4. UDCA treatment induced no Changes in Cell Type Expression within the Dentate Gyrus of the Hippocampus

Treatment with UDCA had no effect on any of the cell types stained within the dentate gyrus. NeuN expression in neurons was similar between all three of the treatment groups (FIG 33A, B, C, D). The percentage of NeuN positive neurons within the dentate gyrus is sustained between this study and the studies in Chapter one, showing that this is likely to be a true effect in the BDL group, as are the inflammatory cell populations the microglia (FIG 33E) and astrocytes (FIG 33F). Thus, there are no anti-inflammatory effects of UDCA drug treatment (prophylactically or therapeutically) within the brain.

Parvalbumin interneuron numbers were marginally reduced in UDCA animals (FIG 33G), however there are highlighted outliers in the BDL group, showing any difference is likely due to variation within the groups.

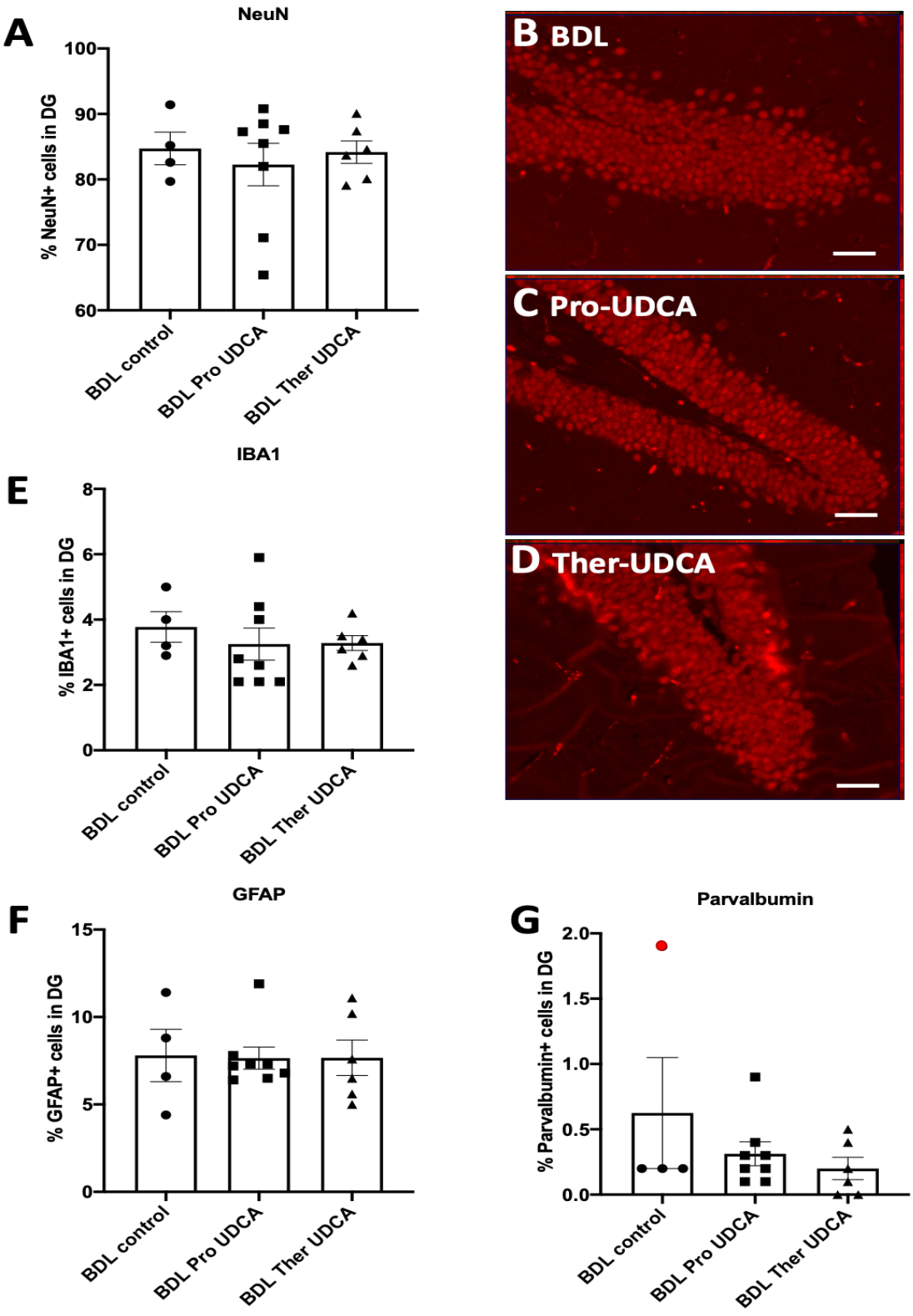

Figure 33. Hippocampal immunofluorescent stain of UDCA study mice. (A) Each group had similar NeuN+ neuron numbers, example image from (B) BDL (C) prophylactic UDCA (D) Therapeutic UDCA mice. UDCA treated mice also had similar numbers of (E) iba1+ microglia (F) GFAP+ astrocytes (G) Parvalbumin + interneurons. Scale = 50 µm. N= 4 BDL N= 8 pro UDCA N= 6 Ther UDCA mice. Data represented as mean +/- SEM statistics ANOVA. Data generated by RuoXie Law UG student under supervision.

4.4.5. UDCA Does not Improve Neuronal Senescence when Compared to BDL control

UDCA treated animals showed no difference from BDL using either the prophylactic or the therapeutic dosing schedule. P21+ RNA ISH shows a similar amount of P21 RNA between BDL control and UDCA treatment groups in both the DG (FIG 34A-C) and CA3 (FIG 34D-F) regions of the hippocampus. P21+ foci per neuron remained similar in both regions between treated and untreated groups (FIG 34G, I), as did the percentage of P21+ neurons present in both the DG (FIG 34H) and CA3 (FIG 34J).

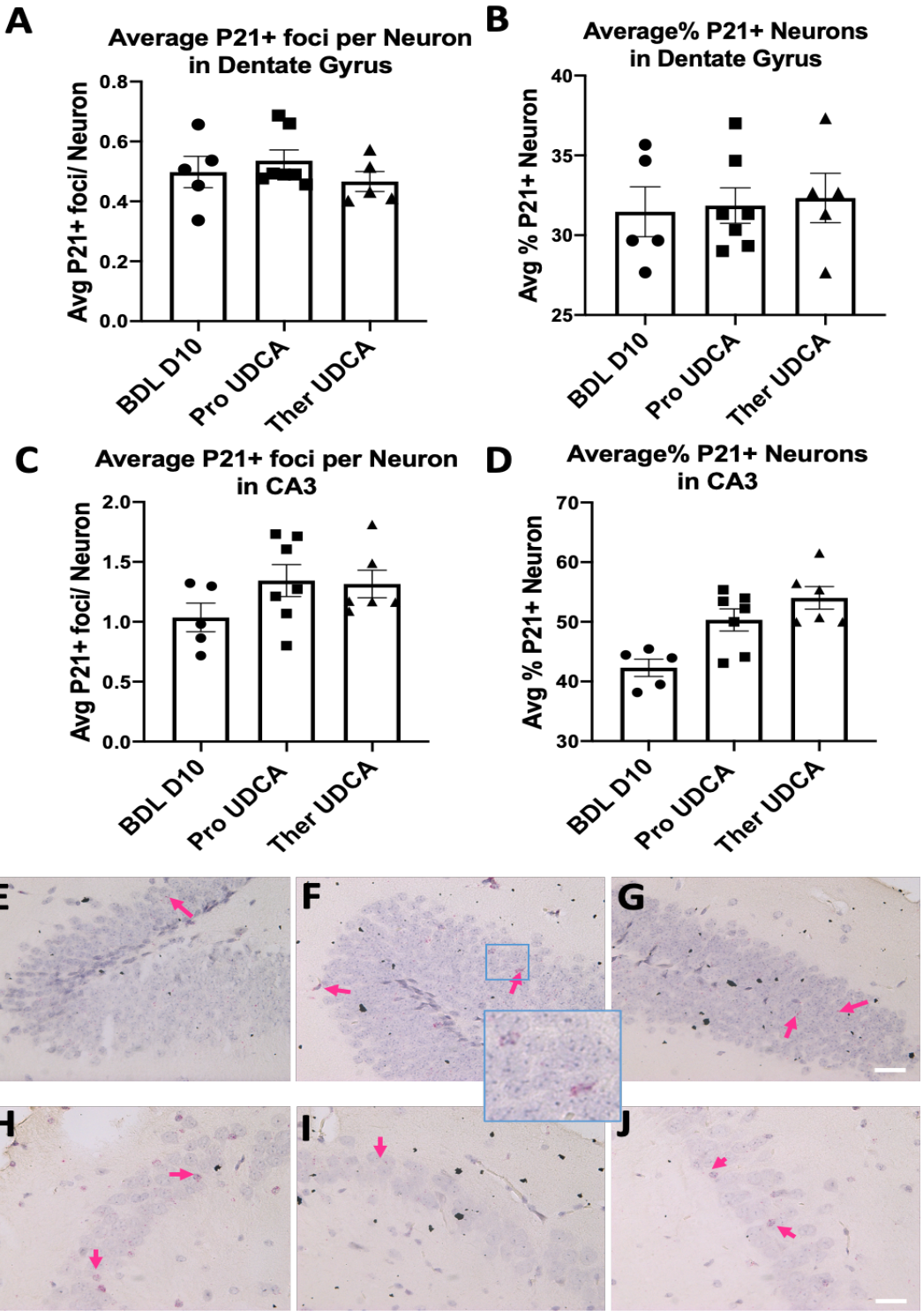

Figure 34. P21 RNA-ISH histology for UDCA dosing study. (A) BDL and UDCA treated animals had similar P21+ foci per neuron and (B) percentage of P21+ neurons in the dentate gyrus. (C) BDL and UDCA treated groups had similar (C) P21+ foci per neuron and (D) percentage of P21+ neurons in the CA3. Example histology showing dentate gyrus P21+ RNA-ISH in (E) BDL (F) Prophylactic UDCA (G) therapeutic UDCA. Example histology showing CA3 P21+ RNA-ISH in (H) BDL (I) Prophylactic UDCA (J) therapeutic UDCA. Scale = 50µm. N= 5 BDL N=7 Pro UDCA N=6 Ther UDCA (one DG broke). Data represented as mean +/- SEM statistics ANOVA. Stain performed by Diana Jurk analysed by me.

4.5. Obeticholic Acid (OCA) Study

4.5.1. Obeticholic Acid Treatment Reduces Fibrosis and DR in the Liver in BDL Mice

Day 10 BDL animals showed comparable levels of activated myofibroblasts (FIG 35A, B, C), fibrosis (FIG 35D, E, F), and DR (FIG 35G, H, I)) to previous studies. Treatment with Obeticholic acid from day of surgery until harvest on day 10 significantly reduced fibrosis, activation of myofibroblasts and DR compared to BDL animals.

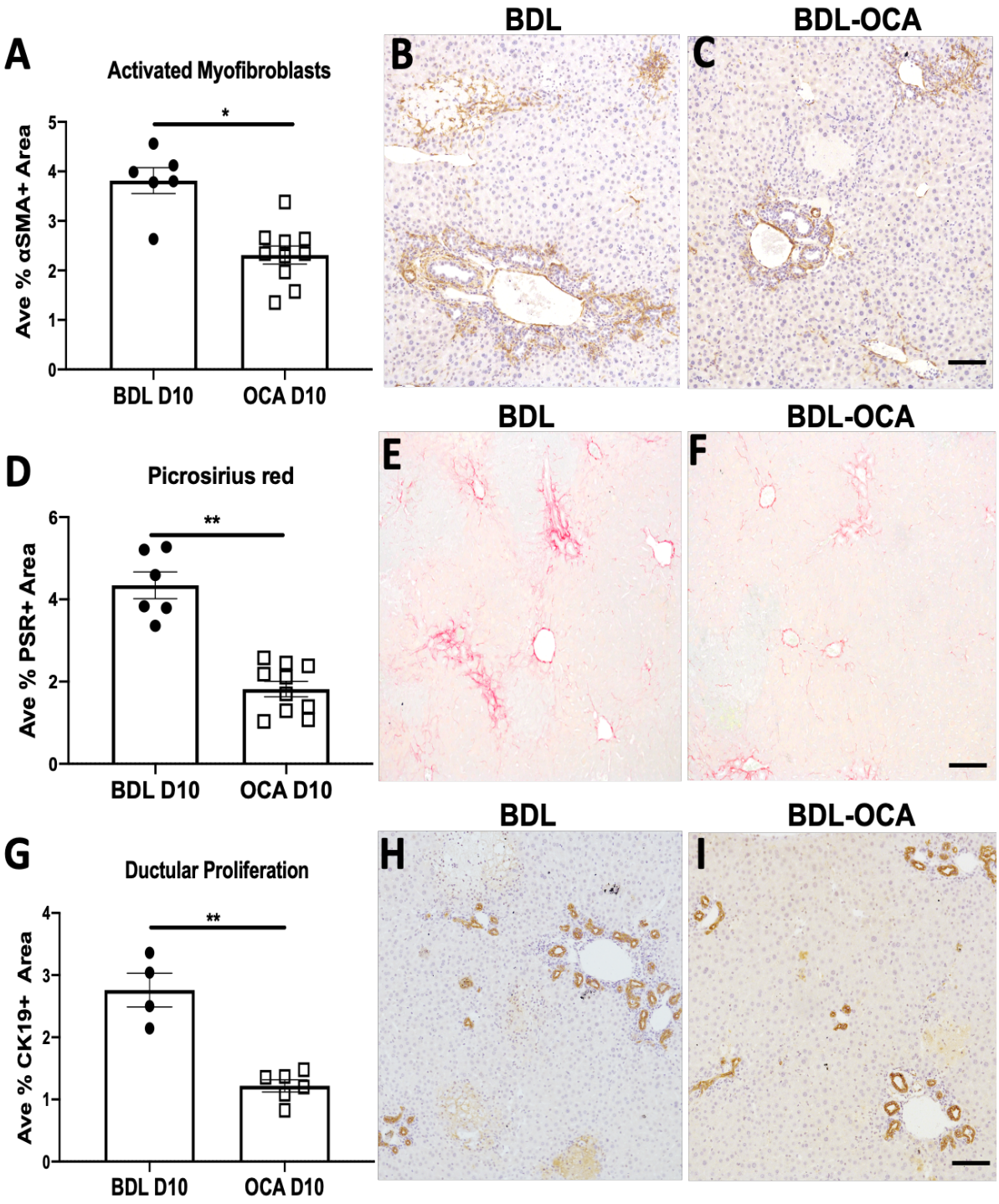

Figure 35. Liver histology for OCA study. (A) OCA treated animals had significantly less activated myofibroblasts. Example α- SMA histology for (B) BDL and (C) OCA treated mice. (D) OCA treated animals had less fibrosis. Example PSR histology for (E) BDL and (F) OCA treated mice. (G) Ductular proliferation is significantly reduced in OCA treated animals. Example PSR histology for (H) BDL and (I) OCA treated mice. Scale= 50µm. N=6 BDL N= 10 OCA. Data represented as mean +/- SEM statistics T.TEST.

4.5.2. Obeticholic Acid Reduces Liver Senescence in the BDL Model

Chapter three established a liver senescence phenotype in BDL mice by day 10, present in both hepatocytes and non-parenchymal cell types. There is also an established DNA damage phenotype by day 10 in the BDL animals, likely to contribute to the senescent phenotype. P21 positivity is reduced in animals treated with OCA in both non-parenchymal (FIG 36A) and hepatocyte (FIG 36B) cell populations. DNA damage is also reduced in OCA treated animals, to significance in non-parenchymal populations (FIG 36C) and to near significance in hepatocyte cell populations (FIG 36D).

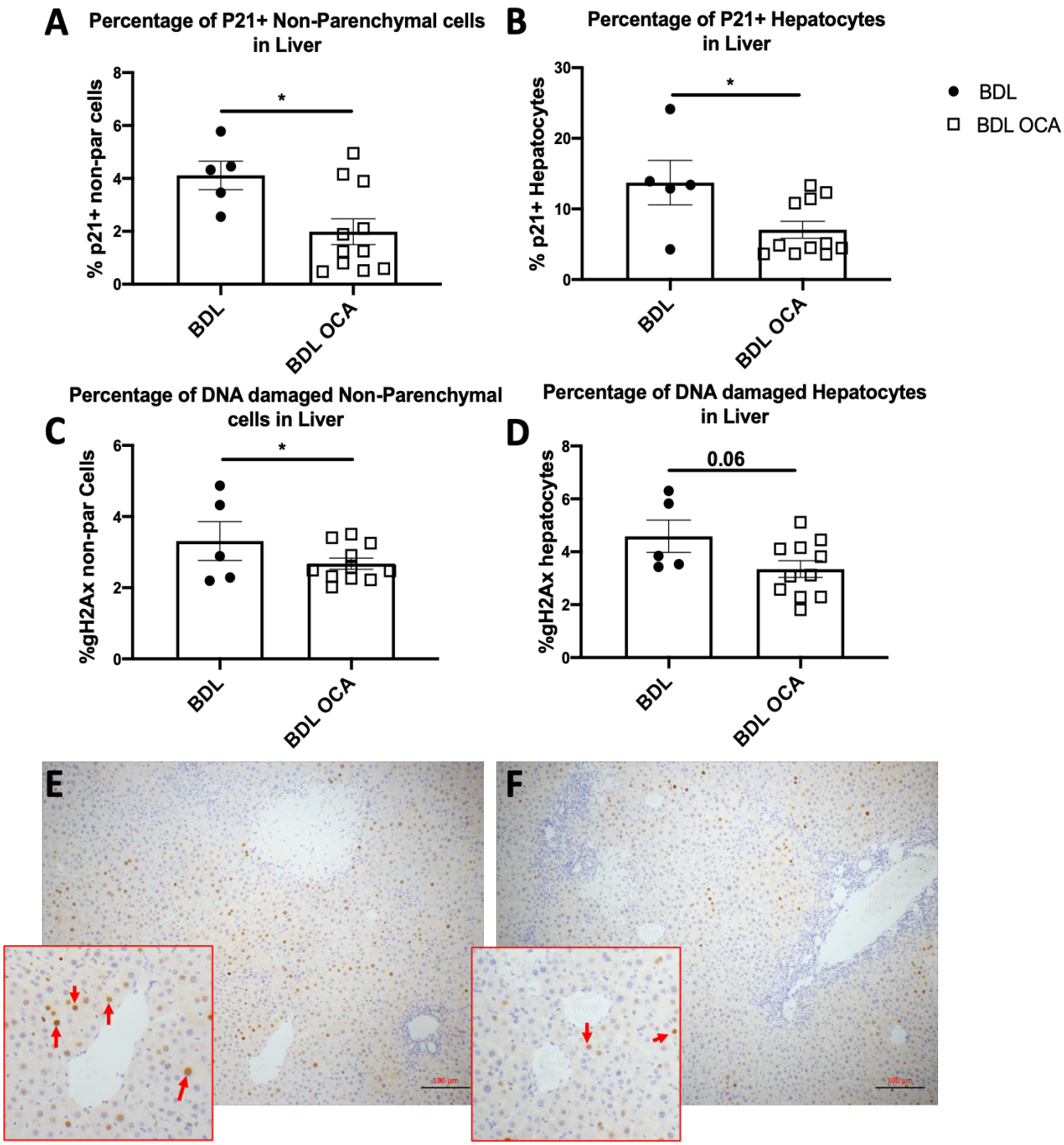

Figure 36. Senescence staining in the liver. (A) percentage of P21+ non parenchymal cells were reduced in OCA treated mice. (B) percentage of P21+ hepatocytes in the liver were reduced in OCA treated mice. (C) percentage of DNA damaged non parenchymal cells in the liver were reduced in OCA treated mice. (D) percentage of DNA damaged hepatocytes in the liver were reduced in OCA treated animals. Histology of P21 in the liver of (E) BDL and (F) OCA treated animals. Scale = 100µm. N=5 BDL N= 11 OCA. Data represented as mean +/- SEM statistics T.TEST. Data analysed using HALO system with thanks to collaborators Thomas Bird and Christos Kiourtis.

4.5.3. OCA Restores BBB damage Associated with BDL

Endothelial wall thickness and vessel circumference remain similar between sham and BDL as reported in the previous study. Treatment with OCA from day 0 led to no significant changes in vessel thickness or circumference between drug treated and either BDL or sham animals (FIG 37B, C). Interestingly loss of astrocyte end-feet coverage at the vessel with BDL was maintained in this repeat study, and OCA treatment led to improved astrocyte coverage at the vessel (FIG 37A). The difference is marginal by day 6 and shows no significant change, however by day 10 the OCA treated animals showed significantly more astrocyte coverage at the vessel (FIG 37E, F, G, H, I), indicative of a more intact BBB.

Pericyte numbers were also reduced in the BDL animals by day 6, when compared to sham though this does not reach significance. Pericyte were increased in both BDL control and OCA treated animals by day 10 with OCA treated animals showing on average significantly more pericytes present within the vessel (FIG 37D). This data could be indicative of more severe BBB breakdown by day 6, accompanied by loss of both astrocyte and pericyte coverage at the vessel.

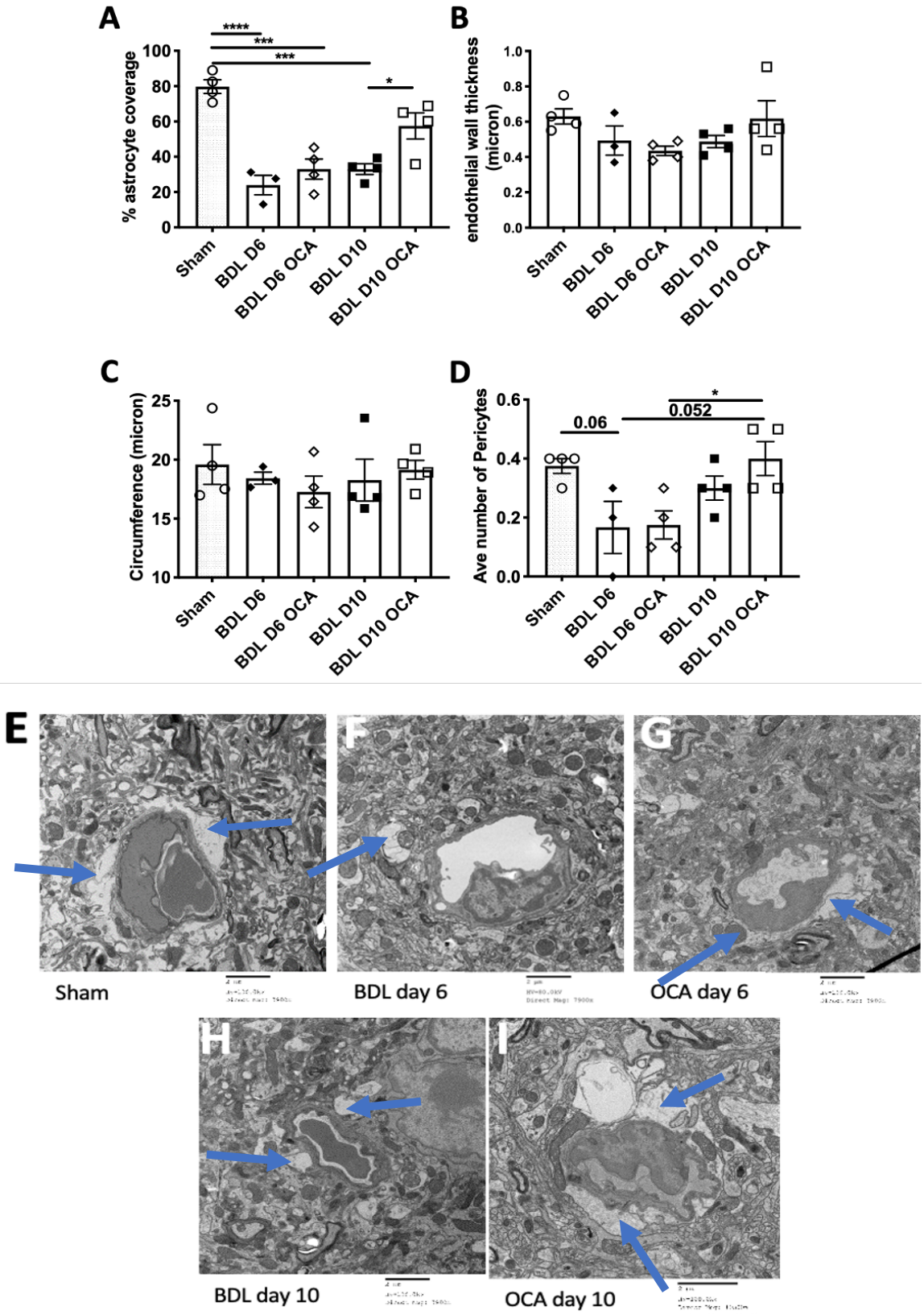

Figure 37. Transmission electron microscopy of hippocampal blood vessels. (A) percentage astrocyte coverage was significantly reduced in day 6 BDL, day 6 OCA treated and day 10 BDL animals when compared to sham animals. Astrocyte coverage is significantly increased between BDL day 10 and OCA day 10 treated

animals. No significant differences in (B) endothelial wall thickness and (C) circumference between groups. (D) number of pericytes around the vessel was significantly increased between day 6 and day 10 OCA treated animals. Images for (E) sham (F) BDL day 6 (G) OCA day 6 (H) BDL day 10 (I) OCA day 10. N= 4 sham N=3 BDL day 6 N=4 day 6 OCA N=4 BDL day 10 N=4 day 10 OCA. Data represented as mean +/- SEM statistics ANOVA. Blue arrows denote astrocyte endfeet.

4.5.4. OCA treated animals show improved behavioural phenotype

BDL animals treated with OCA showed no changes in Open field testing (FIG 38A XB), however these mice spent more time in the novel arm in the Y maze (FIG 38C). Spatial memory deficits but not fatigue appeared ameliorated in animals treated with OCA either prophylactically or therapeutically when compared with untreated BDL animals. This data indicate that OCA may have positive effect on deficits of cognitive domain but not fatigue symptoms. Heatmaps indicate example for each group of time spent in novel arm when the novel arm is A2 (FIG 38D, E).

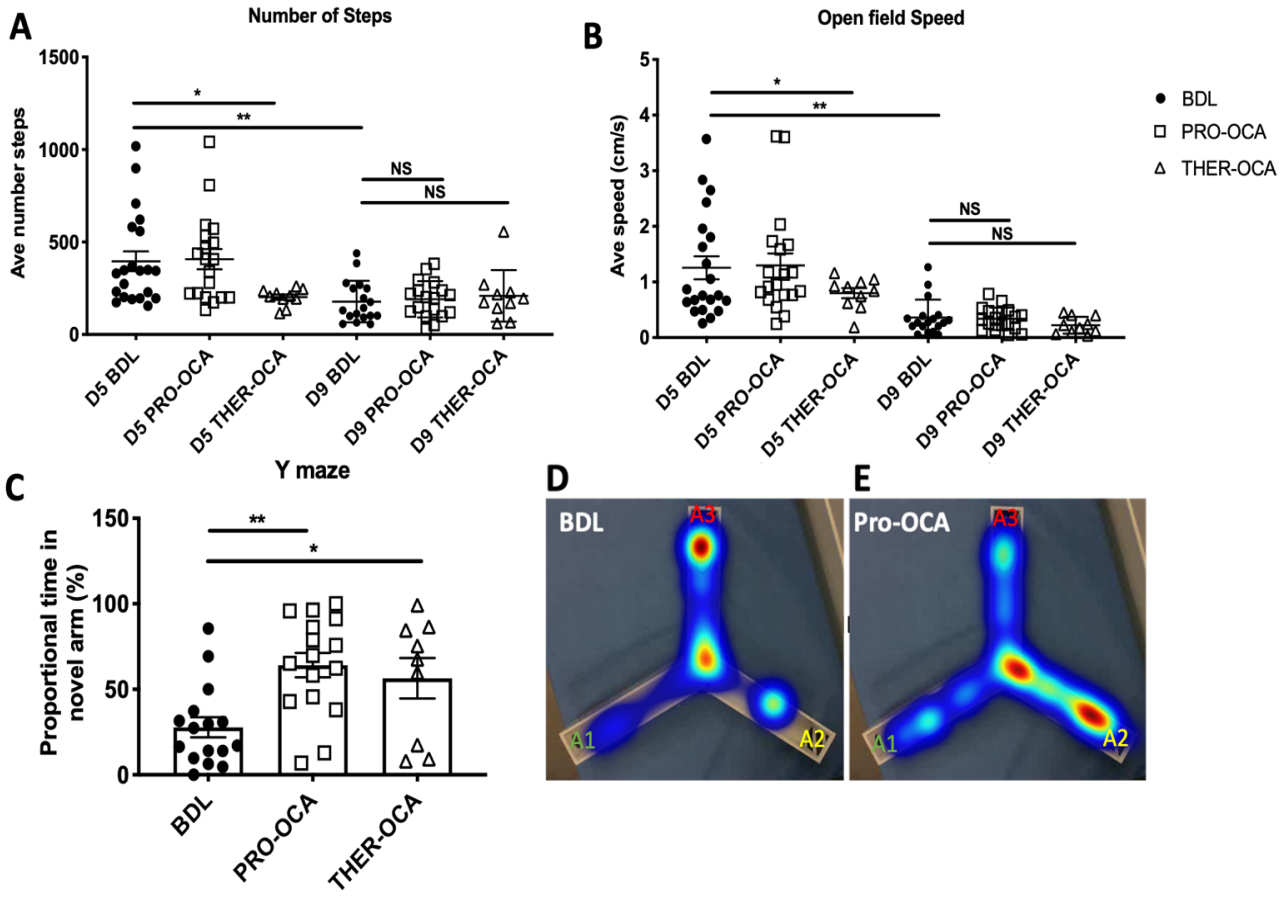

Figure 38. Behavioural testing for OCA drug dosing study. (A) Number of steps taken was significantly reduced between day 5 and day 10 BDL. (B) open field speed of travel was reduced between day 5 and day 9 BDL. (C) Time spent in the novel arm in the Y maze was significantly increased in OCA animals treated with prophylactically or therapeutically on day 10. Y maze heatmaps for (D) BDL and (E) prophylactically OCA where A1 is the start arm and A2 is the novel arm. N= 20 D5 BDL N=20 D5 pro-OCA N= 10 Ther-OCA N= 16 BDL day 9 N=15 pro-OCA N=9 Ther-OCA. Data represented as mean +/-SEM statistics ANOVA.

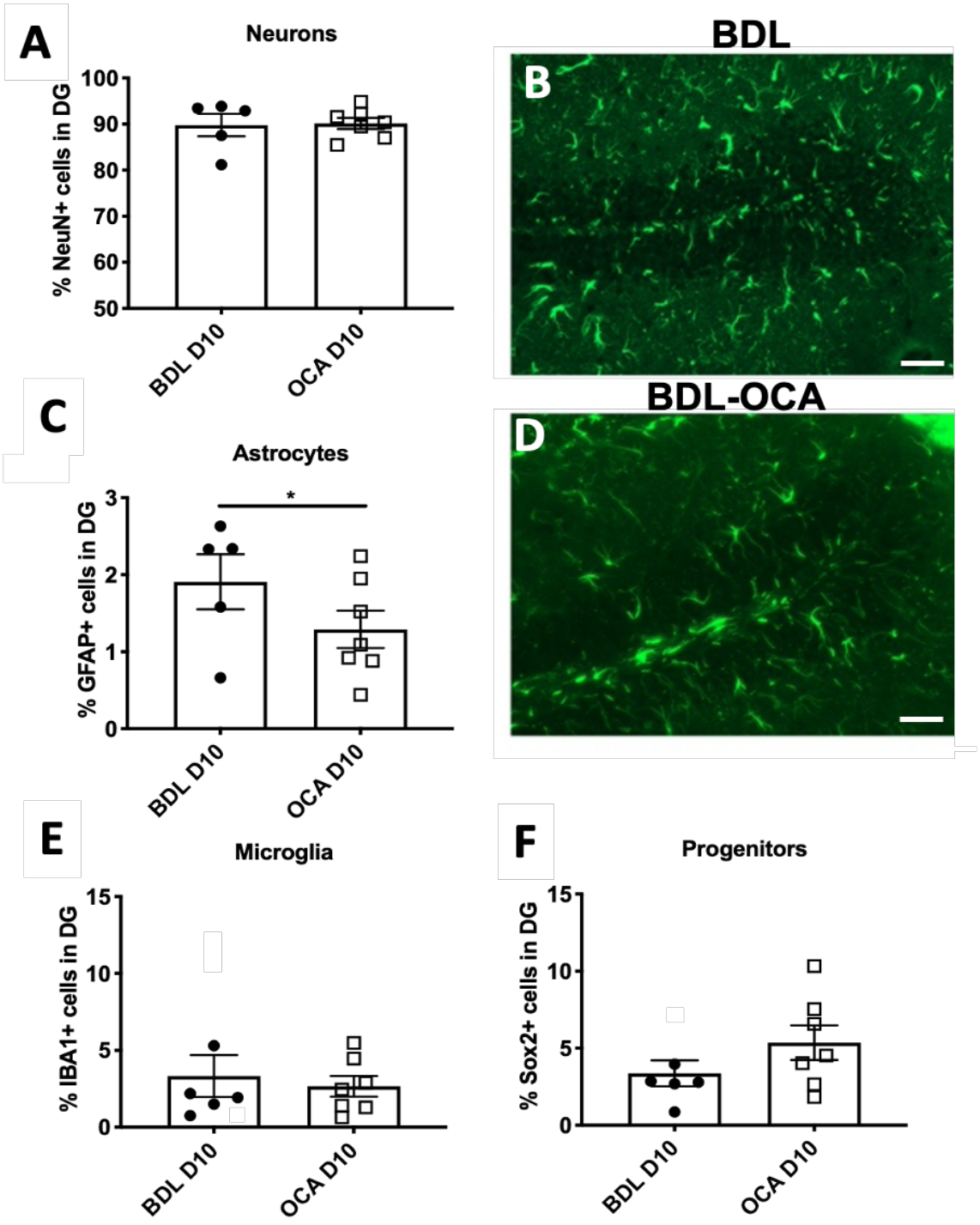

Figure 39 Immunofluorescent stains in the dentate gyrus of mice from BDL OCA study. (A) NeuN+ neurons were similar between BDL and BDL OCA animals. (C) Astrocytes were significantly more in (B) BDL animals compared to (D) OCA. (E) Iba1+ microglia were similar between BDL and BDL OCA groups. (F) SOX2+ progenitors were similar between BDL and BDL OCA animals. Scale = 50 µm. N=5 BDL N= 7 BDL OCA. Data represented as mean +/- SEM Statistics T.TEST.

4.5.1. Obeticholic Acid treatment affects astrocyte activation

There was no significant difference in neuron number between the BDL control and BDL OCA treated groups (FIG 39A). Animals treated with OCA maintained the reduced NeuN expression found in the BDL animals. However, OCA treatment did have an effect on the astrocyte numbers present in the hippocampus during BDL. OCA treated animals had significantly less astrocytes recruited to the hippocampus than comparative BDL control animals (FIG 39C, D), this is likely to indicate lower levels of neuroinflammation in the hippocampus in these mice. Interestingly microglia did not show the same reduction (FIG 39E). Neural progenitors were slightly increased in the OCA treated animals, though not to significant levels (FIG 39F). Overall the brain resident cells show minor changes with OCA treatment when compared to BDL.

4.5.2. OCA Treatment Reduces Neuronal Senescence in BDL Mice

Neuronal senescence was assessed in BDL untreated animals at day 10 post BDL and compared with OCA treated day 10 BDL animals. In the CA3, both the P21 foci per neuron (FIG 40G) and percentage of P21+ neurons (FIG 40H) were significantly reduced in OCA treated animals. In the dentate gyrus there is also some reduction in the 21+ foci per neuron (FIG 40C), and percentage of P21+ neurons (FIG 40D), but it doesn't each significance in this region. Part of the reason for this is likely to be that the senescence phenotype isn't as severe in this region, with the percentage of P21+ neurons in the BDL in the DG only reaching 27%, whereas in the CA3 this is nearly double at 55%.

Telomere associated foci in the CA3 are significantly reduced in the OCA treated animals when compared to the BDL controls. percentage of TAF positive neurons (FIG 40I) and TAF per neuron (FIG 40K) were both halved on average in OCA treated animals (FIG 40L).

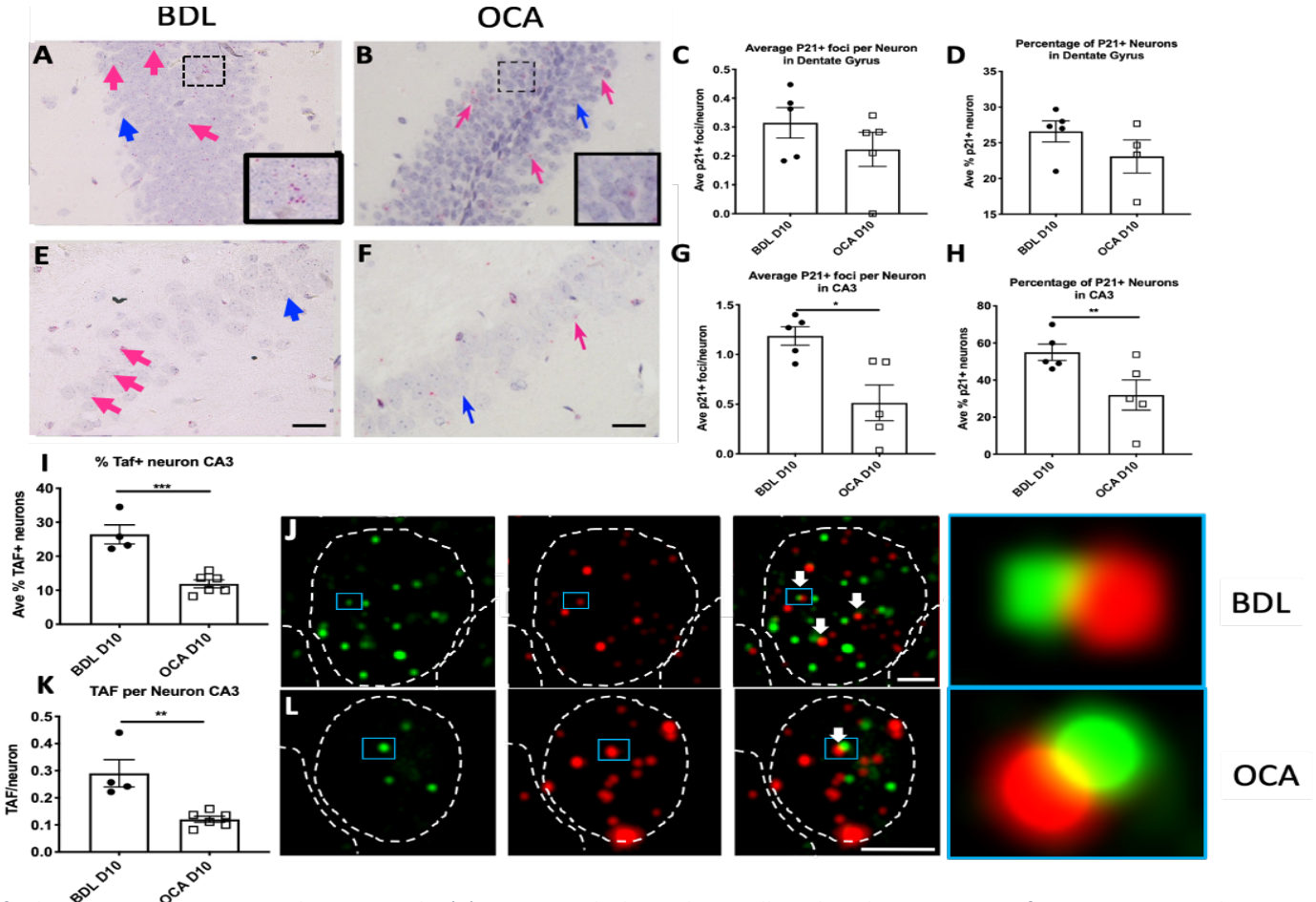

Figure 40. Senescence data for hippocampal neurons in the OCA study. (C) P21 RNA ish showed partially reduced average P21+ foci per neuron in dentate gyrus between (A) BDL and (B) BDL OCA mice. (D) OCA treated mice also had partially reduced percentage of P21+ neurons in the dentate gyrus. (G) There significantly more P21+ foci in the CA3 of (E) BDL mice than (F) BDL OCA mice. (I) percentage of telomere associated foci (TAF)+ neurons in the CA3 were reduced in OCA treated mice. (K) TAF per neuron was also reduced in the OCA treated mice. (J) Example TAF image from BDL mouse showing co-localisation of DNA damage (green) and telomere fish probe (red). (L) example TAF image from OCA. Scale for P21 RNA ish = 50 µm. BDL TAF image = 0.8 µm OCA TAF image 1.2 µm. P21 N= 5 BDL, N=5 OCA. TAF N= 4 BDL N=6 OCA. Data represented as mean +/- SEM statistics T.TEST. Stain performed by Diana Jurk and analysed by me. Pink arrows denote P21+ RNA stain, blue indicate negative cell

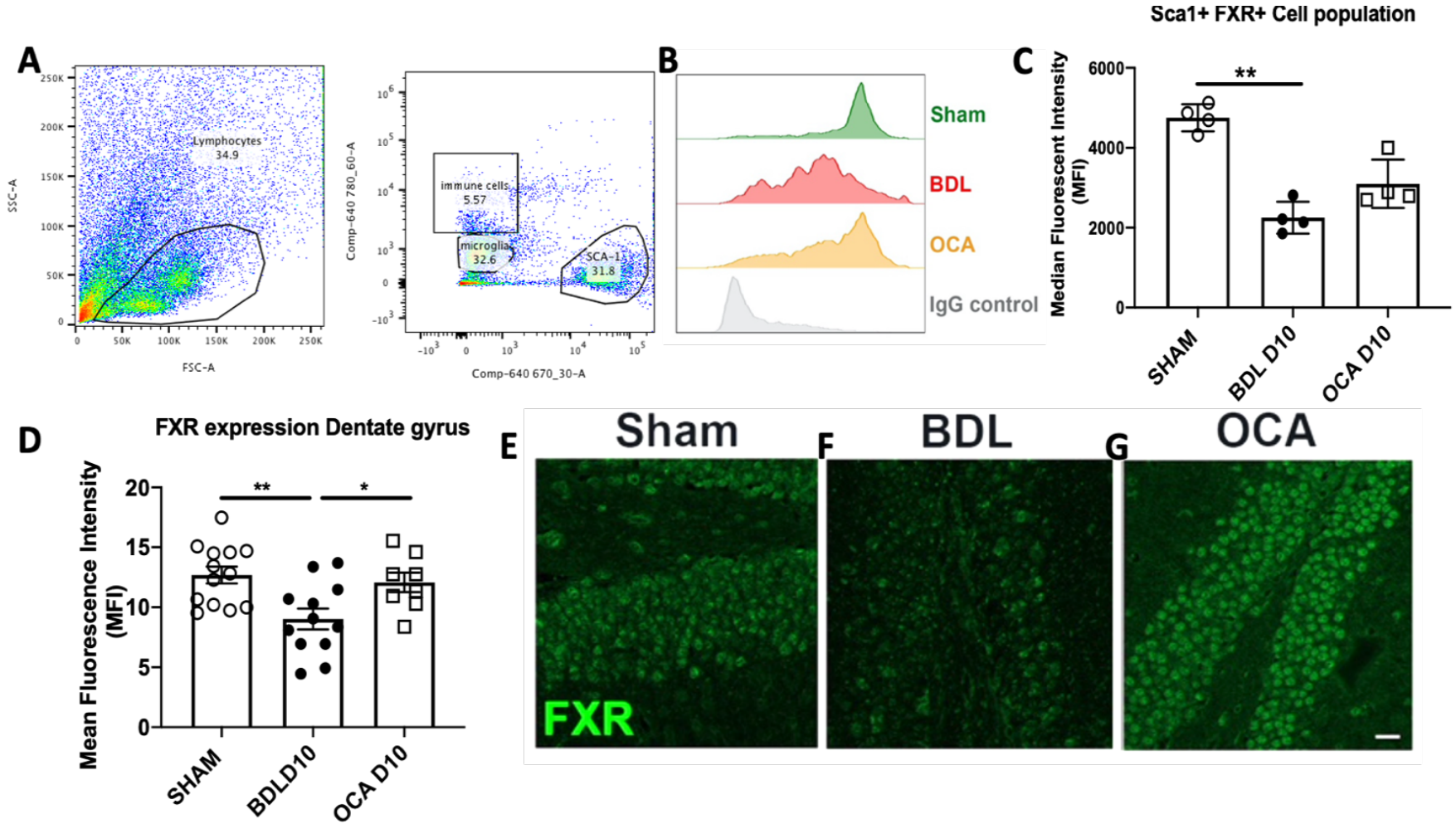

Figure 41. FXR expression profile at the BBB and in hippocampal neurons. (A) gating for endothelial cells as SCa1+ (B) Histogram for sham BDL and OCA animals. (C) BDL animals had significantly less FXR expression than sham animals. (D) FXR expression was also significantly reduced in the dentate gyrus in BDL animals. Histology from (E) sham (F) BDL and (G) BDL OCA mice. FACs N=4 Sham N=4 BDL day 10 N=4 OCA day 10. Histology N=13 sham, N=12 BDL N=8 OCA. Scale = 50 µm. Data represented as mean +/- SEM statistics ANOVA.

4.5.3. Assessment of FXR expression within the BBB and Brain

In order to explore the mechanistic basis of therapeutic benefit of OCA within the brain, flow cytometry was undertaken to assess FXR expression in brain microvascular endothelial cells (BMEC) of the BBB. FXR was expressed in the BMECs from sham BDL and BDL OCA animals (FIG 41), and expression was depressed in BDL, suggesting the action of FXR on the barrier could be through direct mechanisms. When FXR expression was quantified in the dentate gyrus it was also found to be expressed in granule cells. The expression pattern in the DG with BDL showed reduced FXR in the BDL group (FIG 41D, 41F), mirroring what is seen at the BBB. OCA treatment led to increased FXR expression in the DG (FIG 41G), to near Sham levels (FIG 41E).

4.6. Bezafibrate Study

4.6.1. Bezafibrate treatment improves liver pathology in BDL

Treatment with Bezafibrates reduced both activated myofibroblasts (α-SMA) (FIG 42A, B, C), and fibrosis (PSR) (FIG 42D, E, F) by day 10 when compared to BDL animals. This indicates bezafibrate has antifibrotic properties. However, ductular reaction as measured by CK19 (FIG 42G, H, I) was comparable between both BDL control and Bezafibrate treated groups. This data highlights the success of Bezafibrate treatment when comparing Bezafibrate and the other drugs on anti-fibrotic action. Bezafibrate performed as well as OCA in all liver histology apart from ductular reaction.

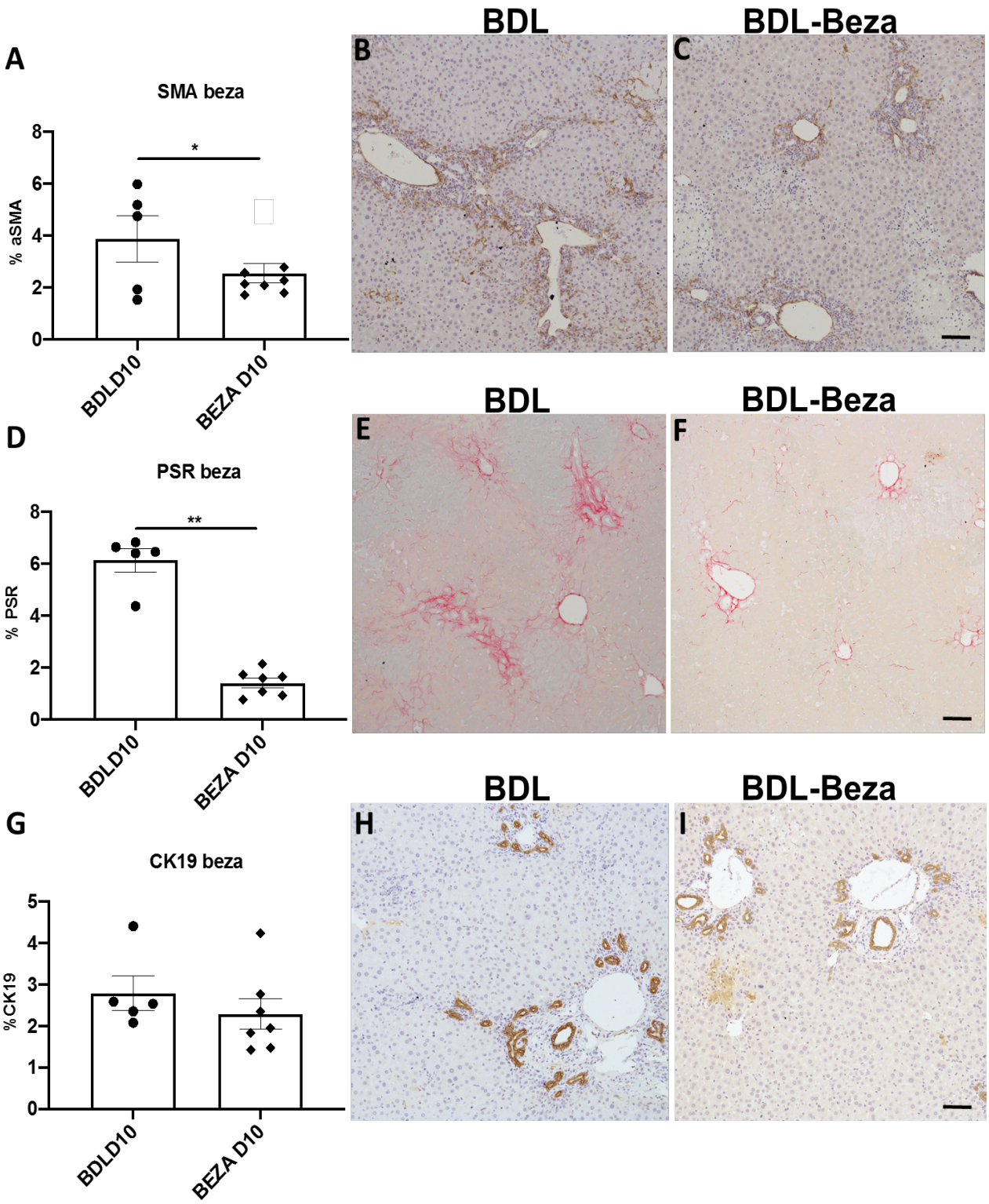

Figure 42. Liver histology images from the Bezafibrate study. (A) activated myofibroblasts (αSMA) were reduced in Bezafibrates (C) compared to BDL (B). (D) fibrosis (PSR) was reduced in (F) bezafibrate compared to (E) BDL. (G) ductular reaction was similar between (H) BDL and (I) Bezafibrate treated mice. N= 5 BDL N=7 Bezafibrate. Scale= 50μm. Data represented as mean +/- SEM statistics T.TEST.

4.6.2. Bezafibrate treatment exacerbates senescence in the liver

Senescence as measured by P21+ count in the liver was significantly increased in the liver of BDL mice treated with bezafibrate (FIG 43C) when compared to BDL control mice (FIG 43A, B). This data indicates that in the context of liver damage Bezafibrate treatment appears to be pro-senescent.

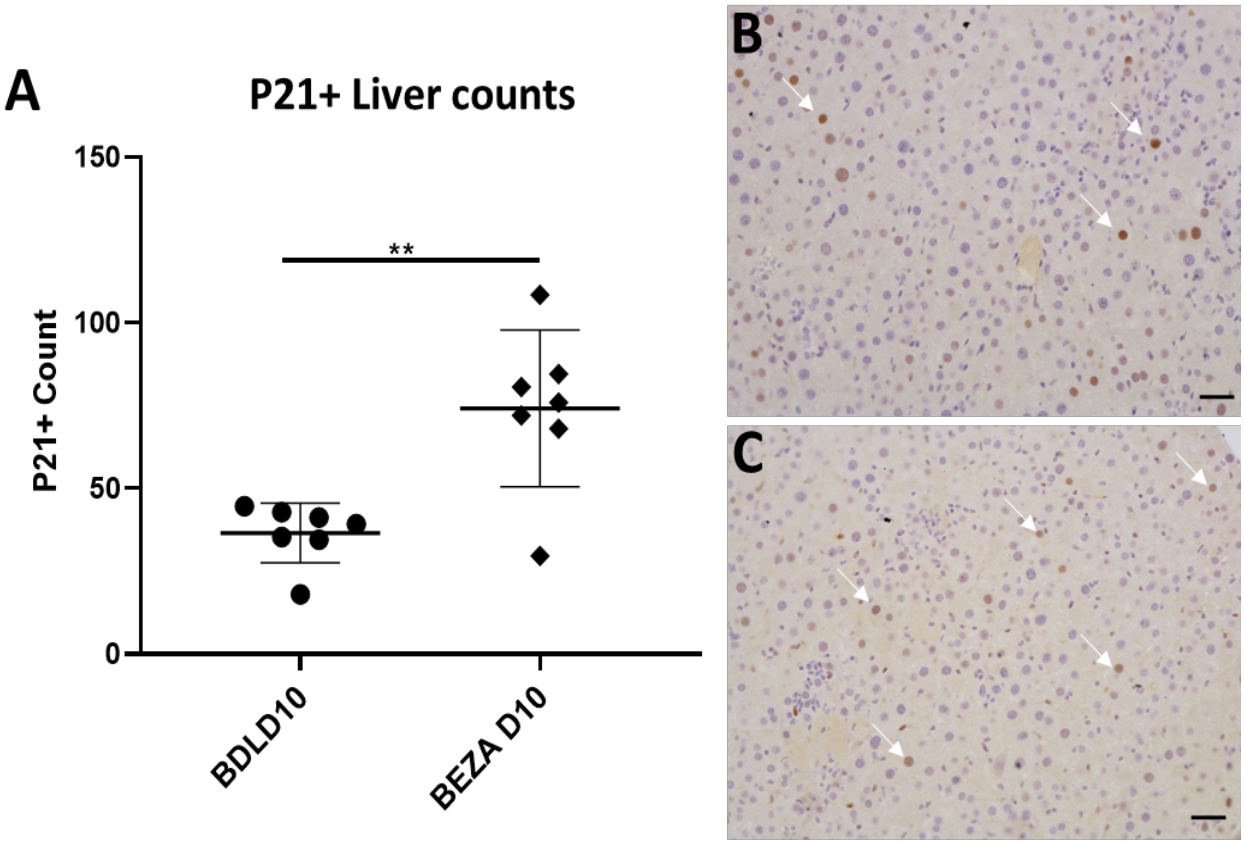

Figure 43. P21+ senescence counts in the liver of BDL and Bezafibrate treated mice. (A) P21+ count in the liver is significantly increased in the (C) Bezafibrate compared to (B) BDL day 10 animals. Scale =50µm. N= 7 BDL N= 7 Bezafibrate. Data represented as mean +/- SEM statistics T.TEST.

4.6.3. Bezafibrate Treatment Does not Improve Behavioural Phenotype in BDL mice

BDL mice treated with Bezafibrate showed similar fatigue to BDL control mice, and travel a similar distance in the open field (FIG 44A), as well as comparable rears (FIG 44B). They also showed comparable time in the novel arm in the Y maze to BDL animals (FIG 44C), indicating there was no reduction in memory impairment or fatigue behaviour in Bezafibrate treated mice.

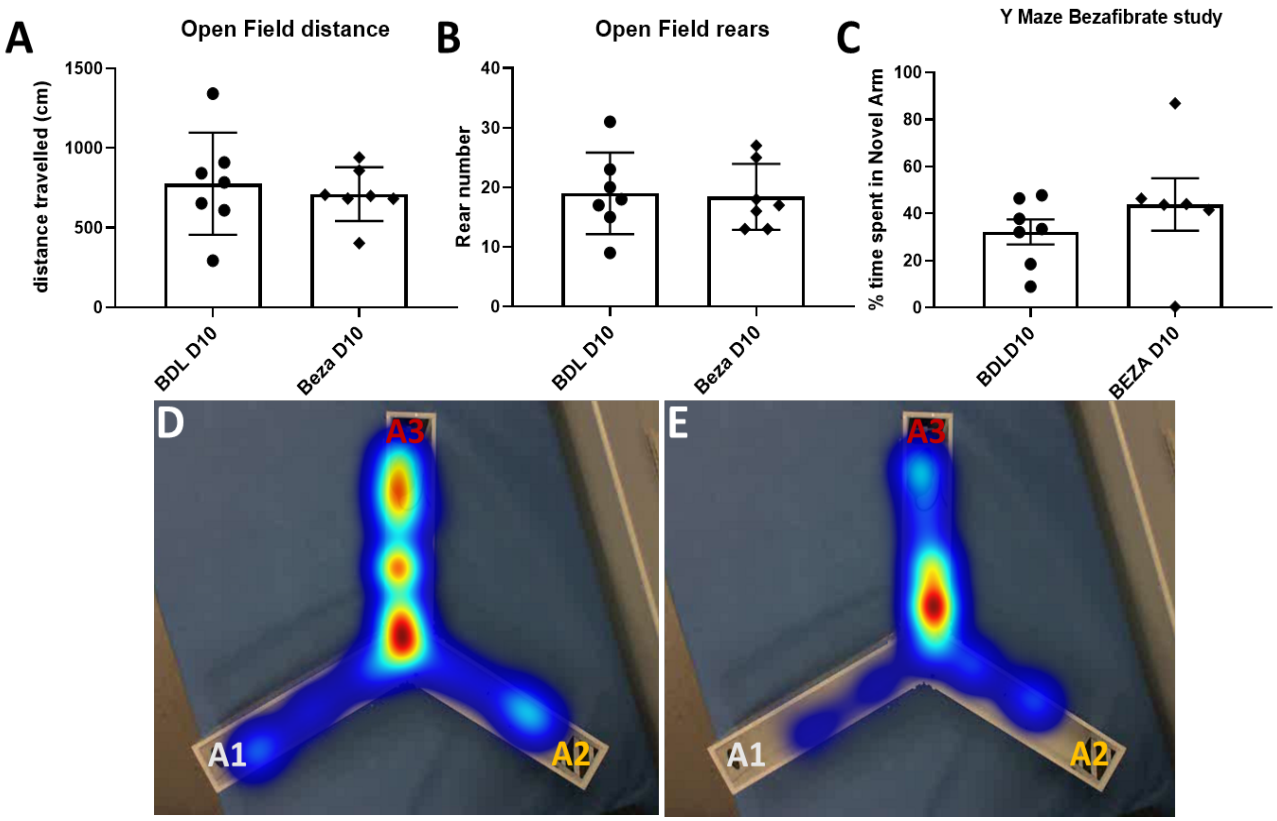

Figure 44. Behavioural testing results from the Bezafibrate study. (A) Open field distance travelled is comparable between groups, as is (B) rear number. (C) Similar time was spent in the novel arm by BDL day 10 and Bezafibrate treated mice. (D) heatmap indicate little time is spent in the novel arm for BDL animals or for (E) Bezafibrate treated animals. Novel arm = A2, start arm = A3. N= 7 BDL mice N= 7 Bezafibrate mice. 1 mouse from Bezafibrate study excluded due to insufficient movement. Data represented as mean +/- SEM statistics T.TEST.

4.6.4. Bezafibrate shows no significant effects on cell types in the Brain

Drug treatment with Bezafibrate showed no significant differences in cell type histology when compared to BDL control animals. Neurons (stained by NeuN) remained reduced in the BDL control animals as reported in chapter 3. Treatment with Bezafibrate had no effect on DG neuronal number (FIG 45A). Similarly, GABAergic Parvalbumin+ interneurons showed no differences between BDL control and Bezafibrate treated animals by day 10 (FIG 45C). Inflammatory cell types microglia (FIG 43B), and astrocytes (FIG 45D, E,F) counts indicate similar levels of neuroinflammation between BDL control (FIG 45E) and bezafibrate treated animals (FIG 45F).

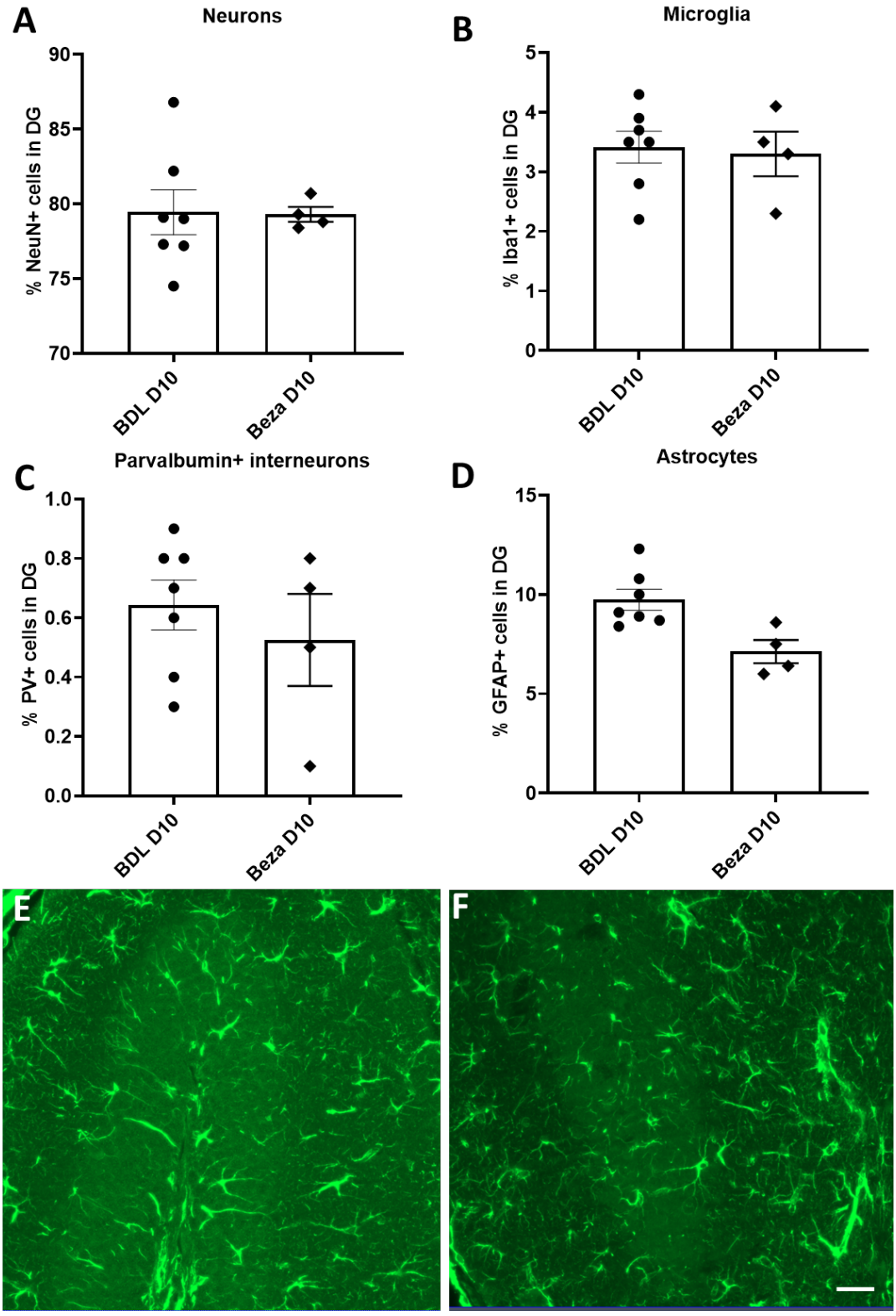

Figure 45. Immunofluorescent histology from the dentate gyrus of BDL mice in the Bezafibrate study. (A) Neuron number was comparable between groups (B) Iba1+ Microglia numbers were comparable between groups. (C) Parvalbumin + interneuron number was comparable between groups (D) Astrocyte numbers were similar between (E) BDL day 10 and (F) Bezafibrate treated mice. N= 7 BDL N=4 Bezafibrate mice. Scale = 50µm. Data represented as mean +/- SEM statistics T.TEST.

4.6.5. Bezafibrate Treatment Exacerbates Hippocampal Neuronal Senescence

P21 RNA ish was used to assess the presence of P21 RNA in neurons in the dentate gyrus and CA3 regions of the hippocampus, as previously described in chapter 3. The P21 RNA ish in the hippocampus seems to reflect what is seen in the liver (FIG 43), in that the Bezafibrate shows largely inflated P21 counts when compared to BDL. When compared to BDL on both P21+ foci per neuron (FIG 46A, E) and percentage of P21+ neurons (FIG 46B, F) Bezafibrate treated animals showed major increase in both DG (FIG 46G, H) and CA3 (FIG 46C, D) regions of the hippocampus. In the CA3 percentage of increased by 15% from 46% in the BDL group to 61% in the Bezafibrate treated group.

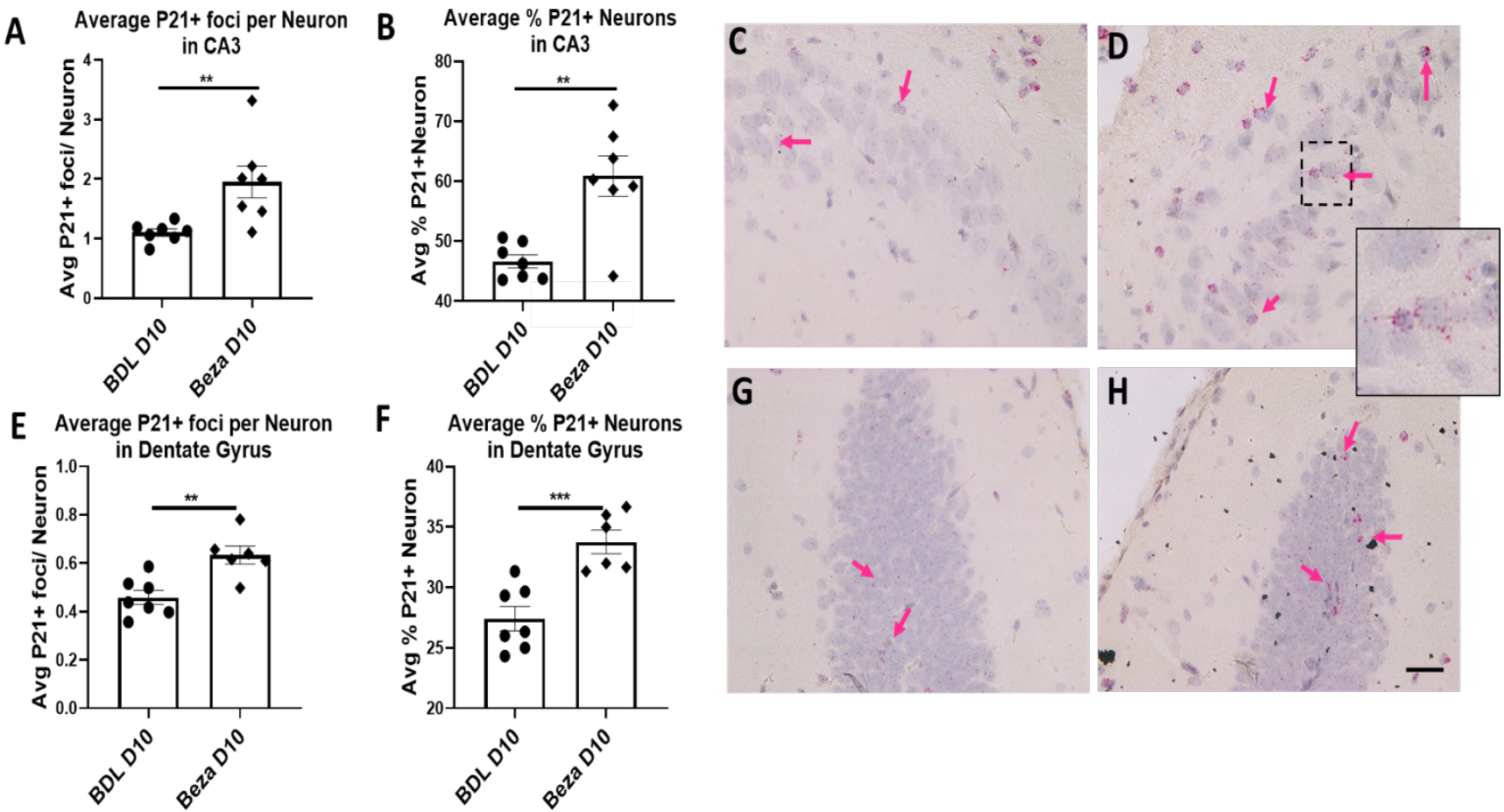

Figure 46. P21+ RNA ish in the hippocampus of mice from the Bezafibrate study. (A) P21 foci per neuron in the CA3 was significantly increased in the (D) Bezafibrate group compared to (C) BDL mice. (B) Average percentage of P21+ neurons in the CA3 was also increased in the Bezafibrate treated mice. (E) P21+ foci per neuron in the dentate gyrus was also significantly increased in the (H) Bezafibrate group compared to (G) BDL group. (F) Average percentage of P21+ neurons were also increased in the Bezafibrate group. Scale = 50µm. N= 7 BDL N=7 Bezafibrate mice. Data represented as mean +/- SEM statistics T.TEST. Stain performed by Diana Jurk analysed by me.

4.7. Summary of Findings from Chapter Four

- When used in the BDL model UDCA does not protect against fibrosis, myofibroblast activation, cellular senescence, or ductular proliferation.

- UDCA provides no protection against cholestasis induced cognitive decline as measured by Y maze behavioural testing.

- UDCA does not improve neuroinflammation or neuronal loss induced by BDL, and shows no improvement in neuronal senescence.

- Bezafibrate improves liver histology in the BDL model, with particular reductions in fibrosis (PSR) and activated myofibroblasts (α-SMA) but not in ductular reaction (CK19).

- Bezafibrate treatment does not result in any improvement in spatial memory (Y maze) or fatigue (Open Field) and does not reduce the neuronal loss or neuroinflammation caused by BDL.

- Bezafibrate exacerbates senescence in the BDL model, in neurons within the hippocampus of the brain as evidenced by P21+ RNA ish.

- OCA produces comparable reduction to Bezafibrate in liver damage related histology stains for fibrosis and activated myofibroblasts, and provided additional reduction in ductular reaction.

- OCA treatment either prophylactically or therapeutically improves spatial memory (Y maze), but not fatigue scores when compared to BDL controls.

- OCA treatment reduces astrocyte neuroinflammation but BDL related neuronal loss remains comparable.

- OCA reduces senescence in both the liver as measured by P21 histology counts, and within neurons in the hippocampus of the brain, both in CA3 and DG regions and as counted by P21 RNA ish and telomere associated foci (TAF) counting.

- OCA impacts morphological changes at the BBB as measured by TEM, Super resolution imaging and MRI scanning. This data indicates that OCA has a positive impact on BBB breakdown caused by BDL surgery.

- FXR is expressed at the BBB and in the hippocampus, meaning these effects could be via direct action on the receptor.

4.8. Conclusions

In our studies, BDL mice treated with UDCA on either a prophylactic or therapeutic dosing schedule showed no significant improvement in any studied parameter. Principally, previous study of the use of UDCA in BDL (both mice and rats) found it to be largely ineffective in treating the liver damage (Zimmermann and Reichen 1992, He, Mennone et al. 2011) caused by the BDL model. One study even found it to aggravate bile infarcts and trigger further necrosis (Fickert, Zollner et al. 2002). Conversely, very few studies find beneficial effects in this model (Poo, Feldmann et al. 1992).

Indeed, even patient studies show inconsistent results regarding symptom improvement following UDCA treatment. Many studies show little histological improvement. One clinical trial showed improved portal and lobular inflammation as well as ductular reaction (Poupon, Balkau et al. 1991) and few have seen beneficial histological effects beneath the level of significance (Leuschner, Fischer et al. 1989, Turner, Myszor et al. 1994, Eriksson, Olsson et al. 1997). Though it is important to note differing clinical criteria of some clinical trials (earlier vs late disease etc) it is clear that UDCA is not a reliable therapeutic approach

for a patient population that can show disparate disease. Given that up to 40% of patients fall into category of UDCA non response, it is clear that better patient disease stratification is needed as are robust biomarkers of UDCA non-response. Currently guidelines require minimum one year's therapy with UDCA to assess non-response (EASL 2017). However, some studies suggest this can be assessed after only 6 months (Zhang, Shi et al. 2013). This would allow earlier intervention with OCA, which could be key for patient outcome.

In our studies, UDCA treatment had no impact on cognition in BDL animals. Spatial memory impairment (Y maze FIG 32) and fatigue (Open field FIG 32) remain prevalent in animals regardless of dosing schedule. These animals also experience similar levels of neuroinflammation to the BDL animals as measured by GFAP+ astrocytes (FIG 33F). NeuN+ neuron loss (FIG 33A) and senescence (FIG 34) in the hippocampus remain similar to BDL, indicating no improvement to neuronal health.

There is currently little literature on the effects of UDCA on cognitive symptoms in BDL or in patients. Large scale Cochrane review of clinical trials shows no beneficial effects on fatigue, but do not specifically mention cognition (Rudic, Poropat et al. 2012), though the prevalence of advanced stage cognitive conditions such as HE were not reduced by UDCA treatment. More recent functional studies in PBC patients indicate that changes in the hippocampus occur regardless of UDCA therapy (Mosher, Swain et al. 2017, Mosher, Swain et al. 2018) suggesting it has little effect on cognitive pathology.

Fibrates such as bezafibrate are from the drug class peroxisome proliferator–activated receptors (PPAR) agonists, and are currently being investigated for use in PBC. Our studies show that although bezafibrate treatment in BDL mice improves many liver outcomes such as reduced activated myofibroblasts (FIG 42A) and fibrosis (FIG 42D), it does not provide any reductions in ductular reaction (FIG 42G) or liver senescence, and in fact exacerbates senescence in this model (FIG 41). These results may mirror selected previous studies using fibrates in the BDL model, that also found reduction in fibrosis and inflammation, however reported an increase in bile duct proliferation (Cindoruk, Kerem et al. 2007). In this study, authors did not look at senescence. Patient trials using Bezafibrate have found promising biochemical improvement (Corpechot, Chazouillères et

al. 2018, Agrawal, Majeed et al. 2019), but no studies so far have published histological changes.

Our studies also show that bezafibrate treatment has no beneficial effects on cognition, when assessed using Y maze (FIG 44C) and animals remain fatigued (FIG 44A). Bezafibrate treatment also had no effect on NeuN+ neuron count (FIG 45A, GFAP+ astrocytes (FIG 45D) and Iba1+ microglia (FIG 45C) in the DG. Interestingly, the increased senescence discovered in the liver, is mirrored in the brain, with Bezafibrate treated animals showing a marked increase in P21 RNA when compared to BDL control animals.

Senescence has been highlighted as a key pathogenic driver in cholestatic disease in both animal models (Sasaki, Ikeda et al. 2005) and human biopsy studies (Tabibian, O'Hara et al. 2014). In this study, we see that both liver and neuronal senescence are increased beyond disease levels in bezafibrate animals (FIG 43, FIG 46), which raises interesting questions about the possibility of cross organ senescence as a mechanism of disease pathology in PBC.

Neuronal senescence has been shown to be key in a number of neurodegenerative diseases including Alzheimer's disease where it has been discovered to be pathologically relevant in both astrocytes and neurons (Bhat, Crowe et al. 2012, He, Jin et al. 2013). In the context of many age-related diseases, clearance of accumulated senescent cells can lead to delay in onset or progression of disease (Baker, Wijshake et al. 2011). Due to the relevance of senescence in the liver pathology of PBC (it is associated with progressive disease), the presence of senescence within the brain is striking, and provides an interesting multi-organ mechanism of disease.

On the other hand, use of OCA in our studies led to significant improvement in many of the studied parameters. Activated myofibroblasts (FIG 35A), liver fibrosis (FIG 35D), and ductular reaction (FIG 35D) were reduced in BDL animals treated with OCA. This mirrors similar reductions in fibrosis observed in other rodent studies (Zhou, Huang et al. 2019) and in recent long term human trials (Bowlus, Pockros et al. 2020), providing positive indications of efficacy.

The OCA treated animals also show improvement in cognitive outputs, making this the first evidence that OCA treatment can benefit cholestasis induced cognitive impairment. Visual spatial memory score in the Y maze was consistently improved across repeated trials and with different observers (FIG 38 C). Fatigue scores were not improved (FIG 38A, B), suggesting this is a specific CNS effect and highlighting the mechanistic separation between cognitive and fatigue symptoms. Astrocyte activation is reduced, as visualised by GFAP (FIG 39C), illustrating reduction in neuroinflammation, although there is no mirrored reduction in Iba+ microglia which represent a relatively low portion of the cell population. Although NeuN+ neuron count isn't increased with OCA treatment (FIG 39A), there is a marked decrease in neuronal senescence as measured by both P21 RNA-ish, and by telomere associated foci (TAF) (FIG 40) in the CA3 and to near significance in the DG.

FXR, the receptor for OCA has been found to be ubiquitously expressed in the central nervous system. In our studies we assessed its expression on the endothelial cells of the BBB (FIG 41A-C) and in granule cell neurons in the hippocampus (FIG 41D-F), and in both found its expression to be repressed by BDL, and increased upon treatment with OCA showing it be a working receptor. While the functional importance of FXR in the brain remains unclear, there are proven consequences of its knockout. Both the expression of neurotransmitters (GABA, NA, 5HT) and behaviour are affected by FXR knockout in mice, including impaired cognitive function and motor coordination (Huang, Wang et al. 2015).

There is also evidence in our data that OCA may directly protect the function integrity of the BBB *in vivo*. BDL mice treated with OCA have fuller astrocyte and pericyte coverage at the vessel (FIG 37A, D) both of which are required for normal barrier function (Iadecola and Nedergaard 2007, Armulik, Genové et al. 2010). The astrocytes present in the OCA animals are also morphologically 'non-reactive' when compared to BDL (FIG 39B-D). In our data we found Sca1+ BMECs at the BBB to express FXR, in sham BDL and OCA treated mice (FIG 41A-C).

Treatment with OCA has been previously found to reduce permeability and inflammation at the intestinal barrier in a variety of animal models (Verbeke, Farre et al. 2015,

Ceulemans, Verbeke et al. 2017), implicating FXR in intestinal barrier functionality. Though direct evidence of FXR signalling at the BBB is scant these studies provide a physiologically relevant insight into the possible functions of FXR in the BBB. In an EAE Multiple sclerosis mouse model, FXR KO increased disease severity and conversely OCA treatment found to have anti-inflammatory effects at the barrier, alleviating disease (Ho and Steinman 2016). These published studies and the studies presented in this thesis implicate an as yet undiscovered role of FXR in modulation of permeability at the BBB.

The data presented in this chapter indicates that early intervention with Obeticholic acid may be beneficial to PBC patients. The current standard treatment plan of PBC involves UDCA therapy as a 1st line (often for up to 18 months), and then combined OCA/UDCA therapy in cases of UDCA non-response. This is a lengthy process, and for patients with cognitive deficit OCA intervention within this timescale may prove too little too late. Evidence shows OCA as currently used has no cognitive benefit, however our evidence shows that in BDL mice when introduced early in the disease process (+3 days), as well at or before disease onset (-3, 0 days) OCA can preserve cognition, and reduce BDL associated neuronal senescence - likely through a combination of indirect (through cytokine signalling from the liver) and direct (through FXR signalling at the BBB and in neurons).

5. Chapter Five – Changes to electrophysiological properties within the hippocampus in BDL mice

5.1. Introduction

5.1.1. The hippocampus

The importance and functions of the human hippocampus were only understood after reports of a patient named HM, who had a bilateral removal of his hippocampi, which lead to an inability to form new memories (Scoville and Milner 1957). This discovery launched an entire field of research, and over the next 20 years several important discoveries were made, for example the discovery of place cells (neurons that respond to specific locations) and their role in spatial memory within the hippocampus (O'Keefe and Dostrovsky 1971) and the discovery of episodic and sequential memory (Suzuki and Eichenbaum 2000).

The hippocampus exists as a bilateral structure in the temporal lobe, and is named so due to its resemblance of the seahorse (in Greek hippo for horse and kampus for sea monster). The hippocampus is comprised of several regions; the dentate gyrus (DG), and the cornu ammonis (CA) regions 3, 2 and 1. Axons from the entorhinal cortex (the major hippocampal input) travel through either the perforant pathway (forming synapses with the CA1), or via the indirect pathway of the trisynaptic circuit (FIG 47), where signaling from the EC first reaches granule cells in the dentate gyrus as a part of the first synapse, then through to the mossy fibers of the CA3 for the second synapse, and finally the Schaffer collaterals (CA3 axons) join to the apical dendrites of the CA1.

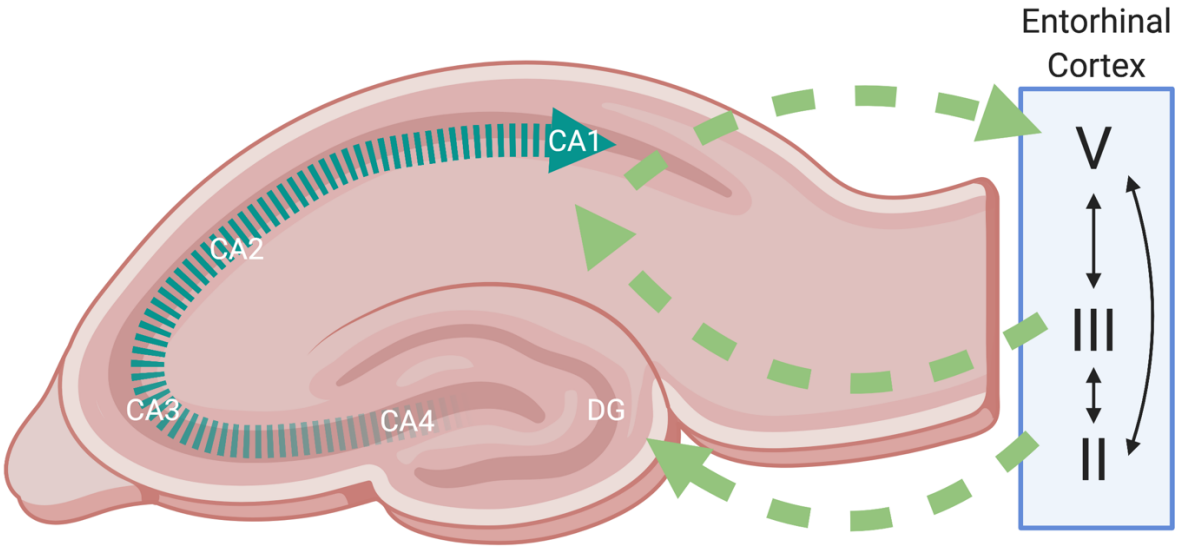

Figure 47. directional flow through the rodent hippocampus (the trisynaptic circuit). The entorhinal cortex provides input to the hippocampus via feedforward to the DG into the trisynaptic loop through CA3 and CA1 via the perforant pathway.

Within the CA regions, there are two major neuronal cell types. Pyramidal cells are the primary excitatory cell of the circuit, providing the major excitatory current. GABAergic basket cells within the CA3 receive excitatory input from pyramidal cells and exert inhibitory outputs, allowing inhibitory feedback loops which can dampen hippocampal excitatory responses.

5.1.2. Pyramidal Cells

Pyramidal cells are so called because of their triangle shaped soma. Pyramidal cells possess apical and basal dendrites – the basal dendrites extend through *stratum pyramidales* through to the *stratum oriens* and the apical dendrites extend through the *stratum radiatum* to *stratum lacunosum moleculare* (FIG 48).

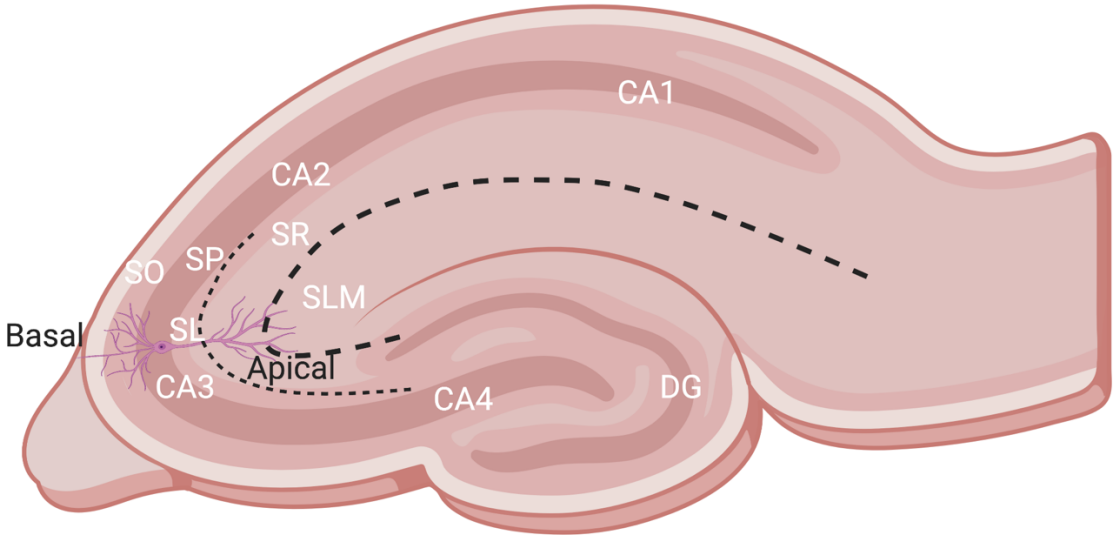

Figure 48. The molecular cell layers of the hippocampus. Stratum Oriens (SO) can be seen distal to the hippocampus, followed by stratum pyramidales (SP, or pyramidal cell layer), then stratum lucunos (SL), through stratum radiatum (SR) and the stratum lacunosum moleculare (SLM).

5.1.3. GABAergic interneurons in the Hippocampus

Interneurons within the hippocampus make up around 11% of cells, and can be largely categorised based on expression of key calcium binding proteins, parvalbumin, calbindin and calretinin. These markers provide an easy way to differentiate the different types of GABAergic interneurons (Kepecs and Fishell 2014).

5.1.3.1. Parvalbumin+ Interneurons

Parvalbumin is only expressed within two subpopulations of interneurons, the basket cells and chandelier (axo-axonic or AAC) cells and bi-stratified. Basket cells make up most of the interneuron population within the CA3, and their cell bodies are located near the *stratum pyramidales* (over 50%), some in the *stratum oriens* (30-40%) and a smaller number in the stratum radiatum (Kosaka, Katsumaru et al. 1987). One basket cell has the ability to innervate the soma of up to 2500 pyramidal cells, giving them control of excitatory outputs within the hippocampus (Kosaka, Katsumaru et al. 1987, Kepecs and Fishell 2014).

The vast majority of parvalbumin+ (PV+) interneurons are fast spiking, meaning they have a high frequency of firing, caused by expression of Kv3.1 potassium channels. The high firing rate of PV+ interneurons means they have an extremely fast turnover of GABA (Kosaka, Katsumaru et al. 1987). This makes these cells extremely demanding of energy (Kann, Papageorgiou et al. 2014).

PV+ interneurons have been implicated in many of the functions of the hippocampus and are largely responsible for co-ordinating the responses of other neurons in processes such as memory consolidation (Ognjanovski, Schaeffer et al. 2017), pattern recognition which allows separation of synaptic inputs (Guzman, Schlögl et al. 2016), and generation of gamma frequency oscillations (Whittington, Traub et al. 1995).

5.1.4. Oscillatory networks within the Hippocampus

Neuronal networks generate different frequencies of oscillation for various sleep-wake states. Depending on the frequency, hippocampal oscillations have diverse biological functions. Oscillations encode region specific outputs, which in the hippocampus and prefrontal cortex is associated with memory formation and processing (Navawongse and Eichenbaum 2013). The synchronous activity of these neuronal networks is responsible for the cognitive processing and storage of information, and produce detectable fluctuations in electric field of the group of neurons (termed local field potential) which can be picked up by electrophysiological recordings in *ex vivo* brain slices. The association of oscillation wavelength with cognitive tasks has been performed largely in rodents, and are categorized below (table 5).

Table 5. the different oscillation wavelengths and their associated functions.

Name	Frequency	Associated function
Delta	0.5 – 4 Hz	Slow wave sleep (Dang-Vu, Schabus et al. 2008)
Theta	4 – 12 Hz	Explorative behaviour (Buzsáki 2005) and REM sleep (Grosmark, Mizuseki et al. 2012)
Alpha	8 – 10 Hz	Relaxed wakefulness (resting with eyes closed) (Niedermeyer 1997)
Beta	I; 15 – 20 Hz II; 20 – 30 Hz	Resting with open eyes (Niedermeyer 1997), motor control and movement planning (Zhang, Chen et al. 2008)
Slow Gamma	20 – 50 Hz	Navigation and visual spatial memory, cognitive processing, learning and memory (Lu, Vreugdenhil et al. 2012)
Fast Gamma	50-80 Hz	Sensory information processing (Colgin, Denninger et al. 2009), spatial memory (object-place pairing) (Zheng, Bieri et al. 2016)

The mechanisms that generate gamma frequency oscillations were initially unclear. Pyramidal cells in the hippocampus (thought to be the cells to encode information with their firing), fire at a frequency of only 3 Hz. In 1995 GABAergic interneurons (aforementioned basket and AAC cells in the hippocampus) were first implicated in the generation of gamma frequency oscillations. Under the antagonism of NMDA, AMPA and kainate, agonism of GABAergic interneurons via a metabotropic glutamate stimulation was able to produce gamma activity in a slice (Whittington, Traub et al. 1995). This showed for the first time that interneurons were responsible for the production of gamma frequency oscillation.

This work gave rise to the interneuron network gamma model (ING model) of attentional gamma oscillations (Whittington, Traub et al. 1995). The ING model suggests that gamma

oscillations are generated solely by interneuron activity in the local networks. However, this raised questions over the mechanism of gamma propagation over larger distances within the brain outside of the hippocampus. Therefore, a more integrative model the pyramidal-cell interneuron network gamma model (PING model) was proposed (Börgers, Epstein et al. 2005). The PING model implicates excitatory firing by the pyramidal cells into reciprocally connected networks of excitatory and inhibitory input. In this model, pyramidal cells fire earlier and interneurons provide necessary inhibitory feedback, producing IPSPs that are sufficient to end firing.

In vitro brain slice models were first published in 1966 (Yamamoto and McIlwain 1966). Since their introduction these models have facilitated investigation into the mechanisms underlying network activity. This has allowed unique insight into not just how networks oscillations are generated, but how network activity can alter during neuropathology. With many *in vitro* models gamma frequency oscillation is found to occur spontaneously, without drug intervention (Pietersen, Patel et al. 2009).

5.1.5. Slow VS Fast Gamma in Memory

In the literature, slow (20-50Hz) and fast gamma (50-80 Hz) events have been associated with different memory integration and processing events. There are several studies implicating slow gamma frequency oscillations with memory recall events. Slow gamma is paired with increase gamma synchronicity between CA3 and CA1, which is proposed to be coupled with memory recall (Montgomery and Buzsáki 2007). Therefore, this associative slow gamma band activity likely promotes the CA3-CA1 synchronicity that allows memory retrieval (Carr, Karlsson et al. 2012)

However, fast gamma activity was found to synchronise with the entorhinal cortex (Colgin, Denninger et al. 2009). The entorhinal cortex primarily processes sensory information, therefore, a role for fast gamma oscillations has been proposed in the integration of sensory information during the encoding of new memories. Fast gamma activity in the hippocampus also becomes the primary gamma frequency oscillation when

novel object and place environments were explored (Zheng, Bieri et al. 2016), and when navigating towards a goal (Cabral, Vinck et al. 2014).

5.1.6. The Role of Gamma frequency Oscillation in Memory Encoding

High frequency gamma oscillations allow the fast transfer of information across the brain. They have thus far been implicated in learning and working memory, spatial navigation (alongside theta activity), and executive function and processing, in humans (Fell, Klaver et al. 2001, Sederberg, Schulze-Bonhage et al. 2007) and rodents (Montgomery and Buzsáki 2007, Zheng, Bieri et al. 2016). Because of this breadth of function, gamma frequency oscillations have been at the centre of scientific investigation of some years.

In human studies into memory, gamma frequency oscillations have been implicated. When human EEG was recorded intracranially and subjects were asked to remember a list of words, an increase in gamma power during encoding was correlated with an increased likelihood of recall (Sederberg, Schulze-Bonhage et al. 2007). In a similar study, a higher level of gamma synchronization was associated with words that were remembered in comparison to those which were later forgotten (Fell, Klaver et al. 2001). In non-human primates, a similar phenomenon has been described – a higher level of synchronisation between LFPs and spiking were seen in the hippocampus when presented with stimuli that were later remembered, as opposed to those which were forgotten (Jutras, Fries et al. 2009).

In rodents, novel object, and novel location testing, has allowed for intricate untangling of the role of gamma activity. In studies where rats were presented with a novel object in a new location (as opposed to a familiar object or familiar location), it was found that fast gamma and CA3-CA1 gamma frequency synchrony were increased (Montgomery and Buzsáki 2007). It is already known that neuron spiking occurs in response to environmental stimuli. In this experiment, place cell spiking was found to increase in

power in conjunction with fast gamma, heavily implicating gamma frequency oscillations in the encoding of novel object-place associations (Zheng, Bieri et al. 2016).

The fast spiking inhibition arising from PV+ interneurons is essential for the generation of gamma frequency activity. When GABAergic interneurons fire, they provide inhibitory input into the pyramidal cell, causing an inhibitory post synaptic potential in the cell, and controlling the timing of the pyramidal firing. When multiple pyramidal cells are stimulated to fire in temporal proximity this spike-timing process generates long-term potentiation in hippocampal neurons thereby encoding memory (Bi and Poo 1998).

In mice, it has been shown that the optogenetic control of PV+ GABAergic interneurons is sufficient to suppress or drive gamma frequency oscillation *in vivo* (Sohal, Zhang et al. 2009). This implicates PV+ interneurons (in in CA3 largely basket cells) as master regulators of network oscillations. Other *in vivo* studies show that gamma oscillations can only be generated in areas such as the CA3 region of the hippocampus, the amygdala, and the neocortex which have a local excitatory network between regions (e.g. in CA3 the Schaffer's collaterals project to the CA1) (Bragin, Jandó et al. 1995). Rodent studies in *ex vivo* hippocampal slices also indicate that CA3 gamma frequency oscillations are dependent on PV+ fast spiking interneurons (Traub, Bibbig et al. 2000, Fuchs, Zivkovic et al. 2007).

5.1.7. The Role of Gamma frequency Oscillation in Memory Recall

Gamma frequency oscillations have been linked to memory recall processes. Rats performing a spatial cue alternation task (that required previous learnt trial knowledge) showed higher gamma synchronicity in LFP between CA3 and CA1, when information was being recalled in order to make the correct choice of arm to traverse (Montgomery and Buzsáki 2007). This indicates that gamma frequency oscillations facilitated transfer of stored memories from CA3 to CA1 for recall.

It is well known that in the rodent hippocampus place cell 'maps' represent visuo-spatial maps of the animal's environment (Johnson and Redish 2007). When an animal pauses to consider a route, place cells are activated in tandem with increased power of gamma oscillations. Primarily, slow gamma activity is generated; oscillations at 30-60 Hz increased in the CA3 upon learned association tasks (Tort, Komorowski et al. 2009).

5.1.8. Neurodegenerative and Psychiatric Disease

Alzheimer's disease (AD) is a progressive neurodegenerative disease, characterised by distinctive pathology of amyloid-ß in plaque deposits in the brain, alongside tau neurofibrillary tangles accumulating in and around neurons (Soto 2003). The hippocampus and associated entorhinal cortex are particularly susceptible to amyloid pathology. The earliest cognitive symptoms associated with AD are episodic and spatial memory impairment.

Recent landmark data suggests that patients may preserve the ability to encode memories but not to retrieve them (Roy, Arons et al. 2016). This is in keeping with reports from rodent models of AD, showing disrupted slow wave gamma power in CA1 region of the hippocampus (Mably, Gereke et al. 2017). In addition, the coordination of slow wave gamma with CA1 place cell firing was reduced (Mably, Gereke et al. 2017). APOE4 knock-in mice have demonstrated that alleviation of slow gamma impairment rescued the learning deficits, specifically implicating slow wave frequency gamma (Gillespie, Jones et al. 2016). The study went one step further, showing that specifically deleting APOE4 only from GABAergic interneurons diminished slow wave gamma disturbance, highlighting the important role of GABAergic interneuron firing. These results were mirrored in a similar study, demonstrating improved slow gamma firing rescued deficit in 5xFAD mouse model (Iaccarino, Singer et al. 2016). It is important to note that slow gamma activity deficits occur across multiple murine models of AD, highlighting the importance of this phenotype.

Changes to network oscillations have long been of interest in psychiatric diseases such as schizophrenia. Post-mortem studies have shown a reduction in GABA synthesizing enzyme GAD , driving a reduction in GABA synthesis in the PV+ interneuron population (Addington, Gornick et al. 2005). This leaves PV+ interneurons unable to fire, or misfiring, in turn causing disruption to gamma frequency oscillations and their associated memory forming mechanisms.

5.1.9. Could Oscillation be impaired in Liver Disease related Cognitive Deficit?

There is currently no evidence of changes to hippocampal gamma frequency oscillations in chronic liver disease during an early disease stage. However, changes to various neurotransmitter systems have been implicated in the pathogenesis of cognitive decline in cholestatic liver disease (Cauli, Mansouri et al. 2009, Dhanda and Sandhir 2015). Research to-date has been around late stage liver disease and hepatic encephalopathy (HE). Using models of hyperammonia, GABA has been shown to be significantly increased in the cerebellum of hyperammonic mice which are cognitively impaired. In this model, behaviour is normalised by treatment with bicuculline, a competitive $GABA_A$ antagonist (Cauli, Mansouri et al. 2009). Other commonly used models of HE such as 4 week BDL have implicated additional neurotransmitter systems, such as the serotonergic system in cognitive decline and dopaminergic system in motor dysfunction (Dhanda and Sandhir 2015).

Even in late stage liver disease models, such as 4-week BDL, very limited evidence is available around changes to network oscillations. Of the evidence that is available, patch clamp electrophysiology was used to assess the electrophysiological properties of single cells in the cerebellum (Aghaei, Hajali et al. 2016), and CA1 (Tahamtan, Aghaei et al. 2017), but not the oscillation patterns of the network. These studies have shown profound differences to the electrophysiological properties of neurons 4 weeks post BDL. The patched Purkinje neurons in the cerebellum were found to be hyperexcitable, with increased firing rates (Aghaei, Hajali et al. 2016), whereas in the CA1 neurons were found to be less excitable with a decreased firing rate (Tahamtan, Aghaei et al. 2017).

Contradictions such as these make it difficult to predict the network firing changes that might occur in the CA3, as the data suggests area specific changes to individual neuron properties. In addition, our cholestatic liver disease model is less severe, choosing only to run the BDL to day 10 to investigate early changes to cognition in cholestatic liver disease, in a pre-cirrhotic state (Chapter 3 and 4).

5.2. Study Rationale

Electrophysiological recordings were undertaken in the CA3 region of the hippocampus in BDL animals and compared to sham control animals (experimental timeline outlined in figure 49). BDL surgery was performed as outlined in Methods section (chapter 2) and animals were maintained for a maximum of 11 days after surgery. Local field potentials (LFP) were recorded from between the *stratum radiatum* and *stratum lacunosum moleculare* regions of the CA3. Behavioural testing was performed as in previous studies on days 9 and 10 where possible. Where this was not possible, open field testing was undertaken on day 8 and Y maze on day 9.

In order to produce a consistent and sustained oscillation, methods to induce hippocampal gamma-frequency oscillations pharmacologically are used. The most commonly used drugs are the cholinergic agonist carbachol (CCH), which activates muscarinic and nicotinic acetylcholine receptors (described in (Fisahn, Pike et al. 1998)) and kainate (KA) which activates ionotropic glutamatergic kainate receptors. To produce comparable results, carbachol was used in each study.

This study was undertaken to provide in depth mechanistic analysis of the effect of pre-cirrhotic liver disease on the generation of gamma frequency oscillations in CA3. Evidence outlined above illustrates that the CA3-generated gamma frequency oscillations are essential for visual spatial memory encoding (Fell, Klaver et al. 2001, Sederberg, Schulze-Bonhage et al. 2007) and retrieval (Montgomery and Buzsáki 2007). PV+ interneurons which are required for the proper maintenance of network oscillations, were also quantified using optical density.

Electrophysiological studies were undertaken on sham (n=8), BDL (n=8), and Obeticholic acid treated animals (0.03% OCA from day 0) (n=7), in order to gain a picture of not just of the effects of cholestatic liver disease on network oscillation, but also the impact (if any) of OCA drug treatment when compared to untreated BDL animals.

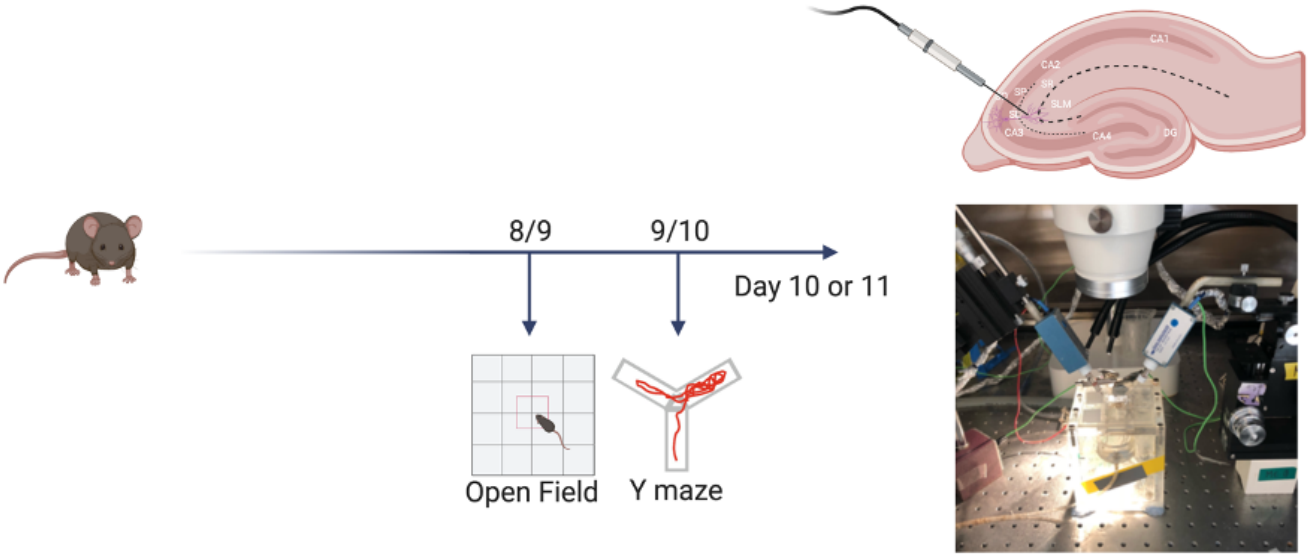

Figure 49. Experimental workflow from day of surgery to in vitro slice recording

5.3. Aims

The aims of these studies were as follows:

- Quantify any possible differences in the ability of the CA3 neuronal networks to generate and maintain gamma frequency oscillations in hippocampal slices from sham or BDL animals.

- Investigate the differences in the properties (area power, amplitude, and frequency) of gamma frequency oscillations generated from hippocampal slices from sham or BDL animals.

- Investigate the changes to gamma frequency oscillations in BDL animals when treated with OCA from surgery date.

- Investigate changes in oscillation propagation proximal and distal to CA3.

- Assess the rhythmicity of stable network oscillations produced by sham, BDL untreated and BDL animals treated with OCA, to investigate changes in stable oscillation phenotype.

- IHC quantification of PV+ interneurons in sham BDL and BDL-OCA, as these are essential for the regulation of hippocampal gamma oscillations.

5.4. Results

5.4.1. BDL animals show significant abnormalities in hippocampal gamma frequency oscillations

Once slices were trimmed and placed in the chamber with aCSF flow, electrodes were placed in the CA3 region. Slices were bathed in the cholinergic agonist carbachol which was applied through the aCSF flow. Carbachol induces oscillations that generally grow in power to a 'stable area power measurement by 3 hours post application (Lu, Wang et al. 2012). In cognitively normal animals' oscillations largely follow this so-called 'stable' pattern (FIG 50E). Rarely, a slice will show a 'fluctuating' pattern, where the oscillation doesn't produce stable oscillations within 3 hours and instead the area power constantly increases and decreases (FIG 50F). Slices may also produce a 'growing' oscillation, where the area power continually increases over 3 hours and never stabilises (FIG 50G), or very rarely the slice will show no oscillation (FIG 50H). In this study I found that in sham mice, 89% of slices produced a stable oscillation phenotype (FIG 50A). Example traces can be seen in Figure 50D.

In contrast, Cholestatic mice showed significant instability in the patterns of carbachol-evoked neuronal network. BDL animals were generally unable to produce stable gamma frequency oscillation within 3 hours recording. Only 18% of BDL mice produced a stable oscillatory pattern (FIG 50B), compared to nearly 90% of sham animals. In contrast, the most frequent pattern of oscillation seen in slices from the BDL was a fluctuating oscillation (FIG 50F). This oscillation pattern is indicative of unstable neuronal network activity. Equal numbers of BDL hippocampal slices produced growing oscillation and no oscillation (FIG 50G, H).

I then assessed the proportions of different oscillation patterns in BDL mice treated with OCA (FIG 50C). The most frequent gamma frequency oscillation pattern in OCA-treated mice was a stable pattern (62%), which may be representative of the improved network health of the neurons. A proportion of slices from OCA treated mice were of unstable oscillatory patterns, for example, fluctuating oscillations represented 26.7%. However, the distribution of oscillation patterns aligns more closely to that seen in sham mice.

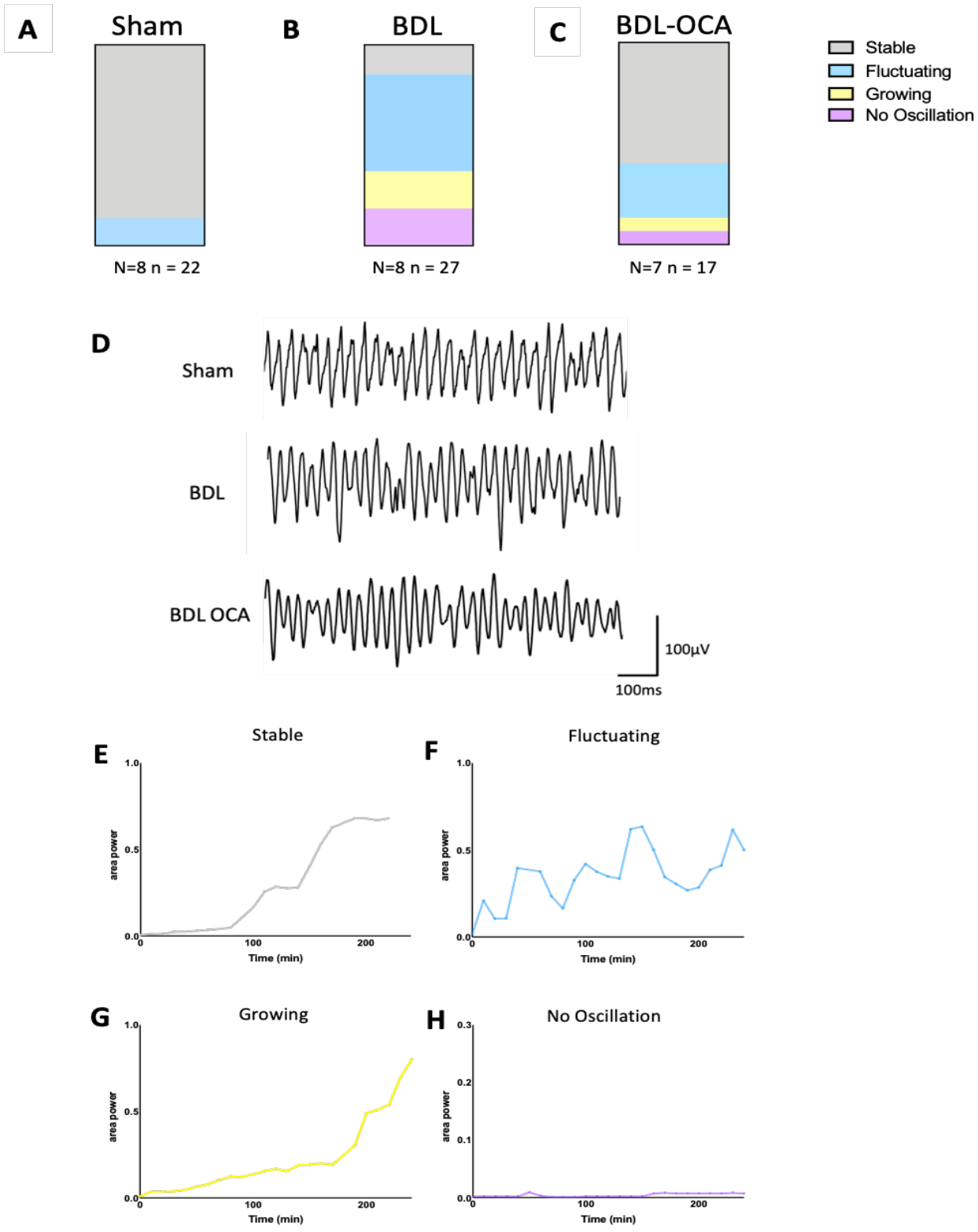

Figure 50. Types of oscillation pattern within gamma frequency. A. the ratio of each oscillation pattern in Sham animals B. the ratio of each oscillation pattern in BDL animals C. the ratio of each oscillation pattern in OCA treated animals. D. Example traces for each group. Outline of oscillation patterns E. stable oscillation F. Fluctuating oscillation pattern G. Growing oscillation pattern H. No oscillation. N = animal number n = slice number N = 8 n=22 BDL N=8 n=27 OCA N= 7 n =17

5.4.2. Changes to Oscillations Over Time

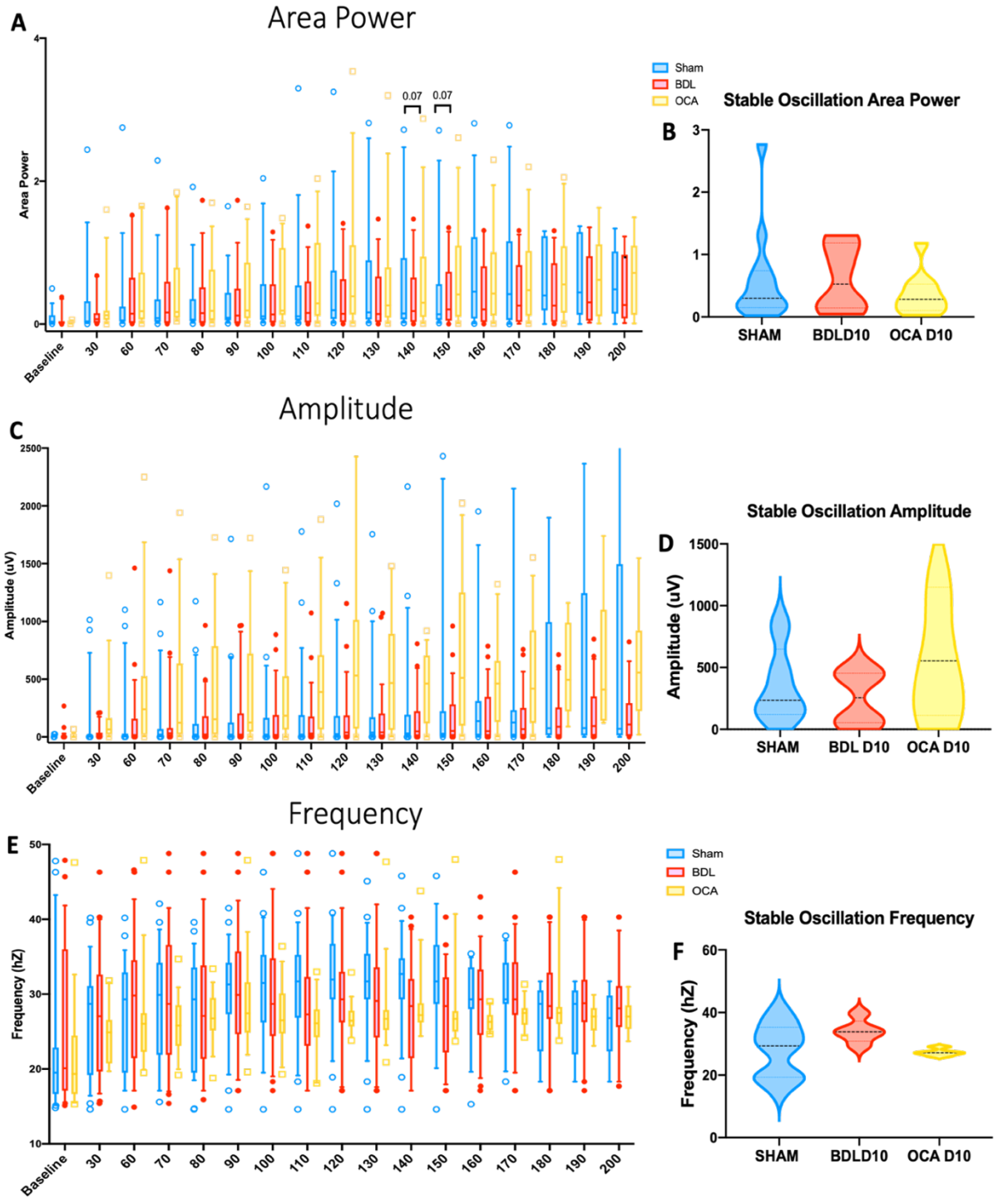

Figure 51. Longitudinal plot showing change to average area power (A), amplitude (C), and Frequency over time. N = 8 n=22 BDL N=8 n=27 OCA N= 7 n =17. Area power (B), amplitude (D), and frequency (F) of stable slices were compared between groups n= 19 sham, 5 BDL, n=10 OCA. N = animal number n = slice number.

When comparing all animals per group over time, generally in the first 90 minutes following carbachol administration area power increased steadily, after which power began to plateau. By 140 minutes post Cb application slices from BDL mice had a larger average area power than sham, to near significance (FIG 51A). However, as all animals were included this may be an artefact, due to BDL animals exhibiting a larger number of 'growing' oscillations. Therefore, the area power, frequency and amplitude were then compared in only the stable slices from each group. Stable oscillation area power showed that BDL animals on average had a larger area power of the oscillation than either sham or OCA treated animals, though this did not reach statistical significance.

However, stable oscillation amplitude (FIG 51B), and amplitude over time (FIG 51A) in OCA mice appeared to have a larger average amplitude than BDL. When comparing area and amplitude, OCA animals have a smaller area power but larger amplitude than BDL animals, possibly indicating that BDL oscillations have a less defined peak in the power spectrum (example seen figure 50D).

In contrast to area power and amplitude, oscillation frequency was initially variable but once oscillations are established the frequency remained constant (FIG 51A). There is a minor increase in the frequency of stable oscillations in BDL animals, on average 34 Hz, compared to 27 Hz for OCA and 28 Hz for sham animals (FIG 51B) though this is not significant. The above compares stable slices from each group n= 19 sham, n=5 BDL, n=10 OCA.

5.4.3. Propagation of oscillations differs Between Sham and BDL Animals

Hippocampal oscillations propagate through the hippocampal structure from CA3 to CA1. Ordinarily oscillations propagate to CA1 via the Schaffer's collaterals generating an oscillation in the CA1 region. This process is important for the encoding and retrieval of spatial memory (Montgomery and Buzsáki 2007) In this experiment once oscillations had

stabilised, one electrode was placed in the *stratum radiatum* region of the CA3, and the other placed initially in a near (proximal) location (FIG 52A), and recorded 3 times for 5 minutes to obtained an average measure. The second electrode was then moved to a more distal location near the CA1 region (FIG 52D), where three X five-minute recordings were again taken. Results were calculated as a percentage difference between the CA3 electrode and the other (proximal or distal) electrode.

Slices from Sham animals on average retained half of their area power and amplitude, with slightly less efficient propagation distally (around 40%). They were able to retain the power of the oscillation even when measured further away in the CA1. In these experiments slices taken from BDL mice appear worse in all measurements when compared to Sham. Stable BDL slice oscillations propagate on average half as well proximally with sham showing mean 60% area power, BDL mean 27% areas power when compared to the ME1 electrode (FIG 52B). Distal area power was almost completely lost in BDL animals, dropping to just 6% of the oscillation area power propagated to CA1, compared to 45% in sham animals (FIG 52E).

The percentage propagation of the oscillation amplitude was also reduced in the BDL animals. Both proximal (FIG 52C) and distal (FIG 52F) propagations of amplitude were reduced by just under a half in the BDL animals when compared to sham (proximal sham mean of 52%, BDL 28%, distal sham mean of 56%, BDL 3%.

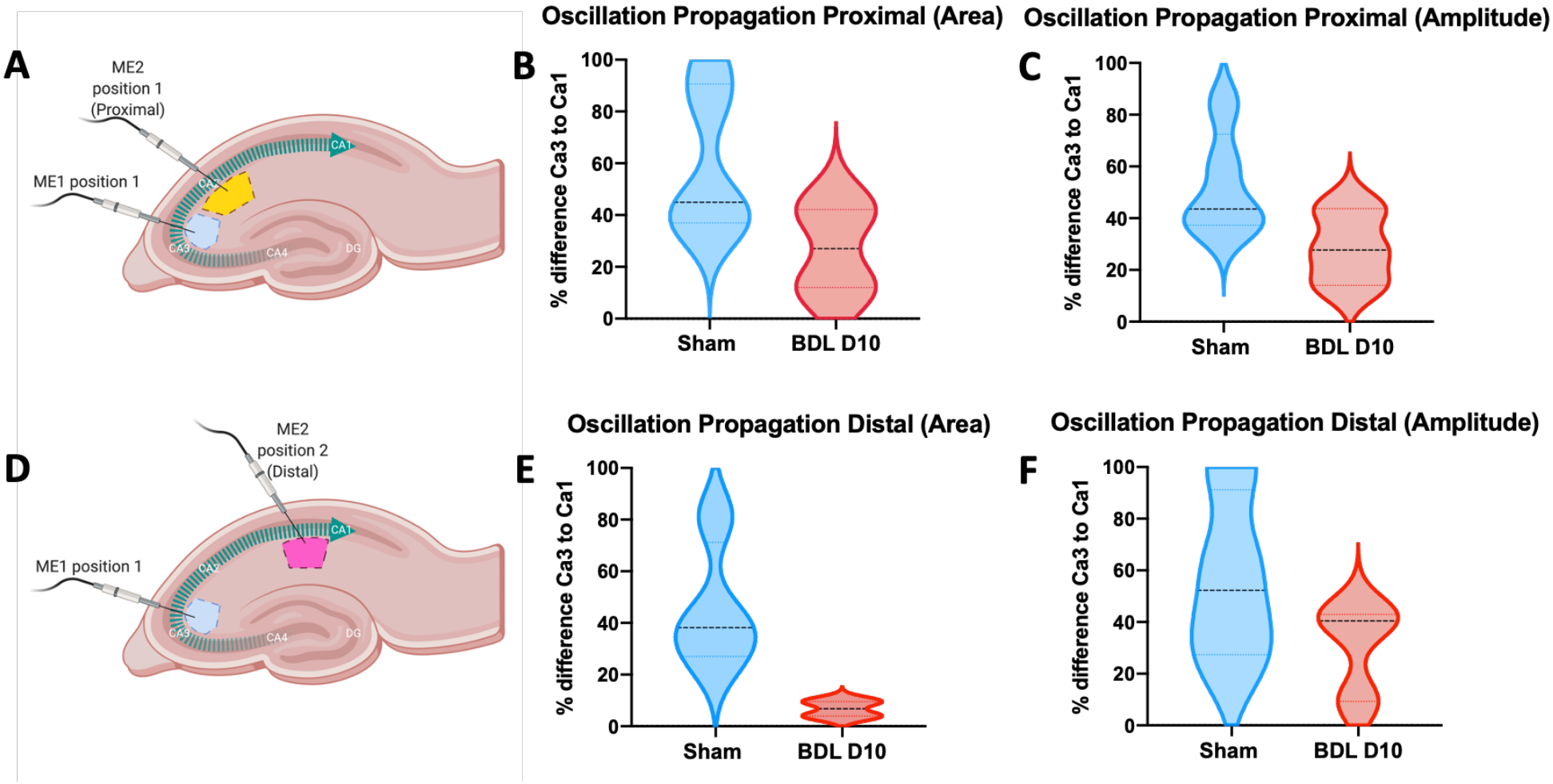

Figure 52. CA3-CA1 propagation was c ompared between sham and BDL groups. Slices were assessed for proximal (near) propagation (A), and distal propagation (D). Area power showed large reduction both proximally (B), and even larger distally (E) in the BDL group. Amplitude also showed reduction proximal (C) and distal (F) though to a lesser extent. N= 5 for sham and N= 3 for BDL.

5.4.4. Changes to Rhythmicity Occur with Bile Duct Ligation

Rhythmicity index (RI) is a way to measure synchronicity of oscillations and sham animals show the highest rhythmicity index with a score of 0.7 +/- (FIG 53A, D). BDL animals produce significantly less rhythmic oscillations, and were very variable (FIG 53B, D). OCA treated animals had more rhythmic oscillations than BDL untreated animals, however this did not reach significance (FIG 53C, D).

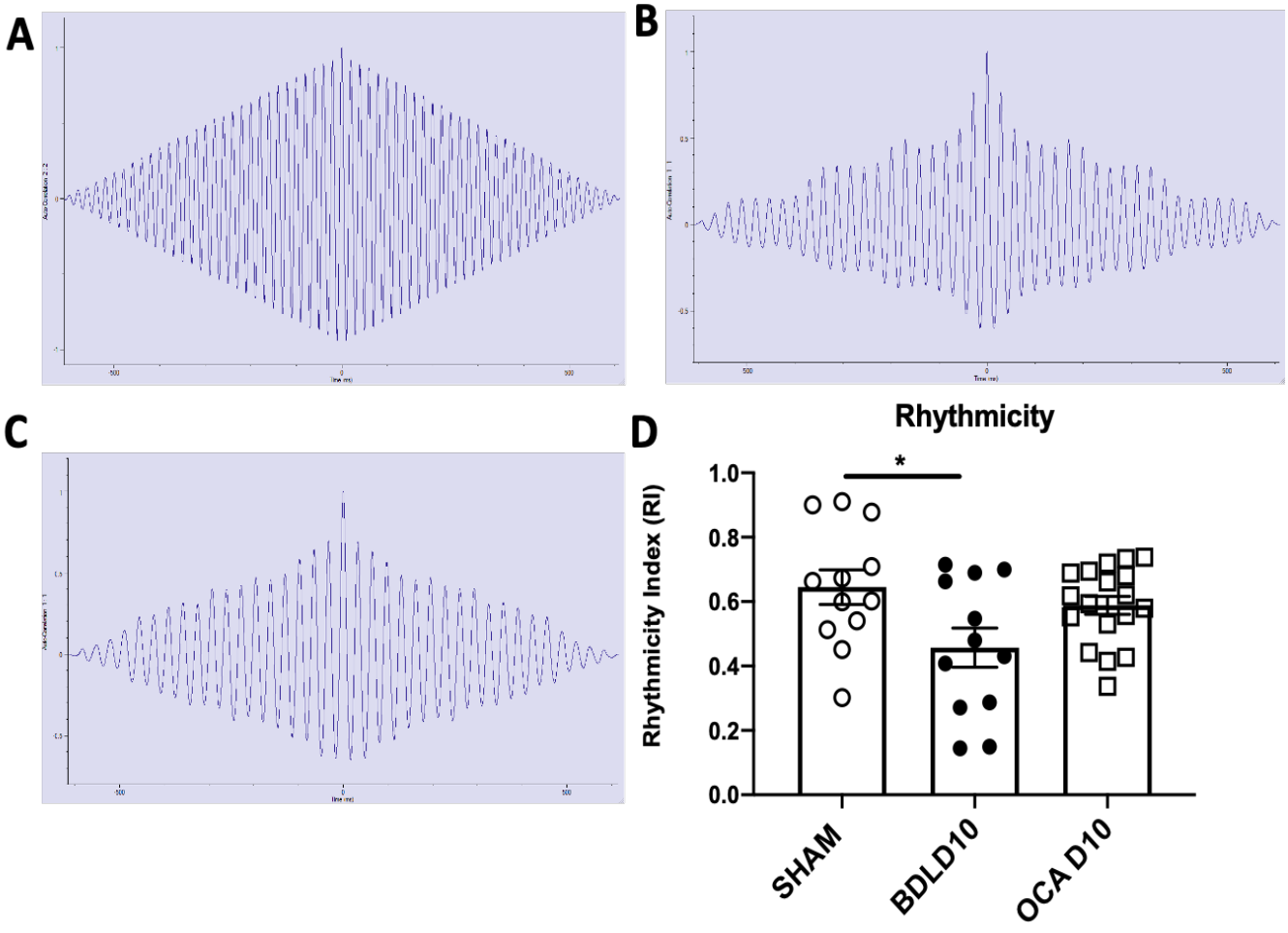

Figure 53. Autocorrelation of traces was performed on a 1second trace to assess oscillation rhythmicity index (RI). An example trace for Sham (A), BDL (B), and OCA treated animals (C). An example of traces from each group (D), rhythmicity index calculations per group (E) n=12 N=6 sham n=12 N=6 BDL, n=14 N=7 OCA. Data presented as mean +/- SEM statistics ANOVA.

5.4.5. Parvalbumin interneurons are partially lost with BDL

Histological assessment of PV+ fast spiking interneurons within the CA3 revealed a significant reduction in both soma number (FIG 54A) and optical density of dendritic spines (FIG 54B) in BDL mice by day 10 (10.08 vs 12.69 in Sham). Optical density is indicative of parvalbumin expression within the entirety of the interneuron, axons and dendrites (neuropil) in addition to the cell body.

Treatment with OCA (FIG 54E) salvaged the PV+ loss, bringing the cell counts back up to near sham level (sham 10.67 OCA 9.66, BDL 4.23 Average counts) (FIG 54A, E). However, OCA treatment did not significantly increase the optical density measurements (11.08) (FIG 54B), suggesting although cell counts remain similar to sham, the total levels of PV+ expression may be reduced.

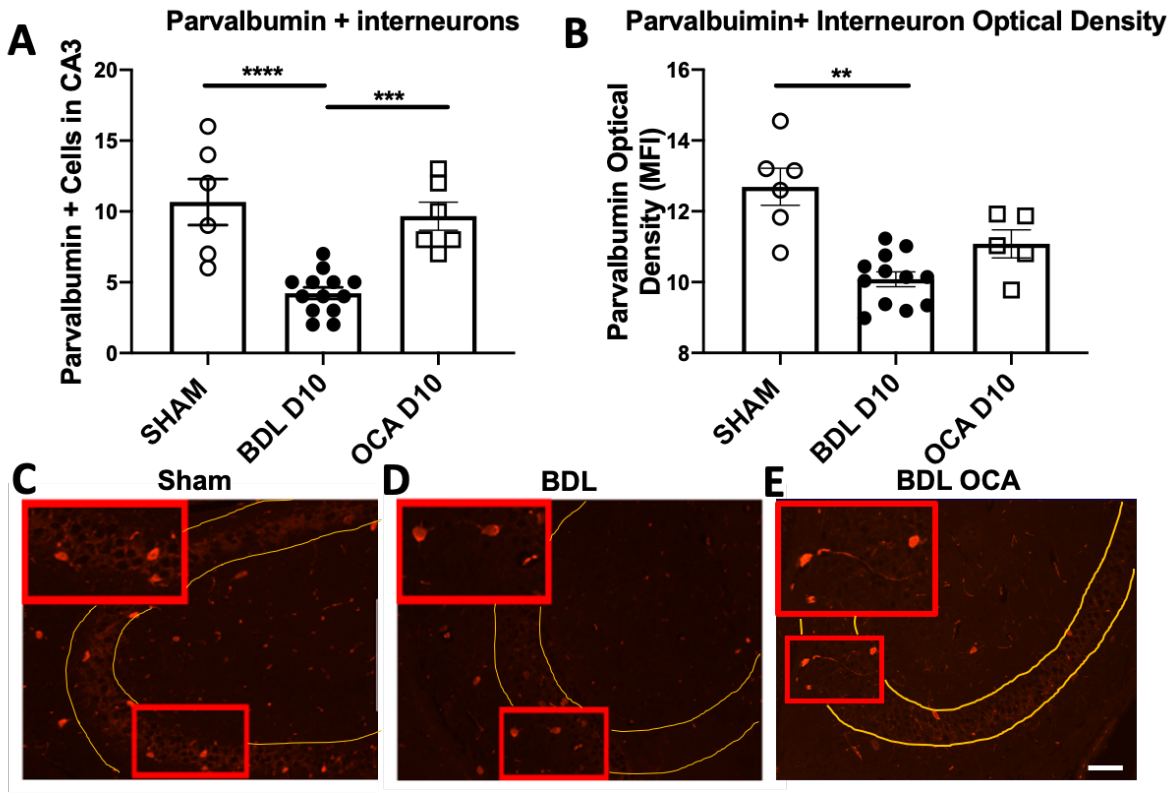

Figure 54. Parvalbumin+ GABAergic interneuron counts (A), and optical density (B) measurements in the CA3. Representative images from sham (C), BDL (D), OCA treated animals (E). These stains were performed on a separate cohort not undergoing electrophysiology. N= 6 sham, N= 12 BDL, N= 6 OCA. Data represented as mean +/- SEM statistics ANOVA. Scale= 100μM

5.5. Summary of findings of Chapter 5

In chapter 5 I aimed to assess changes to circuit functionality in animals undergoing BDL surgery, when compared to sham and OCA treated BDL mice. The key findings from the chapter are as follows:

- Gamma frequency oscillation are impaired as measured in the CA3 *stratum radiatum* region in BDL animals. Only 18% of BDL produced stable oscillations by 3 hours post carbachol administration, compared to 89% of sham animals.

- This phenotype is partially improved with OCA treatment from day of surgery. 62% of slices from OCA treated animals produced stable oscillations within 3 hours.

- Although there are a few differences in key parameters, such as area power, amplitude and frequency longitudinally, of the BDL slices that do stabilize on average they have a slightly higher frequency and area power, though these don't reach significance.

- The propagation of gamma oscillations from CA3 to CA1 is also affected in BDL mice - propagation was reduced both at proximal and distal locations, and in both area power and amplitude, though area power shows a larger reduction to just 6% power in distal regions.

- BDL animals also produce less synchronous oscillations than sham, with a significantly reduced rhythmicity index.

- Parvalbumin+ interneuron counts revealed a significant loss of interneuron soma in the CA3, as well as a reduced staining throughout the neuropil, resulting in reduced optical density in BDL animals when compared to sham. OCA treated animals retained more soma than BDL untreated mice, however still exhibited reduced optical density.

5.6. Conclusions

Previous data from this thesis showed that BDL mice display visual-spatial memory deficit by day 10 post-surgery (Chapter 3). The aim of this chapter was to characterise changes occurring in the gamma frequency oscillations of the hippocampus, which facilitate short term memory process (Montgomery and Buzsáki 2007). We also assessed histologically alterations in PV+ interneurons in the CA3, as they directly contribute to the generation of gamma oscillations by inhibiting the firing of pyramidal cells(Ognjanovski, Schaeffer et al. 2017, Antonoudiou, Tan et al. 2020).

I found BDL mice exhibited several changes to hippocampal networks and subsequently to gamma frequency oscillation. Hippocampal slices from BDL mice were found to be 70% less likely than sham slices to produce stable oscillations by 3 hours post carbachol administration (18% stable vs 89%). This loss of network stability could be directly related to the memory deficit seen in the previous behavioural testing. Stable gamma frequency oscillations are important for the encoding of several types of memory, such as visual spatial memory and executive function (Lu, Vreugdenhil et al. 2012) and object-place recognition (Zheng, Bieri et al. 2016).

We also assessed the rhythmicity of the gamma frequency oscillation and found BDL animals showed significantly less rhythmic oscillations at 180 minutes post-carbachol application (FIG 53). Synchrony of the neuronal network has been proposed to form neural correlates of cognitive information and facilitate memory encoding (Singer 1999). Loss of network synchrony can be seen in various pathological conditions including in Alzheimer's disease, Parkinson's disease, schizophrenia (Uhlhaas and Singer 2006), and to a smaller extent in normal ageing. The loss of this network synchrony is a common pathological marker indicating reduced network capacity and health.

Gamma frequency oscillations are generated in the CA3 and propagate through to CA1 (Csicsvari, Jamieson et al. 2003) via the Schaffer collaterals. This process has long been implicated in the storage and retrieval of memory (Steffenach, Sloviter et al. 2002), and

gamma CA3-CA1 synchrony is seen in tasks such as the Y maze, where retrieval of memories from previous trials affects arm choice (Montgomery and Buzsáki 2007). In this study BDL mice showed decreased propagation with reduced area power and amplitude of the oscillations in the CA1 compared to sham animals, both proximally and distally (FIG 50. Therefore, a loss of CA3-CA1 propagation may underpin the short-term memory recall deficit seen in BDL mice in the Y-maze.

We also found a significant loss of parvalbumin PV+ interneurons, as both the number of cell bodies and the overall optical density in the BDL group was reduced (FIG 54). This loss of parvalbumin expression could provide an underpinning mechanism for the circuit dysfunction and asynchrony. Fast spiking GABAergic interneurons (basket cells) within the CA3 initiate oscillations via the reciprocal firing interactions of pyramidal cell and fast-spiking GABAergic interneurons which are PV+ (Gulyás, Szabó et al. 2010, Whittington, Cunningham et al. 2011). The synchronous firing of Parvalbumin+ interneurons is linked directly to the encoding of short-term and visual spatial memory (Colgin, Denninger et al. 2009).

However, these parvalbumin+ interneurons are highly sensitive to oxidative damage (Kann, Papageorgiou et al. 2014), leading to cell loss during old age. The death or dysfunction of Parvalbumin+ interneurons is associated with cognitive decline in both healthy aged (Vreugdenhil and Toescu 2005) mice and in rodent models of neurodegenerative conditions (Robson, Tweedy et al. 2018).

Oxidative damage can be caused by several biological processes. The dysfunction of mitochondria is a common cause of oxidative stress, with impaired mitochondria overproducing reactive oxygen species (ROS) and leading to oxygen free radicals, an excess of which cause oxidative stress. ROS can damage cells in a number of ways, by oxidising proteins and causing DNA damage which can lead to cellular senescence. Though we have not assessed mitochondrial function in the BDL model, we do see a senescence phenotype within the CA3 in BDL mice (Chapter 3). We also see an increase in DNA damage as measured by γH2AX (Chapter 3). There is also an abundance of evidence of oxidative stress and mitochondrial dysfunction in the liver during cholestasis (Heidari, Ghanbarinejad et al. 2018). Therefore, it is likely that oxidative damage and resulting senescence is causing harm to

sensitive PV+ interneurons, and that the senescence seen within the CA3 region is affecting the generation and transmission of gamma frequency oscillations.

Even if the senescent neurons are not themselves the PV+ interneurons, the presence of senescent cells could damage surrounding neurons. Senescent cells actively release SASP, and cytokines such as IL-6 and IL-8 are commonly produced, triggering damage to nearby cells. IL-6, for example, is associated with cognitive dysfunction in several disease states, including a exacerbator role in Alzheimer's disease (Bauer, Ganter et al. 1992).

Previous data from this thesis has also shown that BDL mice have increased neuroinflammation within the hippocampus (Chapter 3). Chronic inflammation has been shown to impair LTP in the Schaffer collaterals (Min, Quan et al. 2009) and, therefore, may play a role in disruption of gamma frequency oscillations, particularly in the CA3-CA1 propagation impairment seen in BDL animals.

From the data shown in this chapter it seems that OCA treated BDL mice have fewer network abnormalities than untreated BDL mice. However, there are still clear differences when compared to the sham group. Slices from OCA treated animals were less likely to produce stable oscillations than sham animals, and had a higher incidence of unstable oscillation phenotypes such as fluctuating oscillations than sham animals.

OCA treated mice also had a slight reduction in rhythmicity index score, and showed a rescue of the PV+ cell loss seen in BDL, but the optical density was only slightly higher. This mixed phenotype may serve as a partial explanation for the circuit abnormalities still occurring in the OCA group. Obeticholic acid treatment may prevent the absolute loss of the PV+ interneurons, but expression of parvalbumin is still reduced in these interneurons.

To date, there is little mechanistic evidence of neuronal dysfunction in cholestatic models, beyond behavioural testing data. Previous papers published on electrophysiology in the BDL model find variable results through patch clamping CA1 neurons, which displayed reduced excitability in the CA1 (Tahamtan, Aghaei et al. 2017), and hyperexcitability in the cerebellum (Aghaei, Hajali et al. 2016). While other studies have found impaired hippocampal LTP from

liver disease using models of hyperammonia, to emulate hepatic encephalopathy (Monfort, Muñoz et al. 2005).

These data provide the first evidence of cholestasis related changes to hippocampal gamma frequency oscillation properties. They also provide further evidence that OCA treatment, when given to cholestatic mice from the day of surgery, can modify disease course and reduce the cognitive dysfunction. In this instance, OCA partially improves PV+ interneurons, reducing the number of cells lost during cholestasis. OCA also prevented loss of synchrony and network stability that is induced by cholestasis in this model. It remains unclear whether senescence is the driver of cognitive decline, inducing oxidative damage, senescence or death in the PV+ interneuron group. This could directly cause the changes seen in the oscillations, and lead to cognitive decline. Alternatively, PV+ interneurons may be damaged or become senescent due to secondary effects of circulating inflammatory liver phenotype. Proposed mechanisms outlined below (figure 55).

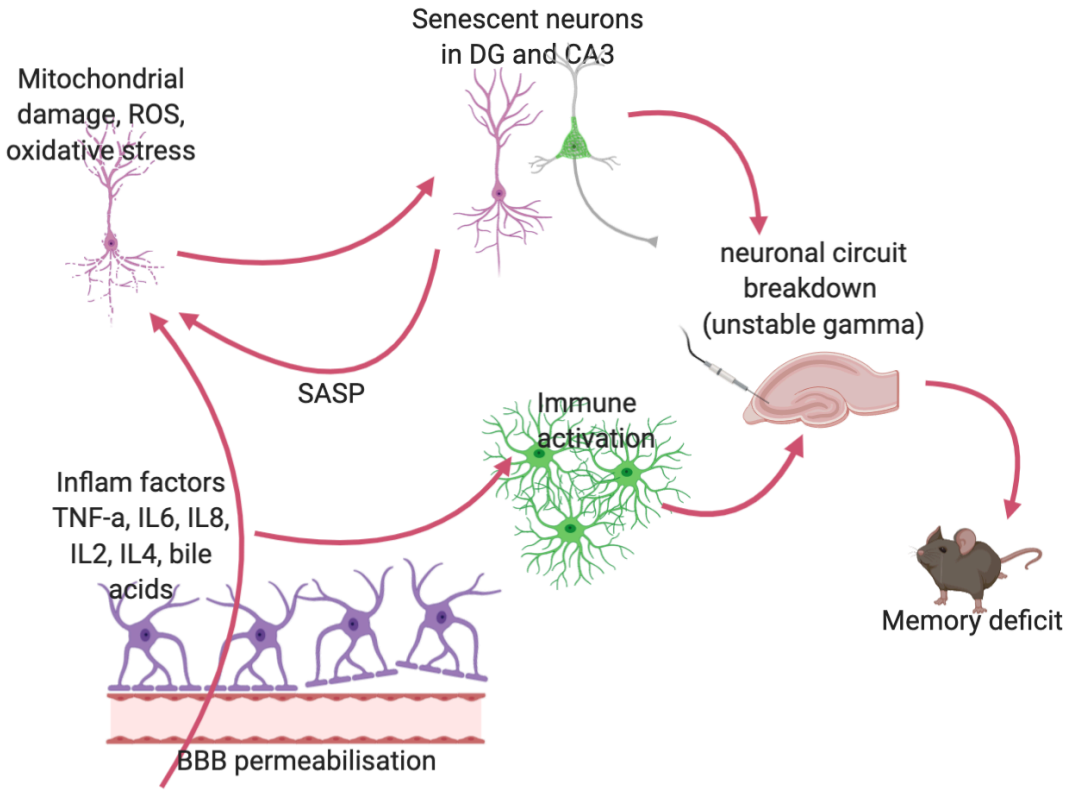

Figure 55. Proposed mechanism for the culmination of direct and indirect effects of circulating inflammatory factors caused by cholestasis in the brain.

6. Chapter Six – In vitro Modelling of cholestasis mediated cognitive decline

6.1. Introduction

In vitro models provide invaluable insight into specific disease pathology that isn't possible with animal models. Though animal models provide a whole system, unless producing a knock in or knock out, it becomes extremely difficult to tease apart the complex signalling pathways and interlinking cellular function in a whole organism model. Therefore in vitro modelling is required to tease apart the specific effects of cholestasis and circulatory toxins on neurons.

6.1.1. A Role for Bile Acid Receptors in the Brain?

Publications investigating the activity of bile acid receptors in the brain have stipulated receptors to be present in several key cell types. TGR5 has been characterised within both neurons and astrocytes within the brain, and it's presence confirmed by different groups (Keitel, Görg et al. 2010, McMillin, Frampton et al. 2015). The presence and functionality of FXR is less well defined. A study published in 2015 found FXR mRNA absent in the brain (Huang, Wang et al. 2015). However, global FXR deletion in mice led to several changes to both neurotransmission and behaviour, with reduced anxiety and impaired memory. Subsequent studies show FXR at mRNA and protein level in neurons in the mouse and human cultured brain. FXR was found to be localised to the nucleus in cultured neurons, but more cytoplasmic in vivo (Huang, Wang et al. 2016). However, the functions of brain resident glia such as astrocytes and microglia do not seem to be modified by activation through FXR (Albrecht, Fleck et al. 2017).

Other bile acids have also been identified in the brain, cholic acid presence was shown to activate liver X Receptor (LXR) present in dopaminergic neurons of the midbrain promoting neurogenesis there (Theofilopoulos, Wang et al. 2013). Knockout mouse models for LXR suffer motor degeneration and astrocytosis, with impaired motor function (Andersson,

Gustafsson et al. 2005). It is clear from these studies that bile acids are able to exert pleotropic effects in the brain – and that signalling is required for normal functions. Bile acids are able to signal in the brain, several bile acid receptors have been found to be expressed, indicating an as yet undiscovered role for bile acids within the brain itself.

6.1.2. In vitro signalling evidence in liver research

6.1.2.1. The Blood Brain Barrier

A lot of research in the field supports the idea that blood brain barrier (BBB) breakdown could facilitate entry into the brain, where bile acid signalling could cause toxic effects and the resultant pathological neurological deficits. Proof of bile acid related BBB breakdown is largely limited to in vitro modelling of human cells. There is in vitro evidence that bilirubin exposure can affect the function of BMECs and render them apoptotic (Palmela, Cardoso et al. 2011), as well as affecting tight junctions (Palmela et al., 2012). The upregulation of IL-6 in these studies was postulated to have a role in BBB breakdown, as in other conditions such as stroke (Blecharz-Lang, Wagner et al. 2018) and systemic inflammation (Hirohata, Matsueda et al. 2017).

In these experiments treatment with bilirubin (UCB) led to a bi-phasic response, of which the second phase caused the reduction in zonula occludens (ZO)-1 and β-catenin levels, thus leading to reduction of tight junctions and cell-to-cell contacts. These changes could potentially increase para- cellular permeability and allow bile acid entry into the brain in pathogenic conditions. Of the few studies that have been performed in vivo, disruption of tight junction proteins occludin and claudin-5 (Quinn et al., 2014) are observed, however other aspects of the cellular matrix, including astrocytic and pericytic modulation of the blood brain barrier, have not been thoroughly studied bar one paper using an in vitro BMEC astrocyte co-culture system (Cardoso, Kittel et al. 2012).

Follow up studies by the same group go on to suggest that certain bile acid properties such as hydrophilicity may affect their actions on the BBB (Palmela, Correia et al. 2015). Hydrophilic bile acids such as ursodeoxycholic acid (UDCA) and glycoursodeoxycholic acid (GUDCA) were

found to have protective effects at the barrier, both reducing apoptotic nuclei. However only GUDCA was effective in reducing caspase 3 activity.

6.1.3. Bile acid Therapies in Neurodegenerative disease

6.1.3.1. Alzheimer's disease

The use of bile acid therapies in Alzheimer's disease (AD) has become a widely researched area, first investigated due to their cholesterol modifying properties. Changes to cholesterol metabolism have been directly implicated in AD progression (Puglielli, Tanzi et al. 2003). One of the major risk factors for Alzheimer' disease, Apolipoprotein E (APOE) mutation 4, is a protein which combines with lipids to form lipoproteins. APOE4 modifies cholesterol homeostasis by altering lipoprotein particle formation.

In vitro modelling of AD is often using cultured neurons treated with amyloid-β (Aβ) peptides, leading to cytotoxicity in the cells. Pre-treatment of cells with tauro-conjugated UDCA (TUDCA) was found to reduce apoptosis in primary cortical rat Aβ cultures through phosphatidylinositide 3'-OH kinase (PI3K) signalling (Solá, Castro et al. 2003). Follow up from the same group showed UDCA and TUDCA both had anti-apoptotic properties through the mineralocorticoid receptor (Solá, Amaral et al. 2006) in neurons, and through NF-κB regulation in microglia (Joo, Won et al. 2004).

The outcomes of these in vitro studies have been so successful that bile acid therapies have since been studied in mouse models. Longitudinal 0.4% (wt/wt) TUDCA dosing for six months in APP/PS1 mice was found to reduce the number of amyloid plaques and resulting neuron damage in the hippocampus and frontal cortex, improving memory (Nunes, Amaral et al. 2012).

Humans studies investigating bile acid composition changes in AD patients found lithocholic acid to be highly increased in the bile acid pool of those with AD. Other implicated bile acids include glycine conjugated bile acids glycodeoxycholic acid (GDCA), glycolithocholic acid (GLCA), glycochenodeoxycholic acid (GCDCA). Other blood based studies identified different glycine conjugated bile acids such as glycoursodeoxycholic acid (GUDCA) as an early

predicator of cognitive impairment (Mapstone, Cheema et al. 2014). Studies from as recently as 2019 find significant changes to bile acid profile in AD patients, finding increased ratio of secondary bile acids strongly associated with progression from mild cognitive impairment to AD, implicating change to secondary transformation processes in the gut. Bile acids highlighted by these studies such as LCA and GLCA are some of the most hydrophobic. Hydrophobicity is known to affect cytotoxic properties of bile acids, reported in the liver to cause damage to mitochondria and inhibit normal cell function (Krähenbühl, Talos et al. 1994).

6.2. Aims of Chapter Six

Bile acids are a diverse group of neuroactive compounds with wide ranging effects. This chapter uses in vitro fetal derived neuronal cells to investigate the effects of patient and mouse serum treatments on neurons, and of the effects of specific bile acids treatments.

We also aim to tease apart specific effects of OCA on the development of senescence. In mouse models we see a reduction in hippocampal neuronal senescence in OCA treated groups. However, as it occurs in parallel with reduced hepatic senescence, it remains unclear whether the OCA effect is driven through primary effects on neuronal cells, or through secondary signalling from the liver. Therefore, we chose to assess the anti-senescent action of OCA when cells are pre-treated for 1 hour before cholestatic serum dosing. This will enable us to see the effects of OCA signalling on neurons treated with cholestatic serum.

The aims of this chapter are as follows:

- Investigate differential effects on neuron death when treated with hydrophobic (lithocholic acid) and hydrophilic (taurocholic acid) using concentrations ranging from 0.5pm to 100µm
- Investigate the effect on viability of direct neuron exposure to serum from cholestatic mice and patients when compared with normal controls
- Assess influence of anti-cholestatic drug treatments such as OCA on cell viability
- Investigate the impact of human and mouse cholestatic serums on senescence of cells by using B-galactosidase assay

- Assess influence of anti-cholestatic treatment OCA on neuronal senescence
- Investigate bile acid receptor FXR and TGR5expression in 97 neuronal cells to elucidate mechanism of OCA effects

6.3. Workflow

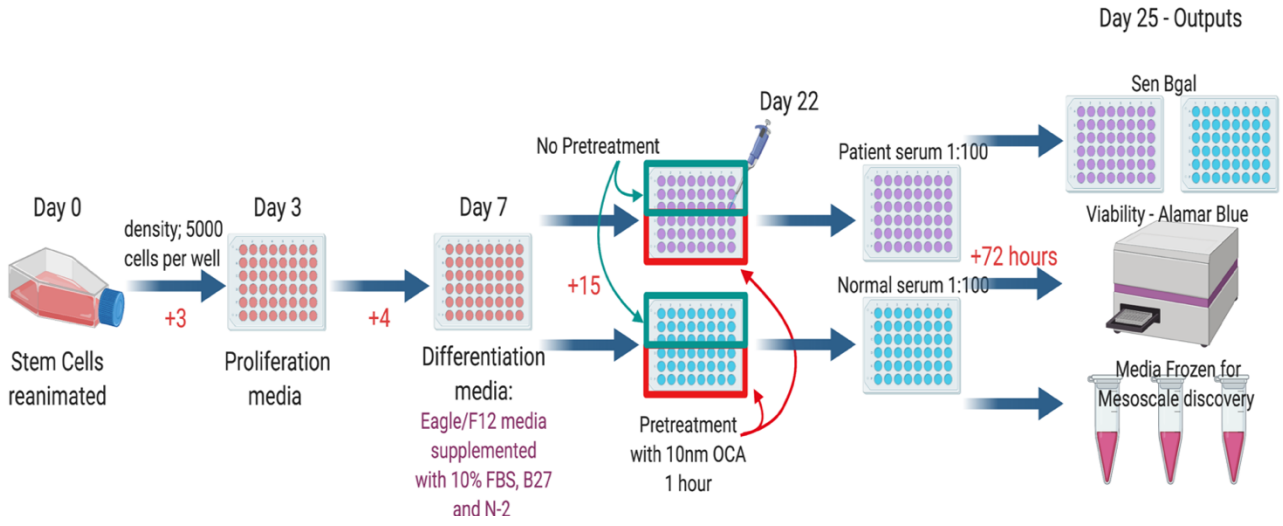

Figure 56. In vitro experimental workflow for 97 neuronal cells

6.4. Results

6.4.1. Differential Effects of Dosing with Cholestatic Versus Normal Serum

6.4.1.1. Mouse Serum Dosing Dilution Testing

Initial dosing experiments with mouse serums from sham, BDL and BDL mice treated with OCA revealed little change to cell viability between groups (FIG 57A).

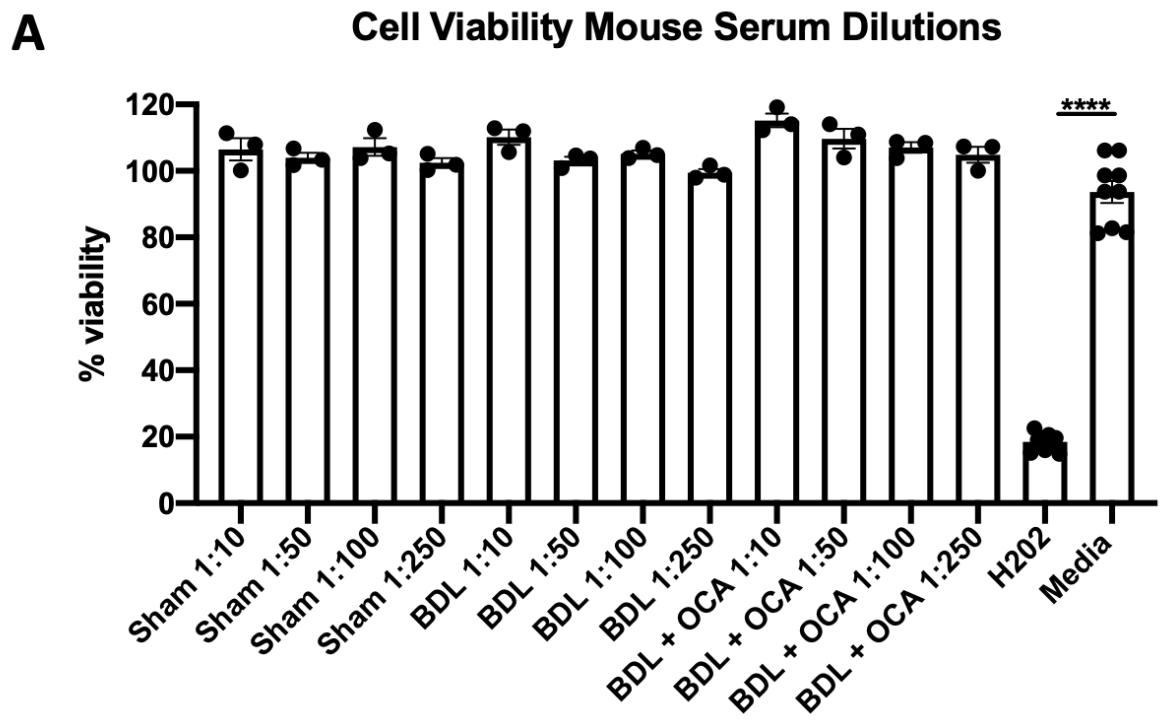

Figure 57. Initial experiment focussed on dosing varying dilutions of serum from sham and BDL mice. H202 was used as a positive control and viaibility was calculated based on media only wells per plate. N= 3 animals per group. Statistical analysis using ANOVA. Data represented as mean +/- SEM

6.4.1.2. BDL Serum Treatments show Mild Effects on Neuron Viability

Using a final concentration of 1:100 for dosing experiment, the experiment was repeated with additional outputs. Wells containing Sham, media only and hydrogen peroxide were also treated with Obeticholic acid. Each of the wells treated with OCA trended towards increased viability, including both sham and BDL treatment groups (FIG 58A). Both sham plus OCA and media only plus OCA groups showed a significant increase in viability as measured by the alamar blue assay. Wells treated with BDL serum showed a minor decrease in viability when compared to media only and sham wells, though this didn't reach significance.

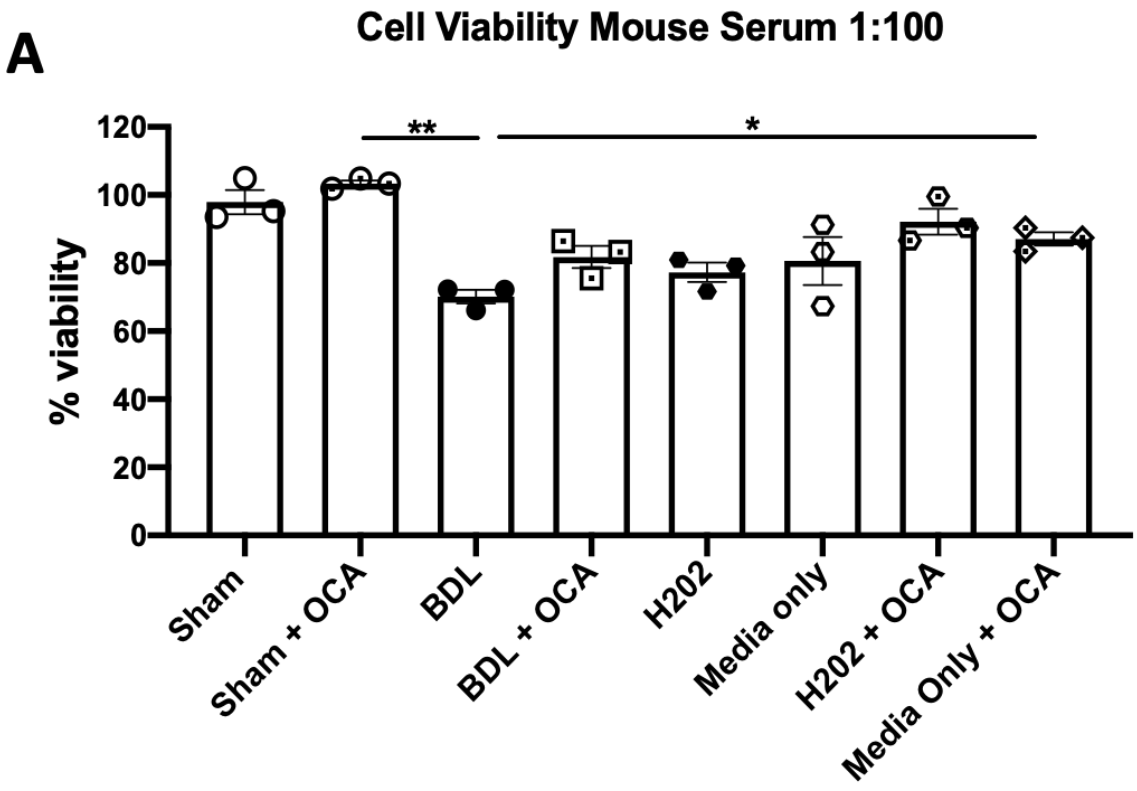

Figure 58. Experiment was repeated at chosen dose of 1:100 serum dilution. Three more sham and BDL mouse serums were tested and compared to media only well. N=3 animals per group. Statistical analysis using ANOVA. Data represented as mean +/- SEM

6.4.1.3. BDL serum treatment causes senescence in Neurons

The same neurons underwent Sen-B galactosidase assay in order to assess levels of senescence induced by each treatment. Peroxide treatment strongly induced senescence as expected (FIG 59). However, 72-hour treatment with serum from BDL mice induced 2x the senescence seen in media only wells. Pre-treatment of neurons with OCA significantly reduced senescence in the BDL treated wells. Pre-treatment of sham serum wells with OCA did not significantly reduce senescence.

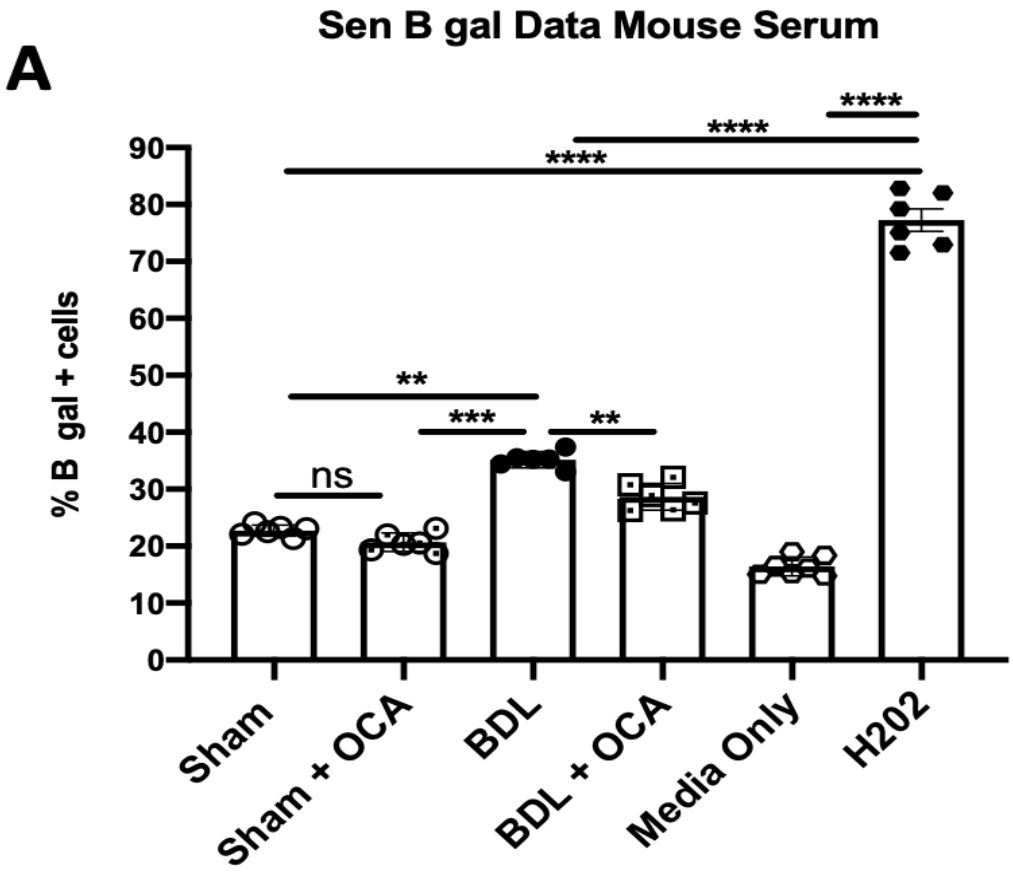

Figure 59. The combined plates were used for sen B gal senescence assay. BDL serum was found to be significantly pro-senescent when compared to media only wells, or those treated with sham serum. Pretreatment with OCA was found to significantly reduce the percentage of senescent cells in BDL serum wells. OCA pretreatment in sham serum treated wells did not significantly reduce senescence. Data are mean +/- sem, N= 6 animals per group.Statistical analysis using ANOVA

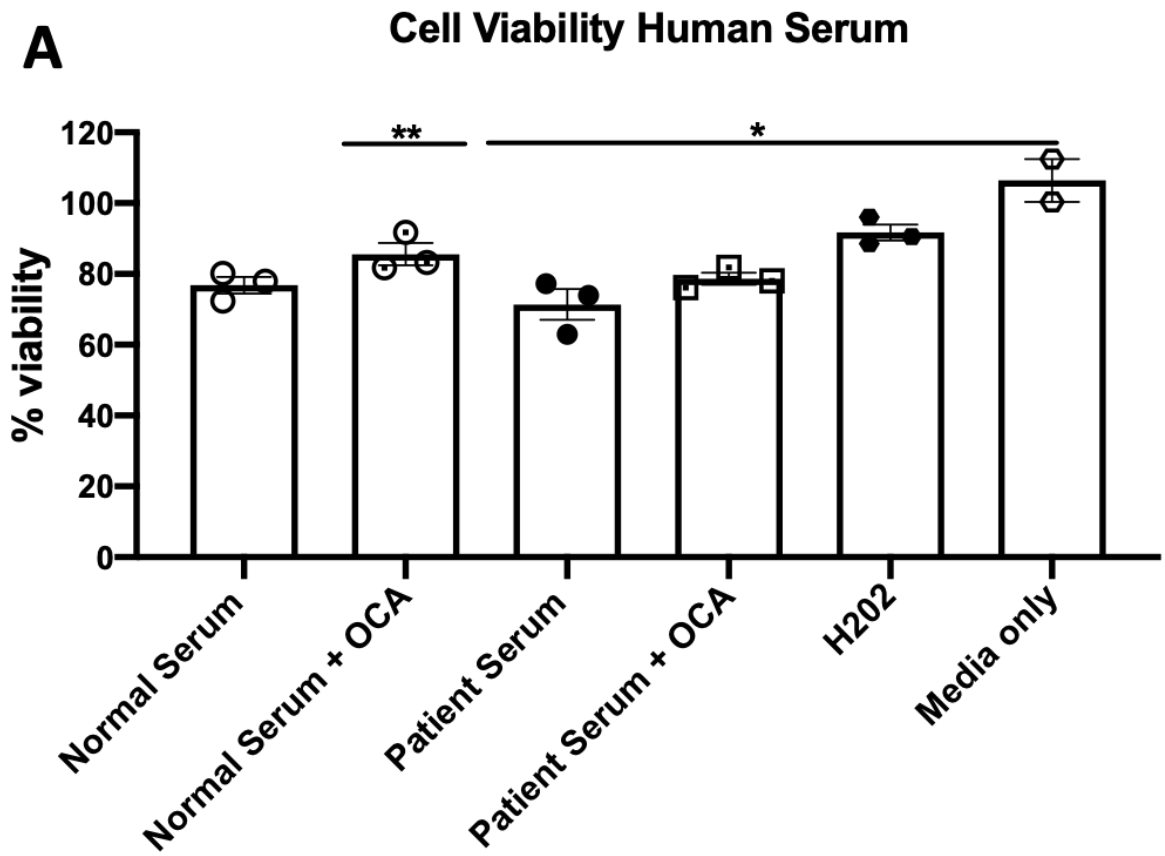

Figure 60. Neurons treated with serums from PBC patients at concentration of 1:100 showed reduced viability when compared to media only wells. Neurons treated with normal human serum did not show reduced viability. Normal serum wells pre-treated with OCA had significantly increased viability when compared to PBC patient serum wells. Data are mean +/- sem, N= 3 samples per group to date. Statistical analysis using ANOVA

6.4.1.1. Treatment with serum from PBC patients and Healthy controls affects neuronal Viability

Similarly, to mice cholestatic serums, serums from PBC patients caused some reduction in cell viability, when compared to media only wells (FIG 60). This indicates that some cell death is likely occurring as a result of serum dosing to the neurons. Viability increases stepwise with OCA pre-treatment, suggesting a protective effect of OCA.

6.4.1.2. Treatment with serum from PBC patients and Healthy controls Induces Neuronal Senescence

Treatment with serum from cognitively dysfunctional PBC patients produced a similar effect to cholestatic mouse serum (FIG 61). Patient serum treatment induced the second highest level of senescence after peroxide treatment, and was significantly more pro-senescent than normal serum or media only wells. Pre-incubation with OCA significantly reduced senescence in neurons treated with patient serums.

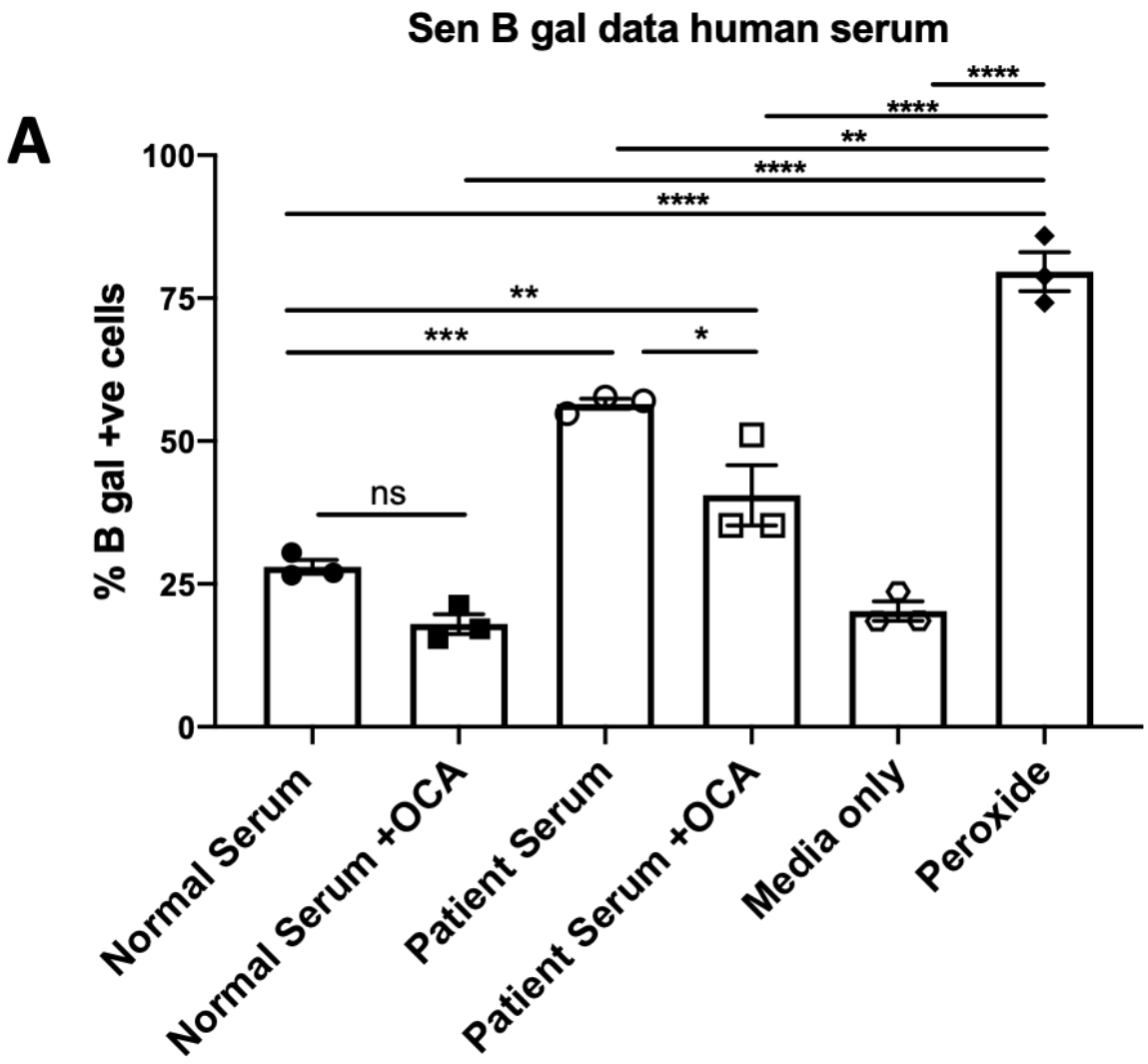

Figure 61. Sen B gal senescence assay on wells in figure 4 showed significant increase in senescence in Patient serum group compared to media only wells, and compared to Normal serum wells +/- OCA. Pretreatment of patient serum with OCA significantly reduced senescence. N= 3 samples per group to date. Statistical analysis using ANOVA. Data represented as +/- SEM.

6.4.2. Effects of Specific Bile acids on Neuronal Health

6.4.2.1. Lithocholic acid Affects the Health of Neurons

Lithocholic acid appears to have a negative impact on neuronal health as measured by the alamar blue assay on days 0, 1, 7 and 14. Treatment at a concentration of 100pm shows the greatest impact on viability, with a decreasing trend from day 1 (FIG 62A) that becomes significant by days 7 and 14 (FIG 62B, C). Higher concentrations such as 500nm and above reduce cell viability. Interestingly, the highest concentrations of LCA 1µm and 100µm have less impact on cell viability than 100pm and 500nm. Change over time measurements show a general downward trend in viability from day 1 to 14 for all concentrations of LCA treatment (FIG 62D).

6.4.2.2. Taurocholic acid has little effect on the Health of Neurons

Opposingly taurocholic acid trends towards an increased viability when compared to media only in all concentrations over time (FIG 63D). The three highest concentrations of TCA 500nm, 1µm and 100µm show significantly increased viability by days 7 (FIG 63B) and 14 (FIG 63C). This data suggest that TCA treatment improves neuronal viability and therefore health.

6.4.3. Bile Acid Receptor Expression Profile of Neuronal Cells

6.4.3.1. Farnesoid X Receptor (FXR)

FXR is the main signalling receptor for OCA. FXR was found to be expressed in several protein samples, including human brain and liver. Interestingly, in the neuronal cells used for the other experiments FXR was relatively highly expressed (FIG 64A). In this sample, FXR can be seen to be expressed at five different molecular weights. This could be due to the different isoforms of FXR, or due to cleavage of the protein in to different molecular weights. There are

reported to be at least four FXR isoforms (Zhang, Kast-Woelbern et al. 2003), which perform differing cellular functions (Ramos Pittol, Milona et al. 2020). Another explanation for the various molecular weights of FXR may be that the protein is undergoing digestion or degradation. Mature neurons were treated with either normal or patient serum (+/- OCA) for 72 hours and co-stained with NeuN and FXR, colocalised positive staining was seen. When ROI was set for whole cell FXR expression was reduced in patient serum treated neurons compared to normal serum treated (FIG 64B, D, E). When ROI was reduced to include only nuclear expression of FXR, there was no difference between groups (FIG 64C).

6.4.3.2. Takeda G Protein 5 Receptor (TGR5)

OCA has been shown to evoke secondary activation of TGR5. The expression of this receptor was very little in the neuronal cells (highlighted) (FIG 65A). TGR5 did show some expression in human liver and brain samples, as well as neuroblastoma cell lines SY5Y. There was also some expression of TGR5 in BBB endothelial cells.

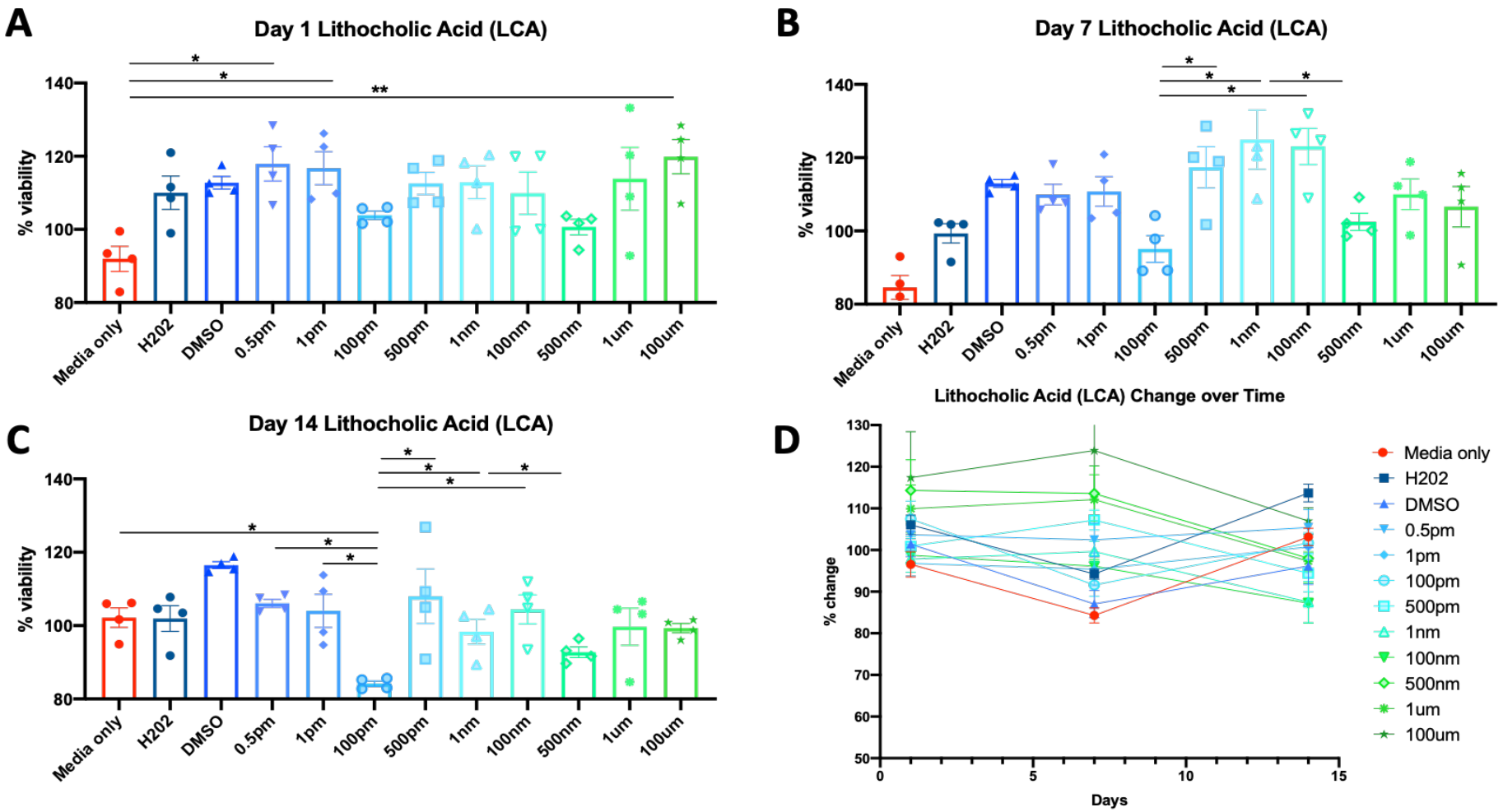

Figure 62. Lithocholic Acid treatment experiments. (A) By day 1 viability was improved in some concentrations. (B) By day 7 some concentrations had reduced viaibiltyand some increased. (D) by day 14 100pm concentration showed reduced viability. (D) Change over time shows a trend for reduced viability. Data represented as mean +/- SEM statistics ANOVA N=4 per concentration

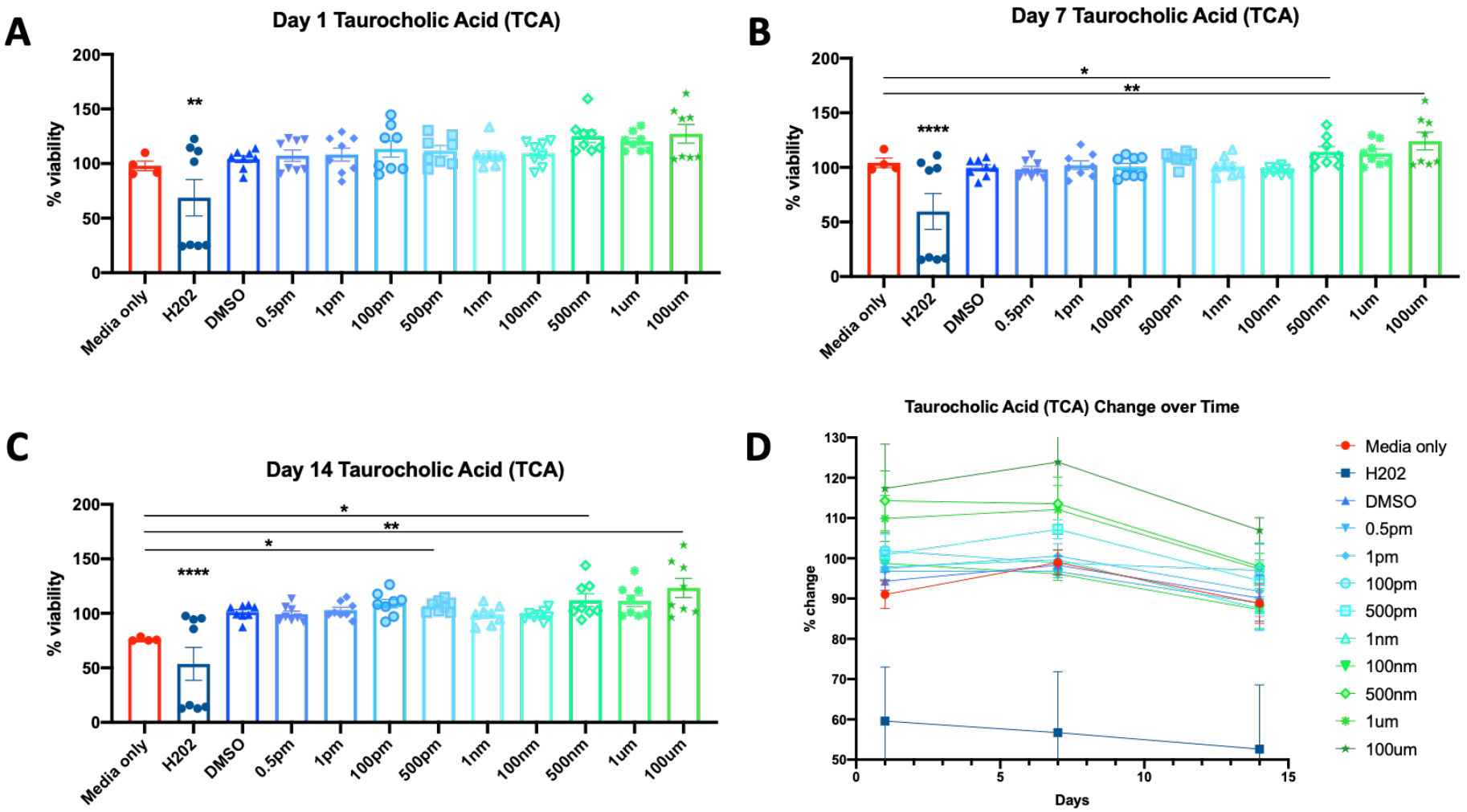

Figure 63 Taurocholic Acid treatment experiments. (A) By day 1 viability remained stable. (B) By day 7 some concentrations had increased viability. (D) by day 14high concentrations showed increased viaibility. (D) Change over time shows a trend for stableviability. Data represented as mean +/- SEM statistics Kruskal Wallis test N=8 per concentration.

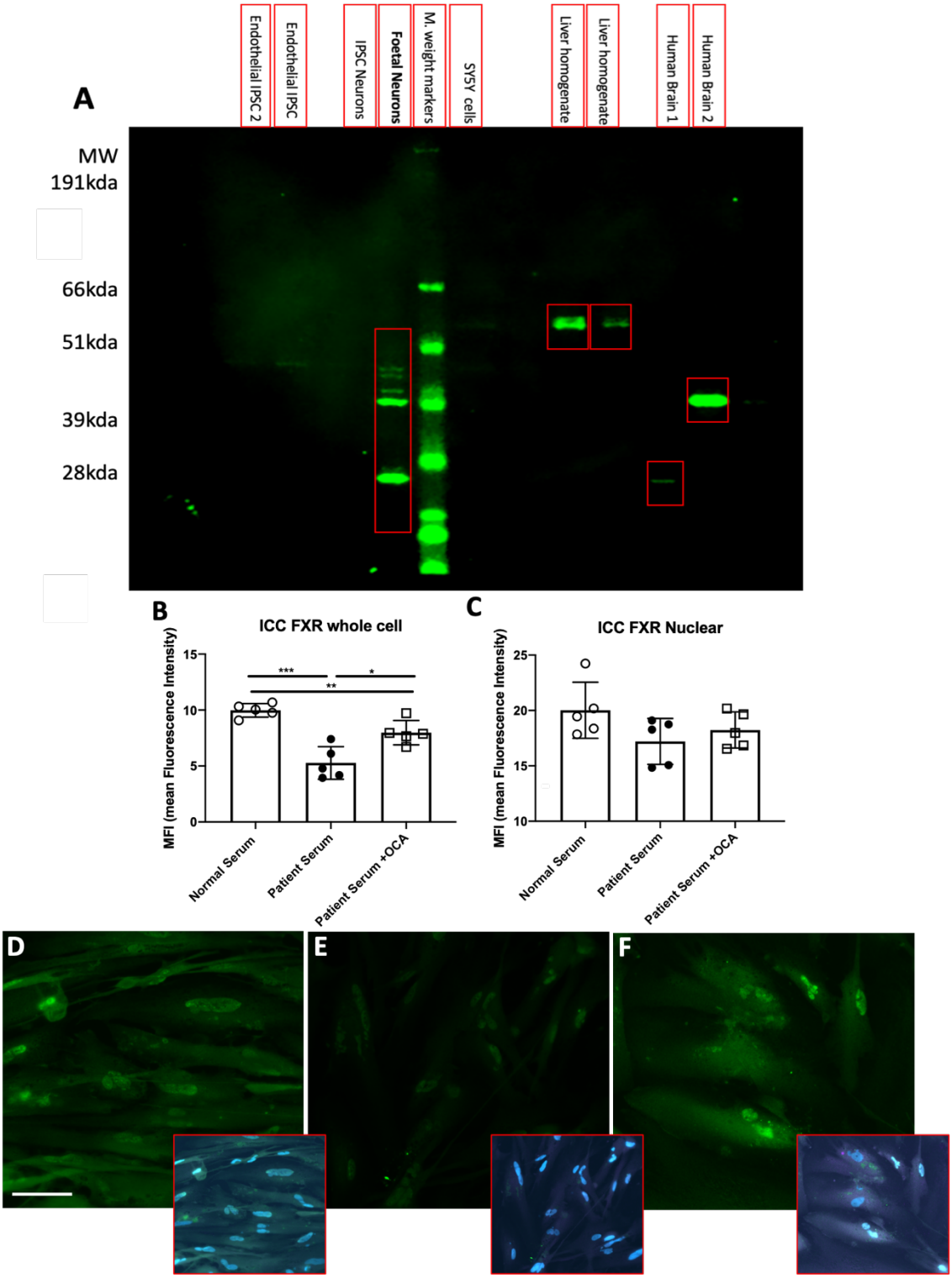

Figure 64. FXR expression in various neuronal cells, endothelial cells and human brain and liver homogenates. (A) FXR is expressed in several isoforms (B)FXR expression is reduced in whole cell patient serum treated neurons, and neurons treated with patient serum +OCA to a smaller extent (C)Nuclear FXR expression shows no differences between normal or patient serum treated neurons (D) representative image showing FXR expression in normal serum treated neurons with NeuN and DAPI overlay image insetted (E) representative image showing FXR expression in patient serum treated neurons with NeuN and DAPI overlay image insetted (F) representative image showing FXR expression in patient serum +OCA treated neurons with NeuN and DAPI overlay image insetted. Represented as mean +/- SEM, statistics ANOVA. Scale = 50 µm. 5 serums tested per group.

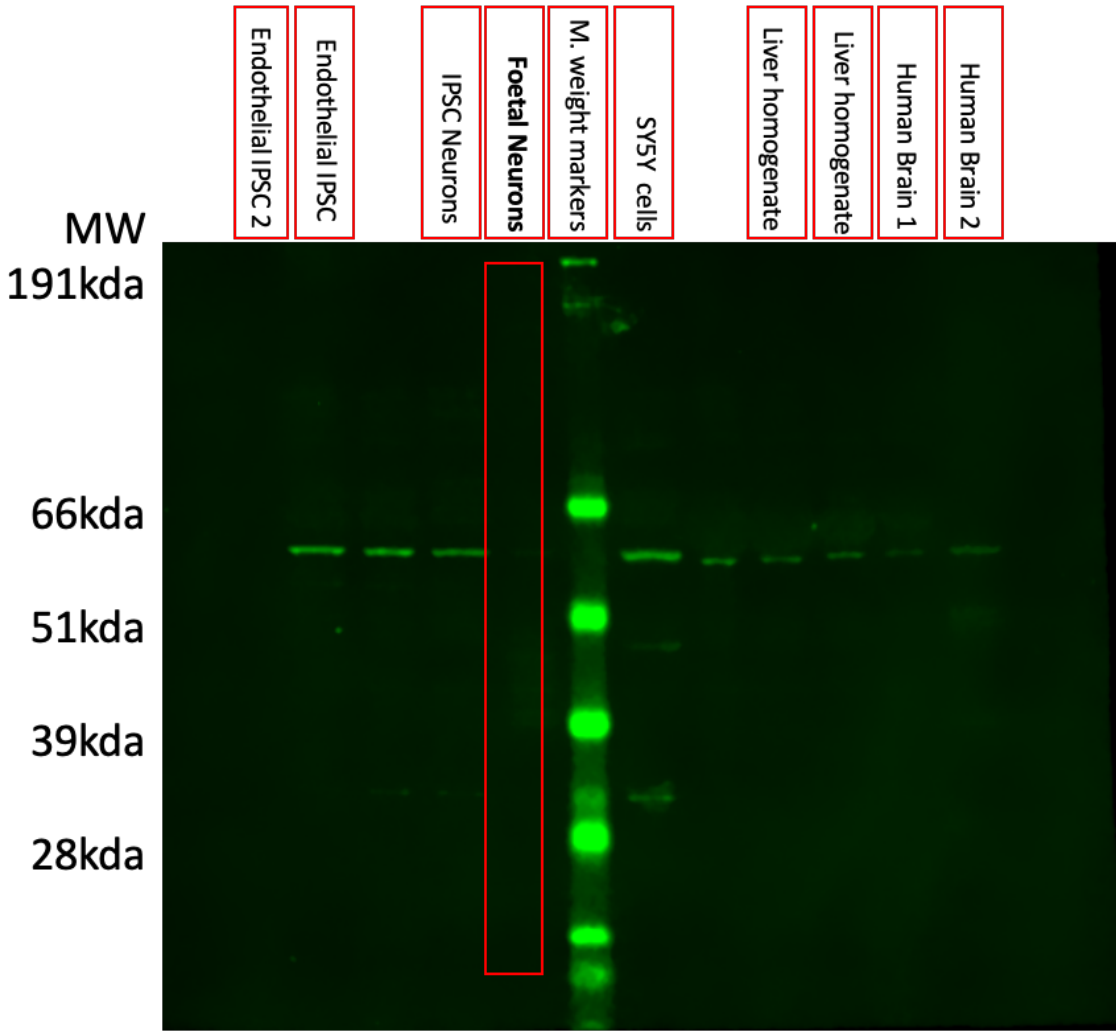

Figure 65. TGR5 expression in various neuronal cells, endothelial cells and human brain and liver homogenates. Western blot showed very little TGR5 expression.

6.5. Summary of findings from Chapter Six:

Main conclusions of this chapter are as follows:

- Cholestatic sera (patient or mouse) possess potent pro-senescent properties.

- Non-cholestatic serum have minimal senescence inducing properties, indicating different pro-senescent molecules present in cholestatic serums.

- Cholestatic serum do have a small but significant effect on cell viability, indicating some cell death occurs as a result of serum dosing.

- Pre-treatment with OCA 1hour prior reduces the effects of cholestatic serums, including significantly reducing senescence – suggests a partial direct mechanism of action for OCA.

- Dosing with specific bile acids with different hydrophobicity profiles produces different effects on cell viability – suggests that the presence of 'harmful' hydrophobic bile acids such as LCA in serum may exert direct effects on neuronal health. Hydrophobic bile acid LCA reduces cell viability in neurons.

- Farnesoid X receptor through which OCA primarily signals is expressed in neurons in vivo (chapter 4), and in vitro.

6.6. Conclusions

In Chapter one I established that cholestasis induces leakiness at the BBB. This fits in with previous observations in vitro (Quinn, McMillin et al. 2014). Therefore, bile acids and other potentially toxic constituents of cholestatic serum such as bilirubin (reviewed in (Hansen 2001)), or ammonia (reviewed in (Braissant, McLin et al. 2013)) can enter the brain. With this in mind, we chose to investigate the direct effects of cholestatic serum on mature neurons *in vitro*.

Previous data (chapters 1 and 2) showed that *in vivo* in the cholestatic bile duct ligation model senescence was induced by cholestasis not just in the liver, but in neurons in the critical CA3 region of the hippocampus. Results from this chapter show that cholestatic serum both from BDL mice, that represent a severe cholestatic model with high levels of circulating bile acids, and serum from PBC patients experiencing a high level of cognitive dysfunction induce senescence *in vitro* in the brain. This indicates factors in the circulation entering the brain may be directly responsible for the senescence phenotype seen in the brain, as oppose to inducing an inflammatory phenotype which might lead indirectly to senescence. This data, along with key publications showing a close relationship between senescence PBC progression (Sasaki, Sato et al. 2020) indicate that senescence is a key pathological feature of the disease, as serum constituents from cholestatic patients induce senescence independently of continued circulatory inflammatory factors, or a pathological neuroinflammatory environment.

In these studies, pharmacological intervention was achieved via pre-treatment incubation with OCA. Our in vivo data from BDL mice shows OCA to be effective in reducing the cognitive deficit in cholestatic mice, and also effective in reducing senescence in the liver and the brain. The use of therapy in a whole organism model makes it difficult to tease apart mechanism. In this case because the OCA was given from the day of surgery or even prophylactically in some experiments, it was impossible to tease apart the mechanism of OCA anti-senescent properties. These may simply have been as a consequence of reduction of cholestatic damage in the liver in the form of fibrosis, senescence etc (chapter 3, 4).

However, the ability of OCA to reduce senescence in an *in vitro* system in neurons indicates a direct mechanism of action on the neurons themselves. This suggests a possible role of FXR in regulation of the cell cycle. FXR is an established tumour suppressor (Yang, Huang et al. 2007) and its downregulation reduces liver regeneration in age (Chen, Wang et al. 2010), and after fibrotic injury (Hong, Lewis et al. 2014). OCA has previously been reported to suppress p53 activation in models of Non-alcoholic Steatohepatitis (NASH) (Goto, Itoh et al. 2018). P53 is a master regulator of the genome and its stimulation regulates the activation of a vast gene set including apoptosis and cell cycle arrest. It directly regulates P21, a well characterised marker of senescence in the small ducts in PBC (Sasaki, Ikeda et al. 2005, Sasaki, Ikeda et al. 2010). In neurodegenerative diseases such as AD, FXR signalling has been found to trigger neuronal apoptosis in areas of amyloid plaque generation (Chen, Ma et al. 2019), suggesting a neuroprotective benefit. These findings implicate FXR as a mediator of cell cycle arrest and potential moderator of senescence (FIG 59, 61) . Further experiments are needed in order to elucidate the specific pathways through which FXR has its anti-senescent effects in our study.

Interestingly, even Sham or normal serum treated wells show a small increase in senescence, showing that exposure of neurons to even small doses of non-cholestatic serum may induce a phenotype that the BBB is usually able to protect from. Also, the idea of a direct anti-senescent effect of OCA is strengthened by the fact that even normal patient serum and media only wells treated with OCA showed a minor reduction in senescence in the Sen-ß-galactosidase assay. This points to a universal role of FXR in cell cycle regulation during normal function not just disease pathology.

Despite the clear pro-senescent effects of dosing with serum from cholestatic patients, it remains unclear which serum components are responsible for the neurotoxic effects. Hydrophobic bile acids such as Lithocholic acid have been linked with senescence (Wu, Menon et al. 2016), hepatotoxicity (Song, Zhang et al. 2011) and the development of neurodegenerative diseases such as Alzheimer's (MahmoudianDehkordi, Arnold et al. 2019). Conversely hydrophilic bile acids such as taurocholic acid and ursodeoxycholic acid are thought to be neuroprotective, with the latter currently being investigated in neurodegenerative diseases Alzheimer's and Parkinson's (reviewed (Ackerman and Gerhard 2016)). Therefore, we tested differential effects of hydrophobic bile acid LCA and hydrophilic

bile acid TCA over a period of 14 days, with cell viability assay (alamar blue) performed at day 0, 1, 7 and 14. A wide range of concentrations were tested from 0.5pm to 100µm.

The cells treated with TCA resulted in almost universally increased cell viability when compared with media only wells. This reached significance by days 7 and 14 at the higher concentrations of 500nm and 100µm. Interestingly, LCA treatment significantly reduced cell viability by day 14 at the medium dose of 100pm when compared to media only. This adds weight to the hypothesis that specific bile acid composition plays a huge factor in its physiological function in the brain.

Despite these results, we are still unable to pull apart the specific contributions of serum components. As previously mentioned, other potentially toxic molecules such as bilirubin and ammonia are likely to be circulating in the serum, and could influence senescence. From MSD data reported in chapter 3, we know that the pro-inflammatory cytokine profile in BDL serum is prolific and pro-senescent due to the upregulation of cytokines such as IL-8, IL-6 and TNFα, known components of SASP. Studies from patients' sera show similar upregulation in proinflammatory cytokines IL-6, TNFα and IFNγ (Golovanova, Il'chenko et al. 2004). With this in mind, more thorough investigation into the componential breakdown of cholestatic serum is needed in order to carefully pick apart the mechanism of cholestasis induced neuronal senescence. In depth bile acid profiling is required in order to distinguish the 'toxic' bile acid profile and the specific actions of hydrophobic 'harmful' bile acids.

It is important to address and discuss the limitations of the neuronal cells used. It is common to use induced pluripotent stem cells for this type of analysis, or alternatively to use immortalised neuronal cell lines. I chose to use stem cells isolated from the forebrain of human embyros. This raises some problems, both ethically and in the context of neuronal phenotype. Ethically the harvest of stem cells from human embryo is complex, though it was approved for use in this study (harvested by my supervisor Peter hanson, differentiated by me). These cells were harvested 8 years ago and can be frozen. The use of these stem cells is advantageous to using IPSC stem cells, due to the fact they are not undergoing a forced de-differentiation. However, there are pit falls. Due to the heterogeneous nature of the culture, I cannot definitively state the identity of the cells in the same way I would be able to from cell

lines. This means that though the rest of my data is focussed on the hippocampus, these mixed neurons are not similar the hippocampal neural cell types and are not a model for the hippocampal environment. The culture also contains subpopulations of both astrocytes and oligodendrocytes, which I am unable to separate form neurons for the basis of my analysis. Feasibly, this could lead to changes in the results, or discrepancies between experiments, where cells may contain varied portions of each of the cell types.

7. Chapter Seven- General Discussion and Future Directions

7.1. Overall Discussion

The data presented in this thesis explore the potential mechanism/s underpinning the cognitive function experienced by a large proportion of cholestatic liver disease patients, with a focus on Primary Biliary Cholangitis. Using the Bile duct ligation mouse model of cholestasis to study this symptomology, I have recapitulated the human disease through liver fibrosis, ductular proliferation and cholestasis resulting in circulating inflammation. Though the BDL model is severe and can lead to cirrhosis after 15 days or more, I chose to study the pre-cirrhotic phase at days 6 and 10, in order to model early disease and intervention. BDL mice showed short-term and spatial memory dysfunction, mirroring the human cognitive symptom set.

identified deficits in key hippocampal functionalities: visual spatial memory deficit and fatigue, loss of NeuN+ neuron and PV+ interneuron expression, key markers of senescence (DNA damage, telomere associated foci (TAF), and P21 RNA), and loss of associated functionality including dysfunction in gamma frequency oscillation. Experiments focussing on Blood-Brain Barrier dysfunction indicated astrocyte activation and proliferation at the barrier, and loss of crucial astrocyte coverage and pilot studies using gadolinium enhanced T1 weighted MRI scanning reveal increased permeability at vessels within the hippocampus. *In vitro* experiments using human embryonic derived neurons allowed direct manipulation of neuron response to circulating cholestatic stimuli in serum, showing the possibility to directly induce senescence without the accompanying neuroinflammation.

Furthermore, we assessed the therapeutic benefits of early intervention drug therapies on the aforementioned deficits. This allowed us to both tease apart mechanism by manipulating cholestasis-mediated cognitive decline, and to evaluate individual drug efficacy specifically on

cognitive related symptoms if used early in the disease-course. The current second line therapy Obeticholic Acid showed promising improvement to key pathology including astrocyte coverage at the BBB, liver and neuronal senescence and restoration of gamma frequency oscillation in the hippocampus. *In vitro* experiments demonstrated a reduction in cholestasis induced senescence in neurons, therefore indicating this effect is likely to be in part at least by direct action and not entirely due to a general reduction in cholestasis and circulating inflammatory stimuli. Below is an implied event cascade to the causes of cognitive deficit through the means assessed during the course of my PhD (FIG 66), and on the right in (B) is the changes I have found to occur with OCA intervention from day -3 or 0.

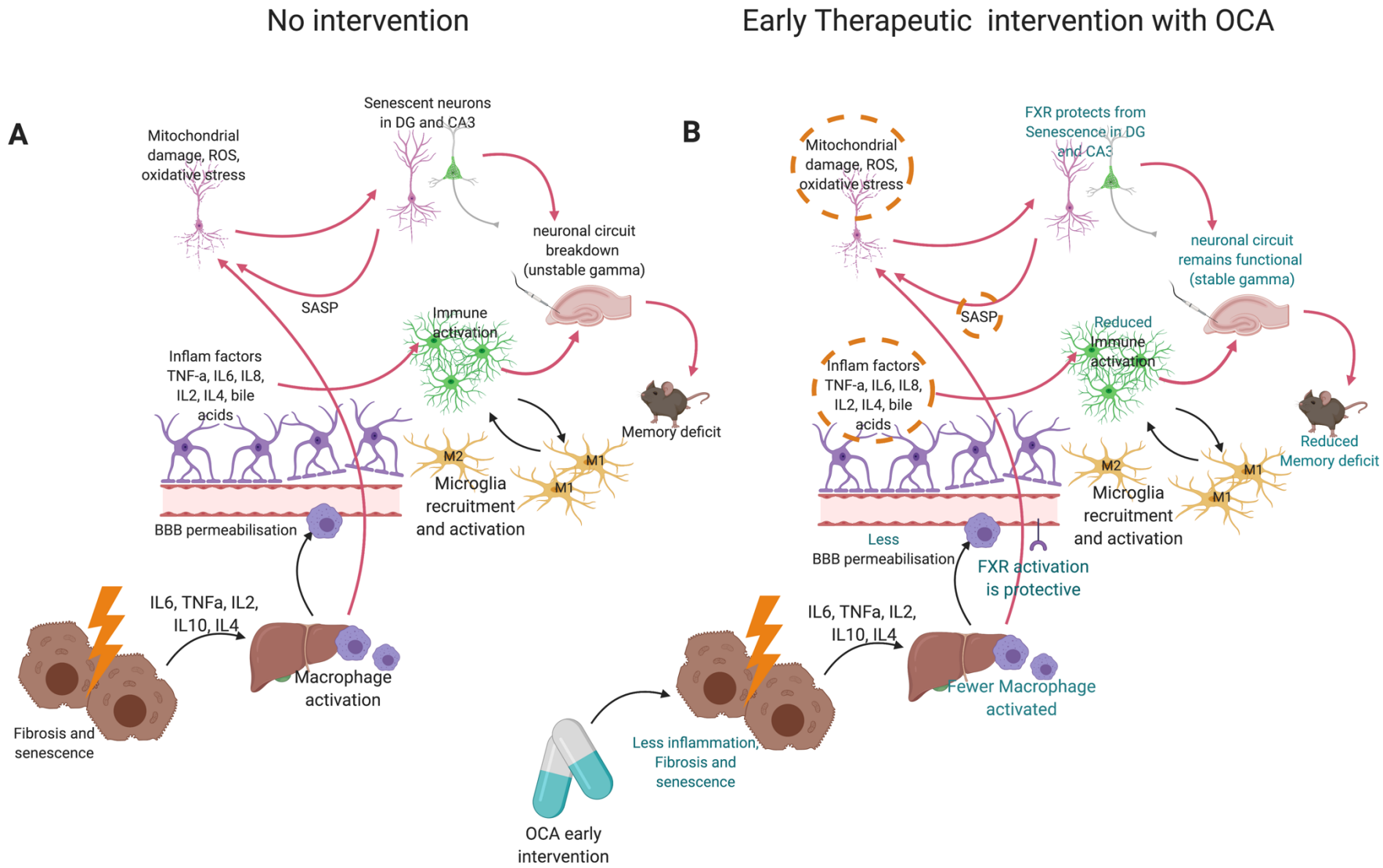

Figure 66. Changes occurring in the BDL model (A) without drug intervention and (B) with the intervention of Obeticholic Acid. Orange circles indicate areas not explored within this thesis.

7.1.1. Blood-Brain Barrier Breakdown is implicated in Cholestatic Liver Disease

BBB breakdown is implicated in the pathogenesis of many chronic diseases such as Alzheimer's disease well as in normal ageing (Montagne, Barnes et al. 2015, Nation, Sweeney et al. 2019). It has been previously shown by other groups that molecules associated with cholestasis such as bilirubin and bile acids have the ability to permeabilise endothelial cell tight junctions in vitro (Palmela, Cardoso et al. 2011, Cardoso, Kittel et al. 2012, Palmela, Sasaki et al. 2012). Additionally, it has been reported that some hydrophilic bile acids can to an extent prevent this increased permeability (Palmela, Correia et al. 2015). Though many of the studies have been limited to *in vitro* modelling, evidence from human imaging studies is beginning to emerge showing brain hypoxia and cerebrovascular changes in the brains of PBC patients (Duszynski, Avati et al. 2020).

My studies focus on astrocytes, which are required for the normal function of the BBB and regulate permeability at the vessel (Iadecola and Nedergaard 2007) via direct connection through the end-feet (Mathiisen, Lehre et al. 2010). I found that disruption occurred early, by the 6-day timepoint, prefacing the other neuronal and cognitive changes. Both EM and super resolution imaging showing proliferative and activated astrocyte with a rounded phenotype surrounding the vessels by day 10, though EM showed few points of contact of the end feet with the vessel itself. The proper function and attachment of astrocytes is imperative to BBB health, and without it vessels become leaky (Heithoff, George et al. 2021).

However, the results of the MRI data remain inconclusive and have a low power of only 3 per group. Because of this I cannot say that BDL definitively induces leakiness. The conclusions that I can draw about the permeability of the barrier come via proxy due to the EM and IF results, which indicate poor astrocyte attachment.

Interestingly, treatment with the FXR agonist OCA from day of surgery resulted in a phenotype closer to sham. This group showed fewer activated astrocytes than cholestatic mice without

treatment and appeared to form more end-feet connections at the barrier. Fluorescence activated cell sorting showed the presence of the receptor FXR on Sca1+ endothelial cells of the BBB within the hippocampus. FXR expression was also found to be significantly increased upon treatment with OCA, suggesting a dynamically active receptor function. Could there be a direct role for FXR modulation of the permeability of the BBB?

FXR signalling has been previously implicated in altering permeability and bile acid translocation at the gut in several pathological conditions (Stojancevic, Stankov et al. 2012), and since then FXR agonists such as OCA have been shown to direct modulate permeability at the gut epithelial (Verbeke, Farre et al. 2015) and vascular barriers (Mouries, Brescia et al. 2019). The latter is of particular interest because it reveals OCAs ability to modulate the vascular barrier not just preventatively (like in our studies where it is administered from the day of surgery) but also therapeutically after the onset of disease. This therefore could be of importance when evaluating the patient benefit of OCA.

7.1.2. Involvement of the Hippocampus in Cognitive Decline

The hippocampus represents the epicentre of human memory processing network. Without the hippocampus, humans are unable to form new memories or to recall them long term, as evidenced by the case study of HM (Scoville and Milner 1957). Previous findings from human imaging studies of PBC patients report structural and functional changes to the hippocampus relatively early in the disease course, from around 6 months (Grover, Southern et al. 2016, Mosher, Swain et al. 2018).

Our work consistently highlights cognitive deficits in hippocampal dependent memory tasks such as the Y-maze are a feature of BDL induced cholestasis. BDL mice (despite the expected individual variability) showed consistent reduction in the primary outcome of time spent in the novel arm across all trials. The Y-maze is widely used experimental procedure for the assessment of short term visual spatial memory, requiring the recognition of environmental cues. This is in keeping with clinical observations indicating deficit occurs in domains of visual

spatial memory and concentration (Jacoby, Rannard et al. 2005, Newton, Hollingsworth et al. 2008).

The authors of Mosher *et al.* postulate that the reduced hippocampal volume observed in their study occurred as an outcome of chronic neuroinflammation. Again, this theory is in part supported by our work showing neuroinflammation in the hippocampus of BDL mice, and the degradation of neurons by day 10, a pre-cirrhotic timepoint comparable to the human disease presented in this publication.

LFP electrophysiology in the gamma frequency oscillation generating region the CA3 allowed us to investigate changes to hippocampal function directly related to cognitive processes. We see large disruption to gamma frequency oscillation by day 10, a process associated with memory encoding and retrieval (Lu, Vreugdenhil et al. 2012). In our studies, BDL mice showed reduction in the ability to produce oscillations of a stable area power, something 89% of slices from sham animals produced within 3 hours, as is consistent with the literature (Lu, Wang et al. 2012). BDL mice also showed reduced CA3-CA1 synchrony, crucial for the recall of spatial cues in visual and working memory tasks such as the Y-maze (Montgomery and Buzsáki 2007) though it is important to note the low n numbers of this analysis.

Crucially, PV+ interneurons were reduced in both number and Parvalbumin expression in the CA3. Parvalbumin positive interneurons are vital for gamma frequency oscillation as they provide inhibitory input to the firing of pyramidal cells (Sohal, Zhang et al. 2009), contributing directly to the generation of gamma (Antonoudiou, Tan et al. 2020). However, parvalbumin interneurons are sensitive to oxidative stress and are often lost as a result of pathology, which may provide mechanistic basis for disorganised oscillation phenotype seen in the BDLs.

I chose to focus on the hippocampus as the primary region of investigation due to primary deficit seen in hippocampal dependent tasks such as the Y maze. Another reason for using the hippocampus as our primary area of investigation was that the hippocampus is sensitive to degradation and damage at the barrier, as was likely to be occurring in a cholestatic model. Additionally, previous studies have highlighted early changes to the hippocampus (as described above), and we were aiming to assess the early invention of therapeutics. However,

this reductionist experimental design may have caused us to overlook whole brain phenomena or the involvement of other key regions. Previous studies have also elucidated changes to other regions such as the globus pallidus, thalamus and putamen (Forton, Patel et al. 2004, Grover, Southern et al. 2016). It is worth noting that many of these studies have a focus largely on fatigue, or on cirrhotic patients which is not what we set out to model. With this aside, these areas warrant further investigation into the pathogenesis of cholestasis induced cognitive decline, questions which can be assessed in future with further utilization of our current experimental design, with a shift in focus.

7.1.3. Does Multi-Organ Senescence play a Role in the Cognitive Decline in PBC?

Senescence is a phenomenon first described by Hayflick in 1961 (Hayflick and Moorhead 1961) and is defined as a cell enters irreversible cell-cycle arrest. This process occurs throughout the body and is contributary to both normal ageing and several disease processes. Senescence is a well characterised feature of cholestatic disease, occurring in the small ducts and periductular hepatocytes in mice models and human patient PBC and PSC (Sasaki, Ikeda et al. 2005, Sasaki, Ikeda et al. 2008, Sasaki, Ikeda et al. 2010, Sasaki, Miyakoshi et al. 2010, Tabibian, O'Hara et al. 2014). More recently, senescence has also been associated with phenotypic presentation of disease. The expression of senescence associated proteins such as p16 have been associated with recurrent PBC (Sasaki, Hsu et al. 2015), and occur in higher levels in UDCA non-responders (Sasaki, Sato et al. 2020).

In neurodegenerative disease models, senescence is known to occur in glial cell types. In AD models the clearance of p16+ cells reduces cognitive decline (Bussian, Aziz et al. 2018). However, there is growing evidence of senescent like phenotype in non-mitotic cells such as neurons (Jurk, Wang et al. 2012, Wei, Chen et al. 2016). Our data provides the first evidence of senescence phenotype occurring in hippocampal neurons during cholestasis, in addition to within hepatocytes and non-parenchymal cells in the liver. This is evidenced not only by the specific senescence staining we performed in collaboration with Diana Jurk and colleagues at

the Mayo Clinic, but by the NeuN expression loss seen in the dentate gyrus, and by the induction of senescence in our *in vitro* model.

This raises interesting questions about the pathological mechanisms of cholestatic liver disease. Is the core mechanism one of bile acid induced senescence, within the liver, that can provoke multi-organ senescence? Is neuronal senescence able to cause cognitive deficit during cholestasis? In studies focussing on neurodegeneration such as Bussian *et al*, clearance of senescent cells can directly improve cognition in disease models, supporting the idea of senescence-driven cognitive decline.

While these questions are not directly answered by the thesis, our experiments with neuronal cell cultures show that senescence is induced in neurons by cholestatic serum even without active liver signalling and independent of neuroinflammatory involvement. The fact that the induction of senescence occurs directly from cholestatic serum and not as a consequence of continued inflammation from the liver implicates it in disease pathogenesis. Patient serums also induced senescence within the neuronal culture, implying that the process may be physiologically relevant in the patient disease, and not just the severe cholestasis induced from bile duct ligation.

7.1.4. Does this Data support the Case for Early Intervention therapy with Obeticholic Acid?

Previous clinical trials into pharmacological improvement with therapies in PBC have thus far shown little tangible improvement in cognition with therapeutic intervention. There could be several reasons for this; clinical trials are rarely designed to assess in detail cognitive symptoms, and cognitively impaired patients generally aren't selected for in trial. This means that any slight improvements may be missed by non-targeted testing. Many of those that do assess cognition are looking solely at fatigue-based symptoms, leaving those with cognitive deficit largely ignored. Different phenotypic presentations of PBC also make it difficult to tease apart the effects on specific sub groups of patients. For example, quick or slow progressors, UDCA non-responders or responders, or AMA-positive or negative PBC that

possess a different disease phenotype. These diverse patient sets may have unique aspects to their pathology, and will respond differently to treatments.

Currently, UDCA is given in the UK as a first line therapy for a minimum of one year in order to assess biochemical response in the liver. After this OCA the only licensed and labelled second-line therapy. Bezafibrate is currently being explored in phase 3 trials, with reported data showing a complete biochemical response in 31% of patients (Corpechot, Chazouillères et al. 2018). In keeping with the literature, we found UDCA intervention even prophylactically to be of little help in reducing cholestasis induced cognitive decline. UDCA treated mice still possessed both cognitive deficits and fatigue, had little improvement to liver pathology such as fibrosis, and had no associated reduction in senescence in the liver or brain, or change to neuroinflammation. Our results indicate therefore in line with previous observations that UDCA treatment has little influence on cognitive symptoms or associated pathology.

However, we see improvement with the therapeutic intervention of OCA in many of the studied parameters. We see vast improvement in liver histology including a reduction in fibrosis in line with previous publications (Goto, Itoh et al. 2018, Zhou, Huang et al. 2019). We also see substantial improvements in key experimental parameters such as in hippocampal dependent memory task the Y-maze when compared to BDL, as well as a reduction in BBB damage, an effect we propose may be due to the direct signalling of FXR at the endothelium. Some of the most striking effects of OCA treatment are within the hippocampus. OCA reduces neuroinflammation and PV+ interneuron loss, producing stable gamma frequency oscillations.

Most convincing are the clear improvements upon OCA pre-incubation of the neuronal cells, before introducing them to cholestatic serum. This data indicates direct therapeutic modulation by OCA of neurons in a way that bolsters them against the detrimental effects of senescence inducing serum. These results show clearly that there is a direct neuroprotective effect of OCA, and its beneficial impact *in vivo* in the BDL model is not just the indirect results of reduced cholestatic signalling at the liver. Therefore, I would hypothesise that early intervention therapy with OCA for those patient experiencing cognitive deficit may prove an effective therapeutic option. However, whether this is practical for clinical practise, when

patients can show few early symptoms and are often not diagnosed or given therapy until more advanced stage of disease, remains to be seen.

On the other hand, though Bezafibrate provides improvement to liver pathology, treatment shows no improvement for cognitive symptoms. In fact, Bezafibrate treatment appears to trigger a pro-senescent phenotype in both the liver and the brain. It is not clear how these outcomes are triggered by Bezafibrate, or whether this has any direct impact on cognition. However, this is an interesting outcome, and of interest to the liver community to explore in more detail.

7.1.5. The use of BDL as a model for PBC

The relevance of the findings displayed in this thesis are of course reliant on the validity of the studied animal models. While mouse models can provide an excellent framework to explore disease, their use has come under scrutiny both ethically and in their biological relevance to human disease. However, it remains crucial for determining whole organism response to disease or pathological injury in a way that *in vitro* modelling cannot recapitulate. Mouse models allow recapitulation of cholestasis as a progressive disease, with immune activation as a systemic response to injury.

The BDL model provides a useful system with which to study cholestatic liver disease. It mirrors many aspects of the patient symptom set such as progressive ductular reaction and fibrogenic response. It presents in 3 well defined phases (outlined below in table 6) allowing for timepoint histological analysis. In contrast, little has been investigated in the cognition and brain histology in mice undergoing BDL surgery, and published studies tend to recreate end stage cirrhotic disease, at later timepoints up to 21 days post-surgery (Huang, Hsieh et al. 2004, Magen, Avraham et al. 2009, Hosseini, Alaei et al. 2014, Dhanda and Sandhir 2015). The use of a model with well characterised liver response allowed us to compare our more investigational findings in the brain alongside liver pathology well recognised in the field.

Table 6. Histological Phases of BDL cholestatic model.

Phase	Days Post-Surgery	Pathological Observations
1	3-5	Biliary and hepatic injury, inflammatory peak
2	5-14	Progressive fibrosis, ductular reaction, inflammatory cytokine profile
3	14-21	Advanced fibrosis and development of cirrhosis, ascites (Abshagen, König et al. 2015, Tag, Sauer-Lehnen et al. 2015)

Despite this, BDL fails to capture some of the key features of the patient disease. The fact that it is such a severe and quick model, though convenient, means that it doesn't faithfully recapitulate the human disease process. PBC is often a slow progressing disease, with patients remaining asymptomatic for several years (Long, Scheuer et al. 1977). The BDL model also fails to emulate any of the auto-immune triggers of PBC, an important factor in the development of the disease.

Another important consideration is that of animal welfare. Bile duct ligation is a severe procedure, and can have a high mortality rate. In our studies, we minimised risk to the animal as much as possible. Creating a smaller wound meant less injury to the animal and quicker wound healing. After their surgery mice were kept in the heated cabinet at 25^{o}C for the duration of the study and administered pain relief and sub-cutaneous fluids. Study numbers were carefully considered for all animal studies.

Despite the pitfalls of any animal model system, BDL provides an effective system in which to study the process of cholestasis at a whole organism level. Using BDL we are able to investigate cross organ interaction between the brain and liver in a way that simply would not be possible using *in vitro* modelling alone. However, the *in vitro* data we have generated compliments the use of animal models and allows deeper mechanistic insight of the specific effects of cholestasis at the neuronal cellular level.

7.2. Future Directions

One of the most interesting aspects of the work has been the multi-organ senescence phenotype that occurs with the BDL model. Currently, it remains impossible to say whether the senescence phenotype within the hippocampus is a direct trigger of cognitive deficit. As it stands, the anecdotal evidence shows that OCA reduces both senescence and cognitive deficit in the BDL animals. In order to assess the causal link between senescence and cognition, it would be beneficial to employ a senescence clearance model, or to treat the mice with senolytic compounds.

The $p16^{Ink4a}$-INK ATTAC mouse is a transgenic mouse model that allows for induced elimination of $p16^{Ink4a}$ positive cells within the body (Baker, Wijshake et al. 2011). Treatment with the drug AP20187 triggers apoptosis in cells expressing the $p16^{Ink4a}$ gene (full schematic below from Baker *et al* 2011). The transgene can also be targeted, triggering clearance within a specific organ or cell type.

Using this transgenic mouse for the BDL model would allow mechanistic insight into the role of senescence in the pathogenesis of cholestasis. If senescent cell clearance within the liver reduces the senescence in the brain or the cognitive deficit this would indicate that the brain senescence is influenced largely by the liver phenotype and not by a separate pathological mechanism. Similarly, clearance of senescent cells only in the brain or in neurons would enable us to establish the specific role of senescence in cognition. Previously, senescence cell clearance in the brain using this technique has been linked to a slowed cognitive decline in neurodegenerative models (Bussian, Aziz et al. 2018). Another exciting experiment would be to treat BDL mice with senolytic compounds such as Dasatinib and Quercetin (D+Q). D+Q are the most thoroughly studied senolytic drugs, and have been shown to alleviate a number of age related conditions with few side effects (Xu, Pirtskhalava et al. 2018). This would be valuable and give indication of whether the use of senolytic compounds may be of therapeutic benefit for those PBC patients experiencing cognitive deficit.

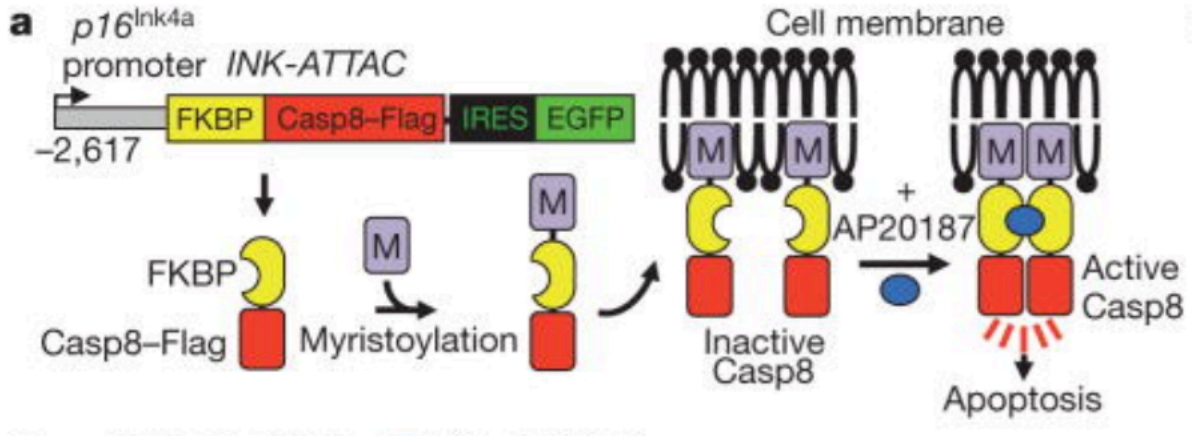

Figure 67 Figure from original paper (Baker, Wijshake et al. 2011) showing a schematic of the generation of the INK-ATTAC model.

Further development of the *in vitro* work would be valuable. Treatment with other therapies such as UDCA to assess therapeutic benefit, and if there are any direct impact of UDCA treatment on senescence. Treatment of neurons with Bezafibrate would identify whether the pro-senescent phenotype persists in vitro, and western blot analysis of protein expression of senescent markers such as P21 and P16 would allow thorough mechanistic evaluation of the pro-senescent properties of Bezafibrate treatment.

Furthermore, the collection of lysates from cells dosed with human patient and normal serum with treatment groups plus and minus drug would elevate the project. This would provide valuable mechanism for the protective effects of OCA within the brain. Western blots can be used to assess FXR modulation by the drug and to evaluate if the receptor is active within the cells by showing a reduction or increase in expression. Western blots of key cell cycle proteins such as p53, p21, and p16 would prove that the effect of OCA is largely anti-senescent (as oppose to anti-apoptotic), and show through which senescence pathways OCA exerts its function. This would provide key knowledge for future drug development and patient trials with OCA or other therapeutic developments. It has not been thoroughly investigated in this thesis; however, OCA also agonises TGR5 receptor. Assessment of the presence and modulation of both FXR and TGR5 in the neurons is required for development of the most efficacious compound.

Finally, a patient clinical trial into the impact of early intervention with OCA is warranted. OCA has positive outcomes when used in our pre-cirrhotic model, yet in the clinic it is not routinely

prescribed until later in the disease. As OCA is already an FDA approved therapy for PBC, it could be an easily implemented therapeutic if it is proven to be beneficial for patients with cognitive symptoms.

8. References

Abshagen, K., M. König, A. Hoppe, I. Müller, M. Ebert, H. Weng, H.-G. Holzhütter, U. M. Zanger, J. Bode, B. Vollmar, M. Thomas and S. Dooley (2015). "Pathobiochemical signatures of cholestatic liver disease in bile duct ligated mice." BMC Systems Biology **9**(1): 83.

Ackerman, H. D. and G. S. Gerhard (2016). "Bile Acids in Neurodegenerative Disorders." Frontiers in aging neuroscience **8**: 263-263.

Acosta, J. C., A. Banito, T. Wuestefeld, A. Georgilis, P. Janich, J. P. Morton, D. Athineos, T.-W. Kang, F. Lasitschka, M. Andrulis, G. Pascual, K. J. Morris, S. Khan, H. Jin, G. Dharmalingam, A. P. Snijders, T. Carroll, D. Capper, C. Pritchard, G. J. Inman, T. Longerich, O. J. Sansom, S. A. Benitah, L. Zender and J. Gil (2013). "A complex secretory program orchestrated by the inflammasome controls paracrine senescence." Nature cell biology **15**(8): 978-990.

Acosta, J. C., A. O'Loghlen, A. Banito, M. V. Guijarro, A. Augert, S. Raguz, M. Fumagalli, M. Da Costa, C. Brown, N. Popov, Y. Takatsu, J. Melamed, F. d'Adda di Fagagna, D. Bernard, E. Hernando and J. Gil (2008). "Chemokine Signaling via the CXCR2 Receptor Reinforces Senescence." Cell **133**(6): 1006-1018.

Addington, A., M. Gornick, J. Duckworth, A. Sporn, N. Gogtay, A. Bobb, D. Greenstein, M. Lenane, P. Gochman and N. Baker (2005). "GAD1 (2q31. 1), which encodes glutamic acid decarboxylase (GAD 67), is associated with childhood-onset schizophrenia and cortical gray matter volume loss." Molecular psychiatry **10**(6): 581-588.

Aghaei, I., V. Hajali, A. Dehpour, M. Haghani, V. Sheibani and M. Shabani (2016). "Alterations in the intrinsic electrophysiological properties of Purkinje neurons in a rat model of hepatic encephalopathy: Relative preventing effect of PPARγ agonist." Brain Research Bulletin **121**: 16-25.

Agrawal, R., M. Majeed, B. M. Attar, Y. A. Omar, C. Mbachi, Y. Wang, E. Flores, S. Shaqib, Y. Wang, V. Udechukwu, M. Demetria and S. Gandhi (2019). "Effectiveness of bezafibrate and ursodeoxycholic acid in patients with primary biliary cholangitis: a meta-analysis of randomized controlled trials." Annals of gastroenterology **32**(5): 489-497.

Albrecht, S., A.-K. Fleck, I. Kirchberg, S. Hucke, M. Liebmann, L. Klotz and T. Kuhlmann (2017). "Activation of FXR pathway does not alter glial cell function." Journal of Neuroinflammation **14**(1): 66.

Allen, D., J. Lannergren and H. Westerblad (1995). "Muscle cell function during prolonged activity: cellular mechanisms of fatigue." Experimental Physiology: Translation and Integration **80**(4): 497-527.

Alpini, G., S. S. Glaser, Y. Ueno, L. Pham, P. V. Podila, A. Caligiuri, G. LeSage and N. F. LaRusso (1998). "Heterogeneity of the proliferative capacity of rat cholangiocytes after bile duct ligation." Am J Physiol **274**(4): G767-775.

Alpini, G., S. Roberts, S. M. Kuntz, Y. Ueno, S. Gubba, P. V. Podila, G. LeSage and N. F. LaRusso (1996). "Morphological, molecular, and functional heterogeneity of cholangiocytes from normal rat liver." Gastroenterology **110**(5): 1636-1643.

Alvaro, D., P. Invernizzi, P. Onori, A. Franchitto, A. De Santis, A. Crosignani, R. Sferra, S. Ginanni-Corradini, M. Grazia Mancino, M. Maggioni, A. F. Attili, M. Podda and E. Gaudio (2004). "Estrogen receptors in cholangiocytes and the progression of primary biliary cirrhosis." Journal of Hepatology **41**(6): 905-912.

Amano, K., P. S. C. Leung, R. Rieger, C. Quan, X. Wang, J. Marik, Y. F. Suen, M. J. Kurth, M. H. Nantz, A. A. Ansari, K. S. Lam, M. Zeniya, E. Matsuura, R. L. Coppel and M. E. Gershwin (2005). "Chemical Xenobiotics and Mitochondrial Autoantigens in Primary Biliary Cirrhosis: Identification of Antibodies against a Common Environmental, Cosmetic, and Food Additive, 2-Octynoic Acid." The Journal of Immunology **174**(9): 5874.
Amodio, P., S. Montagnese, A. Gatta and M. Y. Morgan (2004). "Characteristics of minimal hepatic encephalopathy." Metab Brain Dis **19**(3-4): 253-267.
Anderson, J. M. and C. M. Van Itallie (1995). "Tight junctions and the molecular basis for regulation of paracellular permeability." Am J Physiol **269**(4 Pt 1): G467-475.
Andersson, S., N. Gustafsson, M. Warner and J.-Å. Gustafsson (2005). "Inactivation of liver X receptor β leads to adult-onset motor neuron degeneration in male mice." Proceedings of the National Academy of Sciences **102**(10): 3857-3862.
Antonoudiou, P., Y. L. Tan, G. Kontou, A. L. Upton and E. O. Mann (2020). "Parvalbumin and Somatostatin Interneurons Contribute to the Generation of Hippocampal Gamma Oscillations." The Journal of Neuroscience: JN-RM-0261-0220.
Armulik, A., G. Genové, M. Mäe, M. H. Nisancioglu, E. Wallgard, C. Niaudet, L. He, J. Norlin, P. Lindblom and K. Strittmatter (2010). "Pericytes regulate the blood–brain barrier." Nature **468**(7323): 557-561.
Au - Martin, E., M. Au - El-Behi, B. Au - Fontaine and C. Au - Delarasse (2017). "Analysis of Microglia and Monocyte-derived Macrophages from the Central Nervous System by Flow Cytometry." JoVE(124): e55781.
Bajaj, J. S., J. G. O'Leary, P. Tandon, F. Wong, G. Garcia-Tsao, P. S. Kamath, B. Maliakkal, S. W. Biggins, P. J. Thuluvath, M. B. Fallon, R. M. Subramanian, H. E. Vargas, J. Lai, L. R. Thacker and K. R. Reddy (2017). "Hepatic Encephalopathy Is Associated With Mortality in Patients With Cirrhosis Independent of Other Extrahepatic Organ Failures." Clinical Gastroenterology and Hepatology **15**(4): 565-574.e564.
Baker, D. J., T. Wijshake, T. Tchkonia, N. K. LeBrasseur, B. G. Childs, B. Van De Sluis, J. L. Kirkland and J. M. van Deursen (2011). "Clearance of p16 Ink4a-positive senescent cells delays ageing-associated disorders." Nature **479**(7372): 232-236.
Banks, W. A. (2009). "Characteristics of compounds that cross the blood-brain barrier." BMC neurology **9 Suppl 1**(Suppl 1): S3-S3.
Barrett, K. E. and W. F. Ganong (2012). Ganong's review of medical physiology. New York; London, McGraw-Hill Medical ; McGraw-Hill [distributor].
Bauer, J., U. Ganter, S. Strauss, G. Stadtmüller, U. Frommberger, H. Bauer, B. Volk and M. Berger (1992). "The participation of interleukin-6 in the pathogenesis of Alzheimer's disease." Res Immunol **143**(6): 650-657.
Beuers, U., M. Bilzer, A. Chittattu, G. A. Kullak-Ublick, D. Keppler, G. Paumgartner and F. Dombrowski (2001). "Tauroursodeoxycholic acid inserts the apical conjugate export pump, Mrp2, into canalicular membranes and stimulates organic anion secretion by protein kinase C-dependent mechanisms in cholestatic rat liver." Hepatology **33**(5): 1206-1216.
Bhat, R., E. P. Crowe, A. Bitto, M. Moh, C. D. Katsetos, F. U. Garcia, F. B. Johnson, J. Q. Trojanowski, C. Sell and C. Torres (2012). "Astrocyte senescence as a component of Alzheimer's disease." PloS one **7**(9): e45069-e45069.
Bi, G. Q. and M. M. Poo (1998). "Synaptic modifications in cultured hippocampal neurons: dependence on spike timing, synaptic strength, and postsynaptic cell type." J Neurosci **18**(24): 10464-10472.

Bitto, A., C. Sell, E. Crowe, A. Lorenzini, M. Malaguti, S. Hrelia and C. Torres (2010). "Stress-induced senescence in human and rodent astrocytes." Experimental Cell Research **316**(17): 2961-2968.
Blecharz-Lang, K. G., J. Wagner, A. Fries, M. Nieminen-Kelhä, J. Rösner, U. C. Schneider and P. Vajkoczy (2018). "Interleukin 6-mediated endothelial barrier disturbances can be attenuated by blockade of the IL6 receptor expressed in brain microvascular endothelial cells." Translational stroke research **9**(6): 631-642.
Boche, D., V. Perry and J. Nicoll (2013). "Activation patterns of microglia and their identification in the human brain." Neuropathology and applied neurobiology **39**(1): 3-18.
Börgers, C., S. Epstein and N. J. Kopell (2005). "Background gamma rhythmicity and attention in cortical local circuits: A computational study." Proceedings of the National Academy of Sciences of the United States of America **102**(19): 7002.
Bowlus, C. L., P. J. Pockros, A. E. Kremer, A. Parés, L. M. Forman, J. P. H. Drenth, S. D. Ryder, L. Terracciano, Y. Jin, A. Liberman, R. Pencek, U. Iloeje, L. MacConell and P. Bedossa (2020). "Long-Term Obeticholic Acid Therapy Improves Histological Endpoints in Patients With Primary Biliary Cholangitis." Clin Gastroenterol Hepatol **18**(5): 1170-1178.e1176.
Boyer, J. L. (1983). "Tight junctions in normal and cholestatic liver: does the paracellular pathway have functional significance?" Hepatology **3**(4): 614-617.
Bragin, A., G. Jandó, Z. Nádasdy, J. Hetke, K. Wise and G. Buzsáki (1995). "Gamma (40-100 Hz) oscillation in the hippocampus of the behaving rat." Journal of Neuroscience **15**(1): 47-60.
Braissant, O., V. A. McLin and C. Cudalbu (2013). "Ammonia toxicity to the brain." Journal of inherited metabolic disease **36**(4): 595-612.
Brown, J. P., W. Wei and J. M. Sedivy (1997). "Bypass of senescence after disruption of p21CIP1/WAF1 gene in normal diploid human fibroblasts." Science **277**(5327): 831-834.
Burroughs, A. K., I. J. Rosenstein, O. Epstein, J. M. Hamilton-Miller, W. Brumfitt and S. Sherlock (1984). "Bacteriuria and primary biliary cirrhosis." Gut **25**(2): 133.
Bussian, T. J., A. Aziz, C. F. Meyer, B. L. Swenson, J. M. van Deursen and D. J. Baker (2018). "Clearance of senescent glial cells prevents tau-dependent pathology and cognitive decline." Nature **562**(7728): 578-582.
Buzsáki, G. (2005). "Theta rhythm of navigation: link between path integration and landmark navigation, episodic and semantic memory." Hippocampus **15**(7): 827-840.
Cabral, H. O., M. Vinck, C. Fouquet, C. M. Pennartz, L. Rondi-Reig and F. P. Battaglia (2014). "Oscillatory dynamics and place field maps reflect hippocampal ensemble processing of sequence and place memory under NMDA receptor control." Neuron **81**(2): 402-415.
Calado, R. T., J. A. Regal, D. E. Kleiner, D. S. Schrump, N. R. Peterson, V. Pons, S. J. Chanock, P. M. Lansdorp and N. S. Young (2009). "A Spectrum of Severe Familial Liver Disorders Associate with Telomerase Mutations." PLOS ONE **4**(11): e7926.
Campisi, J. and F. d'Adda di Fagagna (2007). "Cellular senescence: when bad things happen to good cells." Nat Rev Mol Cell Biol **8**(9): 729-740.
Carbone, M., S. Bufton, A. Monaco, L. Griffiths, D. E. Jones and J. M. Neuberger (2013). "The effect of liver transplantation on fatigue in patients with primary biliary cirrhosis: a prospective study." Journal of hepatology **59**(3): 490-494.
Carbone, M., G. F. Mells, G. Pells, M. F. Dawwas, J. L. Newton, M. A. Heneghan, J. M. Neuberger, D. B. Day, S. J. Ducker, R. N. Sandford, G. J. Alexander and D. E. J. Jones (2013). "Sex and Age Are Determinants of the Clinical Phenotype of Primary Biliary Cirrhosis and Response to Ursodeoxycholic Acid." Gastroenterology **144**(3): 560-569.e567.

Cardoso, F. L., A. Kittel, S. Veszelka, I. Palmela, A. Tóth, D. Brites, M. A. Deli and M. A. Brito (2012). "Exposure to lipopolysaccharide and/or unconjugated bilirubin impair the integrity and function of brain microvascular endothelial cells." PLoS One **7**(5): e35919.
Carr, M. F., M. P. Karlsson and L. M. Frank (2012). "Transient slow gamma synchrony underlies hippocampal memory replay." Neuron **75**(4): 700-713.
Cauch-Dudek, K., S. Abbey, D. Stewart and E. Heathcote (1998). "Fatigue in primary biliary cirrhosis." Gut **43**(5): 705-710.
Cauli, O., M. T. Mansouri, A. Agusti and V. Felipo (2009). "Hyperammonemia increases GABAergic tone in the cerebellum but decreases it in the rat cortex." Gastroenterology **136**(4): 1359-1367, e1351-1352.
Ceulemans, L. J., L. Verbeke, J.-P. Decuypere, R. Farré, G. De Hertogh, K. Lenaerts, I. Jochmans, D. Monbaliu, F. Nevens, J. Tack, W. Laleman and J. Pirenne (2017). "Farnesoid X Receptor Activation Attenuates Intestinal Ischemia Reperfusion Injury in Rats." PLOS ONE **12**(1): e0169331.
Chen, Q., H. Ma, X. Guo, J. Liu, T. Gui and Z. Gai (2019). "Farnesoid X Receptor (FXR) Aggravates Amyloid-β-Triggered Apoptosis by Modulating the cAMP-Response Element-Binding Protein (CREB)/Brain-Derived Neurotrophic Factor (BDNF) Pathway In Vitro." Medical science monitor : international medical journal of experimental and clinical research **25**: 9335-9345.
Chen, W.-D., Y.-D. Wang, L. Zhang, S. Shiah, M. Wang, F. Yang, D. Yu, B. M. Forman and W. Huang (2010). "Farnesoid X receptor alleviates age-related proliferation defects in regenerating mouse livers by activating forkhead box m1b transcription." Hepatology (Baltimore, Md.) **51**(3): 953-962.
Chiang, J. Y. (2009). "Bile acids: regulation of synthesis." Journal of lipid research **50**(10): 1955-1966.
Childs, S., R. L. Yeh, E. Georges and V. Ling (1995). "Identification of a Sister Gene to P-Glycoprotein." Cancer Research **55**(10): 2029.
Cindoruk, M., M. Kerem, T. Karakan, B. Salman, O. Akin, M. Alper, O. Erdem and S. Ünal (2007). "Peroxisome proliferators-activated alpha agonist treatment ameliorates hepatic damage in rats with obstructive jaundice: an experimental study." BMC Gastroenterology **7**(1): 44.
Clarke, L. E., S. A. Liddelow, C. Chakraborty, A. E. Münch, M. Heiman and B. A. Barres (2018). "Normal aging induces A1-like astrocyte reactivity." Proceedings of the National Academy of Sciences **115**(8): E1896.
Cohen, Z., M. Ehret, M. Maitre and E. Hamel (1995). "Ultrastructural analysis of tryptophan hydroxylase immunoreactive nerve terminals in the rat cerebral cortex and hippocampus: their associations with local blood vessels." Neuroscience **66**(3): 555-569.
Colgin, L. L., T. Denninger, M. Fyhn, T. Hafting, T. Bonnevie, O. Jensen, M. B. Moser and E. I. Moser (2009). "Frequency of gamma oscillations routes flow of information in the hippocampus." Nature **462**(7271): 353-357.
Colicos, M. A. and P. K. Dash (1996). "Apoptotic morphology of dentate gyrus granule cells following experimental cortical impact injury in rats: possible role in spatial memory deficits." Brain Research **739**(1): 120-131.
Collado, M., M. A. Blasco and M. Serrano (2007). "Cellular senescence in cancer and aging." Cell **130**(2): 223-233.

Colton, C. A., R. T. Mott, H. Sharpe, Q. Xu, W. E. Van Nostrand and M. P. Vitek (2006). "Expression profiles for macrophage alternative activation genes in AD and in mouse models of AD." Journal of neuroinflammation **3**(1): 27.
Coluzzi, E., S. Leone and A. Sgura (2019). "Oxidative Stress Induces Telomere Dysfunction and Senescence by Replication Fork Arrest." Cells **8**(1).
Cornell-Bell, A. H., S. M. Finkbeiner, M. S. Cooper and S. J. Smith (1990). "Glutamate induces calcium waves in cultured astrocytes: long-range glial signaling." Science **247**(4941): 470-473.
Corpechot, C., L. Abenavoli, N. Rabahi, Y. Chretien, T. Andreani, C. Johanet, O. Chazouilleres and R. Poupon (2008). "Biochemical response to ursodeoxycholic acid and long-term prognosis in primary biliary cirrhosis." Hepatology **48**(3): 871-877.
Corpechot, C., O. Chazouillères, S. Lemoinne and A. Rousseau (2019). "Letter: reduction in projected mortality or need for liver transplantation associated with bezafibrate add-on in primary biliary cholangitis with incomplete UDCA response." Aliment Pharmacol Ther **49**(2): 236-238.
Corpechot, C., O. Chazouillères, A. Rousseau, A. Le Gruyer, F. Habersetzer, P. Mathurin, O. Goria, P. Potier, A. Minello, C. Silvain, A. Abergel, M. Debette-Gratien, D. Larrey, O. Roux, J.-P. Bronowicki, J. Boursier, V. de Ledinghen, A. Heurgue-Berlot, E. Nguyen-Khac, F. Zoulim, I. Ollivier-Hourmand, J.-P. Zarski, G. Nkontchou, S. Lemoinne, L. Humbert, D. Rainteau, G. Lefèvre, L. de Chaisemartin, S. Chollet-Martin, F. Gaouar, F.-H. Admane, T. Simon and R. Poupon (2018). "A Placebo-Controlled Trial of Bezafibrate in Primary Biliary Cholangitis." New England Journal of Medicine **378**(23): 2171-2181.
Crowe, J., E. Christensen, D. Doniach, H. Popper, N. Tygstrup and R. Williams (1985). "Early features of primary biliary cirrhosis: an analysis of 85 patients." Am J Gastroenterol **80**(6): 466-468.
Cruz-Sánchez, F. F., X. Gironès, A. Ortega, F. Alameda and J. V. Lafuente (2010). "Oxidative stress in Alzheimer's disease hippocampus: a topographical study." J Neurol Sci **299**(1-2): 163-167.
Csicsvari, J., B. Jamieson, K. D. Wise and G. Buzsaki (2003). "Mechanisms of gamma oscillations in the hippocampus of the behaving rat." Neuron **37**(2): 311-322.
d'Adda di Fagagna, F., P. M. Reaper, L. Clay-Farrace, H. Fiegler, P. Carr, T. Von Zglinicki, G. Saretzki, N. P. Carter and S. P. Jackson (2003). "A DNA damage checkpoint response in telomere-initiated senescence." Nature **426**(6963): 194-198.
D'Mello, C., T. Le and M. G. Swain (2009). "Cerebral microglia recruit monocytes into the brain in response to tumor necrosis factoralpha signaling during peripheral organ inflammation." The Journal of neuroscience : the official journal of the Society for Neuroscience **29**(7): 2089-2102.
D'Mello, C., T. Le and M. G. Swain (2009). "Cerebral microglia recruit monocytes into the brain in response to tumor necrosis factorα signaling during peripheral organ inflammation." Journal of Neuroscience **29**(7): 2089-2102.
D'Mello, C., K. Riazi, T. Le, K. M. Stevens, A. Wang, D. M. McKay, Q. J. Pittman and M. G. Swain (2013). "P-Selectin-Mediated Monocyte–Cerebral Endothelium Adhesive Interactions Link Peripheral Organ Inflammation To Sickness Behaviors." The Journal of Neuroscience **33**(37): 14878.
Dang-Vu, T. T., M. Schabus, M. Desseilles, G. Albouy, M. Boly, A. Darsaud, S. Gais, G. Rauchs, V. Sterpenich, G. Vandewalle, J. Carrier, G. Moonen, E. Balteau, C. Degueldre, A. Luxen, C.

Phillips and P. Maquet (2008). "Spontaneous neural activity during human slow wave sleep." Proceedings of the National Academy of Sciences **105**(39): 15160.
Datto, M. B., Y. Li, J. F. Panus, D. J. Howe, Y. Xiong and X. F. Wang (1995). "Transforming growth factor beta induces the cyclin-dependent kinase inhibitor p21 through a p53-independent mechanism." Proc Natl Acad Sci U S A **92**(12): 5545-5549.
Davalos, D., J. Grutzendler, G. Yang, J. V. Kim, Y. Zuo, S. Jung, D. R. Littman, M. L. Dustin and W.-B. Gan (2005). "ATP mediates rapid microglial response to local brain injury in vivo." Nature neuroscience **8**(6): 752-758.
Davson, H. and W. H. Oldendorf (1967). "Symposium on membrane transport. Transport in the central nervous system." Proc R Soc Med **60**(4): 326-329.
Dawson, P. A., M. Hubbert, J. Haywood, A. L. Craddock, N. Zerangue, W. V. Christian and N. Ballatori (2005). "The heteromeric organic solute transporter α-β, Ostα-Ostβ, is an ileal basolateral bile acid transporter." Journal of Biological Chemistry **280**(8): 6960-6968.
de Lange, T. (2005). "Shelterin: the protein complex that shapes and safeguards human telomeres." Genes Dev **19**(18): 2100-2110.
De Magalhaes Filho, C. D., M. Downes and R. Evans (2016). "Bile Acid Analog Intercepts Liver Fibrosis." Cell **166**(4): 789.
Delerive, P., K. De Bosscher, S. Besnard, W. Vanden Berghe, J. M. Peters, F. J. Gonzalez, J.-C. Fruchart, A. Tedgui, G. Haegeman and B. Staels (1999). "Peroxisome Proliferator-activated Receptor α Negatively Regulates the Vascular Inflammatory Gene Response by Negative Cross-talk with Transcription Factors NF-κB and AP-1." Journal of Biological Chemistry **274**(45): 32048-32054.
Dember, W. N. and H. Fowler (1959). "Spontaneous alternation after free and forced trials." Canadian Journal of Psychology/Revue canadienne de psychologie **13**(3): 151-154.
Dhanda, S. and R. Sandhir (2015). "Role of dopaminergic and serotonergic neurotransmitters in behavioral alterations observed in rodent model of hepatic encephalopathy." Behavioural Brain Research **286**: 222-235.
Dirac, A. M. and R. Bernards (2003). "Reversal of senescence in mouse fibroblasts through lentiviral suppression of p53." J Biol Chem **278**(14): 11731-11734.
Dombrowski, F., B. Stieger and U. Beuers (2006). "Tauroursodeoxycholic acid inserts the bile salt export pump into canalicular membranes of cholestatic rat liver." Lab Invest **86**(2): 166-174.
Driver, J. E., C. Racca, M. O. Cunningham, S. K. Towers, C. H. Davies, M. A. Whittington and F. E. N. LeBeau (2007). "Impairment of hippocampal gamma (γ)-frequency oscillations in vitro in mice overexpressing human amyloid precursor protein (APP)." European Journal of Neuroscience **26**(5): 1280-1288.
Duszynski, C. C., V. Avati, A. P. Lapointe, F. Scholkmann, J. F. Dunn and M. G. Swain (2020). "Near-Infrared Spectroscopy Reveals Brain Hypoxia and Cerebrovascular Dysregulation in Primary Biliary Cholangitis." Hepatology **71**(4): 1408-1420.
Dyson, J., A. Blain, M. Hudson, S. Rushton and D. Jones (2019). "FRI-015-Environmental triggering in primary biliary cholangitis: Disease risk relates to coal mining activity." Journal of Hepatology **70**(1, Supplement): e390.
Dyson, J. K., N. Wilkinson, L. Jopson, G. Mells, A. Bathgate, M. A. Heneghan, J. Neuberger, G. M. Hirschfield, S. J. Ducker, U. K. P. B. C. C. The, R. Sandford, G. Alexander, D. Stocken and D. E. J. Jones (2016). "The inter-relationship of symptom severity and quality of life in 2055 patients with primary biliary cholangitis." Alimentary Pharmacology & Therapeutics **44**(10): 1039-1050.

EASL (2009). EASL Clinical Practice Guidelines: management of cholestatic liver diseases. E. A. S. L. (EASL). J Hepatol. **51:** 237-267.
EASL (2017). "EASL Clinical Practice Guidelines: The diagnosis and management of patients with primary biliary cholangitis." J Hepatol **67**(1): 145-172.
Eriksson, L. S., R. Olsson, H. Glauman, H. Prytz, R. Befrits, B. O. Rydén, K. Einarsson, S. Lindgren, S. Wallerstedt and M. Wedén (1997). "Ursodeoxycholic Acid Treatment in Patients with Primary Biliary Cirrhosis: A Swedish Multicentre, Double-Blind, Randomized Controlled Study." Scandinavian Journal of Gastroenterology **32**(2): 179-186.
Eroglu, C., N. J. Allen, M. W. Susman, N. A. O'Rourke, C. Y. Park, E. Özkan, C. Chakraborty, S. B. Mulinyawe, D. S. Annis and A. D. Huberman (2009). "Gabapentin receptor α2δ-1 is a neuronal thrombospondin receptor responsible for excitatory CNS synaptogenesis." Cell **139**(2): 380-392.
Fabris, L. and M. Strazzabosco (2011). Epithelial–mesenchymal interactions in biliary diseases. Seminars in liver disease, NIH Public Access.
Fell, J., P. Klaver, K. Lehnertz, T. Grunwald, C. Schaller, C. E. Elger and G. Fernández (2001). "Human memory formation is accompanied by rhinal-hippocampal coupling and decoupling." Nat Neurosci **4**(12): 1259-1264.
Ferrebee, C. B., J. Li, J. Haywood, K. Pachura, B. S. Robinson, B. H. Hinrichs, R. M. Jones, A. Rao and P. A. Dawson (2018). "Organic Solute Transporter α-β Protects Ileal Enterocytes From Bile Acid–Induced Injury." Cellular and Molecular Gastroenterology and Hepatology **5**(4): 499-522.
Fickert, P., G. Zollner, A. Fuchsbichler, C. Stumptner, A. H. Weiglein, F. Lammert, H. U. Marschall, O. Tsybrovskyy, K. Zatloukal, H. Denk and M. Trauner (2002). "Ursodeoxycholic acid aggravates bile infarcts in bile duct–ligated and Mdr2 knockout mice via disruption of cholangioles." Gastroenterology **123**(4): 1238-1251.
Fielder, E., C. Tweedy, C. Wilson, F. Oakley, F. E. N. LeBeau, J. F. Passos, D. A. Mann, T. von Zglinicki and D. Jurk (2020). "Anti-inflammatory treatment rescues memory deficits during aging in nfkb1−/− mice." Aging Cell **n/a**(n/a): e13188.
Fiorucci, S., E. Antonelli, G. Rizzo, B. Renga, A. Mencarelli, L. Riccardi, S. Orlandi, R. Pellicciari and A. Morelli (2004). "The nuclear receptor SHP mediates inhibition of hepatic stellate cells by FXR and protects against liver fibrosis." Gastroenterology **127**(5): 1497-1512.
Fisahn, A., F. G. Pike, E. H. Buhl and O. Paulsen (1998). "Cholinergic induction of network oscillations at 40 Hz in the hippocampus in vitro." Nature **394**(6689): 186-189.
Floreani, A., D. Caroli, A. Variola, E. R. Rizzotto, S. Antoniazzi, M. Chiaramonte, N. Cazzagon, C. Brombin, L. Salmaso and V. Baldo (2011). "A 35-year follow-up of a large cohort of patients with primary biliary cirrhosis seen at a single centre." Liver Int **31**(3): 361-368.
Floreani, A., M. Marchiori, S. Bonato, M. Zucchetto, R. Naccarato and M. Chiaramonte (1995). "Cognitive Assessment in Primary Biliary Cirrhosis: A Case--Control Study." American Journal of Gastroenterology **90**(2).
Forton, D. M., N. Patel, M. Prince, A. Oatridge, G. Hamilton, J. Goldblatt, J. M. Allsop, J. V. Hajnal, H. C. Thomas, M. Bassendine, D. E. Jones and S. D. Taylor-Robinson (2004). "Fatigue and primary biliary cirrhosis: association of globus pallidus magnetisation transfer ratio measurements with fatigue severity and blood manganese levels." Gut **53**(4): 587-592.
Franceschi, C., M. Bonafè, S. Valensin, F. Olivieri, M. De Luca, E. Ottaviani and G. De Benedictis (2000). "Inflamm-aging: an evolutionary perspective on immunosenescence." Annals of the new York Academy of Sciences **908**(1): 244-254.

Fuchs, E. C., A. R. Zivkovic, M. O. Cunningham, S. Middleton, F. E. Lebeau, D. M. Bannerman, A. Rozov, M. A. Whittington, R. D. Traub, J. N. Rawlins and H. Monyer (2007). "Recruitment of parvalbumin-positive interneurons determines hippocampal function and associated behavior." Neuron **53**(4): 591-604.
Gatselis, N. K., K. Zachou, G. L. Norman, S. Gabeta, P. Papamichalis, G. K. Koukoulis and G. N. Dalekos (2013). "Clinical significance of the fluctuation of primary biliary cirrhosis-related autoantibodies during the course of the disease." Autoimmunity **46**(7): 471-479.
Gershwin, M. E., C. Selmi, H. J. Worman, E. B. Gold, M. Watnik, J. Utts, K. D. Lindor, M. M. Kaplan and J. M. Vierling (2005). "Risk factors and comorbidities in primary biliary cirrhosis: a controlled interview-based study of 1032 patients." Hepatology **42**(5): 1194-1202.
Gillespie, A. K., E. A. Jones, Y.-H. Lin, M. P. Karlsson, K. Kay, S. Y. Yoon, L. M. Tong, P. Nova, J. S. Carr and L. M. Frank (2016). "Apolipoprotein E4 causes age-dependent disruption of slow gamma oscillations during hippocampal sharp-wave ripples." Neuron **90**(4): 740-751.
Ginhoux, F., M. Greter, M. Leboeuf, S. Nandi, P. See, S. Gokhan, M. F. Mehler, S. J. Conway, L. G. Ng and E. R. Stanley (2010). "Fate mapping analysis reveals that adult microglia derive from primitive macrophages." Science **330**(6005): 841-845.
Glaser, S., H. Francis, S. Demorrow, G. Lesage, G. Fava, M. Marzioni, J. Venter and G. Alpini (2006). "Heterogeneity of the intrahepatic biliary epithelium." World J Gastroenterol **12**(22): 3523-3536.
Glaser, S., I. P. Lam, A. Franchitto, E. Gaudio, P. Onori, B. K. Chow, C. Wise, S. Kopriva, J. Venter, M. White, Y. Ueno, D. Dostal, G. Carpino, R. Mancinelli, W. Butler, V. Chiasson, S. DeMorrow, H. Francis and G. Alpini (2010). "Knockout of secretin receptor reduces large cholangiocyte hyperplasia in mice with extrahepatic cholestasis induced by bile duct ligation." Hepatology (Baltimore, Md.) **52**(1): 204-214.
Goldblatt, J., O. F. James and D. E. Jones (2001). "Grip strength and subjective fatigue in patients with primary biliary cirrhosis." Jama **285**(17): 2196-2197.
Goldblatt, J., P. J. Taylor, T. Lipman, M. I. Prince, A. Baragiotta, M. F. Bassendine, O. F. James and D. E. Jones (2002). "The true impact of fatigue in primary biliary cirrhosis: a population study." Gastroenterology **122**(5): 1235-1241.
Golgi, C., M. Bentivoglio and L. Swanson (2001). "On the fine structure of the pes Hippocampi major (with plates XIII-XXIII). 1886." Brain research bulletin **54**(5): 461-483.
Golovanova, E. V., L. Il'chenko, T. M. Tsaregorodtseva, T. I. Serova and R. B. Gudkova (2004). "[Cytokines in primary biliary cirrhosis (diagnostic and prognostic value)]." Ter Arkh **76**(2): 8-11.
Goodwin, B., S. A. Jones, R. R. Price, M. A. Watson, D. D. McKee, L. B. Moore, C. Galardi, J. G. Wilson, M. C. Lewis and M. E. Roth (2000). "A regulatory cascade of the nuclear receptors FXR, SHP-1, and LRH-1 represses bile acid biosynthesis." Molecular cell **6**(3): 517-526.
Gordon, G. R., H. B. Choi, R. L. Rungta, G. C. Ellis-Davies and B. A. MacVicar (2008). "Brain metabolism dictates the polarity of astrocyte control over arterioles." Nature **456**(7223): 745-749.
Goto, T., M. Itoh, T. Suganami, S. Kanai, I. Shirakawa, T. Sakai, M. Asakawa, T. Yoneyama, T. Kai and Y. Ogawa (2018). "Obeticholic acid protects against hepatocyte death and liver fibrosis in a murine model of nonalcoholic steatohepatitis." Scientific Reports **8**(1): 8157.
Gregory, J. L., E. F. Morand, S. J. McKeown, J. A. Ralph, P. Hall, Y. H. Yang, S. R. McColl and M. J. Hickey (2006). "Macrophage Migration Inhibitory Factor Induces Macrophage Recruitment via CC Chemokine Ligand 2." The Journal of Immunology **177**(11): 8072.

Grosmark, A. D., K. Mizuseki, E. Pastalkova, K. Diba and G. Buzsáki (2012). "REM sleep reorganizes hippocampal excitability." Neuron **75**(6): 1001-1007.
Grover, V. P., L. Southern, J. K. Dyson, J. U. Kim, M. M. Crossey, M. Wylezinska-Arridge, N. Patel, J. A. Fitzpatrick, A. Bak-Bol, A. D. Waldman, G. J. Alexander, G. F. Mells, R. W. Chapman, D. E. Jones and S. D. Taylor-Robinson (2016). "Early primary biliary cholangitis is characterised by brain abnormalities on cerebral magnetic resonance imaging." Aliment Pharmacol Ther **44**(9): 936-945.
Gulyás, A. I., G. G. Szabó, I. Ulbert, N. Holderith, H. Monyer, F. Erdélyi, G. Szabó, T. F. Freund and N. Hájos (2010). "Parvalbumin-containing fast-spiking basket cells generate the field potential oscillations induced by cholinergic receptor activation in the hippocampus." The Journal of neuroscience : the official journal of the Society for Neuroscience **30**(45): 15134-15145.
Guzman, S. J., A. Schlögl, M. Frotscher and P. Jonas (2016). "Synaptic mechanisms of pattern completion in the hippocampal CA3 network." Science **353**(6304): 1117-1123.
Haczeyni, F., H. Wang, V. Barn, A. R. Mridha, M. M. Yeh, W. G. Haigh, G. N. Ioannou, Y. J. Choi, C. A. McWherter, N. C. Teoh and G. C. Farrell (2017). "The selective peroxisome proliferator-activated receptor-delta agonist seladelpar reverses nonalcoholic steatohepatitis pathology by abrogating lipotoxicity in diabetic obese mice." Hepatol Commun **1**(7): 663-674.
Hale, M., J. L. Newton and D. E. J. Jones (2012). "Fatigue in primary biliary cirrhosis." BMJ : British Medical Journal **345**: e7004.
Haley, M. J. and C. B. Lawrence (2016). "The blood–brain barrier after stroke: Structural studies and the role of transcytotic vesicles." Journal of Cerebral Blood Flow & Metabolism **37**(2): 456-470.
Hansen, T. W. (2001). "Bilirubin brain toxicity." J Perinatol **21 Suppl 1**: S48-51; discussion S59-62.
Harder, D. R., C. Zhang and D. Gebremedhin (2002). "Astrocytes Function in Matching Blood Flow to Metabolic Activity." Physiology **17**(1): 27-31.
Harley, C. B., A. B. Futcher and C. W. Greider (1990). "Telomeres shorten during ageing of human fibroblasts." Nature **345**(6274): 458-460.
Hayflick, L. and P. S. Moorhead (1961). "The serial cultivation of human diploid cell strains." Exp Cell Res **25**: 585-621.
Hayflick, L. and P. S. Moorhead (1961). "The serial cultivation of human diploid cell strains." Experimental cell research **25**(3): 585-621.
He, H., A. Mennone, J. L. Boyer and S.-Y. Cai (2011). "Combination of retinoic acid and ursodeoxycholic acid attenuates liver injury in bile duct-ligated rats and human hepatic cells." Hepatology (Baltimore, Md.) **53**(2): 548-557.
He, N., W. Jin, K. Lok, Y. Wang, M. Yin and Z. Wang (2013). "Amyloid-β 1–42 oligomer accelerates senescence in adult hippocampal neural stem/progenitor cells via formylpeptide receptor 2." Cell death & disease **4**(11): e924-e924.
Heathcote, E. J., K. Cauch-Dudek, V. Walker, R. J. Bailey, L. M. Blendis, C. N. Ghent, P. Michieletti, G. Y. Minuk, S. C. Pappas and L. J. Scully (1994). "The Canadian Multicenter Double-blind Randomized Controlled Trial of ursodeoxycholic acid in primary biliary cirrhosis." Hepatology **19**(5): 1149-1156.
Heidari, R., V. Ghanbarinejad, H. Mohammadi, A. Ahmadi, M. M. Ommati, N. Abdoli, F. Aghaei, A. Esfandiari, N. Azarpira and H. Niknahad (2018). "Mitochondria protection as a

mechanism underlying the hepatoprotective effects of glycine in cholestatic mice." Biomedicine & Pharmacotherapy **97**: 1086-1095.
Heithoff, B. P., K. K. George, A. N. Phares, I. A. Zuidhoek, C. Munoz-Ballester and S. Robel (2021). "Astrocytes are necessary for blood–brain barrier maintenance in the adult mouse brain." Glia **69**(2): 436-472.
Herbig, U., W. A. Jobling, B. P. Chen, D. J. Chen and J. M. Sedivy (2004). "Telomere shortening triggers senescence of human cells through a pathway involving ATM, p53, and p21(CIP1), but not p16(INK4a)." Mol Cell **14**(4): 501-513.
Herland, A., A. D. van der Meer, E. A. FitzGerald, T.-E. Park, J. J. Sleeboom and D. E. Ingber (2016). "Distinct contributions of astrocytes and pericytes to neuroinflammation identified in a 3D human blood-brain barrier on a chip." PLoS One **11**(3).
Hernandez-Segura, A., J. Nehme and M. Demaria (2018). "Hallmarks of Cellular Senescence." Trends Cell Biol **28**(6): 436-453.
Heuman, D. M., P. B. Hylemon and Z. R. Vlahcevic (1989). "Regulation of bile acid synthesis. III. Correlation between biliary bile salt hydrophobicity index and the activities of enzymes regulating cholesterol and bile acid synthesis in the rat." J Lipid Res **30**(8): 1161-1171.
Hewitt, G., D. Jurk, F. D. M. Marques, C. Correia-Melo, T. Hardy, A. Gackowska, R. Anderson, M. Taschuk, J. Mann and J. F. Passos (2012). "Telomeres are favoured targets of a persistent DNA damage response in ageing and stress-induced senescence." Nature Communications **3**(1): 708.
Hirohata, S., Y. Matsueda, T. Yanagida and T. Yoshio (2017). "FRI0297 Role of serum interleukin-6 in blood brain barrier damages in neuropsychiatric systemic lupus erythematosus." Annals of the Rheumatic Diseases **76**(Suppl 2): 598.
Hirschfield, G. M. (2011). "Diagnosis of primary biliary cirrhosis." Best Pract Res Clin Gastroenterol **25**(6): 701-712.
Hirschfield, G. M., J. K. Dyson, G. J. Alexander, M. H. Chapman, J. Collier, S. Hübscher, I. Patanwala, S. P. Pereira, C. Thain and D. Thorburn (2018). "The British Society of Gastroenterology/UK-PBC primary biliary cholangitis treatment and management guidelines." Gut **67**(9): 1568-1594.
Hirschfield, G. M. and P. Invernizzi (2011). Progress in the genetics of primary biliary cirrhosis. Seminars in Liver Disease, © Thieme Medical Publishers.
Hirschfield, G. M., X. Liu, C. Xu, Y. Lu, G. Xie, Y. Lu, X. Gu, E. J. Walker, K. Jing and B. D. Juran (2009). "Primary biliary cirrhosis associated with HLA, IL12A, and IL12RB2 variants." New England Journal of Medicine **360**(24): 2544-2555.
Hirschfield, G. M., A. Mason, V. Luketic, K. Lindor, S. C. Gordon, M. Mayo, K. V. Kowdley, C. Vincent, H. C. Bodhenheimer, Jr., A. Parés, M. Trauner, H.-U. Marschall, L. Adorini, C. Sciacca, T. Beecher-Jones, E. Castelloe, O. Böhm and D. Shapiro (2015). "Efficacy of Obeticholic Acid in Patients With Primary Biliary Cirrhosis and Inadequate Response to Ursodeoxycholic Acid." Gastroenterology **148**(4): 751-761.e758.
Hiscock, R., L. Bauld, A. Amos and S. Platt (2012). "Smoking and socioeconomic status in England: the rise of the never smoker and the disadvantaged smoker." Journal of Public Health **34**(3): 390-396.
Ho, P. P. and L. Steinman (2016). "Obeticholic acid, a synthetic bile acid agonist of the farnesoid X receptor, attenuates experimental autoimmune encephalomyelitis." Proceedings of the National Academy of Sciences **113**(6): 1600.

Hofmann, A. F., J. Sjövall, G. Kurz, A. Radominska, C. D. Schteingart, G. S. Tint, Z. R. Vlahcevic and K. D. Setchell (1992). "A proposed nomenclature for bile acids." Journal of Lipid Research **33**(4): 599-604.
Hollingsworth, K. G., J. L. Newton, R. Taylor, C. McDonald, J. M. Palmer, A. M. Blamire and D. E. Jones (2008). "Pilot study of peripheral muscle function in primary biliary cirrhosis: potential implications for fatigue pathogenesis." Clinical Gastroenterology and Hepatology **6**(9): 1041-1048.
Hong, I.-H., K. Lewis, P. Iakova, J. Jin, E. Sullivan, N. Jawanmardi, L. Timchenko and N. Timchenko (2014). "Age-associated change of C/EBP family proteins causes severe liver injury and acceleration of liver proliferation after CCl4 treatments." The Journal of biological chemistry **289**(2): 1106-1118.
Hong, S., V. F. Beja-Glasser, B. M. Nfonoyim, A. Frouin, S. Li, S. Ramakrishnan, K. M. Merry, Q. Shi, A. Rosenthal, B. A. Barres, C. A. Lemere, D. J. Selkoe and B. Stevens (2016). "Complement and microglia mediate early synapse loss in Alzheimer mouse models." Science **352**(6286): 712.
Hosseini, N., H. Alaei, M. Nasehi, M. Radahmadi and Z. Mohammad Reza (2014). "Effects of cholestasis on learning and locomotor activity in bile duct ligated rats." The Malaysian journal of medical sciences : MJMS **21**(1): 19-28.
Huang, C., W. Han, C. Wang, Y. Liu, Y. Chen and Z. Duan (2019). "Early Prognostic Utility of Gp210 Antibody-Positive Rate in Primary Biliary Cholangitis: A Meta-Analysis." Dis Markers **2019**: 9121207.
Huang, C., J. Wang, W. Hu, C. Wang, X. Lu, L. Tong, F. Wu and W. Zhang (2016). "Identification of functional farnesoid X receptors in brain neurons." FEBS Letters **590**(18): 3233-3242.
Huang, F., T. Wang, Y. Lan, L. Yang, W. Pan, Y. Zhu, B. Lv, Y. Wei, H. Shi, H. Wu, B. Zhang, J. Wang, X. Duan, Z. Hu and X. Wu (2015). "Deletion of mouse FXR gene disturbs multiple neurotransmitter systems and alters neurobehavior." Frontiers in behavioral neuroscience **9**: 70-70.
Huang, L.-T., C.-S. Hsieh, M.-H. Chou, J.-H. Chuang, C.-W. Liou, M.-M. Tiao and M.-C. Lai (2004). "Obstructive Jaundice in Rats: Cause of Spatial Memory Deficits with Recovery after Biliary Decompression." World Journal of Surgery **28**(3): 283-287.
Huber, R. M., K. Murphy, B. Miao, J. R. Link, M. R. Cunningham, M. J. Rupar, P. L. Gunyuzlu, T. F. Haws, A. Kassam, F. Powell, G. F. Hollis, P. R. Young, R. Mukherjee and T. C. Burn (2002). "Generation of multiple farnesoid-X-receptor isoforms through the use of alternative promoters." Gene **290**(1-2): 35-43.
Hylemon, P. B., H. Zhou, W. M. Pandak, S. Ren, G. Gil and P. Dent (2009). "Bile acids as regulatory molecules." J Lipid Res **50**(8): 1509-1520.
Iaccarino, H. F., A. C. Singer, A. J. Martorell, A. Rudenko, F. Gao, T. Z. Gillingham, H. Mathys, J. Seo, O. Kritskiy and F. Abdurrob (2016). "Gamma frequency entrainment attenuates amyloid load and modifies microglia." Nature **540**(7632): 230-235.
Iadecola, C. and M. Nedergaard (2007). "Glial regulation of the cerebral microvasculature." Nature neuroscience **10**(11): 1369-1376.
Inagaki, T., M. Choi, A. Moschetta, L. Peng, C. L. Cummins, J. G. McDonald, G. Luo, S. A. Jones, B. Goodwin and J. A. Richardson (2005). "Fibroblast growth factor 15 functions as an enterohepatic signal to regulate bile acid homeostasis." Cell metabolism **2**(4): 217-225.
Insull, W., Jr. (2006). "Clinical utility of bile acid sequestrants in the treatment of dyslipidemia: a scientific review." South Med J **99**(3): 257-273.

Invernizzi, P., M. Miozzo, P. M. Battezzati, I. Bianchi, F. R. Grati, G. Simoni, C. Selmi, M. Watnik, M. E. Gershwin and M. Podda (2004). "Frequency of monosomy X in women with primary biliary cirrhosis." The Lancet **363**(9408): 533-535.
Irvine, K. M., R. Skoien, N. J. Bokil, M. Melino, G. P. Thomas, D. Loo, B. Gabrielli, M. M. Hill, M. J. Sweet, A. D. Clouston and E. E. Powell (2014). "Senescent human hepatocytes express a unique secretory phenotype and promote macrophage migration." World journal of gastroenterology **20**(47): 17851-17862.
Ito, D., Y. Imai, K. Ohsawa, K. Nakajima, Y. Fukuuchi and S. Kohsaka (1998). "Microglia-specific localisation of a novel calcium binding protein, Iba1." Molecular brain research **57**(1): 1-9.
Jacoby, A., A. Rannard, D. Buck, N. Bhala, J. L. Newton, O. F. James and D. E. Jones (2005). "Development, validation, and evaluation of the PBC-40, a disease specific health related quality of life measure for primary biliary cirrhosis." Gut **54**(11): 1622-1629.
Jazrawi, R. P., J. S. de Caestecker, P. M. Goggin, A. J. Britten, A. E. Joseph, J. D. Maxwell and T. C. Northfield (1994). "Kinetics of hepatic bile acid handling in cholestatic liver disease: effect of ursodeoxycholic acid." Gastroenterology **106**(1): 134-142.
Johnson, A. and A. D. Redish (2007). "Neural ensembles in CA3 transiently encode paths forward of the animal at a decision point." J Neurosci **27**(45): 12176-12189.
Jones, D., P. F. Boudes, M. G. Swain, C. L. Bowlus, M. R. Galambos, B. R. Bacon, Y. Doerffel, N. Gitlin, S. C. Gordon, J. A. Odin, D. Sheridan, M. A. Worns, V. Clark, L. Corless, H. Hartmann, M. E. Jonas, A. E. Kremer, G. F. Mells, P. Buggisch, B. L. Freilich, C. Levy, J. M. Vierling, D. E. Bernstein, M. Hartleb, E. Janczewska, F. Rochling, H. Shah, M. L. Shiffman, J. H. Smith, Y. J. Choi, A. Steinberg, M. Varga, H. Chera, R. Martin, C. A. McWherter and G. M. Hirschfield (2017). "Seladelpar (MBX-8025), a selective PPAR-delta agonist, in patients with primary biliary cholangitis with an inadequate response to ursodeoxycholic acid: a double-blind, randomised, placebo-controlled, phase 2, proof-of-concept study." Lancet Gastroenterol Hepatol **2**(10): 716-726.
Jones, D. E., K. Hollingsworth, G. Fattakhova, G. MacGowan, R. Taylor, A. Blamire and J. L. Newton (2010). "Impaired cardiovascular function in primary biliary cirrhosis." American Journal of Physiology-Gastrointestinal and Liver Physiology **298**(5): G764-G773.
Joo, S. S., T. J. Won and D. I. Lee (2004). "Potential role of ursodeoxycholic acid in suppression of Nuclear factor kappa B in microglial cell line (BV-2)." Archives of Pharmacal Research **27**(9): 954.
Jurk, D., C. Wang, S. Miwa, M. Maddick, V. Korolchuk, A. Tsolou, E. S. Gonos, C. Thrasivoulou, M. J. Saffrey, K. Cameron and T. von Zglinicki (2012). "Postmitotic neurons develop a p21-dependent senescence-like phenotype driven by a DNA damage response." Aging cell **11**(6): 996-1004.
Jutras, M. J., P. Fries and E. A. Buffalo (2009). "Gamma-band synchronization in the macaque hippocampus and memory formation." J Neurosci **29**(40): 12521-12531.
Kann, O., I. E. Papageorgiou and A. Draguhn (2014). "Highly Energized Inhibitory Interneurons are a Central Element for Information Processing in Cortical Networks." Journal of Cerebral Blood Flow & Metabolism **34**(8): 1270-1282.
Keitel, V., B. Görg, H. J. Bidmon, I. Zemtsova, L. Spomer, K. Zilles and D. Häussinger (2010). "The bile acid receptor TGR5 (Gpbar-1) acts as a neurosteroid receptor in brain." Glia **58**(15): 1794-1805.
Kepecs, A. and G. Fishell (2014). "Interneuron cell types are fit to function." Nature **505**(7483): 318-326.

Kerfoot, S. M., C. D'Mello, H. Nguyen, M. N. Ajuebor, P. Kubes, T. Le and M. G. Swain (2006). "TNF-α–secreting monocytes are recruited into the brain of cholestatic mice." Hepatology **43**(1): 154-162.
Kerr, T. A., S. Saeki, M. Schneider, K. Schaefer, S. Berdy, T. Redder, B. Shan, D. W. Russell and M. Schwarz (2002). "Loss of nuclear receptor SHP impairs but does not eliminate negative feedback regulation of bile acid synthesis." Developmental cell **2**(6): 713-720.
Kita , H., Z.-X. Lian , J. Van de Water , X.-S. He , S. Matsumura , M. Kaplan , V. Luketic , R. L. Coppel , A. A. Ansari and M. E. Gershwin (2002). "Identification of HLA-A2–restricted CD8+ Cytotoxic T Cell Responses in Primary Biliary Cirrhosis : T Cell Activation Is Augmented by Immune Complexes Cross-Presented by Dendritic Cells." Journal of Experimental Medicine **195**(1): 113-123.
Kita, H., S. Matsumura, X.-S. He, A. A. Ansari, Z.-X. Lian, J. Van de Water, R. L. Coppel, M. M. Kaplan and M. E. Gershwin (2002). "Quantitative and functional analysis of PDC-E2–specific autoreactive cytotoxic T lymphocytes in primary biliary cirrhosis." The Journal of clinical investigation **109**(9): 1231-1240.
Kitani, K., M. Ohta and S. Kanai (1985). "Tauroursodeoxycholate prevents biliary protein excretion induced by other bile salts in the rat." American Journal of Physiology-Gastrointestinal and Liver Physiology **248**(4): G407-G417.
Kobayashi, M., Y. Kakuda, K. Harada, Y. Sato, M. Sasaki, H. Ikeda, M. Terada, M. Mukai, S. Kaneko and Y. Nakanuma (2014). "Clinicopathological study of primary biliary cirrhosis with interface hepatitis compared to autoimmune hepatitis." World journal of gastroenterology **20**(13): 3597-3608.
Kornienko, J. S., I. S. Smirnova, N. A. Pugovkina, J. S. Ivanova, M. A. Shilina, T. M. Grinchuk, A. N. Shatrova, N. D. Aksenov, V. V. Zenin, N. N. Nikolsky and O. G. Lyublinskaya (2019). "High doses of synthetic antioxidants induce premature senescence in cultivated mesenchymal stem cells." Sci Rep **9**(1): 1296.
Kosaka, T., H. Katsumaru, K. Hama, J. Y. Wu and C. W. Heizmann (1987). "GABAergic neurons containing the Ca2+-binding protein parvalbumin in the rat hippocampus and dentate gyrus." Brain Res **419**(1-2): 119-130.
Kraeuter, A.-K., P. C. Guest and Z. Sarnyai (2019). "The Y-Maze for Assessment of Spatial Working and Reference Memory in Mice." Methods in molecular biology (Clifton, N.J.) **1916**: 105-111.
Krähenbühl, S., C. Talos, S. Fischer and J. Reichen (1994). "Toxicity of bile acids on the electron transport chain of isolated rat liver mitochondria." Hepatology **19**(2): 471-479.
Krizhanovsky, V., M. Yon, R. A. Dickins, S. Hearn, J. Simon, C. Miething, H. Yee, L. Zender and S. W. Lowe (2008). "Senescence of activated stellate cells limits liver fibrosis." Cell **134**(4): 657-667.
Kuiper, E. M., B. E. Hansen, R. A. de Vries, J. W. den Ouden-Muller, T. J. van Ditzhuijsen, E. B. Haagsma, M. H. Houben, B. J. Witteman, K. J. van Erpecum and H. R. van Buuren (2009). "Improved prognosis of patients with primary biliary cirrhosis that have a biochemical response to ursodeoxycholic acid." Gastroenterology **136**(4): 1281-1287.
Kuipers, F., T. Claudel, E. Sturm and B. Staels (2004). "The Farnesoid X Receptor (FXR) as modulator of bile acid metabolism." Rev Endocr Metab Disord **5**(4): 319-326.
Kurzawa-Akanbi, M., P. S. Hanson, P. G. Blain, D. J. Lett, I. G. McKeith, P. F. Chinnery and C. M. Morris (2012). "Glucocerebrosidase Mutations alter the endoplasmic reticulum and lysosomes in Lewy body disease." Journal of Neurochemistry **123**(2): 298-309.

Lai, C. H. and K. H. Kuo (2005). "The critical component to establish in vitro BBB model: Pericyte." Brain Res Brain Res Rev **50**(2): 258-265.
Lan, R. Y., T. L. Salunga, K. Tsuneyama, Z. X. Lian, G. X. Yang, W. Hsu, Y. Moritoki, A. A. Ansari, C. Kemper, J. Price, J. P. Atkinson, R. L. Coppel and M. E. Gershwin (2009). "Hepatic IL-17 responses in human and murine primary biliary cirrhosis." J Autoimmun **32**(1): 43-51.
Lawson, L. J., V. H. Perry and S. Gordon (1992). "Turnover of resident microglia in the normal adult mouse brain." Neuroscience **48**(2): 405-415.
Layden, T. J. and J. L. Boyer (1978). "Influence of bile acids on bile canalicular membrane morphology and the lobular gradient in canalicular size." Lab Invest **39**(2): 110-119.
Lazaridis, K. N., B. D. Juran, G. M. Boe, J. P. Slusser, M. De Andrade, H. A. Homburger, K. Ghosh, E. R. Dickson, K. D. Lindor and G. M. Petersen (2007). "Increased prevalence of antimitochondrial antibodies in first-degree relatives of patients with primary biliary cirrhosis." Hepatology **46**(3): 785-792.
LeSage, G. D., A. Benedetti, S. Glaser, L. Marucci, Z. Tretjak, A. Caligiuri, R. Rodgers, J. L. Phinizy, L. Baiocchi, H. Francis, J. Lasater, L. Ugili and G. Alpini (1999). "Acute carbon tetrachloride feeding selectively damages large, but not small, cholangiocytes from normal rat liver." Hepatology **29**(2): 307-319.
Leuschner, U., H. Fischer, W. Kurtz, S. Güldütuna, K. Hübner, A. Hellstern, M. Gatzen and M. Leuschner (1989). "Ursodeoxycholic acid in primary biliary cirrhosis: Results of a controlled double-blind trial." Gastroenterology **97**(5): 1268-1274.
Li, Y., K. Jadhav and Y. Zhang (2013). "Bile acid receptors in non-alcoholic fatty liver disease." Biochem Pharmacol **86**(11): 1517-1524.
Liddelow, S. A., K. A. Guttenplan, L. E. Clarke, F. C. Bennett, C. J. Bohlen, L. Schirmer, M. L. Bennett, A. E. Münch, W.-S. Chung, T. C. Peterson, D. K. Wilton, A. Frouin, B. A. Napier, N. Panicker, M. Kumar, M. S. Buckwalter, D. H. Rowitch, V. L. Dawson, T. M. Dawson, B. Stevens and B. A. Barres (2017). "Neurotoxic reactive astrocytes are induced by activated microglia." Nature **541**(7638): 481-487.
Limbad, C., T. R. Oron, F. Alimirah, A. R. Davalos, T. E. Tracy, L. Gan, P.-Y. Desprez and J. Campisi (2020). "Astrocyte senescence promotes glutamate toxicity in cortical neurons." PloS one **15**(1): e0227887-e0227887.
Lin, H., S. Patel, V. S. Affleck, I. Wilson, D. M. Turnbull, A. R. Joshi, R. Maxwell and E. A. Stoll (2017). "Fatty acid oxidation is required for the respiration and proliferation of malignant glioma cells." Neuro-Oncology **19**(1): 43-54.
Lindgren, S., H. Glaumann, S. Almer, A. Bergquist, E. Bjornsson, U. Broome, A. Danielsson, B. Lebrun, H. Prytz and R. Olsson (2009). "Transitions between variant forms of primary biliary cirrhosis during long-term follow-up." Eur J Intern Med **20**(4): 398-402.
Liu, X., P. Invernizzi, Y. Lu, R. Kosoy, Y. Lu, I. Bianchi, M. Podda, C. Xu, G. Xie and F. Macciardi (2010). "Genome-wide meta-analyses identify three loci associated with primary biliary cirrhosis." Nature genetics **42**(8): 658-660.
Long, R. G., P. J. Scheuer and S. Sherlock (1977). "Presentation and course of asymptomatic primary biliary cirrhosis." Gastroenterology **72**(6): 1204-1207.
Lu, C.-b., Z.-h. Wang, Y.-h. Zhou and M. Vreugdenhil (2012). "Temperature- and concentration-dependence of kainate-induced γ oscillation in rat hippocampal slices under submerged condition." Acta Pharmacologica Sinica **33**(2): 214-220.
Lu, C. B., M. Vreugdenhil and E. C. Toescu (2012). "The effect of aging-associated impaired mitochondrial status on kainate-evoked hippocampal gamma oscillations." Neurobiol Aging **33**(11): 2692-2703.

Lu, W.-Y., T. G. Bird, L. Boulter, A. Tsuchiya, A. M. Cole, T. Hay, R. V. Guest, D. Wojtacha, T. Y. Man, A. Mackinnon, R. A. Ridgway, T. Kendall, M. J. Williams, T. Jamieson, A. Raven, D. C. Hay, J. P. Iredale, A. R. Clarke, O. J. Sansom and S. J. Forbes (2015). "Hepatic progenitor cells of biliary origin with liver repopulation capacity." Nature cell biology **17**(8): 971-983.
Ludwig, J. (1987). "New concepts in biliary cirrhosis." Semin Liver Dis **7**(4): 293-301.
Ludwig, J., E. R. Dickson and G. S. McDonald (1978). "Staging of chronic nonsuppurative destructive cholangitis (syndrome of primary biliary cirrhosis)." Virchows Arch A Pathol Anat Histol **379**(2): 103-112.
Mably, A. J., B. J. Gereke, D. T. Jones and L. L. Colgin (2017). "Impairments in spatial representations and rhythmic coordination of place cells in the 3xTg mouse model of Alzheimer's disease." Hippocampus **27**(4): 378-392.
Maciel-Baron, L. A., S. L. Morales-Rosales, A. A. Aquino-Cruz, F. Triana-Martinez, S. Galvan-Arzate, A. Luna-Lopez, V. Y. Gonzalez-Puertos, N. E. Lopez-Diazguerrero, C. Torres and M. Konigsberg (2016). "Senescence associated secretory phenotype profile from primary lung mice fibroblasts depends on the senescence induction stimuli." Age (Dordr) **38**(1): 26.
Magen, I., Y. Avraham, Z. Ackerman, L. Vorobiev, R. Mechoulam and E. M. Berry (2009). "Cannabidiol ameliorates cognitive and motor impairments in mice with bile duct ligation." Journal of Hepatology **51**(3): 528-534.
MahmoudianDehkordi, S., M. Arnold, K. Nho, S. Ahmad, W. Jia, G. Xie, G. Louie, A. Kueider-Paisley, M. A. Moseley, J. W. Thompson, L. St John Williams, J. D. Tenenbaum, C. Blach, R. Baillie, X. Han, S. Bhattacharyya, J. B. Toledo, S. Schafferer, S. Klein, T. Koal, S. L. Risacher, M. A. Kling, A. Motsinger-Reif, D. M. Rotroff, J. Jack, T. Hankemeier, D. A. Bennett, P. L. De Jager, J. Q. Trojanowski, L. M. Shaw, M. W. Weiner, P. M. Doraiswamy, C. M. van Duijn, A. J. Saykin, G. Kastenmüller, R. Kaddurah-Daouk, I. Alzheimer's Disease Neuroimaging and C. the Alzheimer Disease Metabolomics (2019). "Altered bile acid profile associates with cognitive impairment in Alzheimer's disease-An emerging role for gut microbiome." Alzheimer's & dementia : the journal of the Alzheimer's Association **15**(1): 76-92.
Mapstone, M., A. K. Cheema, M. S. Fiandaca, X. Zhong, T. R. Mhyre, L. H. MacArthur, W. J. Hall, S. G. Fisher, D. R. Peterson, J. M. Haley, M. D. Nazar, S. A. Rich, D. J. Berlau, C. B. Peltz, M. T. Tan, C. H. Kawas and H. J. Federoff (2014). "Plasma phospholipids identify antecedent memory impairment in older adults." Nature Medicine **20**(4): 415-418.
Maragakis, N. J. and J. D. Rothstein (2006). "Mechanisms of Disease: astrocytes in neurodegenerative disease." Nature Clinical Practice Neurology **2**(12): 679-689.
Mathiisen, T. M., K. P. Lehre, N. C. Danbolt and O. P. Ottersen (2010). "The perivascular astroglial sheath provides a complete covering of the brain microvessels: an electron microscopic 3D reconstruction." Glia **58**(9): 1094-1103.
McMaster, P. D. (1922). "DO SPECIES LACKING A GALL BLADDER POSSESS ITS FUNCTIONAL EQUIVALENT?" The Journal of experimental medicine **35**(2): 127-140.
McMillin, M., G. Frampton, R. Tobin, G. Dusio, J. Smith, H. Shin, K. Newell-Rogers, S. Grant and S. DeMorrow (2015). "TGR5 signaling reduces neuroinflammation during hepatic encephalopathy." Journal of neurochemistry **135**(3): 565-576.
Mells, G. F., G. Pells, J. L. Newton, A. J. Bathgate, A. K. Burroughs, M. A. Heneghan, J. M. Neuberger, D. B. Day, S. J. Ducker, R. N. Sandford, G. J. Alexander, D. E. J. Jones and U.-P. Consortium (2013). "Impact of primary biliary cirrhosis on perceived quality of life: The UK-PBC national study." Hepatology **58**(1): 273-283.

Meng, Z., Y. Wang, L. Wang, W. Jin, N. Liu, H. Pan, L. Liu, L. Wagman, B. M. Forman and W. Huang (2010). "FXR regulates liver repair after CCl4-induced toxic injury." Mol Endocrinol **24**(5): 886-897.
Metcalf, J. and O. James (1997). "The geoepidemiology of primary biliary cirrhosis." Semin Liver Dis **17**(1): 13-22.
Milani, S., H. Herbst, D. Schuppan, K. Y. Kim, E. O. Riecken and H. Stein (1990). "Procollagen expression by nonparenchymal rat liver cells in experimental biliary fibrosis." Gastroenterology **98**(1): 175-184.
Min, S. S., H. Y. Quan, J. Ma, J.-S. Han, B. H. Jeon and G. H. Seol (2009). "Chronic brain inflammation impairs two forms of long-term potentiation in the rat hippocampal CA1 area." Neuroscience Letters **456**(1): 20-24.
Monfort, P., M.-D. Muñoz and V. Felipo (2005). "Chronic hyperammonemia in vivo impairs long-term potentiation in hippocampus by altering activation of cyclic GMP-dependent-protein kinase and of phosphodiesterase 5." Journal of Neurochemistry **94**(4): 934-942.
Montagne, A., S. R. Barnes, M. D. Sweeney, M. R. Halliday, A. P. Sagare, Z. Zhao, A. W. Toga, R. E. Jacobs, C. Y. Liu, L. Amezcua, M. G. Harrington, H. C. Chui, M. Law and B. V. Zlokovic (2015). "Blood-brain barrier breakdown in the aging human hippocampus." Neuron **85**(2): 296-302.
Montagnese, S., L. M. Nsemi, N. Cazzagon, S. Facchini, L. Costa, N. V. Bergasa, P. Amodio and A. Floreani (2013). "Sleep-wake profiles in patients with primary biliary cirrhosis." Liver International **33**(2): 203-209.
Montes, S., M. Alcaraz-Zubeldia, P. Muriel and C. Ríos (2001). "Striatal manganese accumulation induces changes in dopamine metabolism in the cirrhotic rat." Brain Research **891**(1): 123-129.
Montgomery, S. M. and G. Buzsáki (2007). "Gamma oscillations dynamically couple hippocampal CA3 and CA1 regions during memory task performance." Proceedings of the National Academy of Sciences of the United States of America **104**(36): 14495-14500.
Morishita, H., J. H. Cabungcal, Y. Chen, K. Q. Do and T. K. Hensch (2015). "Prolonged Period of Cortical Plasticity upon Redox Dysregulation in Fast-Spiking Interneurons." Biol Psychiatry **78**(6): 396-402.
Mosher, V. A. L., M. G. Swain, J. X. Q. Pang, G. G. Kaplan, K. A. Sharkey, G. M. MacQueen and B. G. Goodyear (2017). "Primary Biliary Cholangitis Alters Functional Connections of the Brain's Deep Gray Matter." Clinical and translational gastroenterology **8**(7): e107-e107.
Mosher, V. A. L., M. G. Swain, J. X. Q. Pang, G. G. Kaplan, K. A. Sharkey, G. M. MacQueen and B. G. Goodyear (2018). "Magnetic resonance imaging evidence of hippocampal structural changes in patients with primary biliary cholangitis." Clinical and translational gastroenterology **9**(7): 169-169.
Mouri, S., H. E. Mourabit, C. Bouzbib, A. Schaefer, C. Housset, N. Weiss and D. Thabut (2017). "Implication of the Blood-Brain Barrier in the Physiopathology of Hepatic Encephalopathy in Cirrhosis." Journal of Clinical and Experimental Hepatology **7**: S45-S46.
Mouries, J., P. Brescia, A. Silvestri, I. Spadoni, M. Sorribas, R. Wiest, E. Mileti, M. Galbiati, P. Invernizzi, L. Adorini, G. Penna and M. Rescigno (2019). "Microbiota-driven gut vascular barrier disruption is a prerequisite for non-alcoholic steatohepatitis development." Journal of Hepatology **71**(6): 1216-1228.
Mudaliar, S., R. R. Henry, A. J. Sanyal, L. Morrow, H. U. Marschall, M. Kipnes, L. Adorini, C. I. Sciacca, P. Clopton, E. Castelloe, P. Dillon, M. Pruzanski and D. Shapiro (2013). "Efficacy and

safety of the farnesoid X receptor agonist obeticholic acid in patients with type 2 diabetes and nonalcoholic fatty liver disease." Gastroenterology **145**(3): 574-582.e571.
Munoz-Espin, D. and M. Serrano (2014). "Cellular senescence: from physiology to pathology." Nat Rev Mol Cell Biol **15**(7): 482-496.
Munoz-Lorente, M. A., A. C. Cano-Martin and M. A. Blasco (2019). "Mice with hyper-long telomeres show less metabolic aging and longer lifespans." Nat Commun **10**(1): 4723.
Nakamura, M., H. Kondo, T. Mori, A. Komori, M. Matsuyama, M. Ito, Y. Takii, M. Koyabu, T. Yokoyama and K. Migita (2007). "Anti-gp210 and anti-centromere antibodies are different risk factors for the progression of primary biliary cirrhosis." Hepatology **45**(1): 118-127.
Nakamura, M., Y. Takii, M. Ito, A. Komori, T. Yokoyama, Y. Shimizu-Yoshida, M. Koyabu, M. Matsuyama, T. Mori, T. Kamihira, M. Daikoku, K. Migita, H. Yatsuhashi, N. Nozaki, S. Shimoda and H. Ishibashi (2006). "Increased expression of nuclear envelope gp210 antigen in small bile ducts in primary biliary cirrhosis." J Autoimmun **26**(2): 138-145.
Nation, D. A., M. D. Sweeney, A. Montagne, A. P. Sagare, L. M. D'Orazio, M. Pachicano, F. Sepehrband, A. R. Nelson, D. P. Buennagel, M. G. Harrington, T. L. S. Benzinger, A. M. Fagan, J. M. Ringman, L. S. Schneider, J. C. Morris, H. C. Chui, M. Law, A. W. Toga and B. V. Zlokovic (2019). "Blood-brain barrier breakdown is an early biomarker of human cognitive dysfunction." Nature medicine **25**(2): 270-276.
Navawongse, R. and H. Eichenbaum (2013). "Distinct pathways for rule-based retrieval and spatial mapping of memory representations in hippocampal neurons." J Neurosci **33**(3): 1002-1013.
Nelson, G., J. Wordsworth, C. Wang, D. Jurk, C. Lawless, C. Martin-Ruiz and T. von Zglinicki (2012). "A senescent cell bystander effect: senescence-induced senescence." Aging Cell **11**(2): 345-349.
Nevens, F., P. Andreone, G. Mazzella, S. I. Strasser, C. Bowlus, P. Invernizzi, J. P. Drenth, P. J. Pockros, J. Regula, U. Beuers, M. Trauner, D. E. Jones, A. Floreani, S. Hohenester, V. Luketic, M. Shiffman, K. J. van Erpecum, V. Vargas, C. Vincent, G. M. Hirschfield, H. Shah, B. Hansen, K. D. Lindor, H. U. Marschall, K. V. Kowdley, R. Hooshmand-Rad, T. Marmon, S. Sheeron, R. Pencek, L. MacConell, M. Pruzanski and D. Shapiro (2016). "A Placebo-Controlled Trial of Obeticholic Acid in Primary Biliary Cholangitis." N Engl J Med **375**(7): 631-643.
Newton, J. L., N. Bhala, J. Burt and D. E. Jones (2006). "Characterisation of the associations and impact of symptoms in primary biliary cirrhosis using a disease specific quality of life measure." J Hepatol **44**(4): 776-783.
Newton, J. L., K. G. Hollingsworth, R. Taylor, A. M. El-Sharkawy, Z. U. Khan, R. Pearce, K. Sutcliffe, O. Okonkwo, A. Davidson, J. Burt, A. M. Blamire and D. Jones (2008). "Cognitive impairment in primary biliary cirrhosis: symptom impact and potential etiology." Hepatology **48**(2): 541-549.
Niedermeyer, E. (1997). "Alpha rhythms as physiological and abnormal phenomena." Int J Psychophysiol **26**(1-3): 31-49.
Nozaki, Y., K. Harada, T. Sanzen and Y. Nakanuma (2013). "PPARgamma ligand attenuates portal inflammation in the MRL-lpr mouse: a new strategy to restrain cholangiopathy in primary biliary cirrhosis." Med Mol Morphol **46**(3): 153-159.
Nunes, A. F., J. D. Amaral, A. C. Lo, M. B. Fonseca, R. J. S. Viana, Z. Callaerts-Vegh, R. D'Hooge and C. M. P. Rodrigues (2012). "TUDCA, a Bile Acid, Attenuates Amyloid Precursor Protein Processing and Amyloid-β Deposition in APP/PS1 Mice." Molecular Neurobiology **45**(3): 440-454.

O'Keefe, J. and J. Dostrovsky (1971). "The hippocampus as a spatial map. Preliminary evidence from unit activity in the freely-moving rat." Brain Research **34**(1): 171-175.
Oakley, F., M. Meso, J. P. Iredale, K. Green, C. J. Marek, X. Zhou, M. J. May, H. Millward-Sadler, M. C. Wright and D. A. Mann (2005). "Inhibition of inhibitor of κB kinases stimulates hepatic stellate cell apoptosis and accelerated recovery from rat liver fibrosis." Gastroenterology **128**(1): 108-120.
Ognjanovski, N., S. Schaeffer, J. Wu, S. Mofakham, D. Maruyama, M. Zochowski and S. J. Aton (2017). "Parvalbumin-expressing interneurons coordinate hippocampal network dynamics required for memory consolidation." Nature Communications **8**(1): 15039.
Ogrodnik, M., S. Miwa, T. Tchkonia, D. Tiniakos, C. L. Wilson, A. Lahat, C. P. Day, A. Burt, A. Palmer, Q. M. Anstee, S. N. Grellscheid, J. H. J. Hoeijmakers, S. Barnhoorn, D. A. Mann, T. G. Bird, W. P. Vermeij, J. L. Kirkland, J. F. Passos, T. von Zglinicki and D. Jurk (2017). "Cellular senescence drives age-dependent hepatic steatosis." Nat Commun **8**: 15691.
Ott, P. and F. S. Larsen (2004). "Blood–brain barrier permeability to ammonia in liver failure: a critical reappraisal." Neurochemistry International **44**(4): 185-198.
Palmela, I., F. L. Cardoso, M. Bernas, L. Correia, A. R. Vaz, R. F. Silva, A. Fernandes, K. S. Kim, D. Brites and M. A. Brito (2011). "Elevated levels of bilirubin and long-term exposure impair human brain microvascular endothelial cell integrity." Curr Neurovasc Res **8**(2): 153-169.
Palmela, I., L. Correia, R. F. Silva, H. Sasaki, K. S. Kim, D. Brites and M. A. Brito (2015). "Hydrophilic bile acids protect human blood-brain barrier endothelial cells from disruption by unconjugated bilirubin: an in vitro study." Front Neurosci **9**: 80.
Palmela, I., L. Correia, R. F. M. Silva, H. Sasaki, K. S. Kim, D. Brites and M. A. Brito (2015). "Hydrophilic bile acids protect human blood-brain barrier endothelial cells from disruption by unconjugated bilirubin: an in vitro study." Frontiers in neuroscience **9**: 80-80.
Palmela, I., H. Sasaki, F. L. Cardoso, M. Moutinho, K. S. Kim, D. Brites and M. A. Brito (2012). "Time-dependent dual effects of high levels of unconjugated bilirubin on the human blood-brain barrier lining." Front Cell Neurosci **6**: 22.
Paolicelli, R. C., G. Bolasco, F. Pagani, L. Maggi, M. Scianni, P. Panzanelli, M. Giustetto, T. A. Ferreira, E. Guiducci, L. Dumas, D. Ragozzino and C. T. Gross (2011). "Synaptic pruning by microglia is necessary for normal brain development." Science **333**(6048): 1456-1458.
Pekny, M. and M. Nilsson (2005). "Astrocyte activation and reactive gliosis." Glia **50**(4): 427-434.
Pellicciari, R., S. Fiorucci, E. Camaioni, C. Clerici, G. Costantino, P. R. Maloney, A. Morelli, D. J. Parks and T. M. Willson (2002). "6alpha-ethyl-chenodeoxycholic acid (6-ECDCA), a potent and selective FXR agonist endowed with anticholestatic activity." J Med Chem **45**(17): 3569-3572.
Pells, G., G. F. Mells, M. Carbone, J. L. Newton, A. J. Bathgate, A. K. Burroughs, M. A. Heneghan, J. M. Neuberger, D. B. Day, S. J. Ducker, U.-P. Consortium, R. N. Sandford, G. J. Alexander and D. E. J. Jones (2013). "The impact of liver transplantation on the phenotype of primary biliary cirrhosis patients in the UK-PBC cohort." Journal of hepatology **59**(1): 67-73.
Pietersen, A. N., N. Patel, J. G. Jefferys and M. Vreugdenhil (2009). "Comparison between spontaneous and kainate-induced gamma oscillations in the mouse hippocampus in vitro." Eur J Neurosci **29**(11): 2145-2156.
Pollak, Y., H. Ovadia, E. Orion, J. Weidenfeld and R. Yirmiya (2003). "The EAE-associated behavioral syndrome: I. Temporal correlation with inflammatory mediators." Journal of Neuroimmunology **137**(1): 94-99.

Poo, J. L., G. Feldmann, S. Erlinger, A. Braillon, C. Gaudin, M. Dumont and D. Lebrec (1992). "Ursodeoxycholic acid limits liver histologic alterations and portal hypertension induced by bile duct ligation in the rat." Gastroenterology **102**(5): 1752-1759.
Poordad, F. F. (2007). "The burden of hepatic encephalopathy." Alimentary pharmacology & therapeutics **25**: 3-9.
Post, S. M., H. Duez, P. P. Gervois, B. Staels, F. Kuipers and H. M. Princen (2001). "Fibrates suppress bile acid synthesis via peroxisome proliferator-activated receptor-alpha-mediated downregulation of cholesterol 7alpha-hydroxylase and sterol 27-hydroxylase expression." Arterioscler Thromb Vasc Biol **21**(11): 1840-1845.
Poupon, R. E., B. Balkau, E. Eschwège and R. Poupon (1991). "A multicenter, controlled trial of ursodiol for the treatment of primary biliary cirrhosis. UDCA-PBC Study Group." N Engl J Med **324**(22): 1548-1554.
Poupon, R. E., A. M. Bonnand, Y. Chretien and R. Poupon (1999). "Ten-year survival in ursodeoxycholic acid-treated patients with primary biliary cirrhosis. The UDCA-PBC Study Group." Hepatology **29**(6): 1668-1671.
Poupon, R. E., Y. Chrétien, O. Chazouillères, R. Poupon, J. Chwalow and P. B. C. S. G. and the French (2004). "Quality of life in patients with primary biliary cirrhosis." Hepatology **40**(2): 489-494.
Powell, B. R., N. R. Buist and P. Stenzel (1982). "An X-linked syndrome of diarrhea, polyendocrinopathy, and fatal infection in infancy." The Journal of pediatrics **100**(5): 731-737.
Prince, M. I., A. Chetwynd, W. L. Craig, J. V. Metcalf and O. F. W. James (2004). "Asymptomatic primary biliary cirrhosis: clinical features, prognosis, and symptom progression in a large population based cohort." Gut **53**(6): 865.
Prince, M. I., A. Chetwynd, P. Diggle, M. Jarner, J. V. Metcalf and O. F. James (2001). "The geographical distribution of primary biliary cirrhosis in a well-defined cohort." Hepatology **34**(6): 1083-1088.
Puglielli, L., R. E. Tanzi and D. M. Kovacs (2003). "Alzheimer's disease: the cholesterol connection." Nature Neuroscience **6**(4): 345-351.
Pullinger, C. R., C. Eng, G. Salen, S. Shefer, A. K. Batta, S. K. Erickson, A. Verhagen, C. R. Rivera, S. J. Mulvihill, M. J. Malloy and J. P. Kane (2002). "Human cholesterol 7alpha-hydroxylase (CYP7A1) deficiency has a hypercholesterolemic phenotype." The Journal of clinical investigation **110**(1): 109-117.
Quinn, M., M. McMillin, C. Galindo, G. Frampton, H. Y. Pae and S. DeMorrow (2014). "Bile acids permeabilize the blood brain barrier after bile duct ligation in rats via Rac1-dependent mechanisms." Digestive and liver disease : official journal of the Italian Society of Gastroenterology and the Italian Association for the Study of the Liver **46**(6): 527-534.
R. Pacheco-Rivera, J. A.-R., M.C. Garcia de Leon, M. Shibayama and J. Serrano-Luna (2017). Liver Pathophysiology - Chapter 23. E. S. T. Pablo Muriel. ProQuest Ebook Central.
Ramos Pittol, J. M., A. Milona, I. Morris, E. C. L. Willemsen, S. W. van der Veen, E. Kalkhoven and S. W. C. van Mil (2020). "FXR Isoforms Control Different Metabolic Functions in Liver Cells via Binding to Specific DNA Motifs." Gastroenterology **159**(5): 1853-1865.e1810.
Ricci, P., A. F. Hofmann, L. Hagey, R. A. Jorgensen, E. R. Dickson and K. D. Lindor (1998). "Adjuvant cholylsarcosine during ursodeoxycholic acid treatment of primary biliary cirrhosis." Digestive diseases and sciences **43**(6): 1292-1295.
Ridlon, J. M., D. J. Kang and P. B. Hylemon (2006). "Bile salt biotransformations by human intestinal bacteria." J Lipid Res **47**(2): 241-259.

Robel, S., B. Berninger and M. Götz (2011). "The stem cell potential of glia: lessons from reactive gliosis." Nature Reviews Neuroscience **12**(2): 88-104.
Robson, E., C. Tweedy, N. Manzanza, J.-P. Taylor, P. Atkinson, F. Randall, A. Reeve, G. J. Clowry and F. E. N. LeBeau (2018). "Impaired Fast Network Oscillations and Mitochondrial Dysfunction in a Mouse Model of Alpha-synucleinopathy (A30P)." Neuroscience **377**: 161-173.
Rodrigues, C. M., G. Fan, P. Y. Wong, B. T. Kren and C. J. Steer (1998). "Ursodeoxycholic acid may inhibit deoxycholic acid-induced apoptosis by modulating mitochondrial transmembrane potential and reactive oxygen species production." Mol Med **4**(3): 165-178.
Rogers, A. B. and R. Z. Dintzis (2012). Liver and Gallbladder. Comparative Anatomy and Histology**:** 193-201.
Roskams, T. (2003). "Progenitor cell involvement in cirrhotic human liver diseases: from controversy to consensus." Journal of hepatology **39**(3): 431-434.
Roskams, T. A., N. D. Theise, C. Balabaud, G. Bhagat, P. S. Bhathal, P. Bioulac-Sage, E. M. Brunt, J. M. Crawford, H. A. Crosby, V. Desmet, M. J. Finegold, S. A. Geller, A. S. Gouw, P. Hytiroglou, A. S. Knisely, M. Kojiro, J. H. Lefkowitch, Y. Nakanuma, J. K. Olynyk, Y. N. Park, B. Portmann, R. Saxena, P. J. Scheuer, A. J. Strain, S. N. Thung, I. R. Wanless and A. B. West (2004). "Nomenclature of the finer branches of the biliary tree: canals, ductules, and ductular reactions in human livers." Hepatology **39**(6): 1739-1745.
Roy, D. S., A. Arons, T. I. Mitchell, M. Pignatelli, T. J. Ryan and S. Tonegawa (2016). "Memory retrieval by activating engram cells in mouse models of early Alzheimer's disease." Nature **531**(7595): 508-512.
Rubin, L. L., D. E. Hall, S. Porter, K. Barbu, C. Cannon, H. C. Horner, M. Janatpour, C. W. Liaw, K. Manning, J. Morales and et al. (1991). "A cell culture model of the blood-brain barrier." J Cell Biol **115**(6): 1725-1735.
Rudic, J. S., G. Poropat, M. N. Krstic, G. Bjelakovic and C. Gluud (2012). "Ursodeoxycholic acid for primary biliary cirrhosis." The Cochrane database of systematic reviews **12**(12): CD000551-CD000551.
Rustenhoven, J., D. Jansson, L. C. Smyth and M. Dragunow (2017). "Brain pericytes as mediators of neuroinflammation." Trends in pharmacological sciences **38**(3): 291-304.
Santello, M., C. Calì and P. Bezzi (2012). "Gliotransmission and the tripartite synapse." Adv Exp Med Biol **970**: 307-331.
Sasaki, M., M. Hsu, M. M. Yeh and Y. Nakanuma (2015). "In recurrent primary biliary cirrhosis after liver transplantation, biliary epithelial cells show increased expression of mitochondrial proteins." Virchows Arch **467**(4): 417-425.
Sasaki, M., H. Ikeda, H. Haga, T. Manabe and Y. Nakanuma (2005). "Frequent cellular senescence in small bile ducts in primary biliary cirrhosis: a possible role in bile duct loss." The Journal of Pathology: A Journal of the Pathological Society of Great Britain and Ireland **205**(4): 451-459.
Sasaki, M., H. Ikeda, J. Yamaguchi, M. Miyakoshi, Y. Sato and Y. Nakanuma (2010). "Bile Ductular Cells Undergoing Cellular Senescence Increase in Chronic Liver Diseases Along With Fibrous Progression." American Journal of Clinical Pathology **133**(2): 212-223.
Sasaki, M., H. Ikeda, J. Yamaguchi, S. Nakada and Y. Nakanuma (2008). "Telomere shortening in the damaged small bile ducts in primary biliary cirrhosis reflects ongoing cellular senescence." Hepatology **48**(1): 186-195.

Sasaki, M., M. Miyakoshi, Y. Sato and Y. Nakanuma (2010). "Modulation of the microenvironment by senescent biliary epithelial cells may be involved in the pathogenesis of primary biliary cirrhosis." J Hepatol **53**: 318-325.
Sasaki, M., Y. Sato and Y. Nakanuma (2020). "Increased p16INK4a-expressing senescent bile ductular cells are associated with inadequate response to ursodeoxycholic acid in primary biliary cholangitis." Journal of Autoimmunity **107**: 102377.
Scoville, W. B. and B. Milner (1957). "Loss of recent memory after bilateral hippocampal lesions." J Neurol Neurosurg Psychiatry **20**(1): 11-21.
Sederberg, P. B., A. Schulze-Bonhage, J. R. Madsen, E. B. Bromfield, D. C. McCarthy, A. Brandt, M. S. Tully and M. J. Kahana (2007). "Hippocampal and neocortical gamma oscillations predict memory formation in humans." Cereb Cortex **17**(5): 1190-1196.
Seibenhener, M. L. and M. C. Wooten (2015). "Use of the Open Field Maze to measure locomotor and anxiety-like behavior in mice." Journal of visualized experiments : JoVE(96): e52434-e52434.
Sell, S. (1998). "Comparison of liver progenitor cells in human atypical ductular reactions with those seen in experimental models of liver injury." Hepatology **27**(2): 317-331.
Selmi, C., F. Cavaciocchi, A. Lleo, C. Cheroni, R. De Francesco, S. A. Lombardi, M. De Santis, F. Meda, M. G. Raimondo, C. Crotti, M. Folci, L. Zammataro, M. J. Mayo, N. Bach, S. Shimoda, S. C. Gordon, M. Miozzo, P. Invernizzi, M. Podda, R. Scavelli, M. R. Martin, M. F. Seldin, J. M. LaSalle and M. E. Gershwin (2014). "Genome-Wide Analysis of DNA Methylation, Copy Number Variation, and Gene Expression in Monozygotic Twins Discordant for Primary Biliary Cirrhosis." Frontiers in Immunology **5**(128).
Selmi, C., M. J. Mayo, N. Bach, H. Ishibashi, P. Invernizzi, R. G. Gish, S. C. Gordon, H. I. Wright, B. Zweiban, M. Podda and M. E. Gershwin (2004). "Primary biliary cirrhosis in monozygotic and dizygotic twins: genetics, epigenetics, and environment." Gastroenterology **127**(2): 485-492.
Sengillo, J. D., E. A. Winkler, C. T. Walker, J. S. Sullivan, M. Johnson and B. V. Zlokovic (2013). "Deficiency in Mural Vascular Cells Coincides with Blood–Brain Barrier Disruption in A lzheimer's Disease." Brain pathology **23**(3): 303-310.
Shepherd, J., C. J. Packard, H. G. Morgan, J. L. Third, J. M. Stewart and T. V. Lawrie (1979). "The effects of cholestyramine on high density lipoprotein metabolism." Atherosclerosis **33**(4): 433-444.
Sinal, C. J., M. Tohkin, M. Miyata, J. M. Ward, G. Lambert and F. J. Gonzalez (2000). "Targeted disruption of the nuclear receptor FXR/BAR impairs bile acid and lipid homeostasis." Cell **102**(6): 731-744.
Singer, W. (1999). "Neuronal synchrony: a versatile code for the definition of relations?" Neuron **24**(1): 49-65, 111-125.
Smogorzewska, A. and T. de Lange (2002). "Different telomere damage signaling pathways in human and mouse cells." EMBO J **21**(16): 4338-4348.
Smyk, D. S., E. I. Rigopoulou, A. Pares, C. Billinis, A. K. Burroughs, L. Muratori, P. Invernizzi and D. P. Bogdanos (2012). "Sex differences associated with primary biliary cirrhosis." Clin Dev Immunol **2012**: 610504.
Sofroniew, M. V. (2009). "Molecular dissection of reactive astrogliosis and glial scar formation." Trends Neurosci **32**(12): 638-647.
Sohal, V. S., F. Zhang, O. Yizhar and K. Deisseroth (2009). "Parvalbumin neurons and gamma rhythms enhance cortical circuit performance." Nature **459**(7247): 698-702.

Solá, S., J. D. Amaral, P. M. Borralho, R. M. Ramalho, R. E. Castro, M. r. M. Aranha, C. J. Steer and C. M. P. Rodrigues (2006). "Functional Modulation of Nuclear Steroid Receptors by Tauroursodeoxycholic Acid Reduces Amyloid β-Peptide-Induced Apoptosis." Molecular Endocrinology **20**(10): 2292-2303.
Solá, S., R. E. Castro, P. A. Laires, C. J. Steer and C. M. P. Rodrigues (2003). "Tauroursodeoxycholic Acid Prevents Amyloid-β Peptide-Induced Neuronal Death Via a Phosphatidylinositol 3-Kinase-Dependent Signaling Pathway." Molecular Medicine **9**(9): 226-234.
Song, P., Y. Zhang and C. D. Klaassen (2011). "Dose-response of five bile acids on serum and liver bile Acid concentrations and hepatotoxicty in mice." Toxicological sciences : an official journal of the Society of Toxicology **123**(2): 359-367.
Soto, C. (2003). "Unfolding the role of protein misfolding in neurodegenerative diseases." Nature Reviews Neuroscience **4**(1): 49-60.
Staels, B., J. Dallongeville, J. Auwerx, K. Schoonjans, E. Leitersdorf and J. C. Fruchart (1998). "Mechanism of action of fibrates on lipid and lipoprotein metabolism." Circulation **98**(19): 2088-2093.
Steffenach, H.-A., R. S. Sloviter, E. I. Moser and M.-B. Moser (2002). "Impaired retention of spatial memory after transection of longitudinally oriented axons of hippocampal CA3 pyramidal cells." Proceedings of the National Academy of Sciences of the United States of America **99**(5): 3194-3198.
Steward, O., E. R. Torre, R. Tomasulo and E. Lothman (1992). "Seizures and the regulation of astroglial gene expression." Epilepsy Res Suppl **7**: 197-209.
Stojancevic, M., K. Stankov and M. Mikov (2012). "The impact of farnesoid X receptor activation on intestinal permeability in inflammatory bowel disease." Canadian journal of gastroenterology = Journal canadien de gastroenterologie **26**(9): 631-637.
Strautnieks, S. S., A. F. Kagalwalla, M. S. Tanner, A. S. Knisely, L. Bull, N. Freimer, S. A. Kocoshis, R. M. Gardiner and R. J. Thompson (1997). "Identification of a Locus for Progressive Familial Intrahepatic Cholestasis PFIC2on Chromosome 2q24." The American Journal of Human Genetics **61**(3): 630-633.
Strazzabosco, M. and L. Fabris (2012). "Development of the bile ducts: essentials for the clinical hepatologist." Journal of hepatology **56**(5): 1159-1170.
Stroup, D., M. Crestani and J. Y. Chiang (1997). "Identification of a bile acid response element in the cholesterol 7 alpha-hydroxylase gene CYP7A." Am J Physiol **273**(2 Pt 1): G508-517.
Suzuki, W. A. and H. Eichenbaum (2000). "The neurophysiology of memory." Ann N Y Acad Sci **911**: 175-191.
Tabibian, J. H., S. P. O'Hara, P. L. Splinter, C. E. Trussoni and N. F. LaRusso (2014). "Cholangiocyte senescence by way of N-ras activation is a characteristic of primary sclerosing cholangitis." Hepatology **59**(6): 2263-2275.
Tag, C. G., S. Sauer-Lehnen, S. Weiskirchen, E. Borkham-Kamphorst, R. H. Tolba, F. Tacke and R. Weiskirchen (2015). "Bile duct ligation in mice: induction of inflammatory liver injury and fibrosis by obstructive cholestasis." J Vis Exp(96).
Tahamtan, M., I. Aghaei, V. Pooladvand, V. Sheibani, M. Khaksari and M. Shabani (2017). "Characterization of the CA1 pyramidal neurons in rat model of hepatic cirrhosis: insights into their electrophysiological properties." Metabolic Brain Disease **32**(3): 881-889.

Takano, S., Y. Ito, O. Yokosuka, M. Ohto, K. Uchiumi, K. Hirota and M. Omata (1994). "A multicenter randomized controlled dose study of ursodeoxycholic acid for chronic hepatitis C." Hepatology **20**(3): 558-564.
Tarter, R. E., A. M. Hegedus, D. H. Van Thiel, N. Edwards and R. R. Schade (1987). "Neurobehavioral correlates of cholestatic and hepatocellular disease: differentiation according to disease specific characteristics and severity of the identified cerebral dysfunction." Int J Neurosci **32**(3-4): 901-910.
Theofilopoulos, S., Y. Wang, S. S. Kitambi, P. Sacchetti, K. M. Sousa, K. Bodin, J. Kirk, C. Saltó, M. Gustafsson and E. M. Toledo (2013). "Brain endogenous liver X receptor ligands selectively promote midbrain neurogenesis." Nature chemical biology **9**(2): 126.
Tort, A. B., R. W. Komorowski, J. R. Manns, N. J. Kopell and H. Eichenbaum (2009). "Theta–gamma coupling increases during the learning of item–context associations." Proceedings of the National Academy of Sciences **106**(49): 20942-20947.
Traub, R. D., A. Bibbig, A. Fisahn, F. E. N. LeBeau, M. A. Whittington and E. H. Buhl (2000). "A model of gamma-frequency network oscillations induced in the rat CA3 region by carbachol in vitro." European Journal of Neuroscience **12**(11): 4093-4106.
Turner, I. B., M. Myszor, H. C. Mitchison, M. K. Bennett, A. D. Burt and O. F. W. James (1994). "A two year controlled trial examining the effectiveness of ursodeoxycholic acid in primary biliary cirrhosis." Journal of Gastroenterology and Hepatology **9**(2): 162-168.
Uhlhaas, P. J. and W. Singer (2006). "Neural Synchrony in Brain Disorders: Relevance for Cognitive Dysfunctions and Pathophysiology." Neuron **52**(1): 155-168.
Varadi, D. P. (1974). "Pruritus induced by crude bile and purified bile acids. Experimental production of pruritus in human skin." Arch Dermatol **109**(5): 678-681.
Verbeke, L., R. Farre, B. Verbinnen, K. Covens, T. Vanuytsel, J. Verhaegen, M. Komuta, T. Roskams, S. Chatterjee, P. Annaert, I. V. Elst, P. Windmolders, J. Trebicka, F. Nevens and W. Laleman (2015). "The FXR Agonist Obeticholic Acid Prevents Gut Barrier Dysfunction and Bacterial Translocation in Cholestatic Rats." The American Journal of Pathology **185**(2): 409-419.
Victorelli, S. and J. F. Passos (2017). "Telomeres and Cell Senescence - Size Matters Not." EBioMedicine **21**: 14-20.
Võikar, V., E. Vasar and H. Rauvala (2004). "Behavioral alterations induced by repeated testing in C57BL/6J and 129S2/Sv mice: implications for phenotyping screens." Genes, Brain and Behavior **3**(1): 27-38.
von Zglinicki, T., G. Saretzki, W. Docke and C. Lotze (1995). "Mild hyperoxia shortens telomeres and inhibits proliferation of fibroblasts: a model for senescence?" Exp Cell Res **220**(1): 186-193.
Vreugdenhil, M. and E. C. Toescu (2005). "Age-dependent reduction of gamma oscillations in the mouse hippocampus in vitro." Neuroscience **132**(4): 1151-1157.
Wahler, J. B., M. G. Swain, R. Carson, N. V. Bergasa and E. A. Jones (1993). "Blood-brain barrier permeability is markedly decreased in cholestasis in the rat." Hepatology **17**(6): 1103-1108.
Wang, H., J. Chen, K. Hollister, L. C. Sowers and B. M. Forman (1999). "Endogenous bile acids are ligands for the nuclear receptor FXR/BAR." Mol Cell **3**(5): 543-553.
Wang, Y.-D., W.-D. Chen, M. Wang, D. Yu, B. M. Forman and W. Huang (2008). "Farnesoid X receptor antagonizes nuclear factor kappaB in hepatic inflammatory response." Hepatology (Baltimore, Md.) **48**(5): 1632-1643.

Warren, D. B., D. K. Chalmers, K. Hutchison, W. Dang and C. W. Pouton (2006). "Molecular dynamics simulations of spontaneous bile salt aggregation." Colloids and Surfaces A: Physicochemical and Engineering Aspects **280**(1): 182-193.
Washington, M. K. (2007). "Autoimmune liver disease: overlap and outliers." Mod Pathol **20 Suppl 1**: S15-30.
Webster, C. R. and M. S. Anwer (1998). "Cyclic adenosine monophosphate-mediated protection against bile acid-induced apoptosis in cultured rat hepatocytes." Hepatology **27**(5): 1324-1331.
Wei, Z., X.-C. Chen, Y. Song, X.-D. Pan, X.-M. Dai, J. Zhang, X.-L. Cui, X.-L. Wu and Y.-G. Zhu (2016). "Amyloid β Protein Aggravates Neuronal Senescence and Cognitive Deficits in 5XFAD Mouse Model of Alzheimer's Disease." Chinese medical journal **129**(15): 1835-1844.
Whittington, M. A., M. O. Cunningham, F. E. N. LeBeau, C. Racca and R. D. Traub (2011). "Multiple origins of the cortical gamma rhythm." Developmental Neurobiology **71**(1): 92-106.
Whittington, M. A., R. D. Traub and J. G. Jefferys (1995). "Synchronized oscillations in interneuron networks driven by metabotropic glutamate receptor activation." Nature **373**(6515): 612-615.
Wilhelmsson, U., E. A. Bushong, D. L. Price, B. L. Smarr, V. Phung, M. Terada, M. H. Ellisman and M. Pekny (2006). "Redefining the concept of reactive astrocytes as cells that remain within their unique domains upon reaction to injury." Proc Natl Acad Sci U S A **103**(46): 17513-17518.
Wilson, J. D., C. A. Lindsey and J. M. Dietschy (1968). "Influence of dietary cholesterol on cholesterol metabolism." Ann N Y Acad Sci **149**(2): 808-821.
Witt-Sullivan, H., J. Heathcote, K. Cauch, L. Blendis, C. Ghent, A. Katz, R. Milner, S. C. Pappas, J. Rankin and I. R. Wanless (1990). "The demography of primary biliary cirrhosis in Ontario, Canada." Hepatology **12**(1): 98-105.
Wong, R. J., R. G. Gish and A. Ahmed (2014). "Hepatic encephalopathy is associated with significantly increased mortality among patients awaiting liver transplantation." Liver Transplantation **20**(12): 1454-1461.
Wright, G., N. A. Davies, D. L. Shawcross, S. J. Hodges, C. Zwingmann, H. F. Brooks, A. R. Mani, D. Harry, V. Stadlbauer and Z. Zou (2007). "Endotoxemia produces coma and brain swelling in bile duct ligated rats." Hepatology **45**(6): 1517-1526.
Wright, M. C., R. Issa, D. E. Smart, N. Trim, G. I. Murray, J. N. Primrose, M. J. P. Arthur, J. P. Iredale and D. A. Mann (2001). "Gliotoxin stimulates the apoptosis of human and rat hepatic stellate cells and enhances the resolution of liver fibrosis in rats." Gastroenterology **121**(3): 685-698.
Wright, R. L. and C. D. Conrad (2005). "Chronic stress leaves novelty-seeking behavior intact while impairing spatial recognition memory in the Y-maze." Stress (Amsterdam, Netherlands) **8**(2): 151-154.
Wu, W.-B., R. Menon, Y.-Y. Xu, J.-R. Zhao, Y.-L. Wang, Y. Liu and H.-J. Zhang (2016). "Downregulation of peroxiredoxin-3 by hydrophobic bile acid induces mitochondrial dysfunction and cellular senescence in human trophoblasts." Scientific Reports **6**(1): 38946.
Wylot, B., K. Konarzewska, L. Bugajski, K. Piwocka and M. Zawadzka (2015). "Isolation of vascular endothelial cells from intact and injured murine brain cortex—technical issues and pitfalls in FACS analysis of the nervous tissue." Cytometry Part A **87**(10): 908-920.
Xu, M., T. Pirtskhalava, J. N. Farr, B. M. Weigand, A. K. Palmer, M. M. Weivoda, C. L. Inman, M. B. Ogrodnik, C. M. Hachfeld, D. G. Fraser, J. L. Onken, K. O. Johnson, G. C. Verzosa, L. G. P.

Langhi, M. Weigl, N. Giorgadze, N. K. LeBrasseur, J. D. Miller, D. Jurk, R. J. Singh, D. B. Allison, K. Ejima, G. B. Hubbard, Y. Ikeno, H. Cubro, V. D. Garovic, X. Hou, S. J. Weroha, P. D. Robbins, L. J. Niedernhofer, S. Khosla, T. Tchkonia and J. L. Kirkland (2018). "Senolytics improve physical function and increase lifespan in old age." Nat Med **24**(8): 1246-1256.
Yamamoto, C. and H. McIlwain (1966). "ELECTRICAL ACTIVITIES IN THIN SECTIONS FROM THE MAMMALIAN BRAIN MAINTAINED IN CHEMICALLY-DEFINED MEDIA IN VITRO." Journal of Neurochemistry **13**(12): 1333-1343.
Yang, C. Y., X. Ma, K. Tsuneyama, S. Huang, T. Takahashi, N. P. Chalasani, C. L. Bowlus, G. X. Yang, P. S. Leung, A. A. Ansari, L. Wu, R. L. Coppel and M. E. Gershwin (2014). "IL-12/Th1 and IL-23/Th17 biliary microenvironment in primary biliary cirrhosis: implications for therapy." Hepatology **59**(5): 1944-1953.
Yang, F., X. Huang, T. Yi, Y. Yen, D. D. Moore and W. Huang (2007). "Spontaneous development of liver tumors in the absence of the bile acid receptor farnesoid X receptor." Cancer Res **67**(3): 863-867.
Yang, Y., M. Zhang, G. Eggertsen and J. Y. Chiang (2002). "On the mechanism of bile acid inhibition of rat sterol 12alpha-hydroxylase gene (CYP8B1) transcription: roles of alpha-fetoprotein transcription factor and hepatocyte nuclear factor 4alpha." Biochim Biophys Acta **1583**(1): 63-73.
Yasoshima, M., N. Kono, H. Sugawara, K. Katayanagi, K. Harada and Y. Nakanuma (1998). "Increased expression of interleukin-6 and tumor necrosis factor-alpha in pathologic biliary epithelial cells: in situ and culture study." Laboratory investigation; a journal of technical methods and pathology **78**(1): 89-100.
Younossi, Z. M., V. Ratziu, R. Loomba, M. Rinella, Q. M. Anstee, Z. Goodman, P. Bedossa, A. Geier, S. Beckebaum, P. N. Newsome, D. Sheridan, M. Y. Sheikh, J. Trotter, W. Knapple, E. Lawitz, M. F. Abdelmalek, K. V. Kowdley, A. J. Montano-Loza, J. Boursier, P. Mathurin, E. Bugianesi, G. Mazzella, A. Olveira, H. Cortez-Pinto, I. Graupera, D. Orr, L. L. Gluud, J.-F. Dufour, D. Shapiro, J. Campagna, L. Zaru, L. MacConell, R. Shringarpure, S. Harrison, A. J. Sanyal, M. Abdelmalek, G. Abrams, H. Aguilar, A. Ahmed, E. Aigner, G. Aithal, A. Ala, W. Alazawi, A. Albillos, M. Allison, S. Al-Shamma, R. Andrade, P. Andreone, M. Angelico, V. Ankoma-Sey, Q. Anstee, R. Anty, V. Araya, J. I. Arenas Ruiz, P. Arkkila, M. Arora, T. Asselah, J. Au, O. Ayonrinde, R. J. Bailey, M. Balakrishnan, K. Bambha, M. Bansal, S. Barritt, J. Bate, J. Beato, S. Beckebaum, J. Behari, P. Bellot, Z. Ben Ari, M. Bennett, M. Berenguer, B. T. Beretta-Piccoli, T. Berg, M. Bonacini, L. Bonet, B. Borg, M. Bourliere, J. Boursier, W. Bowman, D. Bradley, M. Brankovic, M. Braun, J.-P. Bronowicki, S. Bruno, E. Bugianesi, C. Cai, J. L. Calleja Panero, E. Carey, M. Carmiel, J. A. Carrión, M. Cave, C. Chagas, T. Chami, A. Chang, A. Coates, J. Cobbold, K. Corey, L. Corless, H. Cortez-Pinto, J. Crespo, O. Cruz Pereira, V. de Ledinghen, A. deLemos, M. Diago, J.-F. Dufour, P. Dugalic, W. Dunn, M. Elkhashab, M. Epstein, M. D. Escudero-Garcia, O. Etzion, L. Evans, R. Falcone, C. Fernandez, J. Ferreira, S. Fink, K. Finnegan, R. Firpi-Morell, A. Floreani, T. Fontanges, R. Ford, E. Forrest, A. Fowell, A. L. Fracanzani, S. Francque, B. Freilich, J. Frias, M. Fuchs, J. Fuentes, M. Galambos, J. Gallegos, A. Geerts, A. Geier, J. George, M. Ghali, R. Ghalib, P. Gholam, P. Gines, N. Gitlin, L. L. Gluud, T. Goeser, J. Goff, S. Gordon, F. Gordon, O. Goria, S. Greer, A. Grigorian, H. Gronbaek, M. Guillaume, N. Gunaratnam, D. Halegoua-De Marzio, B. Hameed, S. Hametner, J. Hamilton, S. Harrison, M. Hartleb, T. Hassanein, D. Häussinger, P. Hellstern, R. Herring, E. Heurich, C. Hezode, H. Hinrichsen, P. Holland Fischer, Y. Horsmans, J. Huang, A. Jakiche, L. Jeffers, B. Jones, R. Jorge, F. Jorquera, A. Kahraman, K. Kaita, N. Karyotakis, Z. Kayali, S. Kechagias, T. Kepczyk, M. Khalili, H. Khallafi, J. Kluwe, W. Knapple, A. Kohli, K. Korenblat, K. Kowdley, A.

Krag, R. Krause, A. Kremer, K. Krok, M. Krstic, M. Kugelmas, S. Kumar, D. Labarriere, M. Lai, P. Lampertico, E. Lawitz, A. Lee, V. Leroy, S. Lidofsky, T. H. Lim, J. Lim, D. Lipkis, E. Little, A. Lonardo, M. Long, R. Loomba, Y. Lurie, G. Macedo, M. Makara, B. Maliakkal, M. Manns, P. Manousou, P. Mantry, G. Marchesini, C. Marinho, P. Marotta, H.-U. Marschall, P. Mathurin, M. Mayo, G. Mazzella, M. McCullen, W. McLaughlin, R. Merriman, A. Modi, E. Molina, A. Montano-Loza, C. Monteverde, S. Moreea, C. Moreno, F. Morisco, A. Mubarak, B. Muellhaupt, S. Mukherjee, T. Müller, A. Nagorni, J. Naik, G. Neff, M. Nevah, P. Newsome, E. Nguyen-Khac, M. Noureddin, J. Oben, A. Olveira, H. Orlent, D. Orr, J. Orr, G. Ortiz-Lasanta, V. Ozenne, P. Pandya, A. Paredes, J. Park, J. Patel, K. Patel, M. Uta, H. Patton, M. Peck-Radosavljevic, S. Petta, S. Pianko, A. Piekarska, N. Pimstone, P. Pockros, S. Pol, M. Porayko, J. Poulos, D. Pound, J. Pouzar, J. Presa Ramos, N. Pyrsopoulos, N. Rafiq, K. Muller, A. Ramji, V. Ratziu, R. Ravinuthala, C. Reddy, G. Reddy K G, K. R. Reddy K R, F. Regenstein, R. Reindollar, A. Riera, M. Rinella, J. Rivera Acosta, G. Robaeys, S. Roberts, F. Rodriguez-Perez, M. Romero-Gomez, R. Rubin, M. Rumi, S. Rushbrook, C. Rust, M. Ryan, R. Safadi, A. Said, K. Salminen, D. Samuel, J. Santoro, A. Sanyal, S. Sarkar, C. Schaeffer, J. Schattenberg, I. Schiefke, E. Schiff, W. Schmidt, J. Schneider, J. Schouten, M. Schultz, G. Sebastiani, D. Semela, T. Sepe, A. Sheikh, M. Sheikh, D. Sheridan, K. Sherman, O. Shibolet, M. Shiffman, A. Siddique, C. Sieberhagen, S. Sigal, K. Sikorska, K. Simon, M. Sinclair, R. Skoien, J. Solis, S. Sood, B. Souder, J. Spivey, P. Stal, L. Stinton, S. Strasser, P. Svorcan, G. Szabo, A. Talal, E. Tam, B. Tetri, P. Thuluvath, H. Tobias, K. Tomasiewicz, D. Torres, M. Trauner, C. Trautwein, J. Trotter, E. Tsochatzis, E. Unitt, V. Vargas, I. Varkonyi, E. Veitsman, U. Vespasiani Gentilucci, D. Victor, J. Vierling, C. Vincent, A. Vincze, M. von der Ohe, N. Von Roenn, R. Vuppalanchi, M. Waters, K. Watt, M. Weltman, A. Wieland, G. Wiener, A. Williams A, J. Williams J, J. Wilson, M. Yataco, E. Yoshida, Z. Younes, L. Yuan, A. Zivony, D. Zogg, H. Zoller, F. Zoulim, E. Zuckerman and M. Zuin (2019). "Obeticholic acid for the treatment of non-alcoholic steatohepatitis: interim analysis from a multicentre, randomised, placebo-controlled phase 3 trial." The Lancet **394**(10215): 2184-2196.

Zamanian, J. L., L. Xu, L. C. Foo, N. Nouri, L. Zhou, R. G. Giffard and B. A. Barres (2012). "Genomic Analysis of Reactive Astrogliosis." The Journal of Neuroscience **32**(18): 6391.

Zenouzi, R., J. von der Gablentz, M. Heldmann, M. Göttlich, C. Weiler-Normann, M. Sebode, H. Ehlken, J. Hartl, A. Fellbrich, S. Siemonsen, C. Schramm, T. F. Münte and A. W. Lohse (2018). "Patients with primary biliary cholangitis and fatigue present with depressive symptoms and selected cognitive deficits, but with normal attention performance and brain structure." PloS one **13**(1): e0190005-e0190005.

Zhang, L., Y. D. Wang, W. D. Chen, X. Wang, G. Lou, N. Liu, M. Lin, B. M. Forman and W. Huang (2012). "Promotion of liver regeneration/repair by farnesoid X receptor in both liver and intestine in mice." Hepatology **56**(6): 2336-2343.

Zhang, L.-N., T.-Y. Shi, X.-H. Shi, L. Wang, Y.-J. Yang, B. Liu, L.-X. Gao, Z.-W. Shuai, F. Kong, H. Chen, W. Han, S.-M. Han, Y.-Y. Fei, Q.-C. Cui, Q. Wang, M. Shen, D. Xu, W.-J. Zheng, Y.-Z. Li, W. Zhang, X. Zhang and F.-C. Zhang (2013). "Early biochemical response to ursodeoxycholic acid and long-term prognosis of primary biliary cirrhosis: Results of a 14-year cohort study." Hepatology **58**(1): 264-272.

Zhang, Y., Y. Chen, S. L. Bressler and M. Ding (2008). "Response preparation and inhibition: the role of the cortical sensorimotor beta rhythm." Neuroscience **156**(1): 238-246.

Zhang, Y., H. R. Kast-Woelbern and P. A. Edwards (2003). "Natural structural variants of the nuclear receptor farnesoid X receptor affect transcriptional activation." J Biol Chem **278**(1): 104-110.

Zhang, Y., Y. Xiong and W. G. Yarbrough (1998). "ARF promotes MDM2 degradation and stabilizes p53: ARF-INK4a locus deletion impairs both the Rb and p53 tumor suppression pathways." Cell **92**(6): 725-734.
Zheng, C., K. W. Bieri, E. Hwaun and L. L. Colgin (2016). "Fast Gamma Rhythms in the Hippocampus Promote Encoding of Novel Object-Place Pairings." eNeuro **3**(2): ENEURO.0001-0016.2016.
Zhou, J., N. Huang, Y. Guo, S. Cui, C. Ge, Q. He, X. Pan, G. Wang, H. Wang and H. Hao (2019). "Combined obeticholic acid and apoptosis inhibitor treatment alleviates liver fibrosis." Acta Pharmaceutica Sinica B **9**(3): 526-536.
Zimmermann, H. and J. Reichen (1992). "Ursodeoxycholate has no beneficial effect on liver function or histology in biliary cirrhosis in the rat." Journal of hepatology **16**(3): 355-359.